Magnetic skyrmions in proximity to an s-wave superconductor

by

Eugene Balkind

Department of Physics
Royal Holloway University of London

Supervisor: Prof. Matthias Eschrig
Advisor: Prof. Jon Goff
Moderator: Dr. Nikolas Kauer

This thesis is submitted for a degree of Doctor of Philosophy
September 2016

Declaration of Authorship

I, Eugene Balkind, hereby declare that this thesis and the work presented in it is entirely my own. Where I have consulted the work of others, this is always clearly stated.

Signed:

Date:

Abstract

In this Thesis we present a new method of theoretical studies of magnetic materials. The method is based on the Fourier expansion of the magnetisation and then using this expansion in order to minimise the free energy functional of a magnetic material, hence obtain the optimal configuration of the system for a certain set of parameters. We also employ Lagrange multiplier technique in order to satisfy the constraint of $\left|\vec{M}\right|^2 = 1$ required by micromagnetics. We have mainly applied this method to a system that obeys a skyrmionic order. Critical fields corresponding to helical-skyrmion and skyrmion-ferromagnetic phase transitions were found exactly. Also, new shapes of skyrmion lattice that have never been observed before were obtained via our method. The method proved itself to be universal, i.e. applicable for any micromagnetic system. As an example of an extended magnetic system, we considered a bilayer of a magnet and a superconductor and used our method along with Brandt's approach to a superconductor, that we used as a guide for our method, in order to describe the combined system and study the magnetic states obtained.

Contents

List of Figures

List of Tables

Chapter 1

Introduction

People have been studying magnetism for centuries, ever since they first noticed that some objects may attract the others without any visible reason. This must have been a great mystery back those days. On the other hand, we grow up accepting the fact of existence of fields around us. We ask our parents how phone and TV signals work and their answer would definitely contain words "electromagnetic waves" in it, no matter of their background. Probably every physicist remembers a demonstration back from high school of a magnet and metal shavings that align along field lines. Magnetic effects became a part of our life long ago and are not mysterious anymore. However, a scientist always tries to look deeper. If a man observes two objects that attract each other, a scientist wants to know why they do. Although magnetism is around us and we constantly use it in our everyday life, there are still mysteries to be revealed, there are still questions to be answered.

We know now that magnetism in solids is induced by spins of charged particles with electrons being the most common case. The magnetic moment of an electron is anti-parallel to the spin angular momentum. The direction is spontaneously chosen from one of the degenerate states with the same ground state energy. In presence of an external field the chosen direction is between the direction of the external field and one of the directions preferred by magnetic anisotropy. This is true for homogeneous states only, i.e. when the magnetisation direction is not spatially varying within the sample. [1] An example of an inhomogeneous state is a domain state in a ferromagnet. Such a state contains regions (domains) with all spins parallel to each other, however the total domain spin is not parallel to other domains' spins. So one can say that a typical ferromagnet consists of homogeneous domains, but as spins are aligned in the same direction within a single domain only, ferromagnet itself is an inhomogeneous system as almost any system in nature. Schematic representation of magnetic domains is demonstrated in Figure 1.1a and magnetic domains actually observed in a ferromagnet can be found in Figure 1.1b.

While a single ferromagnetic domain is a special example of a homogeneous system, the

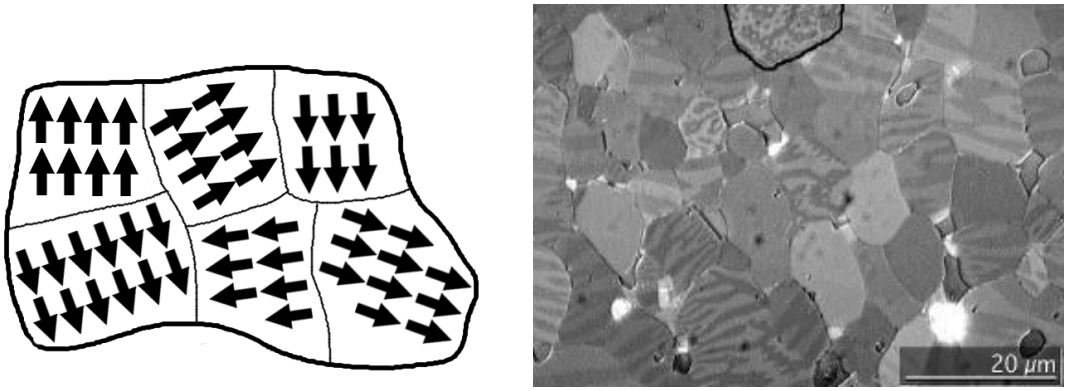

(a) Schematic representation of magnetic domains. [2]

(b) Magnetic domains observed in NdFeB. [3]

Figure 1.1: Schematic representation of magnetic domains along with the actual picture of magnetic domains in NdFeB. Spins are aligned in the same direction within a single domain only, though the total spins of domains are aligned in a random order with respect to each other.

full bulk ferromagnet is inhomogeneous. Once a large enough external field is turned on, the domain structure gets progressively destroyed and the whole system turns into a homogeneous one with all the spins pointing in one direction, determined by the field. Magnetic domains are separated by domain walls – regions where spins are smoothly rotating from one neighbouring direction to another. One can distinguish between two main types of domain walls: Bloch wall – the one that corresponds to the rotation of domain wall spins through the plane of the domain wall, and Néel wall – the one that corresponds to the rotation within the domain wall plane. Schematic representation of spin behaviour in both Bloch and Néel walls is demonstrated in Figure 1.2. Note that other types of domain walls are possible, but they are less common and are not to be discussed here.

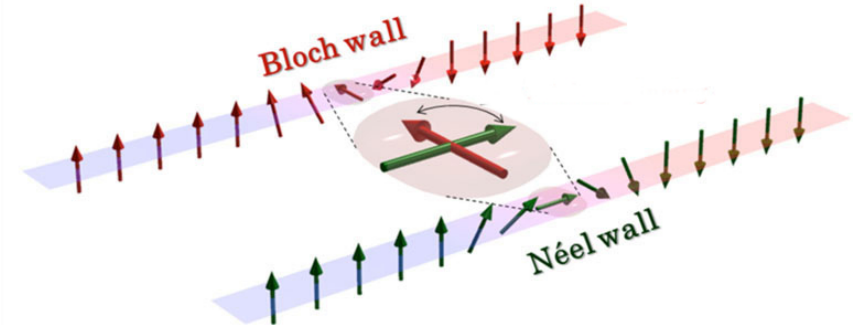

Figure 1.2: Schematic representation of spin behaviour in Bloch (red) and Néel (green) domain walls. In the Bloch case spin rotates from one terminal position (either “up” or “down”) to another through the plane and in the Néel case the rotation occurs within the plane. [4]

Ferromagnets are permanent magnets, i.e. once magnetised by an external field, they preserve their magnetisation even when the field is switched off. Typical examples of ferromagnets are iron, cobalt, nickel and their alloys. [5] Among the first studying ferromagnetism was Aleksandr Stoletov who demonstrated a non-linear dependence between $\vec{B}$ and $\vec{H}$. The Bohr-van Leeuwen theorem [6] tells us that ferromagnetism is of pure quantum nature. [5] The main quantum mechanic origin of (electronic) ferromagnets is the exchange interaction. [7]

It is well known from basic quantum mechanics that two electrons in one shell (subshell) cannot have the same spin. [8] When orbitals of the outer unpaired valence electrons overlap, electrons with parallel spins would repel even more than electrons usually do, hence the total spatial charge distribution would decrease, and therefore the total electrostatic energy would become smaller. So it is actually energetically favourable for an electron to change its spin to align with neighbouring atom's electron's spin in order to maintain the total minimal free energy. In a simple way one may think about the exchange interaction this way: two electrons of the same spins would never ever go to the same place, hence they would not need any energy to repulse if they were not repulsing already. For a system of many particles in the case where there are no other interactions present spins would tend to align with their neighbours until all the spins are aligned in one direction. This explanation, though, does not take into account on-site Coulomb interactions that would make the picture more complicated (favouring anti-ferromagnetic alignment). Often one works with effective Hamiltonians, in which case the effective exchange interactions includes a large part of on-site correlations due to Coulomb interactions.

Ferromagnetic exchange interactions can be modelled by Heisenberg Hamiltonian for all the atoms in a solid: [9]

$$\hat{H}_H = -\sum_{ij} J_{ij} \vec{S}_i \cdot \vec{S}_j, \tag{1.1}$$

where $\vec{S}_i$ and $\vec{S}_j$ are spins of electrons localised at sites i and j respectively, and J_{ij} is the exchange coupling. [10] However, it is often possible to set $J_{ij} = J = const$ for neighbouring atoms and zero otherwise, as this would correspond to the exchange between nearest neighbours only, that is often the most likely exchange to occur; in this case the summation then goes over the nearest neighbour pairs only:

$$\hat{H}_H = -J \sum_{\langle ij \rangle} \vec{S}_i \cdot \vec{S}_j, \tag{1.2}$$

and $J > 0$ corresponds to a ferromagnet, whereas $J < 0$ corresponds to an anti-ferromagnet. This classification rises from the fact that spins are parallel in a ferromagnet, just as they are in the equal-spin triplet state and anti-parallel in an anti-ferromagnet and singlet state. J is defined as $J = E_s - E_t$, hence its sign depends on whether the energy of a singlet state, E_s,

is lower (hence anti-ferromagnet is favourable) or the energy of a triplet state, E_t, is lower (ferromagnet is preferred in this case). [10] The full Hamiltonian of a ferromagnetic system then writes as

$$\hat{H}_F = -J \sum_{\langle ij \rangle} \vec{S}_i \cdot \vec{S}_j + g\mu_B \sum_j \vec{S}_j \cdot \vec{B}, \tag{1.3}$$

where the last term is the Zeeman energy, that is nothing else but the energy of an electron (a particle with spin S_j) in an external magnetic field. [7] More generally, under continuum approximation (see later) the Zeeman energy can be written as

$$E_z = -\mu_0 \int \vec{M} \cdot \vec{H} dV, \tag{1.4}$$

where $\vec{H}$ is the external field and $\vec{M}$ is the local magnetisation. [5]

Let us now pay more attention to inhomogeneous magnetic states. The most famous inhomogeneous state is the domain state in ferromagnets, with magnetic domains separated by domain walls, just as we discussed earlier. Another typical source of inhomogeneity are spin waves, or magnons, that are excited states of a typical Heisenberg magnet. [13] Inhomogeneous states can be also favoured by spin-orbit coupling, hence an anisotropic chiral exchange interaction that is described by Dzyaloshinsky-Moriya Hamiltonian: [15]

$$\hat{H}_{DM} = -\sum_{ij} \vec{D}_{ij} \cdot \left(\vec{S}_i \times \vec{S}_j \right), \tag{1.5}$$

where $\vec{D}_{ij}$ is the Dzyaloshinsky-Moriya coupling vector. Clearly, for the case of parallel or anti-parallel spins the whole term would be equal to zero due to the cross product. Schematic representation of a two-spin system described by Hamiltonian (1.5) can be found in Figure 1.3. In Figure 1.3 we see two spins suffering strong spin-orbit interaction; the vector $\vec{D}_{12}$ is perpendicular to the plane where the spins are located.

While the exchange interaction tends to align all the spins in one direction, Dzyaloshinsky-Moriya interaction gives a spin a twist. This effect results from the fact that electron's spin interacts with the atom as well as with other electrons in the system. Spin-orbit interaction then gives the shift to the direction of the spin with respect to its perfect alignment governed by the exchange interaction only. It shall be noted, though, that this effect is significant in non-centrosymmetric materials only.

This anisotropic interaction was first derived by *Igor Dzyaloshinsky* in 1958 [15] and clarified by *Toru Moriya* in 1960 (spin-orbit coupling was used to explain the phenomenological approach of Dzyaloshinsky). [16] The total Hamiltonian of a magnetic material (that is not

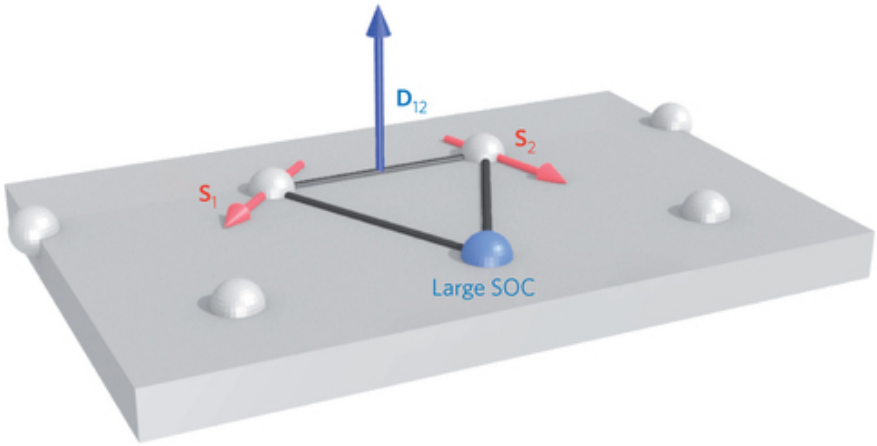

Figure 1.3: Schematic representation of neighbouring spins behaviour under strong spin-orbit coupling. [14]

necessarily homogeneous) would then be written as

$$\hat{H}_M = -J \sum_{\langle ij \rangle} \vec{S}_i \cdot \vec{S}_j - \sum_{ij} \vec{D}_{ij} \cdot \left(\vec{S}_i \times \vec{S}_j \right) + g\mu_B \sum_j \vec{S}_j \cdot \vec{B}. \tag{1.6}$$

When effects of Dzyaloshinsky-Moriya interaction are strong enough, thus cannot be neglected, and the field is weak enough, hence Zeeman term cannot dominate, spins in a magnet align in a helical order, as demonstrated in Figure 1.4.

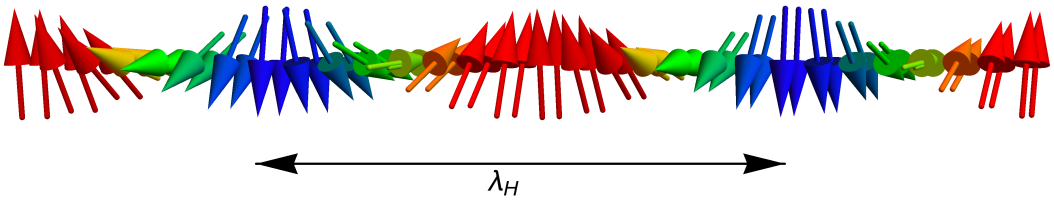

Figure 1.4: Spin helix with a period of λ_H. By analogy to any wavelength, λ_H is defined as the shortest non-zero distance between two spins aligned in the same direction.

It is also important to notice that the inversion symmetry gets broken when the Dzyaloshinsky-Moriya term is dominant and the solution is in helical (like in Figure 1.4) or skyrmion (see later) form.

From Figure 1.4 we also see that helices have their pitch period, λ_H, that is related to the helical pitch vector, $\vec{k}_H = k_H \hat{e}_x$, via

$$\lambda_H = \frac{2\pi}{k_H}. \tag{1.7}$$

A typical way to describe the magnetisation of a helix is to parametrise it as

$$\vec{M} = \begin{pmatrix} 0 \\ -\sin\left(\vec{k}_H \cdot \vec{r}\right) \\ \cos\left(\vec{k}_H \cdot \vec{r}\right) \end{pmatrix}, \tag{1.8}$$

where $\vec{r} = (x, y)$ and $\vec{k}_H = \left(k_{H_x}, k_{H_y}\right)$. [17]

If the field is large enough, however, the Zeeman term becomes the dominating one and the system then collapses into a ferromagnetic (homogeneous) state.

So effects of Dzyaloshinsky-Moriya interaction, should they be strong enough, result into inhomogeneous magnetic ordering, like spiral magnets or helimagnets. However, there is always space for topological defects, and thus from the competition between exchange and anisotropic terms new pattern may rise: magnetic skyrmions.

A magnetic skyrmion is a topologically stable field configuration that can be pictured as spin helices of unit period length packed next to each other in circular direction, i.e. a side view of a skyrmion is nothing more but a helix! An example of a single (Bloch) skyrmion can be found in Figure 1.5 and a schematic spin-helix is demonstrated in Figure 1.6. We see then that if we follow radial direction only within a skyrmion, we observe half a helix turn. Boxed regions in Figure 1.5 and Figure 1.6 match exactly.

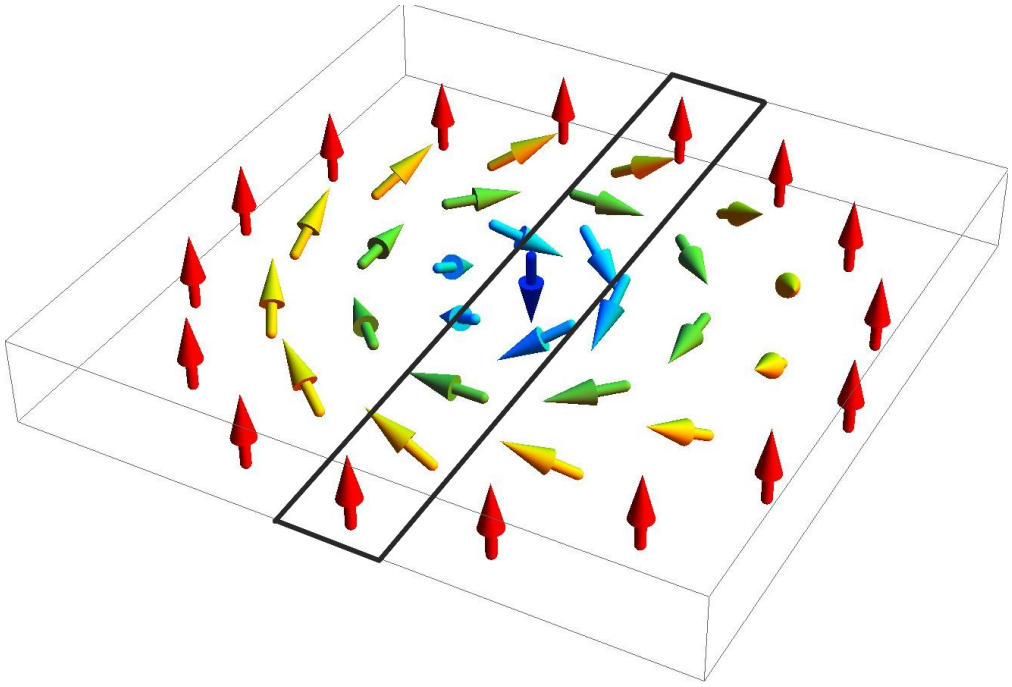

Figure 1.5: A single skyrmion with a radial direction emphasised and a unit period of a helix boxed. [18]

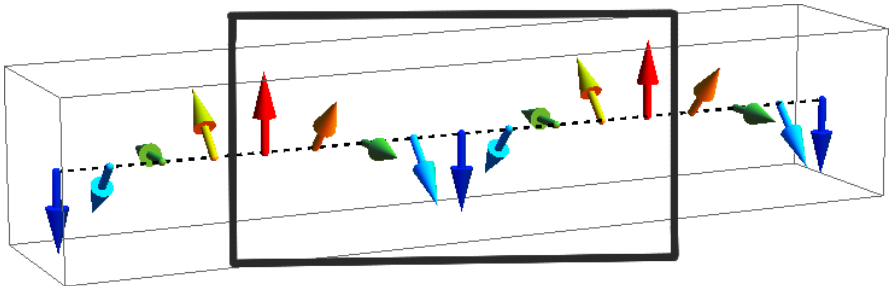

Figure 1.6: A spin helix with period boxed. [18]

One can then consider a skyrmion to be an intermediate state between helical state and ferromagnetic state in a magnetic material as it rises from the competition between the exchange interaction that is responsible for the ferromagnetic state and the anisotropic exchange that generates helical behaviour. Such states are demonstrated in Figure 1.7.

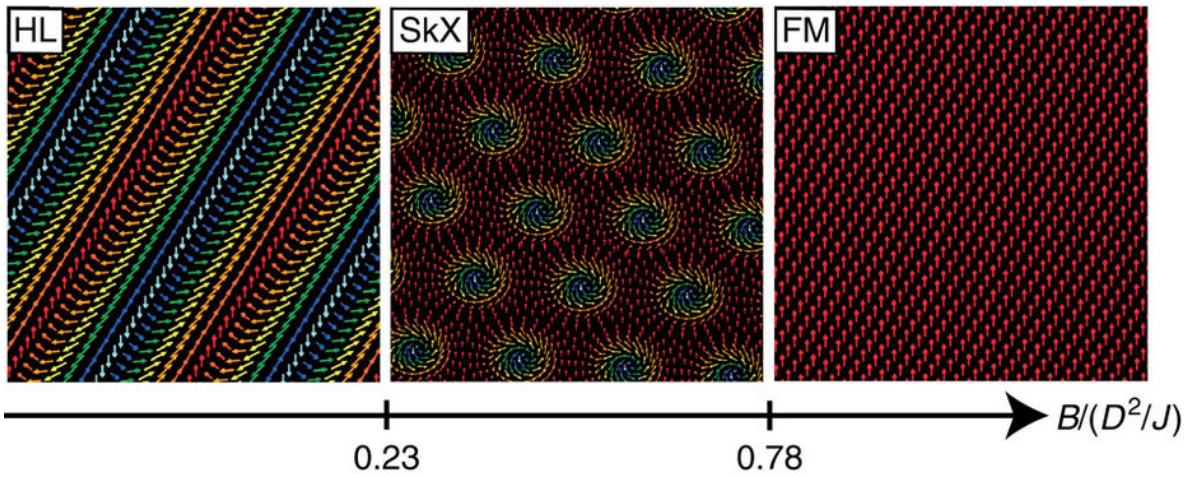

Figure 1.7: Schematic representation of possible spin configurations in a magnetic material with Dzyaloshinsky-Moriya interaction for different values of an external field. Below B_{c_1} we observe a helix, between B_{c_1} and B_{c_2} – skyrmion lattice, above B_{c_2} – ferromagnetic configuration. Values of critical fields demonstrated in dimensionless units are claimed by *Iwasaki et al* and we are to discuss them later. [19]

Experimentally observed phase diagrams of materials that exhibit skyrmion lattices under certain conditions are demonstrated in Figure 1.8.

It might be found curious that skyrmions (the actual word "skyrmion" along with the mathematical model it stands for, to be precise) came to condensed matter field from nuclear physics. Originally, skyrmions are named after *Tony Skyrme*. [22] He was developing a nonlinear field theory for interacting pions and came up with quantised and topologically stable solutions. He explained stability of particles by the fact that they are topologically protected. [22] Tony Skyrme studied 3D systems and his original skyrmion solution is therefore 3D as

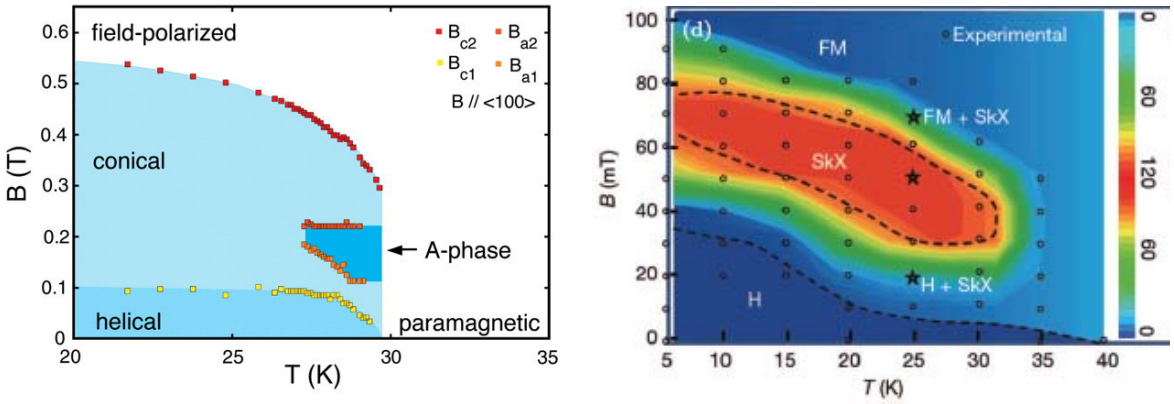

(a) Phase diagram of MnSi. [20]

(b) Phase diagram of $Fe_{1-x}Co_xSi$. [21]

Figure 1.8: Phase diagrams of magnetic materials that demonstrate skyrmion lattice under certain conditions.

well. We are, however, interested in 2D skyrmions referred to as "baby skyrmions" by some early researchers.

Having been introduced in nuclear physics, Skyrme model was exposed to other areas where people were interested in multidimensional localised structures. People were looking for localised solutions of non-linear field equations with particle-like properties. It was proven, however, that these localised states are actually unstable in many areas of interest, [23] since inhomogeneous states often appear as excitations, hence static configurations collapse into topological singularities. [24] Though, the instability of localised field configurations can be overcome. In condensed matter systems the instability of localised states can be avoided by adding chiral interactions to the functional, i.e. considering materials with broken inversion symmetries. The most obvious place to study would be magnetic non-centrosymmetric crystals, but skyrmions are found as stable or metastable localised states also in non-centrosymmetric ferroelectrics, [25] multi-component ferromagnetic Bose-Einstein condensates, [26] quantum Hall systems, [27] superfluid helium-A, [28] liquid crystals [29] and glasses. [30] Moreover, a 3D skyrmion lattice is proposed for the dense nuclear matter of neutron stars [31] and neutron stars themselves. [32]

In this research we are in the first place interested in 2D magnetic skyrmions that are mainly found in cubic helimagnets, such as MnSi, [20] $Fe_{1-x}Co_xSi$, [21] FeGe, [33] $Cr_{1-x}Mn_xGe$ alloys, [34] and also in easy-plane hexagonal magnets like $CsCuCl_3$ [35] and $RuCuCl_3$, [36] polar magnetic semiconductor GaV_4S_8, [39] multiferroic films of Cu_2OSeO_3, [37] tetragonal antiferromagnets [38] and other magnetically ordered crystals.

Existence of (2D or 3D) skyrmion solution in helimagnets as an alternative to (1D) helical solutions of the field equations of Dzyaloshinsky theory was first introduced by *A. N. Bogdanov and D. A. Yablonsky* in 1989 while studying anisotropic non-centrosymmetric magnetic ma-

terials that experience the spin-orbit interaction subject to an external field. [40] They have, however, pointed out that this skyrmion solution (they referred to skyrmions as "magnetic vortices") are thermodynamically metastable, i.e. the energy of helical states would always be lower than that of skyrmion states. Despite that, stable skyrmion solutions were found later.

Since skyrmions were introduced to condensed matter physics, a lot of research has been carried out in the field. For example, Bogdanov carried on with his research on single isolated skyrmions, [41] ending up proving that skyrmion state might be thermodynamically stable as well as metastable; [42] *Han et al* focused on skyrmion lattices in chiral magnets, [43] *Iwasaki et al* dealt with magnon-skyrmion scattering, [19] *Marcus Garst* mainly focused on the dynamics of skyrmions, [44] *Leonov et al* considered skyrmions in liquid crystals [45] and many other skyrmion systems, *T. Yokoyama and J. Linder* studied Josephson effect through magnetic skyrmion [46] and a lot more work has been put in the field.

Finally, in 2009 skyrmions were first observed experimentally in MnSi. [20] With the aid of neutron scattering *Mühlbauer et al* have observed a lattice of two dimensional skyrmions that is perpendicular to the external field itself. [20] In 2010 *Yu et al* observed skyrmion lattice in $Fe_{1-x}Co_xSi$ using Lorentz transmission electron microscopy, [21] following up finding skyrmions in FeGe. [33] An example of the skyrmion lattice observed in FeGe can be found in Figure 1.9. Spin-resolved scanning tunnelling microscopy helped to find triangular skyrmion lattices in monolayer iron on Ir(111). [47] *Romming et al* studied size and shape of a single skyrmion. [48] Stable skyrmions have been even found at room temperature in ultrathin transition metal ferromagnets (Pt/Co/Ta and Pt/CoFeB/MgO) with magnetic transmission soft X-ray microscopy. [49]

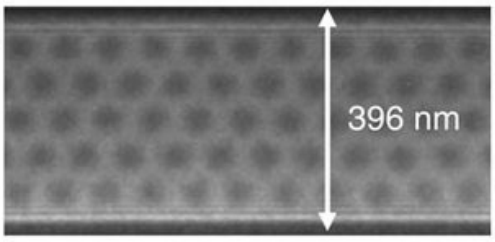

Figure 1.9: Skyrmion lattice in FeGe by high-resolution Lorentz transmission electron microscopy. In it $\vec{M}(\vec{r})$ observed that is demonstrated in the Figure. Black regions correspond to skyrmions. [50]

Skyrmion structures in bulk materials have also been observed. Those were found to be translationally invariant along the field direction, hence one can say that the magnetic texture of these materials consists of skyrmion tubes aligned in the triangular lattice. [17] Schematic representation of these structures can be found in Figure 1.10. Later other types of 3D skyrmion structures were found. [17]

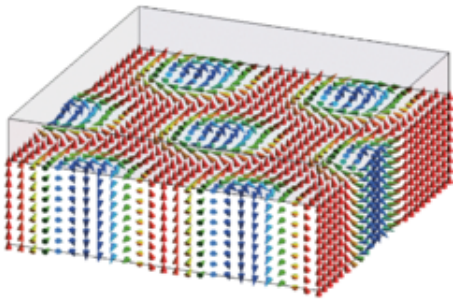

Figure 1.10: Schematic representation of possible configuration of spins in a bulk magnetic material. The magnetisation is translationally invariant in the direction of an external field. [17]

It does not matter now if those theorists that used to call 2D magnetic skyrmions "baby" had anything ironic on their mind or not, 2D magnetic skyrmions

are not "baby" anymore. Skyrmions have been researched a lot theoretically and stabilised experimentally. People even see magnetic skyrmions as a perspective direction for data storage devices. *Romming et al* have already managed to create ("write") and destroy ("remove") a single skyrmion that seems to be a great step towards new generation of digital memory devices. [51] It was also proposed to use magnetic skyrmions as logic gates [52] and transistors. [53]

The discussion of lattices of topological defects is rather incomplete should we study skyrmion lattices only. There are other examples of topological defects to be considered even in condensed matter physics. One of them is found in superconductors.

The phenomenon of superconductivity was discovered by a master of low temperatures Heike Kamerlingh Onnes in mercury below $4.12K$ in 1911. [54] In his experiment at $T = 4.12K$ the resistivity spontaneously jumped down to zero (immeasurably small quantity at least). The state of zero resistance was called to be superconducting and the state above the critical temperature – normal. This discovery had a huge impact on the scientific community and in following years many other materials proved to be superconducting at certain circumstances. In fact, it was demonstrated that almost half of the known metals exhibit superconductivity at low temperatures with niobium being high-temperature champion – its critical temperature is $T_c = 9.3K$, that is the highest result for a pure metal – and there are of course thousands of superconducting alloys as well. [5] The highest T_c reached at the moment of writing this Thesis is $T_c \sim 133K$ at normal pressure and it is $HgBa_2Ca_2Cu_3O_8$ that demonstrates it. [55] Overall, the highest T_c reached is $T_c \sim 203K$ in H_2S under pressure of $150GPa$. [56]

Superconductors are well-known for their perfect conductance, hence zero resistance at low temperatures. However, according to the modern definition, the main characteristic of a superconducting state is its ability to completely repel an external magnetic field, should it be below the critical field, B_c. [57] If the applied field is higher than B_c (that depends on temperature itself) superconductivity is destroyed. The state of complete field repulsion and perfect conductivity is called to be a Meissner phase – after Walther Meissner who discovered this complete repulsion of an external field by a superconductor in 1933 along with Robert Ochsenfeld. [57] The Meissner state is a thermodynamic state that depends uniquely on the applied field and temperature (i.e. there is no difference, whether we first cool the sample down or turn the field on), but not on the previous configuration of the system. [58]

By analogy to ferromagnets, one can describe superconductors by an order parameter, that is zero for a non-superconducting (normal) state, but is non-zero in the superconducting (Meissner) phase. This was first done by *Vitaly Ginzburg* and *Lev Landau* in 1952. [59] For a superconductor the order parameter is a macroscopic wave function of Cooper pairs condensate, $\psi = |\psi|e^{i\theta}$. Then the free energy functional is expanded around the critical point in powers of the order parameter and hence the macroscopic wave function can be found by minimising the obtained functional with respect to $|\psi|$. The famous Ginzburg-Landau functional per unit volume for a superconductor in an external magnetic field is then written

as

$$F_s = F_n + \int \left\{ \alpha|\psi|^2 + \frac{\beta}{2}|\psi|^2 + \frac{\left|\left(-i\hbar\nabla - q\vec{A}\right)\psi\right|^2}{2m} + \frac{|\vec{B}|^2}{2\mu_0} \right\} \frac{d^3r}{V}, \tag{1.9}$$

where F_n is the free energy density of a normal state averaged over the volume V, $\vec{B}$ is the internal field of a superconductor (zero in the bulk), $\vec{A}$ is the corresponding vector potential and α and β are phenomenological constants.[1] It is also often convenient to define $F = F_s - F_n$ and study the difference only.

Notice that in Meissner state $|\psi| = const$ and $\theta = const$, hence it follows that the Meissner state is homogeneous, as the ferromagnetic state in a single domain is.

However, as there are inhomogeneous magnetic states in magnets, there are inhomogeneous states in superconductors as well, when magnetic field can partially penetrate a sample without destroying superconductivity. This can be an intermediate state that is formed near the surface of a superconductor (so the field is not exactly zero there, but decays towards zero on some penetration depth depending on the geometry of a sample) [60, 61] or a superconducting vortex lattice.

In 1935 Wander Johannes de Haas and Josina Maria Casimir-Jonker discovered a smooth transition from the normal state to the Meissner state with two critical fields. [62] They thought, though, that the effect was due to bad quality of their samples and did not pay much attention to it. In 1937 Lev Shubnikov considered material with not doubtable quality and discovered the same effect: some materials demonstrated a mixed state between normal and Meissner states. [64]

Hence one can distinguish between superconductors that change their phase from normal to Meissner directly – call them "type-I superconductors" – that have one critical field, and superconductors that exhibit a mixed state between normal and Meissner states – "type-II superconductors"[2] – that have two critical fields: B_{c_1} for Meissner-mixed state transition and B_{c_2} for mixed-normal phase transition. Both B_{c_1} and B_{c_2} depend on temperature. It was found later that most of the known superconductors, especially high-temperature ones, i.e. those of particular interest of the scientific community, are type-II superconductors. A comparison between phase diagrams of a magnetic material and a type-II superconductor is demonstrated in Figure 1.11.

Nonetheless, the true nature of the mixed state had not been discovered until in 1957 *Alexei Abrikosov* predicted its existence theoretically. [63] In his work he suggested that "flux tubes" may be present in a superconductor when an external field lies between B_{c_1} and B_{c_2}. The field would then penetrate the superconductor through these flux tubes, but in the bulk

[1] The are constant with respect to spatial coordinates, though might depend on other parameters, such as temperature, pressure, etc.

[2] In fact, formal classification is based on the value of Ginzburg-Landau parameter, κ, that we would discuss later.

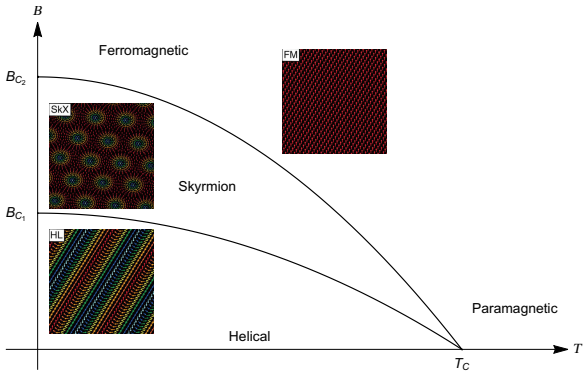

(a) Phase diagram of a magnetic material exhibiting helical, skyrmion, ferromagnetic and paramagnetic states. Pictures of phases are taken from [19].

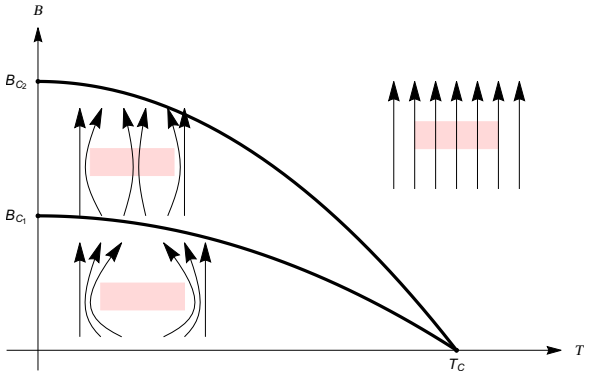

(b) Phase diagram of a type-II superconductor exhibiting Meissner, mixed and normal states. In Meissner state a superconductor completely repells the field, while in the mixed state some field can penetrate.

Figure 1.11: Comparison between phase diagrams of a magnetic material and a typpe-II superconductor. Both have two critical temperatures, hence two phase transitions, and a mixed state between two states of a completely different order.

superconductor magnetic induction would still remain zero. Abrikosov identified these flux tubes as superconducting vortices and the corresponding state as a vortex state. This state would of course be inhomogeneous, hence the order parameter, ψ, shall acquire some spatial dependence. The order parameter is still constant in the bulk superconductor, but then decays down to zero when approaching the vortex core. Abrikosov also suggested a vortex lattice (called sometimes "Abrikosov lattice" or "Abrikosov vortex lattice" nowadays) as a solution of Ginzburg-Landau equations derived from the functional (1.9) for a system in the mixed state. [63] Later it was calculated that for a system to maintain the minimal free energy the lattice has to be triangular. [65]

A vortex lattice was first observed in niobium in 1964 by *D. Criber et al* via neutron diffraction [66] and later directly – using electron microscopy – by *U. Essman and H. Träuble.* [67] The actual lattice found was triangular and periodic, as it had been predicted, though it might be deformed by defects in the crystal lattice. Examples of superconducting vortex lattices observed can be found in Figure 1.12.

Since a superconducting vortex lattice was predicted theoretically and observed experimentally a lot of research has been carried out in the field. Many research groups around the world have been focusing on finding high T_c superconductivity, grinding microscopic explanation of unconventional superconductivity, studying effects of lattice defects on Abrikosov vortices and unvealing other mysteries of this fascinating phenomena. Extensive theoretical studies of vortex lattices have been carried out by, for example, *Daniel Agterberg* [70] and *Ernst Helmut Brandt* [71]. We shall focus on the methods and results of the last one later on the go.

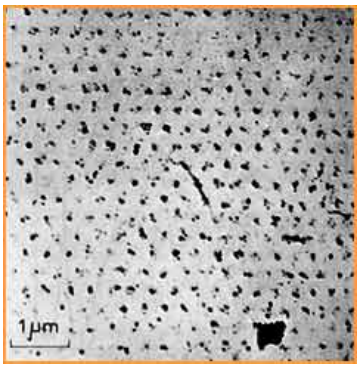

(a) Abrikosov vortex lattice observed in $Pb - 4at\%In$ by U. Essman and H. Träuble in 1967 using electron microscopy. [67]

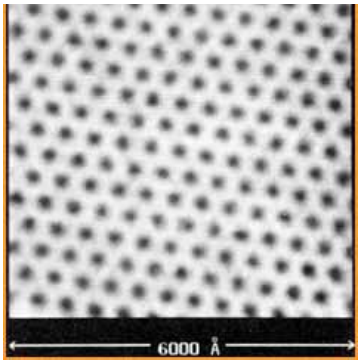

(b) Abrikosov vortex lattice observed in $NbSe_2$ by H. F. Hess et al in 1989 via scanning tunnel microscopy. [68]

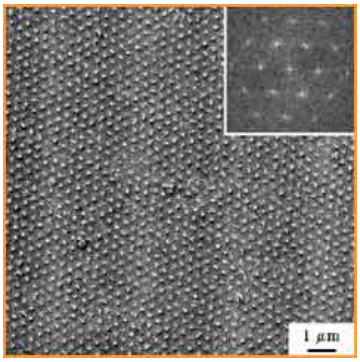

(c) Abrikosov vortex lattice observed in MgB_2 by L. Y. Vinnikov et al in 2003 by bitter decoration. [69]

Figure 1.12: Examples of superconducting vortex lattices observed in different materials by different techniques.

Many people that used to work with skyrmions have noticed similarities between skyrmion lattice and Abrikosov vortex lattice: lattice structure, topological nature, requirement of an external field to exist, etc. [43]

Skyrmions had been studied in conjunction with superconductors. For example, *Agterberg et al* have considered magnetic superconductors, [72] *Knigavko et al* focused on skyrmions in triplet superconductors. [73]

In this Thesis we investigate the case of a superconducting vortex lattice next to the skyrmion lattice (i.e. the bilayer of a magnetic material and a type-II superconductor) and see if the ground state of both systems is to change; as we are mainly focused on magnetic materials and skyrmion lattices in this Thesis, our main goal is to see if we can stabilise metastable magnetic states found in the skyrmion material by presence of a superconductor next to the magnet.

We will combine the two systems via electromagnetic coupling; i.e. an external field that penetrates the vortex in a superconductor would not be uniform anymore, but rather stand as a combination of the uniform external field and the magnetisation stray field of the skyrmion lattice. On the other hand, the field external to the skyrmion lattice would not remain uniform either, as it would be the field that penetrated a superconductor, and had been modified therefore.

We start off with Brandt's approach to type-II superconductors [71] and extend it to the combined system.

In this Thesis we first discuss single skyrmions, then, in chapter 2 turn to skyrmion lattices and study their stable and metastable states, emphasising energies of these states with respect to each other, size and shape of skyrmions and critical magnetic fields that were found exactly.

Being inspired by Brandt's approach, we consider Fourier representation of the magnetisation. The method introduced in chapter 2 proved to be very efficient, universal and more accurate than any other known technique. In chapter 3 we recall type-II superconductors and superconducting vortices, and henceforth in chapter 4 consider a bilayer of a skyrmion material and type-II superconductor. We then see if one can use a superconductor in order to stabilise magnetic states that used to be metastable in pure magnetic material.

Chapter 2

Skyrmion Lattice

2.1 Introduction and Motivation

Skyrmion lattices were first introduced by *Igor Klebanov* [79] in 1985 for neutron crystals. *Bogdanov and Yablonskii* [40] then introduced the skyrmion lattice model for magnetic materials (they referred to skyrmions as "magnetic vortices", though) in 1989, and in 2009 (after a period of twenty years!) a skyrmion lattice was finally spotted experimentally by *Mühlbauer et al* [20] in MnSi and by *Yu et al* [21] in $Fe_{1-x}Co_xSi$ (these materials were predicted by *Bogdanov and Hubert* in 1994 to support skyrmion lattices [42]).

It is known from both theoretical predictions [42] and experimental evidence [75] that skyrmions form 2D triangular lattices[1] that are perpendicular to the external field and translation invariant in the parallel direction. Skyrmion lattices have been observed in non-centrosymmetric magnets, such as MnSi, $Fe_{1-x}Co_xSi$, FeGe, $Mn_{1-x}Fe_xGe$, and some other materials. [75] An example of experimentally observed skyrmion lattice can be found in Figure 2.1.

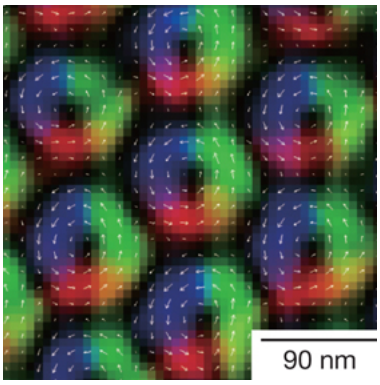

Figure 2.1: Skyrmion lattice structure observed experimentally in $Fe_{1-x}Co_xSi$ for a weak magnetic field ($50mT$). Colour scheme and arrows represent the magnetisation direction. [21]

Clearly, being proposed back in 1989, skyrmion lattices have been studied widely. Various methods had been used: for example, *Bogdanov* introduced analogy to the Abrikosov solution for a superconducting vortex lattice [40] in his first work and then conducted the study of free energy functional of a magnetic material using polar coordinates and tried the finite-difference method [42, 80] and Runge-Kutta method, [81] in order to solve Eu-

[1] Triangular lattice was first imposed for skyrmions due to the analogy to Abrikosov vortices in type-II superconductors. [42]

ler equation for helical-like structures obtained. *Yu et al* performed Monte-Carlo simulations, [21] *Han et al* applied variational analysis of the free energy functional with the aid of CP^1 mapping and analogy of skyrmion lattice to the Abrikosov vortex lattice, [43] *Karin Everschor* and *Markus Garst* solved Landau-Lifshitz-Gilbert equation [82] and many other approaches have been carried out. In this survey we are going to apply a different method of investigation of skyrmion lattices – as the skyrmion lattice is periodic, we will use the probably most convenient way of investigation for periodic structures: introduce Fourier decomposition of the magnetisation on a triangular lattice and use it in order to minimise the free energy functional of a magnetic system. We will start with the systems that have been already studied, for example, by *Han et al*, [43] in order make sure our approach is consistent with the results obtained before; then we would carry on the research to reveal unknown mysteries of this piece of the microworld.

In this chapter we discuss single skyrmions and their origin, then introduce Fourier decomposition of the magnetisation components, then with the aid of the Lagrange multiplier we find optimal lattice spacing for a given field that minimises the free energy functional and then investigate stable solutions, paying extra attention to transition points and determining exact values of critical fields. Although the lattice of the stable system was confirmed to be triangular during this research, another lattice type was found in metastable regions. It appeared that some metastable skyrmion configurations follow honeycomb lattices in oppose to their stable counterparts. However, if one compares free energy functionals of systems that obey triangular and honeycomb lattices, one realises that they are close to each other near the skyrmion-ferromagnet transition. We will study these honeycomb lattice solutions deeper in comparison with triangular lattice solutions and thus think of their applications in the future.

2.2 Magnetic Skyrmions

As it was mentioned in the introduction, magnetic skyrmions mainly arise from the competition between ferromagnetic exchange and anisotropic interaction. The exchange interaction tends to bring all the spins to a single alignment, whereas Dzyaloshinsky-Moriya interaction tends to curl spins in helices. So when these terms are of similar magnitude and the Zeeman term is small enough, magnetic skyrmions can be formed. Typical length scale of magnetic skyrmions is $5 - 100nm$, which is larger than the lattice constant,[2] hence the continuum approximation is valid for magnetic skyrmion systems. [75]

There are, however, other possible origins of skyrmions or skyrmion-like structures. Let us briefly discuss several of them, though we would still focus on those resulting from the competition between exchange and Dzyaloshinsky-Moriya interactions. The most popular alternative origin of skyrmions is the long-ranged magnetic dipolar interaction. [76] These

[2]Lattice constant of a material, not to be confused with skyrmion lattice constant.

are common in magnetic thin films with perpendicular easy-axis anisotropy. The dipolar interaction in this case enhances an in-plane magnetisation, whereas the natural anisotropy favours an out-of-plane magnetisation. So we have two competing interactions again, hence the skyrmion state may arise. Typical length scale of skyrmions arising from the competition of the dipolar interaction and the anisotropic interaction is in order of $100nm$ to $1\mu m$, which is larger than the length scale in the system of our interest. These skyrmions are often referred to as "magnetic bubbles". [77]

Other skyrmion formation mechanisms include frustrated exchange interactions, [74] where one considers second nearest neighbour interactions, and four-spin exchange interactions, that lead to square skyrmion lattices. [47] In these cases the size of the skyrmion is of order of $1nm$, which is of order of the lattice constant, hence the continuum approximation cannot be applied here. [75] Luckily, here and later on we are going to focus on skyrmions formed by the competition between the exchange interaction and anisotropic interaction, hence shall not worry about the validity of the continuum approximation.

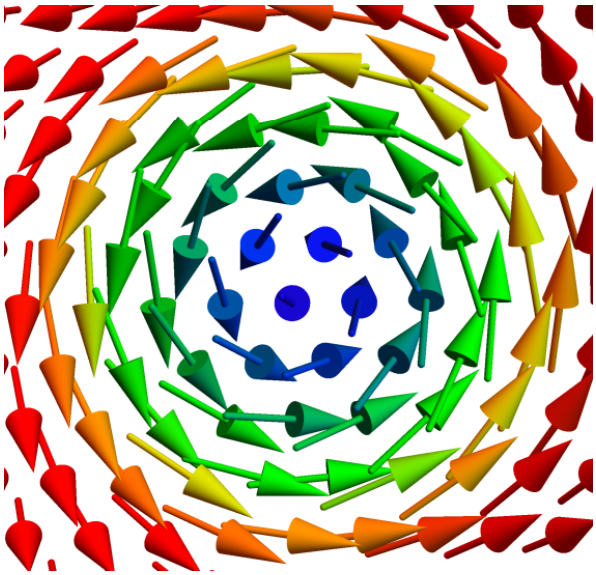

Figure 2.2: Single magnetic skyrmion in spin representation.

Let us now consider a single skyrmion as depicted in Figure 2.2. We see that the spins are in their "up" position at the edge of the skyrmion and in the "down" position in the centre of a skyrmion. On the other hand, in polar coordinates, the component of the spins in circular direction is independent of the polar angle, and thus we can claim that the direction of a spin in a single skyrmion has the radial dependence only.

In continuum approximation a magnetic system is described by the following free energy functional per unit area: [75]

$$F = \int \left\{ \frac{J}{2} \sum_{\mu} \left(\partial_\mu \vec{M}\right) \cdot \left(\partial_\mu \vec{M}\right) + D\vec{M} \cdot \left(\nabla \times \vec{M}\right) - \vec{B} \cdot \vec{M} \right\} \frac{dxdy}{A}, \tag{2.1}$$

where the integration goes over the unit cell with area A and $\vec{M}$ is the direction of the magnetisation, hence must satisfy

$$\left|\vec{M}\right|^2 = 1. \tag{2.2}$$

We also introduce $\kappa = \frac{D}{2J}$ and $\vec{\beta} = \frac{\vec{B}}{2J}$ in order to simplify our functional to

$$F = 2J \int \left\{ \frac{1}{4} \sum_{\mu} \left(\partial_\mu \vec{M}\right) \cdot \left(\partial_\mu \vec{M}\right) + \kappa \vec{M} \cdot \left(\nabla \times \vec{M}\right) - \vec{\beta} \cdot \vec{M} \right\} \frac{dxdy}{A}. \tag{2.3}$$

A single skyrmion is a magnetic system, hence it is convenient to describe it by the functional (2.1). However, following the symmetries described above it is also convenient to parametrise the magnetisation in polar coordinates:

$$\vec{M} = (\cos\phi \sin\theta, \sin\phi \sin\theta, \cos\theta)\,, \tag{2.4}$$

with θ and ϕ angles demonstrated in Figure 2.3.

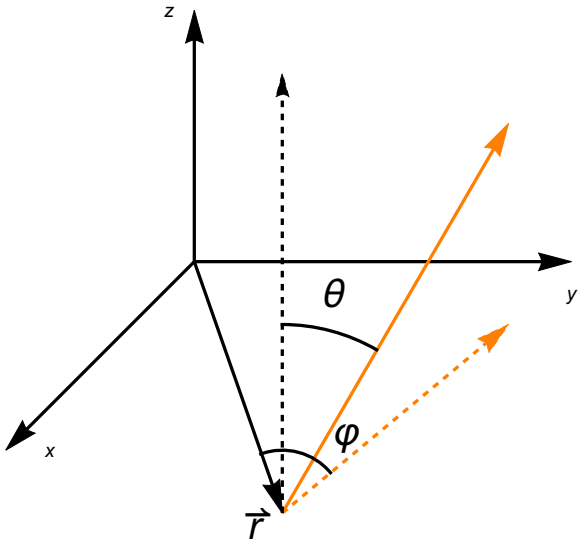

Figure 2.3: Definition of angles θ and ϕ for a spin within a skyrmion.

Combining this definition with the knowledge we obtained from Figure 2.2, conclude that θ depends on the radial component only and ϕ – only on the angular one. So if one defines a radius-vector in our new coordinate system as

$$\vec{r} = (r, \varphi)\,,^{3} \tag{2.5}$$

then $\theta = \theta(r)$ only and $\phi = \phi(\varphi)$ only. While the $\theta(r)$ dependence is non-trivial, $\phi(\varphi)$ can be written as

$$\phi(\varphi) = m\varphi + \gamma, \tag{2.6}$$

where $m = \pm 1$ and $\gamma = 0, \pm\frac{\pi}{2}, \pi$. Their values depend on the anisotropy and its origin. For

[3] This is in fact $\vec{r} = (r, \vartheta, \varphi)$ in 3D, but we are working on a plane, hence with the case of $\vartheta = \frac{\pi}{2}$.

the system of our interest (Bloch skyrmion) $m = 1$ and $\gamma = \frac{\pi}{2}$. The sign of γ is determined by the Dzyaloshinsky-Moriya constant, D. The form of $\phi(\varphi)$ stated in equation (2.6) comes from the topological skyrmion number. [75] Topological skyrmion number is defined as

$$N_{sk} = \frac{1}{4\pi} \int\int \vec{M} \cdot \left(\frac{\partial \vec{M}}{\partial x} \times \frac{\partial \vec{M}}{\partial y} \right) dxdy, \tag{2.7}$$

where $\vec{M}$ can be parametrised as in (2.4). The skyrmion number then turns into (see below for the detailed conversion of the integral)

$$N_{sk} = \frac{1}{4\pi} \int_0^{\infty} dr \int_0^{2\pi} d\varphi \frac{d\theta}{dr} \frac{d\phi}{d\varphi} \sin\theta = \frac{1}{4\pi} \Big[\cos\theta \Big]_{r=0}^{r=\infty} \Big[\phi(\varphi) \Big]_0^{2\pi}. \tag{2.8}$$

Suppose now that all spins point up at $r \to \infty$ and all spins point down at $r = 0$. Then

$$\Big[\cos\theta \Big]_{r=0}^{r=\infty} = 2. \tag{2.9}$$

One can define the vorticity, m, such that

$$N_{sk} = m \tag{2.10}$$

once the condition $r \to \infty$ is fixed. Then obtain

$$m = \frac{1}{2\pi} \Big[\phi(\varphi) \Big]_0^{2\pi}. \tag{2.11}$$

Such a formulation then leads to

$$\phi = m\varphi, \tag{2.12}$$

or

$$\phi = m\varphi + \gamma. \tag{2.13}$$

Let us now convert the functional (2.1) to the form that is consistent with our new parametrisation of $\vec{M}$. Notice that although we have parametrised our magnetisation in polar coordinates, the derivatives involved in functional (2.1) still remain Cartesian. In the representation of $\vec{r} = (r, \vartheta, \varphi)$ the derivatives become[4]

$$\partial_x = \cos\vartheta \sin\varphi \partial_r - \frac{\sin\vartheta}{r\sin\varphi} \partial_\vartheta + \frac{\cos\vartheta\cos\varphi}{r} \partial_\varphi, \tag{2.14}$$

$$\partial_y = \sin\vartheta \sin\varphi \partial_r + \frac{\cos\vartheta}{r\sin\varphi} \partial_\vartheta + \frac{\sin\vartheta\cos\varphi}{r} \partial_\varphi, \tag{2.15}$$

and there is no z-dependence in our model. With the aid of transformations (2.14) and

[4]See Appendix A.1 for the derivation.

(2.15) and polar parametrisation of the magnetisation, (2.4), one can transform the functional (2.23) into pure polar form. While the transformation of the Zeeman term (the last term in the functional) is trivial, let us focus on the transformation of the exchange term and Dzyaloshinsky-Moriya term.

The exchange term can be expanded as

$$\mathcal{T}_{ex} = \frac{1}{4}\left[(\partial_x M_x)^2 + (\partial_y M_x)^2 + (\partial_x M_y)^2 + (\partial_y M_y)^2 + (\partial_x M_z)^2 + (\partial_y M_z)^2\right]. \tag{2.16}$$

Taking the parametrisation of M_x, M_y and M_z from (2.4), the parametrisation of ∂_x and ∂_y from (2.14) and (2.15) respectively and recalling the fact that $\theta = \theta(r)$ only and $\phi = \phi(\varphi) = m\varphi + \gamma$, with $m = 1$, $\gamma = \frac{\pi}{2}$ and $\vartheta = \frac{\pi}{2}$ for Bloch skyrmions, we obtain

$$\mathcal{T}_{ex} = \frac{1}{4}\left(\frac{d\theta}{dr}\right)^2 + \frac{1}{4r}\sin^2\theta. \tag{2.17}$$

The easiest way to deal with the anisotropic term is to apply derivatives, (2.14) and (2.15) and do the algebra just as we did it for the exchange term above.[5] The anisotropic term then becomes

$$\mathcal{T}_{DM} = \kappa\frac{d\theta}{dr} + \frac{\kappa}{r}\sin\theta\cos\theta. \tag{2.18}$$

Combining results from (2.17) and (2.18) along with the parametrised form of the Zeeman term, we obtain the polar form of the free energy functional:

$$F = 2\pi J\int_0^R \left\{\left(\frac{1}{2}\frac{d\theta}{dr} + \kappa\right)^2 - \kappa^2 + \frac{\kappa}{r}\sin\theta\cos\theta + \frac{1}{4r}\sin^2\theta - \beta\left(\cos\theta - 1\right)\right\} r dr, \tag{2.19}$$

where $\kappa = \frac{D}{2J}$, $\beta = \frac{B}{2J}$, as $\vec{B} = (0, 0, B)$ with $B = const$ and R is the radius of a skyrmion. Technically, the integration should have taken place on the interval of $[0, \infty)$, but we fix the outer boundary to R as θ collapses to a trivial solution for $r > R$.

Now we can minimise the obtained functional with respect to θ either directly or via solving corresponding Euler-Lagrange equation in order to obtain $\theta(r)$ for a skyrmion of a given radius, R. In either way we start with the linear initial guess,

$$\theta_0(r) = \pi\left(1 - r\right), \tag{2.20}$$

with boundary conditions of

$$\theta(0) = \pi \tag{2.21}$$

[5] Alternatively, one can recall curl in polar coordinates, transform $\vec{M}$ into pure polar form (i.e. to M_r, M_ϑ, M_φ, not the parametrised form used in (2.4)) and do the curl directly. Both methods would work.

and

$$\theta(R) = 0. \tag{2.22}$$

Before proceeding with calculations of θ, one shall find the optimal radius of a skyrmion. In his early works *Bogdanov* defined the radius of a skyrmion as lattice constant halved. [42] Later he used more accurate circular-cell approximation. [41] However, while working with a single skyrmion, the relation between the radius of a skyrmion and lattice constant does not really matter, so we can use any definition. In any case, the radius of a skyrmion is roughly the distance from a "down" spin to the nearest "up" spin. We also need to employ another minimisation procedure in order to find the optimal radius for given values of κ and β. This was done directly and the results obtained are demonstrated in Figure 2.4.

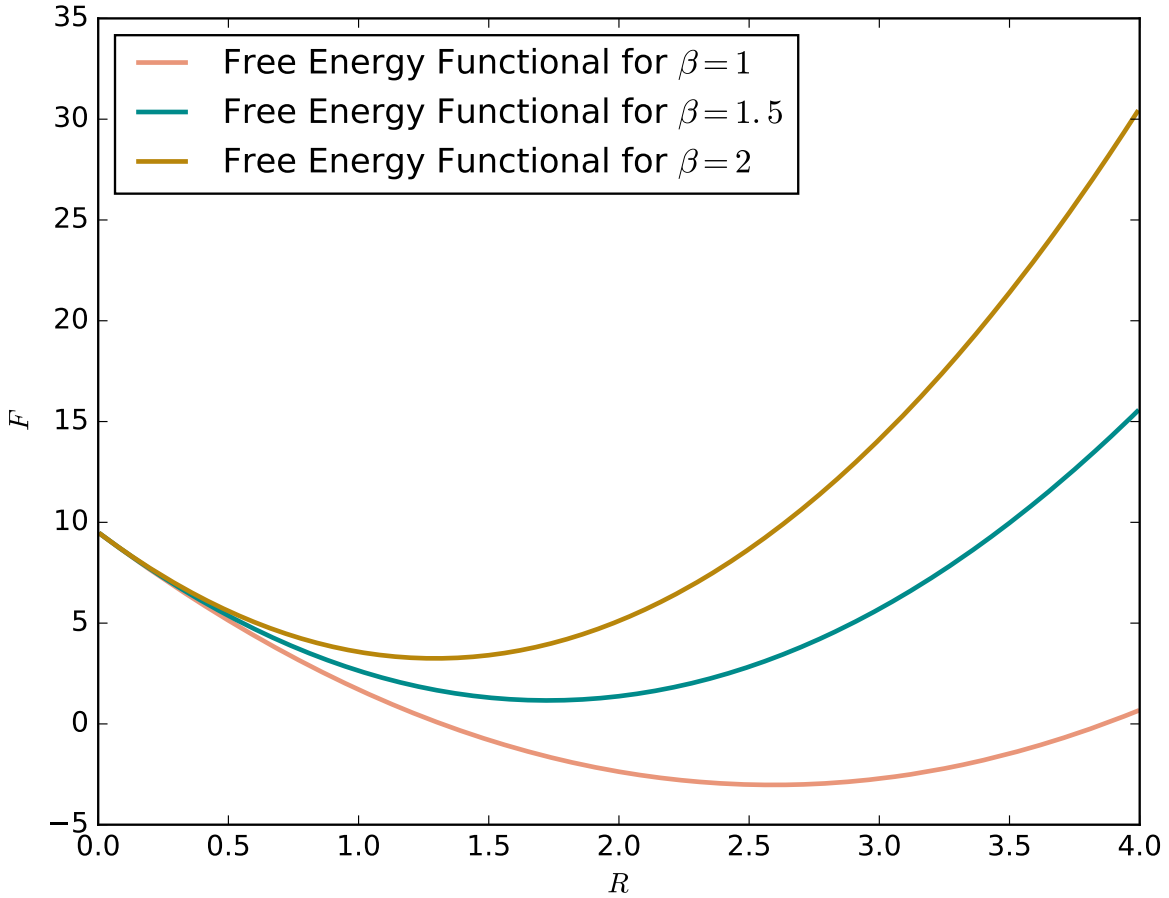

Figure 2.4: Free energy functional for a single skyrmion minimised with respect to the radius of a skyrmion with optimal radius found. All the calculations were performed for $\kappa = 1$. Lines of different colours correspond to calcualtions for corresponding values of β.

From Figure 2.4 we can notice that the optimal radius of a skyrmion does not vary much with β, however, the dependence exists. It is demonstrated in Figure 2.5a. We see then that the radius decreases with applied field increasing, i.e. the skyrmion becomes smaller at high

fields. Physically this means that if we consider the same number of spins for any system, for large external field more spins would rather align in the direction of the field (as in a typical ferromagnet), than follow the skyrmion distribution. And as we consider the skyrmion radius to be the distance from " down" spin to the nearest "up" spin, this distance would become smaller, as fewer spins would make it up.

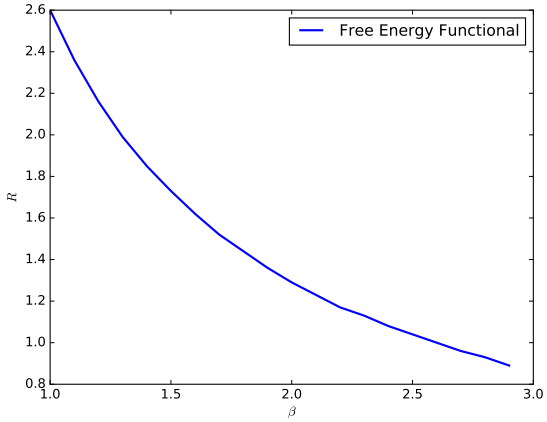

(a) Optimal radius of a skyrmion against β.

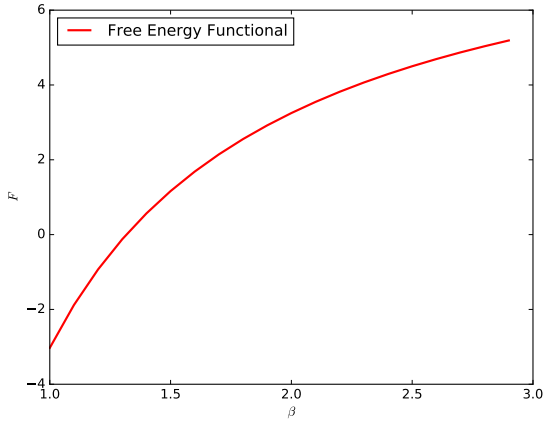

(b) Free energy functional of a signgle skyrmion against β.

Figure 2.5: Optimal radius of a skyrmion and free energy functional for a single skyrmion calculated for the optimal radius configuration against β.

The free energy functional, (2.19), was calculated for an optimal radius configuration using $\theta(r)$ found for this radius from the minimisation of the functional (2.19). The functional against the applied field for fixed $\kappa = 1$ is demonstrated in Figure 2.5b.

Let us also plot $\theta(r)$ as it was found from the minimisation of the free energy functional with the optimal radius. This is shown in Figure 2.6. The coordinate is scaled with the optimal radius for a studied configuration in order to provide better comparisonal view.

Results demonstrated in Figure 2.6 can be compared against those obtained experimentally by *Romming et al.* [48] We would see then that the correspondence between these results is quite good. Also, from Figure 2.6 one can conclude that the linear guess is rather good only for small values of an applied field and for the region around the centre of a skyrmion. In other cases the linear formulation of $\theta(r)$ should not be accepted.

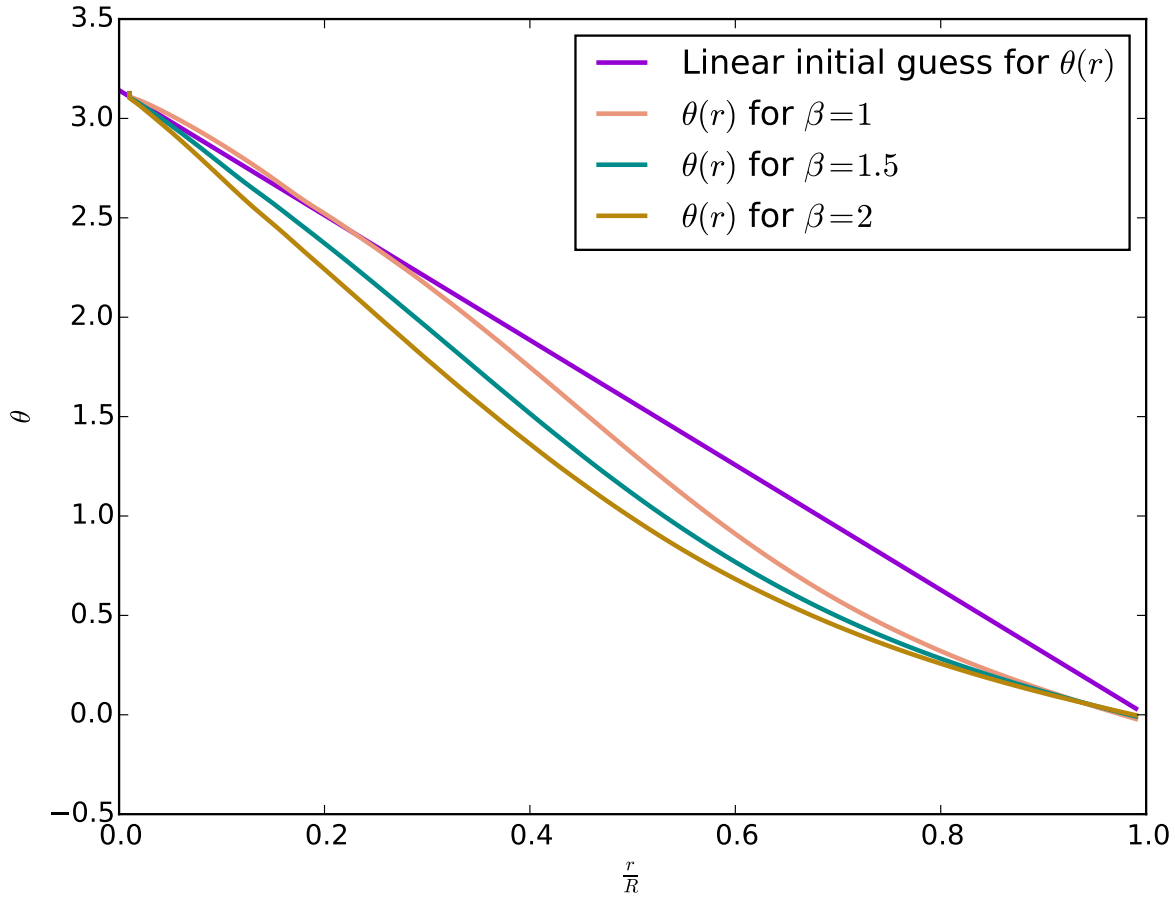

Figure 2.6: $\theta(r)$ found from the minimisation of the free energy functional with the optimal radius for different values of β. Lines of different colours correspond to calcualtions for various values of β. The purple line stands for the initial linear guess for θ. The terminal point varies for different configurations as it is nothing but the optimal radius itself.

2.3 Euler-Lagrange Equations for a Magnetic System in Fourier Space

2.3.1 Free Energy Functional in Cartesian Coordinates

So far we have dealt with a single magnetic skyrmion only. A single skyrmion is a great toy model, a wonderful self-consistent piece of quantum magnetism. Despite the fact that one can extract surprisingly a lot from single skyrmion studies and the fact that single (isolated) skyrmions still can act as stable and metastable solutions of the actual systems [41, 78], we would rather move to the survey of their collective behaviour: study 2D lattices formed by skyrmions.

At the first glance one could try to formulate a structure factor [83] for a single skyrmion and work with it on a lattice. Such an approach would not work for skyrmions, however, as

skyrmions are known to be dynamic. Moreover, skyrmion lattice as well as the skyrmion itself can get deformed. So let us start our study of skyrmion lattices with the formulation of the free energy functional in Cartesian coordinates. It is convenient to work in polar coordinates with a single skyrmion, that is a 2D circular object itself, i.e. obeys rotational symmetry,[6] however, this does not hold for lattices. A formulation in terms of Cartesian coordinates is preferable in the case of skyrmion lattices. It is also easier to construct square and triangular lattices in Cartesian coordinates due to their rectangular nature. As it was demonstrated in section 2.2, the free energy functional per unit volume (from here onwards – just the free energy functional) of a magnetic system in Cartesian coordinates goes as follows:

$$F\left[\vec{M}\right] = \int \left\{ \frac{J}{2} \sum_{\mu} \left(\partial_\mu \vec{M}\right) \cdot \left(\partial_\mu \vec{M}\right) + D\vec{M} \cdot \left(\nabla \times \vec{M}\right) - \vec{B} \cdot \vec{M} \right\} \frac{dxdy}{A}, \tag{2.23}$$

where J is the ferromagnetic exchange constant, D is the Dzyaloshinsky-Moriya coupling constant and $\vec{B}$ is the external field applied. Here $\vec{M} = \vec{M}(x, y)$ with components

$$\vec{M}(x, y) = (M_x(x, y), M_y(x, y), M_z(x, y)), \tag{2.24}$$

obeying $\left|\vec{M}\right|^2 = 1$ and $\vec{B} = (0, 0, B)$ with $B = const$, which corresponds to the uniform external field in z-direction.

Many equations that are to be derived in the following chapters cannot be solved analytically, hence have to be attempted numerically. The most convenient way to do numerical analysis is to convert the equations of interest to the dimensionless form, as in this case one does not have to worry about extremely small or extremely large quantities as well as the dimensions themselves. Hence let us convert the free energy functional, (2.23), into dimensionless form. Introduce

$$\kappa = \frac{D}{2J} \tag{2.25}$$

that would scale the anisotropic (Dzyaloshinsky-Moriya) constant, and

$$\beta = \frac{B}{2J} \tag{2.26}$$

to scale the applied field as we did for single skyrmion studies in the previous section, in order to obtain dimensionless formulation of the free energy functional:

$$F\left[\vec{M}(x, y)\right] = 2J \int \left\{ \frac{1}{4} \sum_{\mu} \left(\partial_\mu \vec{M}\right) \cdot \left(\partial_\mu \vec{M}\right) + \kappa \vec{M} \cdot \left(\nabla \times \vec{M}\right) - \vec{\beta} \cdot \vec{M} \right\} \frac{dxdy}{A}, \tag{2.27}$$

[6] In this case we need to deal with $\theta = \theta(r)$ only, hence simplify our life by dealing with a quasi 1D system.

or just

$$F\left[\vec{M}(x,y)\right] = 2J\int \mathcal{F}[\vec{M}(x,y)]\frac{dxdy}{A}, \tag{2.28}$$

where $\mathcal{F}$ is the free energy functional density. Notice that β and κ are not dimensionless themselves, moreover, κ has dimensions of $\vec{r}^{-1}$ and β has dimensions of $\vec{r}^{-2}$. However, functional

$$\tilde{F} = \int \mathcal{F}[\vec{M}(x,y)]\frac{dxdy}{A} \tag{2.29}$$

is dimensionless.

Let us now introduce dimensionless coordinates, $\vec{\tilde{r}} = \vec{r}_\kappa$, via

$$\vec{r}_\kappa = (\tilde{x},\tilde{y}) = \kappa\vec{r}, \tag{2.30}$$

with $\tilde{x} = \kappa x$ and $\tilde{y} = \kappa y$, as κ has dimensions of $\vec{r}^{\,-1}$. This is the usual convention for coordinates in skyrmion systems. [43]

In correspondence with (2.30) define

$$\tilde{A} = \kappa^2 A, \tag{2.31}$$

$$\tilde{\partial}_\mu = \frac{1}{\kappa}\partial_\mu, \tag{2.32}$$

so the functional, $\tilde{F}$, transforms to

$$\tilde{F} = \kappa^2\int\left\{\frac{1}{4}\sum_\mu\left(\tilde{\partial}_\mu\vec{M}_\kappa\right)\cdot\left(\tilde{\partial}_\mu\vec{M}_\kappa\right) + \vec{M}_\kappa\cdot\left(\tilde{\nabla}\times\vec{M}_\kappa\right) - \vec{\beta}_\kappa\cdot\vec{M}_\kappa\right\}\frac{d\tilde{x}d\tilde{y}}{\tilde{A}} = \kappa^2\tilde{F}_\kappa, \tag{2.33}$$

where we have also defined

$$\vec{\beta}_\kappa = \frac{\vec{\beta}}{\kappa^2} \tag{2.34}$$

to make $\vec{\beta}$ dimensionless as well.

Another important quantity now is $\vec{M}_\kappa$, that is defined as

$$\vec{M}_\kappa = \vec{M}_\kappa\left(\frac{\vec{r}_\kappa}{\kappa}\right). \tag{2.35}$$

In order to shorthand the notation in the future, we relabel

$$\vec{r}_\kappa \to \vec{r}, \tag{2.36}$$

$$\tilde{F}_\kappa \to \tilde{F}, \tag{2.37}$$

$$\vec{\beta}_\kappa \to \vec{\beta}, \tag{2.38}$$

$$\vec{M}_\kappa \to \vec{M}, \tag{2.39}$$

etc.

Despite the fact that the formulation of the free energy functional given in (2.27) is convenient for lattice studies, magnetisation formulated in Cartesian components, as stated in (2.24), does not automatically satisfy the crucial constraint of

$$|\vec{M}(x,y)|^2 = 1. \tag{2.40}$$

In order to take this constraint into account we introduce the Lagrange multiplier, $\lambda = \lambda(x,y)$, and hence add the constraint to the functional, as one usually does for constraint systems:

$$\tilde{\mathcal{F}} = \frac{1}{4}\sum_\mu \left(\partial_\mu \vec{M}\right)\cdot\left(\partial_\mu \vec{M}\right) + \vec{M}\cdot\left(\nabla\times\vec{M}\right) - \vec{\beta}\cdot\vec{M} + \lambda\left(|\vec{M}|^2 - 1\right), \tag{2.41}$$

or in component form:

$$\begin{aligned}\tilde{\mathcal{F}} &= \frac{1}{4}\left[(\partial_x M_x)^2 + (\partial_x M_y)^2 + (\partial_x M_z)^2 + (\partial_y M_x)^2 + (\partial_y M_y)^2 + (\partial_y M_z)^2\right] \\ &+ \left[M_x\partial_y M_z - M_y\partial_x M_z + M_z\left(\partial_x M_y - \partial_y M_x\right)\right] - \beta M_z \\ &+ \lambda\left(M_x^2 + M_y^2 + M_z^2 - 1\right),\end{aligned} \tag{2.42}$$

for better demonstration.

We want to figure out the optimal spin (magnetisation) configuration for given parameters, so we need to minimise functional (2.41), and thus derive Euler-Lagrange equations for M_x, M_y and M_z. Following the general form of

$$\frac{\partial\mathcal{F}}{\partial M_\mu} - \partial_\nu \frac{\partial\mathcal{F}}{\partial\left(\partial_\nu M_\mu\right)} = 0, \tag{2.43}$$

with summation convention applied for ν, that is $\nu = x, y$, Euler-Lagrange equations come as follows:

$$\left(\partial_x^2 + \partial_y^2\right) M_x - 4\partial_y M_z - 4\lambda M_x = 0, \tag{2.44}$$

$$\left(\partial_x^2 + \partial_y^2\right) M_y + 4\partial_x M_z - 4\lambda M_y = 0, \tag{2.45}$$

$$\left(\partial_x^2 + \partial_y^2\right) M_z - 4\left(\partial_x M_y - \partial_y M_x\right) - 4\lambda M_z = -2\beta. \tag{2.46}$$

2.3.2 Fourier Representation of the Magnetisation

As it was mentioned before, there are many methods to study skyrmion lattices. None of them is perfect, however. One of the most popular methods (developed by *Bogdanov et al* [42])

involves so-called *circular cell approximation*, i.e. it assumes a unit cell to be a circle with the corresponding radius. This method does its job, however results obtained are not nessesarily in a good agreement with experimental evidences (see later). Another method, introduced by *Han et al*, [43] that takes into account similarity between the skyrmion lattice and Abrikosov vortex lattice does not take the constraint of $\left|\vec{M}\right|^2 = 1$ for all $\vec{r}$ into account, hence the results obtained cannot be precise either. Therefore we are not going to follow any of the existing methods; instead develop a very new one: being inspired by Brandt's approach for Abrikosov vortices in type-II superconductors (see section 3.5) we Fourier transform the magnetisation components (and the Lagrange multiplier as well) and do all the important calculations in Fourier space. As our skyrmion lattice is a periodic structure (hence the magnetisation is a periodic quantity) and in general is expected to be similar to the Abrikosov vortex lattice, Fourier approach is completely legitimate. Following Brandt's motivation, [71] we expect our approach to be fast and universal, i.e. converging fast enough for any combination of parameters.

Prior to doing the transformation itself, let us introduce the space and the lattice. We define lattice vectors to be $\vec{a}_1$ and $\vec{a}_2$ with

$$\vec{a}_1 = a\hat{e}_x \tag{2.47}$$

and

$$\vec{a}_2 = \frac{a}{2}\hat{e}_x + \frac{\sqrt{3}}{2}a\hat{e}_y. \tag{2.48}$$

An example of a triangular lattice is given in Figure 2.7.

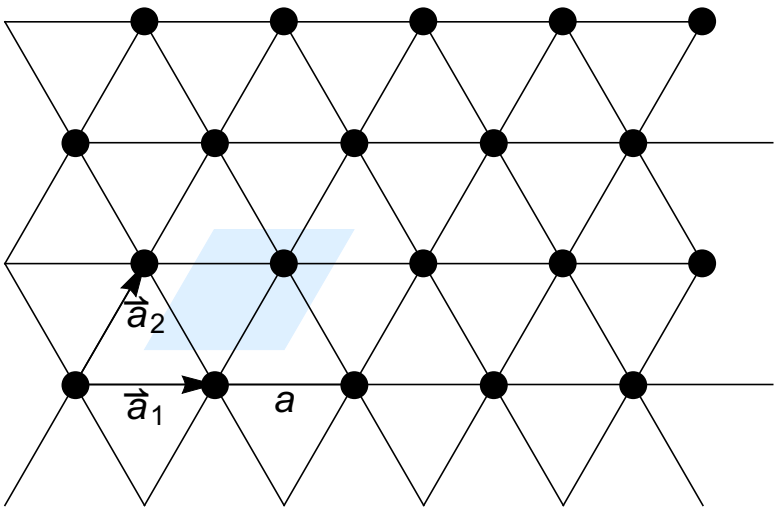

Figure 2.7: Sample triangular lattice with primitive lattice vetors $\vec{a}_1$ and $\vec{a}_2$ and lattice spacing a. A unit cell is depicted by a shaded paralellogram and contains exactly one vertex (skyrmion, in our case).

Any point within the unit cell now can be described by

$$\vec{r} = x_i \vec{a}_1 + y_j \vec{a}_2, \tag{2.49}$$

where $x_i \in [0, 1]$ and $y_j \in [0, 1]$ within a unit cell. See Figure 2.8 for the demonstration of such a unit cell.

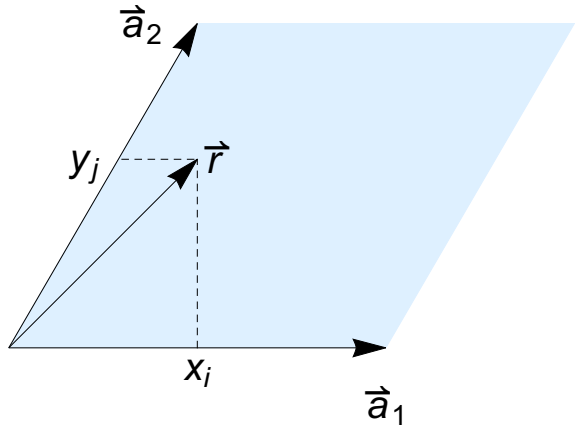

Figure 2.8: A unit cell of a triangular lattice with primitive vectors, $\vec{a}_1$ and $\vec{a}_2$. Position vector, $\vec{r}$, is defined via $\vec{a}_1$ and $\vec{a}_2$ as in equiation (2.49) and $x_i \in [0, 1]$ and $y_j \in [0, 1]$.

Positions of skyrmions (or any vertices, in general) on a triangular lattice can be denoted by

$$\vec{R}_{vw} = (vx_1 + wx_2, wy_2), \tag{2.50}$$

with

$$x_1 = a, \tag{2.51}$$

$$x_2 = \frac{a}{2}, \tag{2.52}$$

$$y_2 = \frac{\sqrt{3}}{2} a, \tag{2.53}$$

where and a is the lattice spacing and v and w are integers. For example, when $v = w = 0$, a skyrmion is located at $\vec{R}_{00} = 0$, etc.

With such a unit cell imposed, any real space function can be periodised as

$$f\left(\vec{r} + \vec{R}_{vw}\right) = f\left(\vec{r}\right). \tag{2.54}$$

On the other hand, one can always Fourier transform any periodic function via

$$f\left(\vec{r}\right) = \sum_{\vec{k}} f_{\vec{k}} e^{-i\vec{k}\vec{r}}, \tag{2.55}$$

where

$$\vec{r} = (x, y)\,, \tag{2.56}$$

and

$$\vec{k} = \left\{\vec{k}_{mn}\right\}, \tag{2.57}$$

with

$$\vec{k}_{mn} = \frac{2\pi}{x_1 y_2}\begin{pmatrix} m y_2 \\ n x_1 - m x_2 \end{pmatrix} = \begin{pmatrix} k_x \\ k_y \end{pmatrix}, \tag{2.58}$$

where m and n are dummy indices. In Fourier space they go from $-\frac{N_x}{2}$ to $\frac{N_x}{2}$ for m and $-\frac{N_y}{2}$ to $\frac{N_y}{2}$ for n, where N_x is the number of points in x-direction used in numerical simulations and N_y is the number of points in y-direction.

Now that as we have fulfilled all the necessary conditions, we can do the (discrete) Fourier transform[7] of the magnetisation components and the Lagrange multiplier.

Discrete Fourier transform of M_x is given as

$$M_x(x, y) = \sum_{m,n} X_{mn}(k_x, k_y) e^{-i\vec{k}_{mn}\vec{r}}, \tag{2.59}$$

where $X_{mn}(k_x, k_y)$ is the Fourier coefficient for M_x and m and n are integer indices as introduced before.

In order to shorthand the notation, we write

$$M_x = \sum_{\vec{k}} X_{\vec{k}} e^{-i\vec{k}\vec{r}}, \tag{2.60}$$

and by analogy:

$$M_y = \sum_{\vec{k}} Y_{\vec{k}} e^{-i\vec{k}\vec{r}}, \tag{2.61}$$

$$M_z = \sum_{\vec{k}} Z_{\vec{k}} e^{-i\vec{k}\vec{r}}, \tag{2.62}$$

for the rest components of the magnetisation and the Lagrange multiplier:

$$\lambda = \sum_{\vec{k}} \lambda_{\vec{k}} e^{-i\vec{k}\vec{r}}. \tag{2.63}$$

Notice that although in this notation we have only one summation index, $\vec{k}$, the actual summation goes over m and n indices, also

$$X_{\vec{k}} = X_{mn}(k_x, k_y) \tag{2.64}$$

[7] Not to be confused with Fourier series.

as well as all the other Fourier coefficients.

Now we can substitute these Fourier expressions into Euler-Lagrange equations (2.44) – (2.46) derived in the previous section.[8] In order to do it we would require formulation of derivatives in Fourier form:

$$\partial_\nu M_\mu = -\sum_{\vec{k}} i k_\nu \hat{M}_\mu(\vec{k}) e^{-i\vec{k}\vec{r}}, \tag{2.65}$$

where $\nu = x, y$, $\mu = x, y, z$ and $\hat{M}_\mu(\vec{k})$ is the Fourier coefficient of a magnetisation component, M_μ, i.e. either of $X_{\vec{k}}$, $Y_{\vec{k}}$ and $Z_{\vec{k}}$. Similarly,

$$\partial_\nu^2 M_\mu = -\sum_{\vec{k}} k_\nu^2 \hat{M}_\mu(\vec{k}) e^{-i\vec{k}\vec{r}}, \tag{2.66}$$

and we also write

$$k_x^2 + k_y^2 = k^2. \tag{2.67}$$

So we can now use auxiliary relations (2.65) – (2.67) along with Fourier formulations (2.60) – (2.63) to obtain Euler-Lagrange equations in Fourier form from (2.44) – (2.46). Note the terms with the Lagrange multiplier. The equations then are:

$$\sum_{\vec{k}} \left[-k^2 X_{\vec{k}} e^{-i\vec{k}\vec{r}} + 4ik_y Z_{\vec{k}} e^{-i\vec{k}\vec{r}} - 4X_{\vec{k}} \sum_{\vec{k}'} \lambda_{\vec{k}'} e^{-i(\vec{k}+\vec{k}')\vec{r}} \right] = 0, \tag{2.68}$$

$$\sum_{\vec{k}} \left[-k^2 Y_{\vec{k}} e^{-i\vec{k}\vec{r}} - 4ik_x Z_{\vec{k}} e^{-i\vec{k}\vec{r}} - 4Y_{\vec{k}} \sum_{\vec{k}'} \lambda_{\vec{k}'} e^{-i(\vec{k}+\vec{k}')\vec{r}} \right] = 0, \tag{2.69}$$

$$\sum_{\vec{k}} \left[-k^2 Z_{\vec{k}} e^{-i\vec{k}\vec{r}} + 4i \left(k_x Y_{\vec{k}} - k_y X_{\vec{k}} \right) e^{-i\vec{k}\vec{r}} - 4Z_{\vec{k}} \sum_{\vec{k}'} \lambda_{\vec{k}'} e^{-i(\vec{k}+\vec{k}')\vec{r}} \right] = -2\beta. \tag{2.70}$$

Multiply equations (2.68) – (2.70) by $\frac{e^{i\vec{k}''\vec{r}}}{A}$ and integrate over $dxdy$:[9]

$$\sum_{\vec{k}} \int \left[-k^2 X_{\vec{k}} e^{-i\vec{k}\vec{r}} + 4ik_y Z_{\vec{k}} e^{-i\vec{k}\vec{r}} - 4X_{\vec{k}} \sum_{\vec{k}'} \lambda_{\vec{k}'} e^{-i(\vec{k}+\vec{k}')\vec{r}} \right] e^{i\vec{k}''\vec{r}} \frac{dxdy}{A} = 0, \tag{2.71}$$

[8] Another option is to Fourier transform the equations directly.

[9] We need this integration step as we are working with Euler-Lagrange equations, though if we had worked with the direct variation of the functional, the integration would have been more straightforward as well as if we had Fourier transformed the equations at once.

$$\sum_{\vec{k}} \int \left[-k^2 Y_{\vec{k}} e^{-i\vec{k}\vec{r}} - 4ik_x Z_{\vec{k}} e^{-i\vec{k}\vec{r}} - 4Y_{\vec{k}} \sum_{\vec{k}'} \lambda_{\vec{k}'} e^{-i(\vec{k}+\vec{k}')\vec{r}} \right] e^{i\vec{k}''\vec{r}} \frac{dxdy}{A} = 0, \tag{2.72}$$

$$\begin{aligned} \sum_{\vec{k}} \int \left[-k^2 Z_{\vec{k}} e^{-i\vec{k}\vec{r}} + 4i \left(k_x Y_{\vec{k}} - k_y X_{\vec{k}} \right) e^{-i\vec{k}\vec{r}} \right. & - \left. 4Z_{\vec{k}} \sum_{\vec{k}'} \lambda_{\vec{k}'} e^{-i(\vec{k}+\vec{k}')\vec{r}} \right] e^{i\vec{k}''\vec{r}} \frac{dxdy}{A} \\ & = -2\beta \int e^{i\vec{k}''\vec{r}} \frac{dxdy}{A}. \end{aligned} \tag{2.73}$$

Now one wants to simplify equations obtained. We will present the derivation step by step, considering several important cases (terms) and do the rest by analogy. Start with a sample term that results from the Dzyaloshinsky-Moriya term:

$$\sum_{\vec{k}} \int 4ik_y Z_{\vec{k}} e^{-i\vec{k}\vec{r}} e^{i\vec{k}''\vec{r}} \frac{dxdy}{A} = \sum_{\vec{k}} \int 4ik_y Z_{\vec{k}} e^{-i(\vec{k}-\vec{k}'')\vec{r}} \frac{dxdy}{A}, \tag{2.74}$$

but the integral of an exponent like the one in the above equation is just a δ-function:

$$\int e^{-i(\vec{k}-\vec{k}'')\vec{r}} \frac{dxdy}{A} = \delta_{\vec{k}\vec{k}''}, \tag{2.75}$$

hence the whole term reduces to

$$\sum_{\vec{k}} \int 4ik_y Z_{\vec{k}} e^{-i(\vec{k}-\vec{k}'')\vec{r}} \frac{dxdy}{A} = 4i \sum_{\vec{k}} k_y Z_{\vec{k}} \delta_{\vec{k}\vec{k}''} \tag{2.76}$$

also re-label $\vec{k} \to \vec{k}'$ and $\vec{k}'' \to \vec{k}$ to get

$$4i \sum_{\vec{k}} k_y Z_{\vec{k}} \delta_{\vec{k}\vec{k}''} \to 4i \sum_{\vec{k}'} k'_y Z_{\vec{k}'} \delta_{\vec{k}\vec{k}'}. \tag{2.77}$$

One can generalise this (call it) d-term as

$$T^d_{\mu k} = 4i\sigma \sum_{\vec{k}'} k'_\mu \hat{M}_\mu(\vec{k}') \delta_{\vec{k}\vec{k}'}, \tag{2.78}$$

where $\sigma = \pm 1$.

Another important term is the one containing the Lagrange multiplier, λ, call it λ-term:

$$-4 \int \sum_{\vec{k}} X_{\vec{k}} \sum_{\vec{k}'} \lambda_{\vec{k}'} e^{-i(\vec{k}+\vec{k}'-\vec{k}'')\vec{r}} \frac{dxdy}{A} = -4 \sum_{\vec{k}} X_{\vec{k}} \sum_{\vec{k}'} \lambda_{\vec{k}'} \delta_{\vec{k}+\vec{k}',\vec{k}''}, \tag{2.79}$$

which yields $\vec{k}+\vec{k}' \to \vec{k}''$, or $\vec{k}' \to k''-\vec{k}$, hence

$$-4\sum_{\vec{k}} X_{\vec{k}} \sum_{\vec{k}'} \lambda_{\vec{k}'} \delta_{\vec{k}+\vec{k}',\vec{k}''} = -4\sum_{\vec{k}} X_{\vec{k}} \lambda_{\vec{k}''-\vec{k}}, \tag{2.80}$$

re-labelling $\vec{k} \to \vec{k}'$ and $\vec{k}'' \to \vec{k}$ in order to remain consistent with the previous example, get

$$-4\sum_{\vec{k}} \sum_{\vec{k}''} X_{\vec{k}} \lambda_{\vec{k}''-\vec{k}} \to -4\sum_{\vec{k}'} X_{\vec{k}'} \lambda_{\vec{k}-\vec{k}'}, \tag{2.81}$$

and this λ-term can be generalised to

$$T^{\lambda}_{\mu k} = -4\sum_{\vec{k}'} \hat{M}_{\mu}(\vec{k}') \lambda_{\vec{k}-\vec{k}'}. \tag{2.82}$$

Dealing with exchange terms is easy compared to d-terms or λ-terms: no underwater rocks, integrate the exponents to obtain δ-functions and re-label $\vec{k} \to \vec{k}'$ for consistence sake.

Finally, the constant term is simplified to:

$$-2\beta \int e^{i\vec{k}''\vec{r}} \frac{dxdy}{A} = -2\beta\delta_{\vec{k},0}, \tag{2.83}$$

where we have re-labelled $\vec{k}'' \to \vec{k}$.

Investigating all the d-terms by following example (2.78), all the λ-terms via (2.82) and employing (2.83) for the constant term, for a given k one obtains:

$$\sum_{\vec{k}'} \left[\left\{ -k'^2 X_{\vec{k}'} + 4ik'_y Z_{\vec{k}'} \right\} \delta_{\vec{k}\vec{k}'} - 4X_{\vec{k}'} \lambda_{\vec{k}-\vec{k}'} \right] = 0, \tag{2.84}$$

$$\sum_{\vec{k}'} \left[\left\{ -k'^2 Y_{\vec{k}'} - 4ik'_x Z_{\vec{k}'} \right\} \delta_{\vec{k}\vec{k}'} - 4Y_{\vec{k}'} \lambda_{\vec{k}-\vec{k}'} \right] = 0, \tag{2.85}$$

$$\sum_{\vec{k}'} \left[\left\{ -k'^2 Z_{\vec{k}'} + 4i \left(k'_x Y_{\vec{k}'} - k'_y X_{\vec{k}'} \right) \right\} \delta_{\vec{k}\vec{k}'} - 4Z_{\vec{k}'} \lambda_{\vec{k}-\vec{k}'} \right] = -2\beta\delta_{\vec{k},0}. \tag{2.86}$$

Equations (2.84) – (2.86) can be rewritten in the matrix form to shorthand notation and make the numerical procedures that are to follow easier and clearer:

$$\sum_{\vec{k}'} \hat{D}_{\vec{k}\vec{k}'} \vec{V}_{\vec{k}'} = \vec{I}_{\vec{k}}, \tag{2.87}$$

where the term on the RHS is just

$$\vec{I}_{\vec{k}} = \begin{pmatrix} 0 \\ 0 \\ -2\beta\delta_{\vec{k},0} \end{pmatrix}, \tag{2.88}$$

$\vec{V}_{\vec{k}}$ is the vector containing Fourier coefficients of the magnetisation components for a given k,

$$\vec{V}_{\vec{k}} = \begin{pmatrix} X_{\vec{k}} \\ Y_{\vec{k}} \\ Z_{\vec{k}} \end{pmatrix}, \tag{2.89}$$

and the matrix $\hat{D}_{\vec{k}\vec{k}'}$ is

$$\hat{D}_{\vec{k}\vec{k}'} = \begin{pmatrix} k'^2\delta_{\vec{k}\vec{k}'} - 4\lambda_{\vec{k}-\vec{k}'} & 0 & 4ik'_y\delta_{\vec{k}\vec{k}'} \\ 0 & k'^2\delta_{\vec{k}\vec{k}'} - 4\lambda_{\vec{k}-\vec{k}'} & -4ik'_x\delta_{\vec{k}\vec{k}'} \\ -4ik'_y\delta_{\vec{k}\vec{k}'} & 4ik'_x\delta_{\vec{k}\vec{k}'} & k'^2\delta_{\vec{k}\vec{k}'} - 4\lambda_{\vec{k}-\vec{k}'} \end{pmatrix}. \tag{2.90}$$

For convenience $\hat{D}_{\vec{k}'}$ matrix can be split onto two terms,

$$\hat{D}_{\vec{k}\vec{k}'} = \hat{K}_{\vec{k}'}\delta_{\vec{k}\vec{k}'} - \hat{L}_{\vec{k}\vec{k}'}, \tag{2.91}$$

where

$$\hat{K}_{\vec{k}'} = \begin{pmatrix} k'^2 & 0 & 4ik'_y \\ 0 & k'^2 & -4ik'_x \\ -4ik'_y & 4ik'_x & k'^2 \end{pmatrix} \tag{2.92}$$

and the second term is related to the Lagrange multiplier,

$$\hat{L}_{\vec{k}\vec{k}'} = 4\lambda_{\vec{k}-\vec{k}'}\hat{I}, \tag{2.93}$$

with $\hat{I}$ being an identity 3×3 matrix.

This step, however, is not necessary, though it simplifies future numerical calculation, as the $\hat{K}_{\vec{k}'}$ matrix contains lattice parameters only and is not modified by Euler-Lagrange equations, hence has to be calculated once per lattice.

Solving equation (2.87) for $\vec{V}_{\vec{k}}$ via

$$\vec{V}_{\vec{k}} = \sum_{\vec{k}'} \hat{D}^{-1}_{\vec{k}\vec{k}'}\vec{I}_{\vec{k}'}, \tag{2.94}$$

one can obtain expressions for Fourier coefficients and hence use the Fourier transform expressions, equations (2.60) – (2.62), to obtain M_x, M_y and M_z.

As one may have noticed, we find $X_{\vec{k}}$, $Y_{\vec{k}}$ and $Z_{\vec{k}}$ and thus M_x, M_y and M_z analytically (matrix inversion and Fourier transform). However, we need to employ a numerical procedure (see Appendix C.1) in order to find the Lagrange multiplier, λ.

2.3.3 Skyrmion Lattice Solution

A typical lattice solution obtained by the procedure described in the previous section may be found in Figure 2.9.

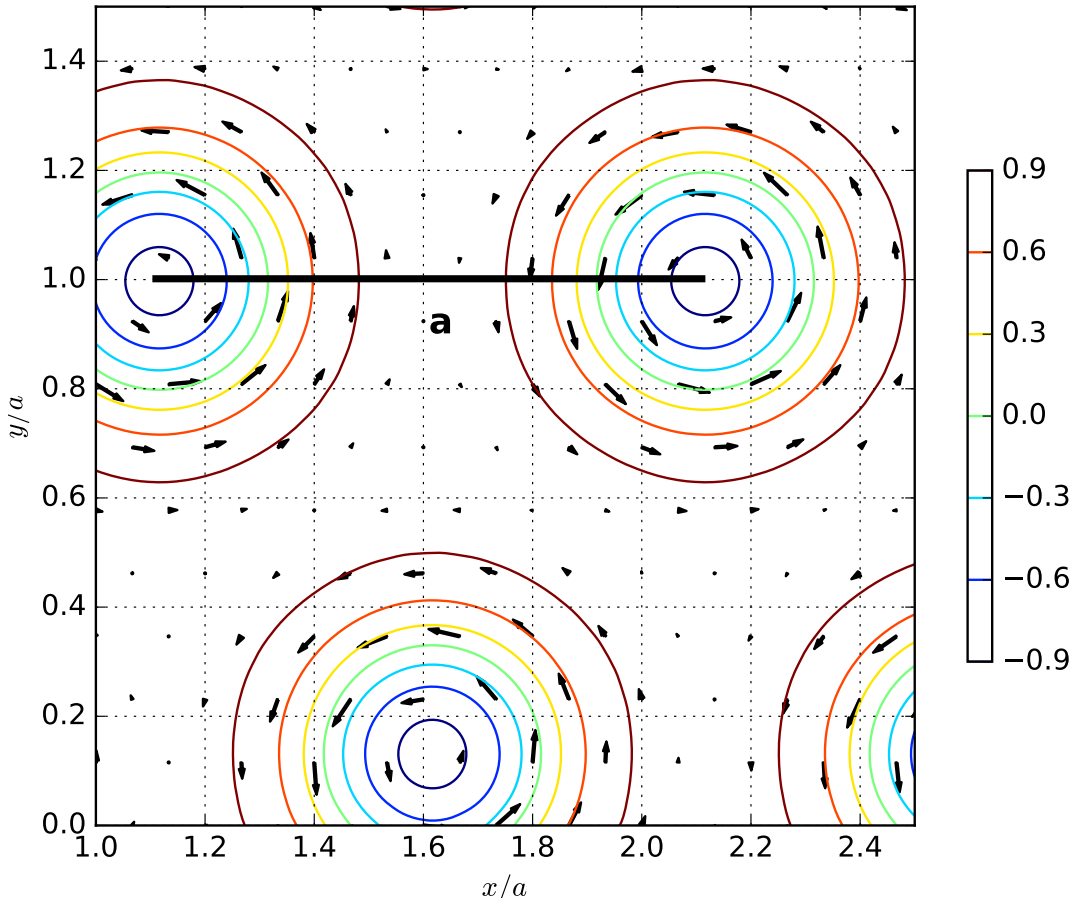

Figure 2.9: Lattice solution for a skyrmion system for the external field of $\beta = 1.4$ and the lattice spacing of $a = 4$. In this figure as well as in all the other figures of this kind to follow one finds the magnetisation of the skyrmion system. M_x and M_y are denoted by arrows curling in the anti-clockwise direction (skyrmion way) and the colour contours stand for M_z that has the value of -1 in the centre of a skyrmion and 1 in the region between skyrmions. The coordinates are normalised with respect to the lattice spacing, a. Note that it is not a unit cell, though a piece of the lattice, represented in this figure.

As we can see from Figure 2.9, the lattice is triangular just as we imposed it to be. Lattice spacing, a, is the distance between the centres of two neighbouring origins of unit cells. Also we see that M_z has its lowest values in the centre of a skyrmion and the highest between

skyrmions. Conventionally, the highest value of z-component of the magnetisation, $M_z = 1$, corresponds to the "up" configuration of spins and the lowest value of z-component of the magnetisation, $M_z = -1$, corresponds to the "down" configuration of spins. Following such a convention, one can see how spins change their position from "down" in the centre of a skyrmion to "up" on the edge just as we have seen it for a single skyrmion in the previous section.

Spin pattern, though, is better seen from Figure 2.10 that demonstrate spin orientation whithin a unit cell of a skyrmion lattice and on a triangular lattice respectively.

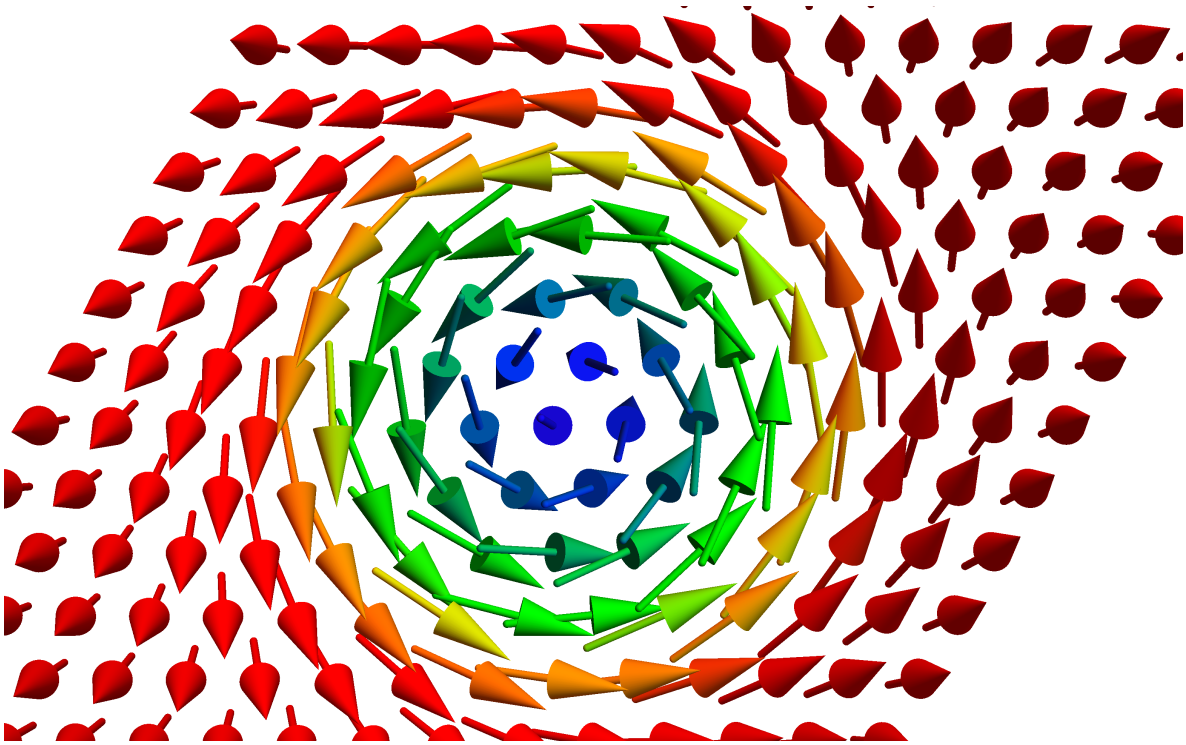

Figure 2.10: Spin orientation within the unit cell of a triangular skyrmion lattice for $\beta = 1.4$ and $a = 4$. Spin changes from "down" position in the centre of a skyrmion to "up" position far away from the centre of a skyrmion.

Keeping in mind that the field applied is positive, we see that spins align along the direction of the field between skyrmions and in the opposite direction in the centres of skyrmions. So one can call the region between skyrmions to be ferromagnetic.

We will stick to the representation style used in Figure 2.9 while speaking about lattice structure and shape of skyrmions, whereas the style used in Figure 2.10 is more convenient when discussing spin patterns and internal structure of skyrmions.

Although it was the magnetisation we have been mainly interested in, we had to employ a numerical procedure in order to find the Lagrange multiplier, λ. If we have a look at λ in the unit cell of our system, we realise that the shape of λ repeats the shape of a skyrmion exactly,

though with the largest value situated in the centre – see Figure 2.11a – and the lowest values distributed in the middle region of a "skyrmion". In other words, λ takes the largest values when the spins are aligned parallel or anti-parallel to the external field and the lowest values when the spins are perpendicular to it (parallel to the xy-plane). It is not surprising, should one remember the actual constraint of $\left|\vec{M}\right|^2 = 1$.

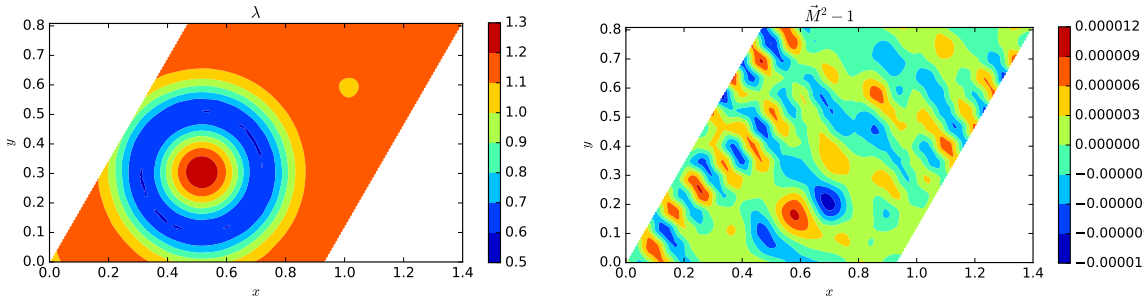

(a) Lagrange multiplier calculated for $\beta = 1.4$, $a = 4$ on a unit cell.

(b) $|\vec{M}|^2$ calculated for $\beta = 1.4$, $a = 4$ on a unit cell.

Figure 2.11: Lagrange multiplier and $|\vec{M}|^2 - 1$ on a unit cell of a skyrmion system. Lagrange Multiplier repeats the shape of a skyrmion exactly and the condition of $|\vec{M}|^2 = 1$ is preserved at any point in the unit cell up to numeric uncertainty.

The only reason to introduce the Lagrange multiplier was to fulfil the condition of $|\vec{M}|^2 = 1$ in every single point of the lattice, as described in section 2.3.1. Figure 2.11b shows us that $|\vec{M}|^2 = 1$ holds everywhere up to the numerical accuracy, which means that our implementation of the constraint and the calculations that followed up are correct. Figure 2.11a and Figure 2.11b are presented in order demonstrate the legitimacy of the method developed in this work. We will not refer to studies of quantities displayed in Figure 2.11a and Figure 2.11b in the future.

Solutions to Euler-Lagrange equations are functions for which a functional is stationary, however, there is no guarantee that such a stationary solution minimises the functional or, in case it does, the minima found is the global minima, not the local one. So solutions found by the method introduced in section 2.3.2 can be metastable as well as stable or not stable at all. Since we work with a thermodynamic system that obeys several first order phase transitions, we expect a huge cluster of metastable solutions, but it is the stable solutions we are looking for in the first place. Hence we need to invent an additional procedure to distinguish stable solutions from those metastable or not stable at all. As in general we are free to vary the lattice spacing (though, the outcome of such a variation may not correspond to the minimal configuration), we can find a lattice spacing that guarantees the most stable solution for a given β and fix it. And this is to be demonstrated in the next section.

2.4 Finding the Optimal Skyrmion Lattice

2.4.1 Additional Condition

In section 2.3.1 we have minimised the free energy functional by deriving Euler-Lagrange equations that can be solved for a stationary solution. However, there is no guaranty for such a solution to be the global minima: it might correspond to a local minima or no minima at all. So we need to think of some additional condition that would help us to make sure the solution we have found is the actual minima of the free energy functional. The only control parameter we have used so far was $\vec{\beta}$ that is related to the external field.

Let us now work with the lattice spacing, a, as with a parameter and develop a procedure to find an optimal one. Parametrise the coordinates via γ that is a dimensionless number:

$$\vec{r} = \gamma \vec{r}', \tag{2.95}$$

with $x = \gamma x'$ and $y = \gamma y'$, which leads to

$$\partial'_\mu = \frac{1}{\gamma}\partial_\mu, \tag{2.96}$$

$$d^2r' = \frac{1}{\gamma^2}d^2r, \tag{2.97}$$

$$A' = \frac{1}{\gamma^2}A, \tag{2.98}$$

hence the functional (2.27) turns into

$$\tilde{F}\left[\vec{M}_\gamma\right] = \int \left\{ \frac{1}{4}\frac{1}{\gamma^2}\sum_\mu \left(\partial'_\mu \vec{M}_\gamma\right)\cdot\left(\partial'_\mu \vec{M}_\gamma\right) + \frac{1}{\gamma}\vec{M}_\gamma \cdot \left(\nabla' \times \vec{M}_\gamma\right) - \vec{\beta}\cdot\vec{M}_\gamma \right\} \frac{dx'dy'}{A'}, \tag{2.99}$$

with $\vec{M}_\gamma = \vec{M}(\gamma\vec{r}')$.

In the end, though, the functional must be independent of the scaling, γ, hence we impose

$$\frac{\partial \tilde{F}}{\partial \gamma} = 0, \tag{2.100}$$

that leads to

$$\int \left\{ -\frac{1}{2}\frac{1}{\gamma^3}\sum_\mu \left(\partial'_\mu \vec{M}_\gamma\right)\cdot\left(\partial'_\mu \vec{M}_\gamma\right) - \frac{1}{\gamma^2}\vec{M}_\gamma \cdot \left(\nabla' \times \vec{M}_\gamma\right) + \frac{\delta \tilde{F}}{\delta \vec{M}}\frac{\partial \vec{M}}{\partial \gamma} \right\} \frac{dx'dy'}{A'} = 0, \tag{2.101}$$

or, in shorthand,

$$\tilde{F}_{ex} = \frac{1}{4}\int \sum_\mu \left(\partial'_\mu \vec{M}_\gamma\right)\cdot\left(\partial'_\mu \vec{M}_\gamma\right)\frac{dx'dy'}{A'} \tag{2.102}$$

for the ferromagnetic exchange term and

$$\tilde{F}_{DM} = \int \vec{M}_\gamma \cdot \left(\nabla' \times \vec{M}_\gamma\right) \frac{dx'dy'}{A'} \tag{2.103}$$

for the Dzyaloshinsky-Moriya term, we get

$$-2\frac{1}{\gamma^3}\tilde{F}_{ex} - \frac{1}{\gamma^2}\tilde{F}_{DM} + \int \frac{\delta\tilde{F}}{\delta\vec{M}} \frac{\partial\vec{M}}{\partial\gamma} \frac{dx'dy'}{A'} = 0. \tag{2.104}$$

But as $\vec{M}$ is a stationary solution of Euler-Lagrange equations, it corresponds to

$$\frac{\delta\tilde{F}}{\delta\vec{M}} = 0. \tag{2.105}$$

On the other hand, we recall that $\vec{M}_\gamma = \vec{M}(\gamma\vec{r}')$. We would like to have $\vec{M}$ unchanged, though, as it is $\vec{M}(\vec{r})$ that is a stationary solution of Euler-Lagrange equations derived, not $\vec{M}(\gamma\vec{r}')$ or any other scaled $\vec{M}$. Hence we impose $\gamma = 1$. This is allowed, as the functional shall be independent of γ anyway. So our condition would actually look like

$$\frac{\partial\tilde{F}}{\partial\gamma}\Big|_{\gamma=1} = 0, \tag{2.106}$$

and thus (2.104) transforms to

$$\int \left\{ -\frac{1}{2}\sum_\mu \left(\partial'_\mu \vec{M}_\gamma\right) \cdot \left(\partial'_\mu \vec{M}_\gamma\right) - \vec{M}_\gamma \cdot \left(\nabla' \times \vec{M}_\gamma\right) \right\} \frac{dx'dy'}{A'} = 0, \tag{2.107}$$

or just

$$-2\tilde{F}_{ex} - \tilde{F}_{DM} = 0, \tag{2.108}$$

that can be rewritten as

$$\frac{\tilde{F}_{DM}}{\tilde{F}_{ex}} = -2, \tag{2.109}$$

which is actually nothing more, but the virial theorem[10] formulated for our problem (call $V = \frac{\tilde{F}_{DM}}{\tilde{F}_{ex}}$ to be a "virial ratio" from here on). We will also stick to the condition (2.109) in our calculations in order to make sure the minimum we find is the global minimum (see later).

As we have used the fact that the free energy functional is stationary with respect to $\vec{M}$ and λ, we conclude that (2.109) holds for a stationary solution, or, on the other hand, if (2.109) holds for a given set of parameters, then the solution obtained is stationary. Employing this additional condition also gives us better numerical accuracy in the position of the minima (see

[10] In general, virial theorem relates the average of the total kinetic energy with the the average of the total potential energy. [85]

later).

2.4.2 Fixing Optimal Spacing

In the previous section we have derived a relation, (2.109), that is supposed to help us achieve a global minima of the system. The question is now how to satisfy this relation? And the answer is: by varying the lattice spacing, a, for a given β. An example of the free energy functional for $\beta = 1.1$ against different values of the spacing is demonstrated in Figure 2.12a.

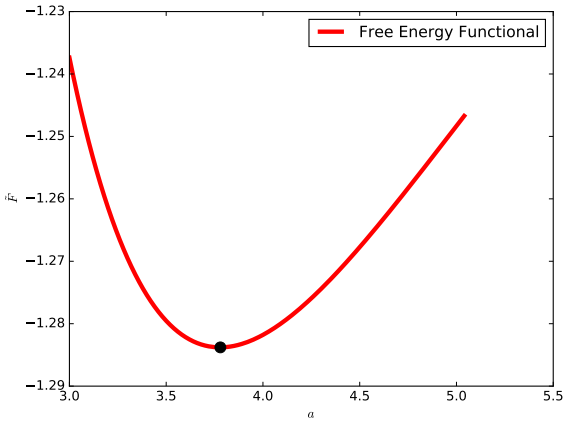

(a) Free energy functional of a skyrmion system for $\beta = 1.1$ against the lattice spacing. The black dot indicates the minima of the functional.

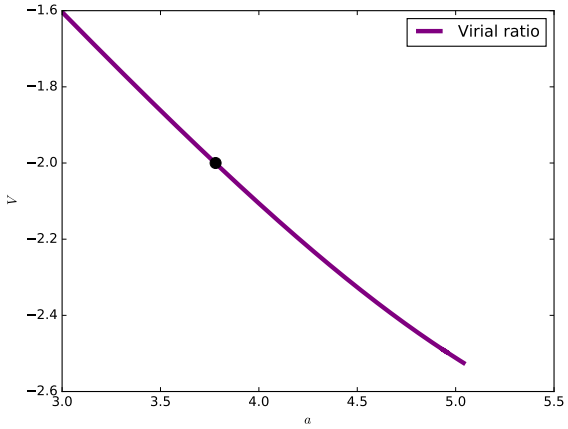

(b) Virial ratio, $\frac{\tilde{F}_{DM}}{\tilde{F}_{ex}}$, for $\beta = 1.1$. The black dot indicates $V = \frac{\tilde{F}_{DM}}{\tilde{F}_{ex}} = -2$ point.

Figure 2.12: Free energy functional and virial ratio against lattice spacing for $\beta = 1.1$.

We see that it is hard to determine the minima from Figure 2.12a solely, as the free energy functional is very shallow around it. One can still determine the minima, though with quite poor precision. This is indicated by a black dot. On the other hand, from Figure 2.12b it is easy to find the spacing that satisfies the virial condition, (2.109), – this point is indicated in Figure 2.12b by a black dot. Comparing position of black dots in Figure 2.12a and Figure 2.12b, realise that they their abscissa coordinates coincide, i.e. the minima of the free energy functional corresponds to $\frac{\tilde{F}_{DM}}{\tilde{F}_{ex}} = -2$, as expected. Though, it is far easier to determine a point precisely from Figure 2.12b than from Figure 2.12a. Moreover, it would also require to consider way fewer points in a due to high precision of the method, hence the efficiency of the method would increase. So we will use condition (2.109) in order to find the optimal spacing, a, that minimises the free energy functional. The state obtained for a that corresponds to the minimal value of the free energy functional aka $\frac{\tilde{F}_{DM}}{\tilde{F}_{ex}} = -2$ is the stable solution.

2.4.3 Analytical Solution for $B = 0$

2.4.3.1 The Solution

Before turning to numerical minimisation of the functional (2.27) using all the scaling and procedures we have presented above, we want to test our approach. In order to do it, let us minimise functional (2.27) analytically for a special case of $B = 0$.

As we know, Dzyaloshinksy-Moriya system in absence of an external field should demonstrate helical behaviour. [15] Let us derive this solution analytically. The dimensionless functional for $\beta = 0$ is

$$\tilde{F}\left[\vec{M}(x,y)\right] = \int \left\{ \frac{1}{4}\sum_{\mu}\left(\partial_\mu \vec{M}\right)\cdot\left(\partial_\mu \vec{M}\right) + \vec{M}\cdot\left(\nabla\times\vec{M}\right) + \lambda\left(\left|\vec{M}\right|^2 - 1\right)\right\}\frac{dxdy}{A}. \tag{2.110}$$

Fourier expand components of $\vec{M}$ as introduced in section 2.3.2:

$$M_\mu = \sum_{\vec{k}} \hat{M}_\mu(\vec{k}) e^{-i\vec{k}\vec{r}}, \tag{2.111}$$

with $\hat{M}_\mu$ being Fourier coefficients for M_x, M_y, M_z, then the derivatives are

$$\partial_\nu M_\mu = -\sum_{\vec{k}} i k_\nu \hat{M}_\mu(\vec{k}) e^{-i\vec{k}\vec{r}}, \tag{2.112}$$

$$\left(\nabla\times\vec{M}\right)_\alpha = \sum_{\beta\gamma}\epsilon_{\alpha\beta\gamma}\sum_{\vec{k}} i k_\beta \hat{M}_\gamma(\vec{k}) e^{-i\vec{k}\vec{r}}, \tag{2.113}$$

and the functional then becomes

$$\begin{aligned}\tilde{F}\left[\vec{M}(x,y)\right] \;=\; & \int\left\{ -\frac{1}{4}\sum_{\alpha\mu}\sum_{\vec{k},\vec{k}'}(ik_\mu)(ik'_\mu)\hat{M}_\alpha(\vec{k})\hat{M}_\alpha(\vec{k}')e^{-i(\vec{k}+\vec{k}')\vec{r}}\right. \\ & + \sum_{\alpha\beta\gamma}\epsilon_{\alpha\beta\gamma}\sum_{\vec{k},\vec{k}'} ik_\beta \hat{M}_\alpha(\vec{k}')\hat{M}_\gamma(\vec{k})e^{-i(\vec{k}+\vec{k}')\vec{r}} \\ & \left. + \lambda\left(\sum_{\alpha}\sum_{\vec{k},\vec{k}'}\hat{M}_\alpha(\vec{k})\hat{M}_\alpha(\vec{k}')e^{-i(\vec{k}+\vec{k}')\vec{r}} - 1\right)\right\}\frac{dxdy}{A}.\end{aligned} \tag{2.114}$$

Recall

$$\int e^{-i(\vec{k}+\vec{k}')\vec{r}}\frac{dxdy}{A} = \delta_{\vec{k},-\vec{k}} \tag{2.115}$$

and work with each term of the functional (2.114) separately:

$$\tilde{F} = \tilde{F}_{ex} + \tilde{F}_{DM} + \tilde{F}_\lambda. \tag{2.116}$$

The exchange term simplifies to

$$\begin{aligned}
\tilde{F}_{ex} &= -\frac{1}{4}\int \sum_{\mu\nu}\sum_{\vec{k},\vec{k}'}(ik_\nu)(ik'_\nu)\hat{M}_\mu(\vec{k})\hat{M}_\mu(\vec{k}')e^{-i(\vec{k}+\vec{k}')\vec{r}}\frac{dxdy}{A} \\
&= -\frac{1}{4}\sum_{\mu\nu}\sum_{\vec{k},\vec{k}'}(ik_\nu)(ik'_\nu)\hat{M}_\mu(\vec{k})\hat{M}_\mu(\vec{k}')\delta_{k,-k} \\
&= -\frac{1}{4}\sum_{\mu\nu}\sum_{\vec{k}}(ik_\nu)(-ik_\nu)\hat{M}_\mu(\vec{k})\hat{M}_\mu(-\vec{k}) \\
&= -\frac{1}{4}\sum_{\mu\nu}\sum_{\vec{k}}k_\nu^2\hat{M}_\mu(\vec{k})\hat{M}^*_\mu(\vec{k}) \\
&= -\frac{1}{4}\sum_{\mu\nu}\sum_{\vec{k}}k_\nu^2\left|\hat{M}_\mu\right|^2, \qquad (2.117)
\end{aligned}$$

as $\hat{M}_\mu(-\vec{k}) = \hat{M}^*_\mu(\vec{k})$.

The Dzyaloshinsky-Moriya term then becomes:

$$\begin{aligned}
\tilde{F}_{DM} &= \sum_{\alpha\beta\gamma}\epsilon_{\alpha\beta\gamma}\int\sum_{\vec{k},\vec{k}'}ik_\beta\hat{M}_\alpha(\vec{k}')\hat{M}_\gamma(\vec{k})e^{-i(\vec{k}+\vec{k}')\vec{r}}\frac{dxdy}{A} \\
&= \sum_{\alpha\beta\gamma}\epsilon_{\alpha\beta\gamma}\sum_{\vec{k},\vec{k}'}ik_\beta\hat{M}_\alpha(\vec{k}')\hat{M}_\gamma(\vec{k})\delta_{k,-k} \qquad (2.118) \\
&= \sum_{\alpha\beta\gamma}\epsilon_{\alpha\beta\gamma}\sum_{\vec{k}}ik_\beta\hat{M}^*_\alpha(\vec{k})\hat{M}_\gamma(\vec{k}).
\end{aligned}$$

Finally, the Lagrange multiplier term turns into:

$$\begin{aligned}
\tilde{F}_\lambda &= \lambda\int\left(\sum_\mu\sum_{\vec{k},\vec{k}'}\hat{M}_\mu(\vec{k})\hat{M}_\mu(\vec{k}')e^{-i(\vec{k}+\vec{k}')\vec{r}}-1\right)\frac{dxdy}{A} \\
&= \sum_\mu\sum_{\vec{k},\vec{k}'}\hat{M}_\mu(\vec{k})\hat{M}_\mu(\vec{k}')\delta_{\vec{k},-\vec{k}}-\lambda \qquad (2.119) \\
&= \lambda\sum_\mu\sum_{\vec{k}}\left|\hat{M}_\mu(\vec{k})\right|^2-\lambda \qquad (2.120)
\end{aligned}$$

Combining all three terms, we obtain

$$\tilde{F} = \sum_{\vec{k}}\left\{\frac{1}{4}\sum_{\mu\nu}k_\nu^2\left|\hat{M}_\mu(\vec{k})\right|^2+\sum_{\mu\beta\gamma}\epsilon_{\mu\beta\gamma}\hat{M}^*_\mu(\vec{k})ik_\beta\hat{M}_\gamma(\vec{k})+\lambda\sum_\mu\left|\hat{M}_\mu(\vec{k})\right|^2\right\}-\lambda. \qquad (2.121)$$

Vary the functional with respect to $\hat{M}^*_\mu(\vec{k})$ by writing the corresponding Euler-Lagrange

equation:

$$\frac{\partial \tilde{F}}{\partial \hat{M}^*_\mu} - \partial_\nu \frac{\partial \tilde{F}}{\partial(\partial_\nu \hat{M}^*_\mu)} = 0 \tag{2.122}$$

with the summation convention applied for ν.

One then finds that all the derivative terms,

$$\frac{\partial \tilde{F}}{\partial(\partial_\nu \hat{M}^*_\mu)} = 0 \tag{2.123}$$

$\forall \nu$, hence we obtain

$$\frac{\partial \tilde{F}}{\partial \hat{M}^*_\mu} = 0, \tag{2.124}$$

which is found to be

$$\frac{\partial \tilde{F}}{\partial \hat{M}^*_\mu} = \sum_{\vec{k}} \left\{ \frac{1}{2} \sum_{\mu\nu} k_\nu^2 \hat{M}_\mu(\vec{k}) + \sum_{\beta\gamma} \epsilon_{\mu\beta\gamma} \left(i k_\beta \hat{M}_\gamma(\vec{k}) - i k_\gamma \hat{M}_\gamma(\vec{k}) \right) + 2\lambda \sum_\mu \hat{M}_\mu(\vec{k}) \right\} = 0, \tag{2.125}$$

leading to three equations for three Fourier coefficients for a given k:

$$k^2 X_{\vec{k}} + 4 i k_y Z_{\vec{k}} + 4\lambda X_{\vec{k}} = 0, \tag{2.126}$$

$$k^2 Y_{\vec{k}} - 4 i k_x Z_{\vec{k}} + 4\lambda Y_{\vec{k}} = 0, \tag{2.127}$$

$$k^2 Z_{\vec{k}} + 4 i k_x Y_{\vec{k}} - 4 i k_y X_{\vec{k}} + 4\lambda Z_{\vec{k}} = 0. \tag{2.128}$$

These equations look similar to equations (2.84) – (2.86) with the only difference in the absence of β.[11] Let us now rewrite our new equations in the matrix form:

$$\hat{D}^{(0)}_{\vec{k}} \vec{V}_{\vec{k}} + 4\lambda \hat{I} \vec{V}_{\vec{k}} = 0, \tag{2.129}$$

where we have separated the Lagrange multiplier from the other terms combined in $\hat{D}^{(0)}_{\vec{k}}$,

$$\hat{D}^{(0)}_{\vec{k}} = \begin{pmatrix} k^2 & 0 & 4 i k_y \\ 0 & k^2 & -4 i k_x \\ -4 i k_y & 4 i k_x & k^2 \end{pmatrix}. \tag{2.130}$$

[11] We could have actually adapted equations (2.84) – (2.86) for $\beta = 0$ case straight away, though we decided to repeat the procedure from scratch for better demonstration.

The Fourier coefficients are now combined in the eigenvector $\vec{V}_{\vec{k}}$,

$$\vec{V}_{\vec{k}} = \begin{pmatrix} X_{\vec{k}} \\ Y_{\vec{k}} \\ Z_{\vec{k}} \end{pmatrix}. \tag{2.131}$$

On the other hand, sometimes it is more convenient to write

$$\hat{D}_{\vec{k}} = \hat{D}^{(0)}_{\vec{k}} + 4\lambda\hat{I}, \tag{2.132}$$

with

$$\hat{D}_{\vec{k}} = \begin{pmatrix} k^2+4\lambda & 0 & 4ik_y \\ 0 & k^2+4\lambda & -4ik_x \\ -4ik_y & 4ik_x & k^2+4\lambda \end{pmatrix} \tag{2.133}$$

then equation (2.129) reduces to

$$\hat{D}_{\vec{k}}\vec{V}_{\vec{k}} = 0 \tag{2.134}$$

that can be easily solved via

$$\det \hat{D}_{\vec{k}} = 0. \tag{2.135}$$

So let us find the determinant of the matrix $\hat{D}$:

$$\det \hat{D} = \left(k^2+4\lambda\right)\left(-16k^2 + \left(k^2+4\lambda\right)^2\right), \tag{2.136}$$

and a characteristic equation

$$\left(k^2+4\lambda\right)\left(-16k^2 + \left(k^2+4\lambda\right)^2\right) = 0 \tag{2.137}$$

solves to

$$\lambda = -\frac{1}{4}\left(k^2+4\sigma k\right), \tag{2.138}$$

where σ can take values of $\sigma = -1, 0, 1$.

Let us now denote

$$k|_{\beta=0} = k_H \tag{2.139}$$

in order to mark the wave vector of a helix and not to confuse it with other possible values of k.

Finally, let us go back to the free energy functional, (2.121), and notice that it can be written in the matrix form as well:

$$\tilde{F} = \sum_{\vec{k}} \hat{D}_{\vec{k}}\vec{V}_{\vec{k}} - \lambda. \tag{2.140}$$

But we had just solved $\hat{D}_{\vec{k}}\vec{V}_{\vec{k}} = 0$, hence the functional reduces to

$$\tilde{F} = -\lambda = \frac{1}{4}k_H^2 + \sigma k_H = \tilde{F}_\sigma. \tag{2.141}$$

Let us now plot $\tilde{F}(k_H)$ for allowed values of σ to determine whichever corresponds to the minimal solution. See the plot in Figure 2.13.

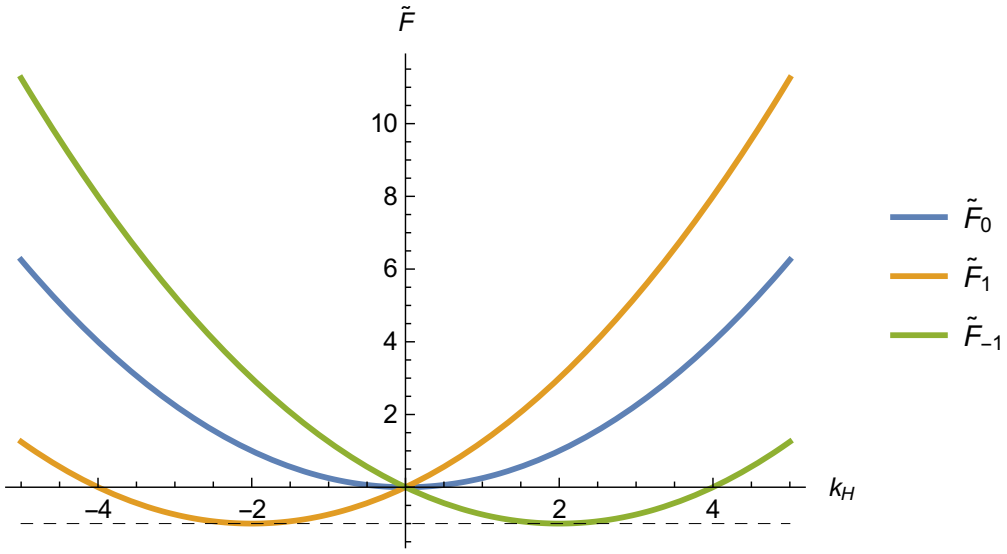

Figure 2.13: $\tilde{F}(k_H)$ for differnet values of σ: blue curve represents the functional for $\sigma = 0$, orange curve stands for $\sigma = 1$ case and green one goes for $\sigma = -1$.

As one can see form Figure 2.13, if we would like to stick to positive values of k_H it is $\sigma = -1$ we should choose. However, if we do not restrict ourselves to positive k_H, $\sigma = 1$ case would also minimise the free energy functional.

On the other hand, one can assume a helical solution from the beginning and parametrise $\vec{M}$ in the usual helical form as it was demonstrated in the introduction:

$$\vec{M} = \begin{pmatrix} 0 \\ -\sin \vec{k}_H \vec{r} \\ \cos \vec{k}_H \vec{r} \end{pmatrix}, \tag{2.142}$$

with $\vec{k} = k_H \hat{e}_x$, then the derivatives become

$$\partial_\mu \vec{M} = -k_{H_\mu} \begin{pmatrix} 0 \\ \cos \vec{k}_H \vec{r} \\ \sin \vec{k}_H \vec{r} \end{pmatrix}, \tag{2.143}$$

$$\nabla \times \vec{M} = -\vec{k}_H \begin{pmatrix} 0 \\ -\sin \vec{k}_H \vec{r} \\ \cos \vec{k}_H \vec{r} \end{pmatrix}, \tag{2.144}$$

hence the ferromagnetic exchange term simplifies to

$$\tilde{F}_{ex} = \frac{1}{4} \sum_{\mu} \left(\partial_\mu \vec{M} \right) \cdot \left(\partial_\mu \vec{M} \right) = \frac{1}{4} k_H^2 \tag{2.145}$$

and the Dzyaloshinsky-Moriya term – to

$$\tilde{F}_{DM} = \vec{M} \cdot \left(\nabla \times \vec{M} \right) = -k_H, \tag{2.146}$$

as an expression $\sin^2 \theta + \cos^2 \theta = 1$ is involved in both (2.145) and (2.146). Hence the total functional becomes

$$\tilde{F} = \frac{1}{4} k_H^2 - k_H, \tag{2.147}$$

just as we got it via λ with $\sigma = -1$ that corresponds to $\vec{k} = k_H \hat{e}_x$ (positive k_H).

Finally, let us plot $\tilde{F}$ vs k_H and compare it with $\frac{\tilde{F}_{DM}}{\tilde{F}_{ex}}$. The plot is demonstrated in Figure 2.14.

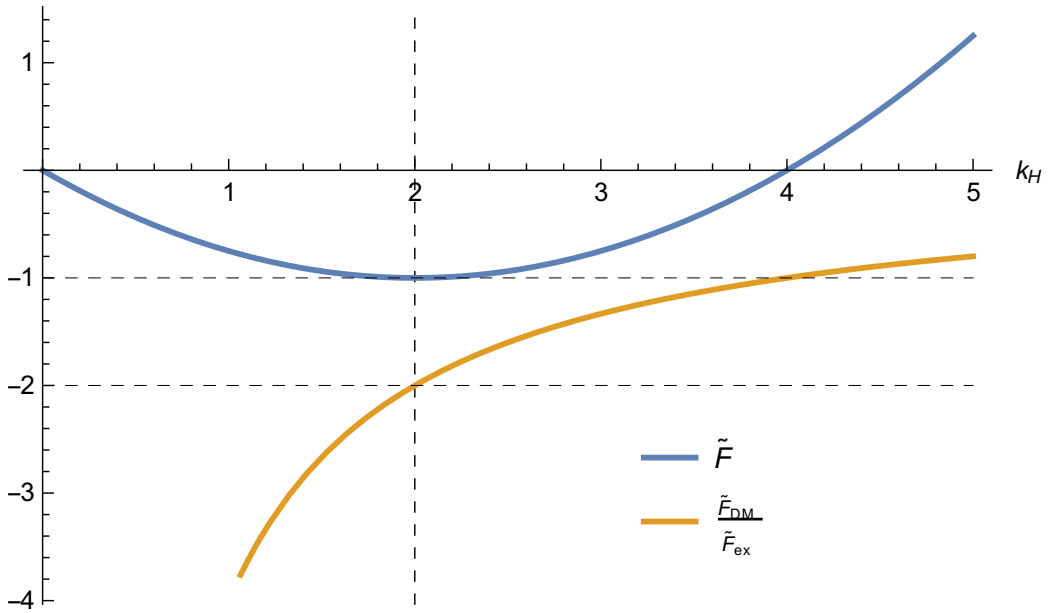

Figure 2.14: $\tilde{F}(k_H)$ and $\frac{\tilde{F}_{DM}}{\tilde{F}_{ex}}$ compared. Blue curve represents $\tilde{F}(k_H)$ for positive values of k_H and orange one – $\frac{\tilde{F}_{DM}}{\tilde{F}_{ex}}$.

In Figure 2.14 we see that it is $k_H = 2$ that corresponds to the minima of $\tilde{F}$ on the one

hand side, and to

$$\frac{\tilde{F}_{DM}}{\tilde{F}_{ex}} = -2 \tag{2.148}$$

on the other hand side, as the condition (2.148) is satisfied precisely at $k_H = 2$. Hence we conclude that it is easy to determine a point at which (2.148) is satisfied exactly. Clearly, for a nonzero β the position of the minima of the functional would change, but the virial theorem would remain valid (i.e. the condition (2.148) would still correspond to the minima), hence the condition (2.148) would hold for any value of an external field as well. Then conclude that it is condition (2.148) one must fulfil in order to make sure the minima one finds for $\tilde{F}$ is the actual global minima.

Notice, that the condition (2.148) is general for any helimagnetic system in its ground state.

2.4.3.2 Comments on the Numerics

Another conclusion one may obtain from Figure 2.14 is the fact that $\tilde{F}$ is very shallow near its minima, hence the error in the position of this minima would be significant. In fact, it is nearly impossible to determine the exact minima from the blue curve in Figure 2.14 with a naked eye. This can be justified by a simple example. Suppose we are looking for a solution of

$$f(x_r) = 0. \tag{2.149}$$

However, it is impossible to reach anything precisely numerically, just up to a certain accuracy, hence what we actually want is

$$|f(x_r)| < \epsilon, \tag{2.150}$$

where ϵ is the numerical error in calculations of f.

Taylor expand

$$f(x_r + \Delta x) = f(x_r) + \Delta x \frac{\partial f}{\partial x}\Big|_{x_r} + \mathcal{O}\left(\Delta x^2\right), \tag{2.151}$$

where Δx is the numerical error in the result; so the condition (2.150) turns into

$$|\Delta x| \left|\frac{\partial f}{\partial x}\Big|_{x_r}\right| < \epsilon, \tag{2.152}$$

as $f(x_r) = 0$ and we neglect terms of the second and higher orders in Δx.

We conclude then that the smaller $\left|\frac{\partial f}{\partial x}\Big|_{x_r}\right|$ is, the higher the error in the result would be. In other words, the shallower the function is around the point of interest, the higher numerical error there is; and according to Figure 2.14, the free energy functional is almost flat around its minima, hence the result obtained would be highly unreliable in terms of the determination

of the actual minima. So this is another motivation for us to employ condition (2.148) in our future calculations.

2.4.4 Summary of the Method

Let us now summarise our method. In order to obtain the optimal configuration of a magnetic system, one needs to

- write the free energy functional in Cartesian coordinates with Lagrange multiplier, λ, imposed for a functional to satisfy the constraint of $\left|\vec{M}\right|^2 = 1$;
- define the lattice – triangular in our case;
- define Fourier decomposition of the magnetisation components and the Lagrange multiplier;
- derive Euler-Lagrange equations in Fourier representation;
- rewrite these equations in the matrix form;
- find Fourier coefficients for λ numerically;
- find Fourier coefficients for the magnetisation components analytically from λ found in the previous stage;
- use the virial ratio, (2.109), to find the optimal spacing, a, for a given value of an external field, β;
- use the optimal spacing found before in order to calculate the optimal configuration of the system for a given β;
- repeat the procedure for other values of β of interest.

2.4.5 Stable Solutions

Following the procedure described in section 2.4.2, we have fixed the optimal spacing that corresponds to a certain value of an external field. Clearly, skyrmion lattice exists for some particular values of an external field only. We study the system for different values of an external field to find the minimal possible free energy for that field starting from $\beta = 0$. The free energy curve obtained is demonstrated in Figure 2.15 (red curve).

Notice that as we have found magnetisation components formulated in Fourier space, there is no need to calculate the free energy functional numerically (hence avoid possible numerical errors, especially while calculating derivatives); we can just formulate it via Fourier coefficients.

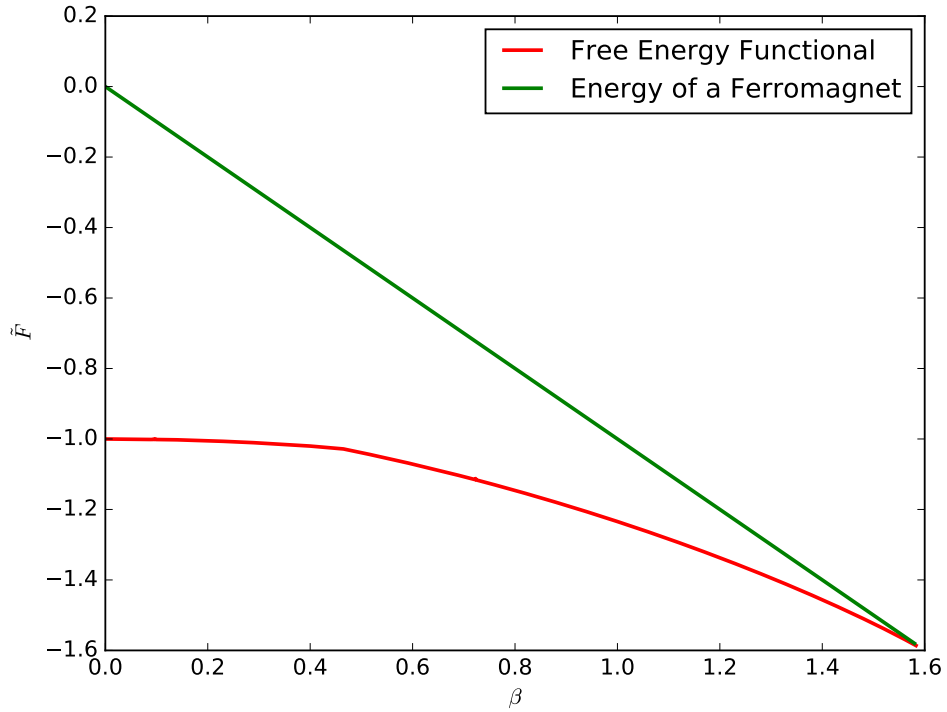

Figure 2.15: Free energy functional of a magnetic system against an external field. Red curve represents the optimal free energy of a system and green line is the free energy of a ferromagnetic system demonstrated for comparison purposes.

Write

$$\tilde{F} = \tilde{F}_{ex} + \tilde{F}_{DM} + \tilde{F}_{Z}, \tag{2.153}$$

as we did for $B = 0$ case, keeping in mind that the condition $\left|\vec{M}\right|^2 = 1$ is now satisfied, hence $\tilde{F}_{\lambda} = 0$.

Use (2.60) – (2.62) for Fourier formulations of magnetisation components and (2.65) for Fourier formulation of their derivatives to obtain:

$$\begin{aligned}
\tilde{F}_{ex} &= \frac{1}{4}\int \sum_{\nu} \left(\partial_\nu \vec{M}\right)\cdot\left(\partial_\nu \vec{M}\right)\frac{dxdy}{A} \\
&= \frac{1}{4}\int \sum_{\nu\mu}\sum_{\vec{k}\vec{k}'}(-ik_\nu)(-ik'_\nu)\hat{M}_\mu(\vec{k})\hat{M}_\mu(\vec{k}')e^{-i(\vec{k}+\vec{k}')\vec{r}}\frac{dxdy}{A} \\
&= -\frac{1}{4}\sum_{\nu\mu}\sum_{\vec{k}\vec{k}'} k_\nu k'_\nu \hat{M}_\mu(\vec{k})\hat{M}_\mu(\vec{k}')\delta_{\vec{k}\vec{k}'} \\
&= -\frac{1}{4}\sum_{\nu\mu}\sum_{\vec{k}} k_\nu(-k_\nu)\hat{M}_\mu(\vec{k})\hat{M}^*_\mu(\vec{k}) \\
&= \frac{1}{4}\sum_{\nu\mu}\sum_{\vec{k}} k_\nu^2\left|\hat{M}_\mu\right|^2 = \frac{1}{4}\sum_{\vec{k}} k^2\left(\left|X_{\vec{k}}\right|^2 + \left|Y_{\vec{k}}\right|^2 + \left|Z_{\vec{k}}\right|^2\right),
\end{aligned} \tag{2.154}$$

where we have noticed that $(-i)(-i) = -1$, $\delta(-x) = \delta(x)$ and $\hat{M}_\mu(-\vec{k}) = \hat{M}^*_\mu(\vec{k})$.

Similarly, for the Dzyaloshinsky-Moriya term:

$$\begin{aligned}\tilde{F}_{DM} &= \int \vec{M} \cdot \left(\nabla \times \vec{M}\right) \frac{dxdy}{A} \\ &= -i \int \sum_{\vec{k}\vec{k}'} \left(X_{\vec{k}} k'_y Z_{\vec{k}'} - Y_{\vec{k}} k'_x Z_{\vec{k}'} + Z_{\vec{k}} k'_x Y_{\vec{k}'} - Z_{\vec{k}} k'_y X_{\vec{k}'}\right) e^{-i(\vec{k}+\vec{k}')\vec{r}} \frac{dxdy}{A} \\ &= i \sum_{\vec{k}} \left(k_y X_{\vec{k}} Z^*_{\vec{k}} - k_x Y_{\vec{k}} Z^*_{\vec{k}} + k_x Y^*_{\vec{k}} Z_{\vec{k}} - k_y X^*_{\vec{k}} Z_{\vec{k}}\right).\end{aligned} \tag{2.155}$$

Finally, for the Zeeman term:

$$\tilde{F}_Z = -\beta \int M_z \frac{dxdy}{A} = -\beta \int \sum_{\vec{k}} Z_{\vec{k}} e^{-i\vec{k}\vec{r}} \frac{dxdy}{A} = -\beta \sum_{\vec{k}} Z_{\vec{k}} \delta_{\vec{k},0} = -\beta Z_0, \tag{2.156}$$

so the total free energy can be formulated via Fourier coefficients of the magnetisation as

$$\tilde{F} = \sum_{\vec{k}} \left\{ \frac{1}{4} k^2 \left(\left|X_{\vec{k}}\right|^2 + \left|Y_{\vec{k}}\right|^2 + \left|Z_{\vec{k}}\right|^2 \right) + i \left(k_y X_{\vec{k}} Z^*_{\vec{k}} - k_x Y_{\vec{k}} Z^*_{\vec{k}} + k_x Y^*_{\vec{k}} Z_{\vec{k}} - k_y X^*_{\vec{k}} Z_{\vec{k}} \right) \right\} - \beta Z_0. \tag{2.157}$$

And it is functional (2.157) demonstrated in Figure 2.15 and all the subsequent figures as a function of β.

In order to prove that the solution we obtained is actually stable, we demonstrate the corresponding virial ratio,

$$V = \frac{\tilde{F}_{DM}}{\tilde{F}_{ex}}, \tag{2.158}$$

and ensure it is equal to -2 $\forall\beta$ up to some numerical uncertainty. This is demonstrated in Figure 2.16.

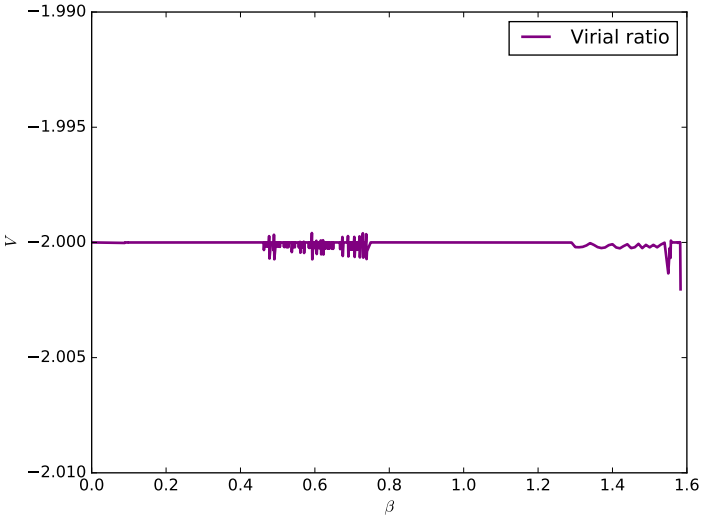

Figure 2.16: $\frac{\tilde{F}_{DM}}{\tilde{F}_{ex}}$ against β. $\frac{\tilde{F}_{DM}}{\tilde{F}_{ex}} = -2$ $\forall\beta$ up to some numerical uncertainty.

In order to get a better understanding of the transitions, it might be handy to demonstrate free energy functional for the metastable regions as well as for the stable ones. This is shown in Figure 2.17, where energies of metastable helices, skyrmions and a ferromagnet are plotted along with the stable solutions.

From Figure 2.17 it is also easy to read off the critical points. So we claim that in our

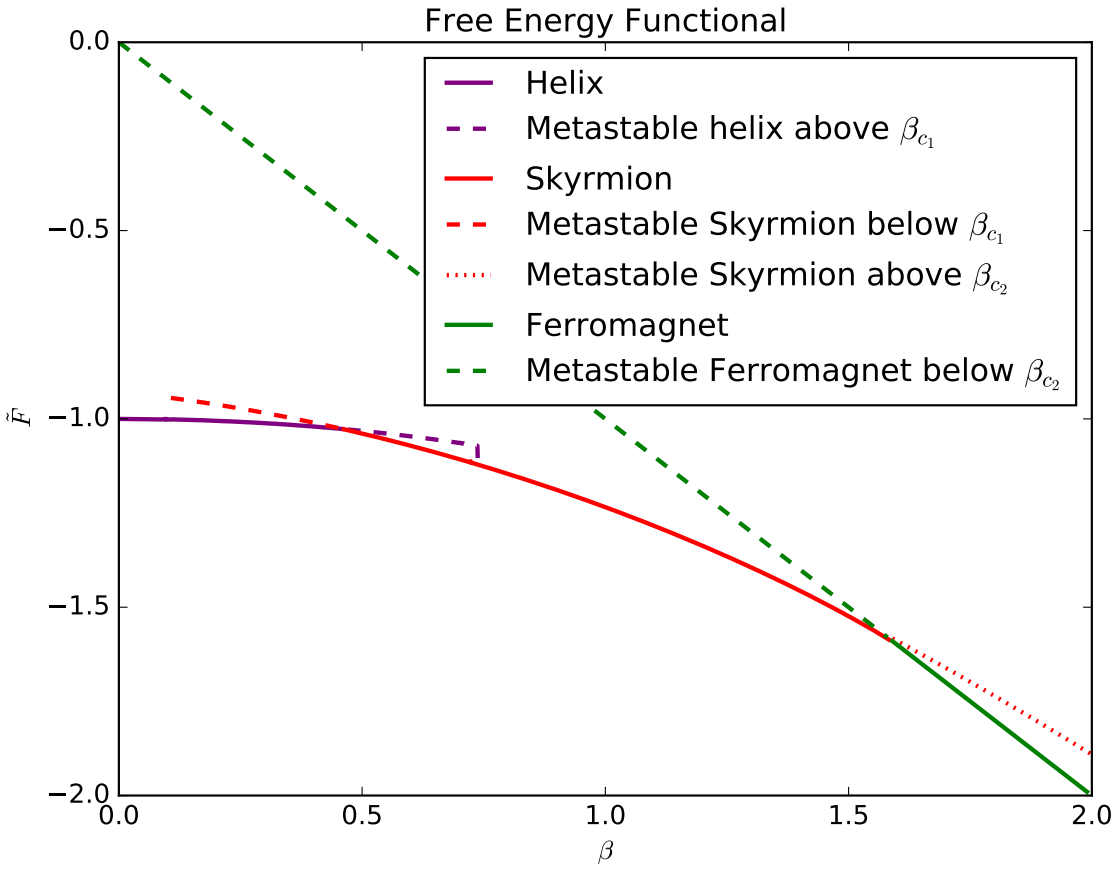

Figure 2.17: Free energy functional of a magnetic system against an external field. Red curve represents the optimal free energy of a skyrmion system, purple one stands for the helial system and green line is the free energy of a ferromagnetic system. Dashed lines of different colours correspond to metastable solutions of corresponding patterns.

units the critical field for the helical-skyrmion phase transition is

$$\beta_{c_1} = 0.46 \tag{2.159}$$

and the critical field for the skyrmion-ferromagnet phase transition is

$$\beta_{c_2} = 1.56. \tag{2.160}$$

It is notable, that although the studies of the free energy functional of a skyrmion lattice system have been performed before (by *Han et al* [43], for example), the constraint of $|\vec{M}|^2 = 1$ had never been implemented in a proper way for a lattice,[12] hence the exact transition points

[12]It had been for a single skyrmion, though, as polar coordinates are sort of the conventional way of working there, and parametrisation of $\vec{M}$ in polars provides $\left|\vec{M}\right|^2 = 1$ in a straighforward way.

had never been found before.

Following Figure 2.17, we can define three regions on β scale: helical region – where a stable system obeys helical ordering, skyrmion region – where a stable solution has the form of the skyrmion lattice and ferromagnetic region – where a system has its minimal configuration as a ferromagnet. Then if for a given β the stable solution for our system is a helix, we say that a system for a given β lies in a helical region or in a helical state. All the regions are demonstrated in Figure 2.18.

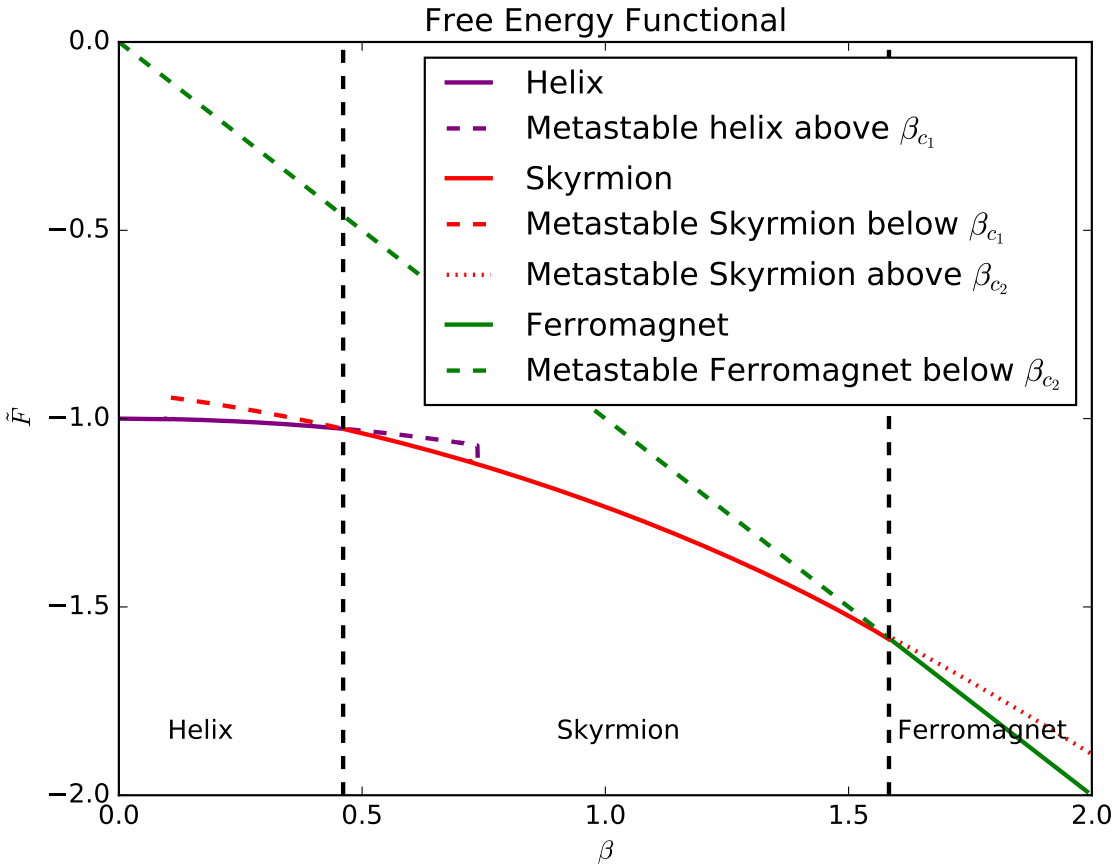

Figure 2.18: Magnetic pattern distribution with respect to β.

We had already mentioned, that the total free energy functional is composite of three terms: ferromagnetic exchange term,

$$\tilde{\mathcal{F}}_{ex} = \frac{1}{4}\sum_{\mu}\left(\partial_\mu \vec{M}\right)\cdot\left(\partial_\mu \vec{M}\right), \tag{2.161}$$

Dzyaloshinksi-Moriya term,

$$\tilde{\mathcal{F}}_{DM} = \vec{M}\cdot\left(\nabla\times\vec{M}\right) \tag{2.162}$$

and Zeeman term,

$$\tilde{\mathcal{F}}_Z = \vec{\beta} \cdot \vec{M}. \tag{2.163}$$

It had been also pointed out before that when the Zeeman term is dominant, the system tends to a ferromagnetic solution, when the Dzyaloshinksi-Moriya term is dominant, the system tends to be helical (and thus turns into a perfect helix at zero field, as demonstrated in section 2.4.1), and when neither is dominant, the stable solution may have a form of a skyrmion lattice. Let us demonstrate these three terms separately to test our propositions.

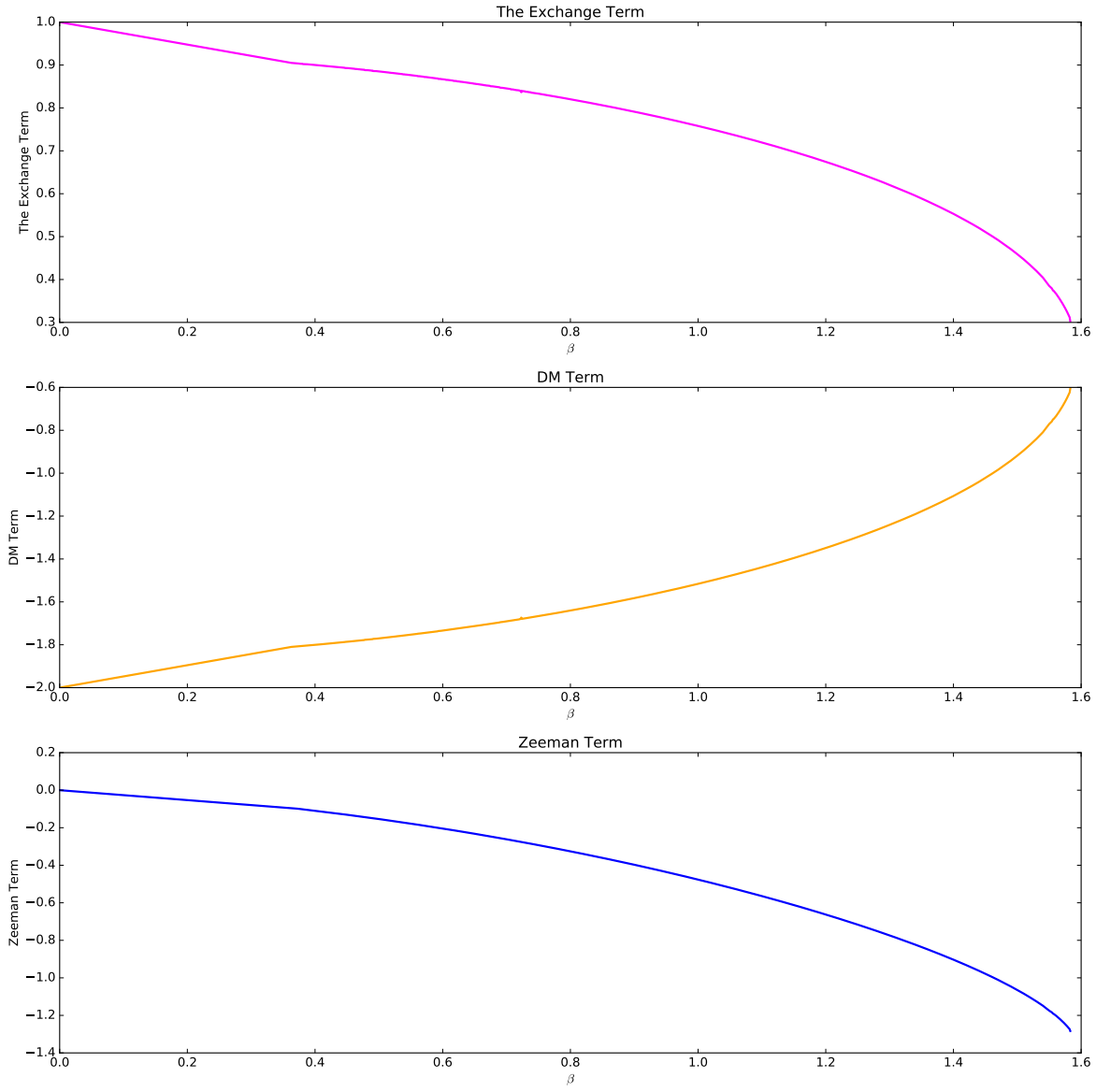

Figure 2.19: Ferromagnetic exchange term (the upper figure), Dzyaloshinksi-Moriya term (the middle figure) and Zeeman term (the last figure) demonstrated separately against β.

Figure 2.19 shows us that our predictions were correct: at low values of the field the Zeeman term is (obviously) very small, whereas the exchange term and anisotropic term have the most of their effect (despite having opposite signs, $|\tilde{F}_{ex}| = \max$ as well as $|\tilde{F}_{DM}| = \max$ at $\beta = 0$). This effect then gets smaller with β increasing. It shall be also clear enough that for large external fields the system would tend to the ferromagnetic ordering, as (mathematically) the Zeeman term would dominate drastically over the others and (physically) spins would tend to align along the field with Dzyaloshinksi-Moriya effects not able to compete any more. When effects of all three terms are comparable to each other, Dzyaloshinsky-Moriya term is able to compete with ferromagnetic ordering and skyrmion lattice results as an outcome of such a competition.

It is also notable, how different the lattice is near transition points. Consider Figure 2.20 for different configurations.

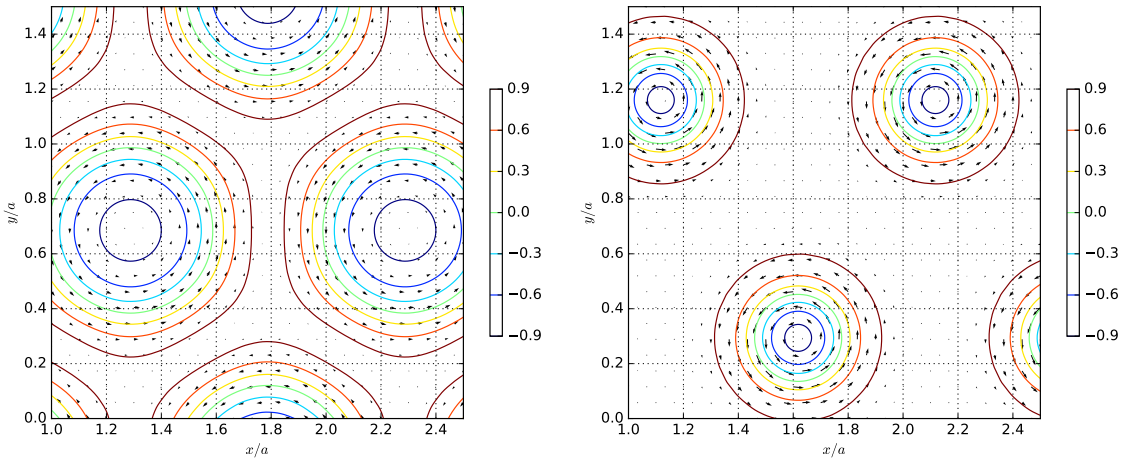

(a) Optimal lattice solution for a skyrmion system for $\beta = 0.478$ and $a = 3.785$ (stable skyrmion region near helix-skyrmion phase transition).

(b) Optimal lattice solution for a skyrmion system for $\beta = 1.55$ and $a = 4.8$ (stable skyrmion region near skyrmion-ferromagnet phase transition).

Figure 2.20: Skyrmion lattice near critical points.

In Figure 2.20a there is a skyrmion system near helix-skyrmion phase transition. Here we see that the radius of skyrmions (i.e. the distance from the centre of a skyrmion to the edge) becomes large, spacing between them – therefore small (not the distance between the cores of skyrmions, though), and the shape of skyrmions is not ideally circular anymore. If we compare skyrmion lattice in Figure 2.21 with a typical helix in Figure 2.22, we would realise that our skyrmions actually tend to helices: more spins undertake the intermediate states between "up" and "down", fewer spins align with the field. The similarities are seen even better if we consider the side view that is demonstrated in Figure 2.23. So the actual phase transition that eventually happens at a point is not surprising at all.

On the other hand, as it is demonstrated in Figure 2.20b, near skyrmion-ferromagnet

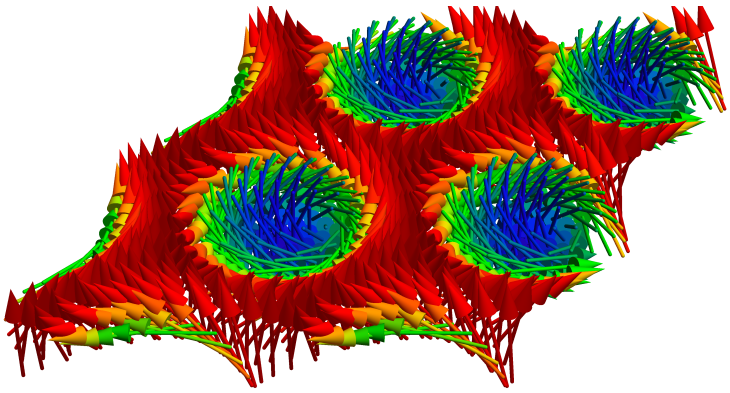

Figure 2.21: Optimal spin configuration for a skyrmion system for $\beta = 0.478$ and $a = 3.785$ (stable skyrmion region near helix-skyrmion phase transition).

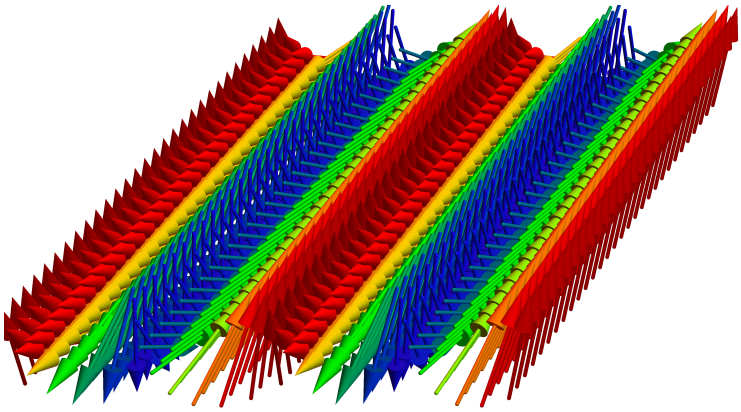

Figure 2.22: Spin configuration of a stable helical structure obtained for $\beta = 0.15$ and $a = 3.81$.

(a) Side view of a helix.

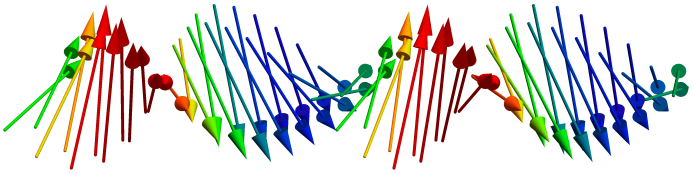

(b) Side view of a skyrmion lattice near helix-skyrmion transition.

Figure 2.23: Side view comparison between helix and skyrmion lattice near helix-skyrmion phase transition.

phase transition skyrmions appear to be smaller and the distance between them increases (this also includes the distance between skyrmion cores), therefore the area with the highest magnetisation increases. But as the field between skyrmions is constant, we can approximate the area between skyrmions as a ferromagnetic region. This is well demonstrated in Figure 2.24 that presents the spin configuration of the skyrmion lattice near β_{c_2}. It is then clear from Figure 2.24 that the ferromagnetic region (i.e. the region of all the spins aligned along the field) is larger than the skyrmions themselves. In fact, spins that are not aligned with the field are in a little fraction in comparison with those that do align. So with β increasing, the area of the ferromagnetic region is increasing as well, and at some point, at β_{c_2}, pure ferromagnet becomes energetically more favourable than the skyrmion system, as there are only few spins that are not aligned with the field left.

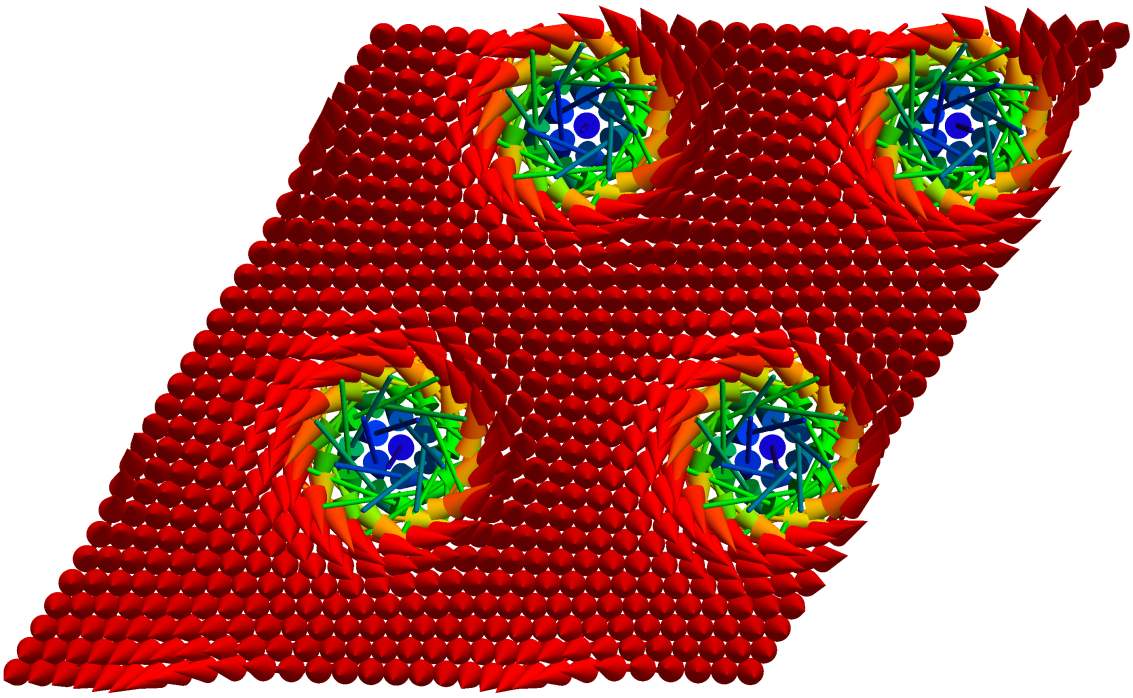

Figure 2.24: Optimal spin configuration for a skyrmion system for $\beta = 1.55$ and $a = 4.8$ (stable skyrmion region near skyrmion-ferromagnet phase transition).

We have already mentioned several times that the lattice spacing that provides an energetically optimal configuration varies for different values of an external field. One can recall the analogy to the Abrikosov vortex lattice: the optimal lattice spacing for a superconducting vortex lattice is also defined by the field. The dependence is universal and well-known (see later). However, from the actual skyrmion configurations demonstrated in Figure 2.20 it is hard to make any conclusions about how does the optimal spacing depend on the applied field, so let us study this dependence explicitly. It is demonstrated in Figure 2.25a. As one

can see from this figure, the spacing increases drastically with β increasing, which agrees with our conclusion based on the lattice configuration demonstrated in Figure 2.20b. Area of the ferromagnetic region is increasing, hence the distance between skyrmions would become larger. However, the spacing is also slightly increasing with β decreasing towards the helical region, and this conclusion is not obvious solely from Figure 2.20a.

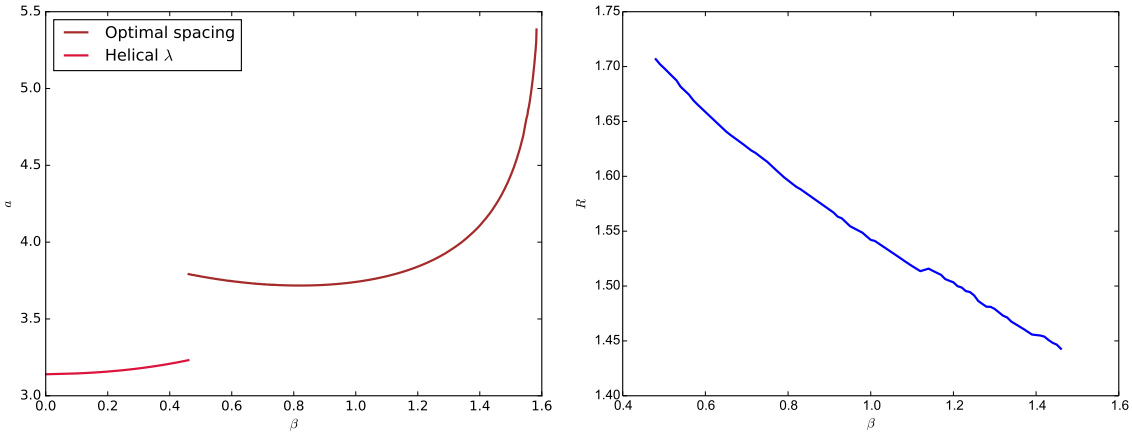

(a) Optimal skyrmion lattice spacing vs β.

(b) Optimal radius of a skyrmion vs β.

Figure 2.25: Lattice spacing and skyrmion radius vs β. Brown curve stands for the optimal lattice spacing, vinous curve – for λ_H and blue one – for the radius of a skyrmion. Both lattice spacing and the radius of a skyrmion are scaled with κ as usual for skyrmion systems. The spacing increases drastically when the field is approaching β_{c_2}, when the field is near β_{c_1}, the spacing slightly increases as well.

One can now define a radius of a skyrmion as the distance from the minimal value of M_z (ideal "down" spin) that lies in the centre of a skyrmion to the largest value of M_z (the closest "up" spin) that happens to be on the edge, just as we did it for a single skyrmion in section 2.2. The definition of the radius of a skyrmion on the lattice is demonstrated in Figure 2.26.

Then if we plot the radius of the skyrmion against the applied field as it is done in Figure 2.25b, we realise that the radius of a skyrmion always decreases with field applied (which means that the area of the ferromagnetic region always increases and while increasing it tears skyrmions apart and makes them smaller), or, in other words, if one prefers moving backwards in β scale, i.e. from the ferromagnetic region towards helices, one would realise that the lattice spacing at a point starts increasing – consult with the corresponding region in Figure 2.25a. This happens because the radius of a skyrmion always increases with decreasing field, hence at a point in order to continue increasing it needs more space, so the lattice then shall expand, as skyrmions cannot overlap.

Also recall the crucial parameter of a helix, λ_H – the period of a helix. It can be calculated

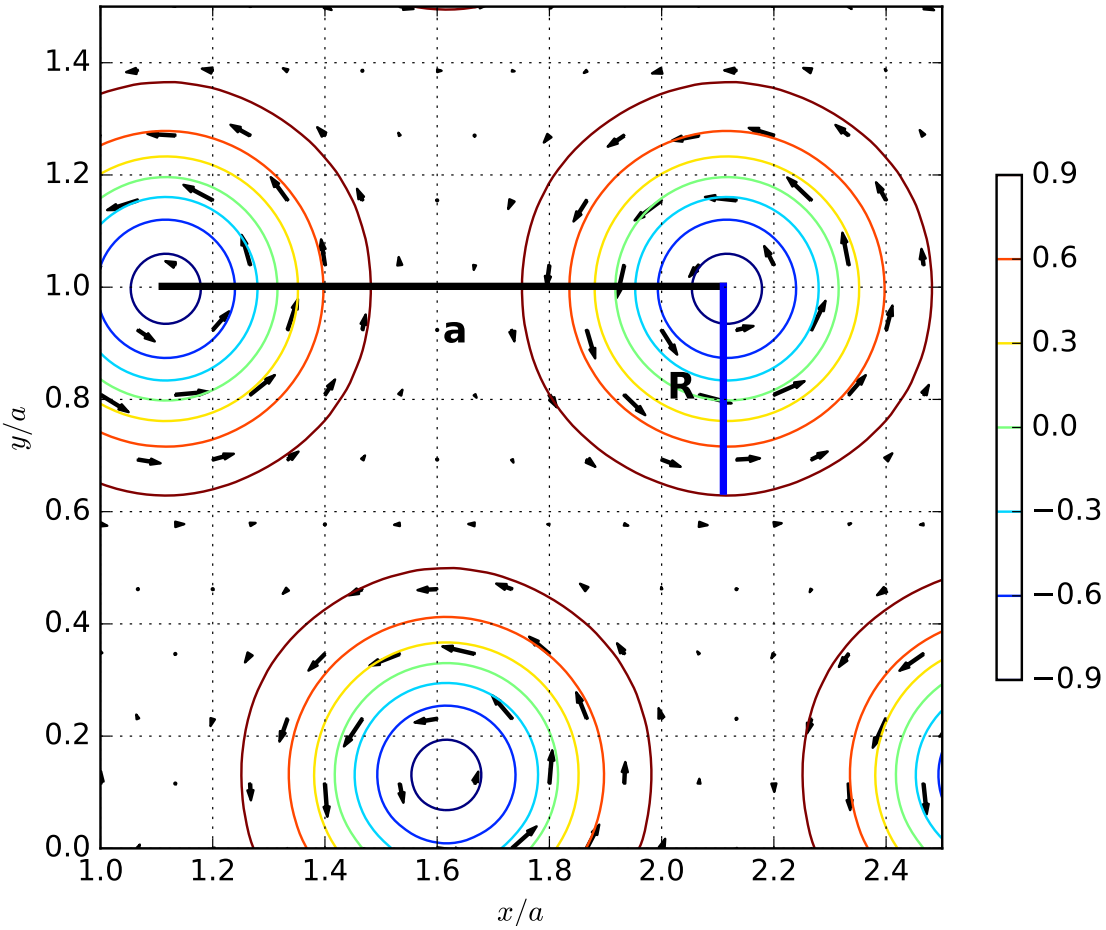

Figure 2.26: Skymion lattice with the radius of a single skyrmion defined. Here a is the lattice spacing and R is the radius of a single skyrmion.

via

$$\lambda_H = \frac{2\pi}{k_H}, \tag{2.164}$$

and for $k_H = 2$ (calculated in section 2.4.3.1 for $\beta = 0$), $\lambda_H = \pi$. We see then from the vinous line in Figure 2.25a that corresponds to $\lambda_H(\beta)$, that λ_H obtained from our calculation is exactly $\lambda_H = \pi$, hence our calculations exactly match analytical predictions as expected.

2.5 Comparison to Earlier Works

2.5.1 Comparison to the Simulations

2.5.1.1 Comparison to the Pioneering Work

Let us now briefly compare our results against those obtained in the past. First consider the pioneering work in skyrmion lattices by *Bogdanov et al.* [40, 42] In this work they started with the same functional we have begun with. Then it was transformed in the spiral form: [42]

$$\tilde{w}_s = \frac{1}{L}\int_0^L \left[\left(\frac{d\theta}{dr}\right)^2 - \frac{d\theta}{dr} + \kappa \sin^2\theta + \beta\left(1-\cos\theta\right)\right] dr, \tag{2.165}$$

where $\tilde{w}_s$ is the average energy density, L is the period of the spiral structure and r is the radial coordinate; κ and β correspond to our definitions given in section 2.3.1. The most important thing, θ, arises from the decomposition of the magnetisation in polar form,

$$\vec{M} = \left(\sin\theta\cos\varphi, \sin\theta\sin\varphi, \cos\theta\right). \tag{2.166}$$

The Euler equation that follows from (2.165) is then

$$\left(\frac{d\theta}{dr}\right)^2 = \kappa\sin^2\theta + \beta\left(1-\cos\theta\right) + C, \tag{2.167}$$

with constant C defined through the following condition:

$$\int_0^\pi \sqrt{\kappa\sin^2\theta + \beta\left(1-\cos\theta\right) + C}\, d\theta = \frac{\pi}{2}. \tag{2.168}$$

Boundary conditions for a single skyrmion were introduced to be

$$\theta(0) = \pi, \tag{2.169}$$

$$\theta(\infty) = 0, \tag{2.170}$$

that transformed to

$$\theta(L) = 0 \tag{2.171}$$

for a lattice with a circular cell approximation embedded, yielding $L = 2R$, where R is the radius of a single skyrmion. [42]

A linear ansatz of

$$\theta_0 = \pi\left(1 - \frac{r}{L}\right) \tag{2.172}$$

was first introduced in [42], but the function $\theta(r)$ was still calculated numerically from (2.167)

via Newton's method.

A good thing to compare with our results is the optimal lattice spacing – twice the radius in the circular cell approximation. Skyrmion radius defined via circular cell approximation for a cell obtained via Newton's method is demonstrated in Figure 2.27a and for a cell obtained by Runge-Kutta method is demonstrated in Figure 2.27b. [84]

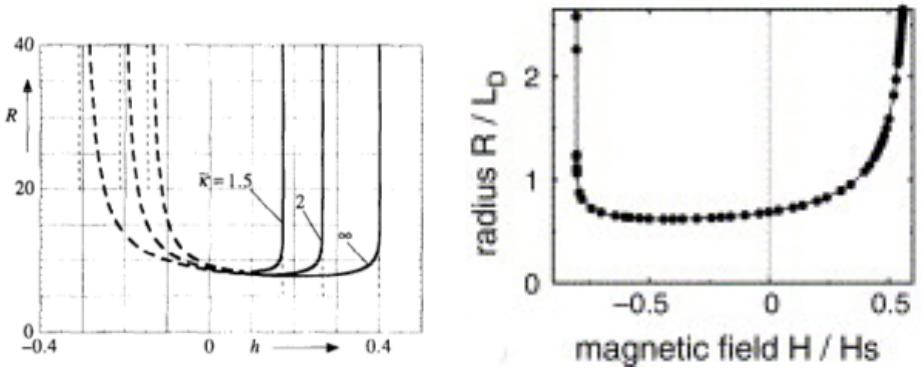

(a) Radius of a cell in circular cell approximation for a cell obtained by Newton's method. [42]

(b) Radius of a cell in circular cell approximation for a cell obtained by Runge-Kutta method. [84]

Figure 2.27: Radius of a cell in circular cell approximation.

In all of his works, however, Bogdanov addressed to a skyrmion lattice as to a periodic structure of single skyrmions with a circular cell approximation. He also had never distinguished stable and metastable states.

We see that radius of a cell in circular cell approximation demonstrated in Figure 2.27 is similar to the optimal lattice spacing calculated in this survey – see Figure 2.25a. However, we are sure to distinguish stable and metastable states, hence demonstrate the optimal lattice spacing or period of a helix in the region where either of them belongs.

All the other works discussed later in this chapter are in one way or another (as well as our work) based on Bogdanov's approach.

2.5.1.2 Comparison to the Other Works

Kawaguchi et al [17] followed the approach developed in [42], i.e. parametrised $\vec{M}$ in polar coordinates and focused on the Euler equation, (2.167).

Then they have employed linear ansatz,

$$\theta(r) = \theta_0(r) = \pi(1 - r), \tag{2.173}$$

and used it in further calculation. As we could see from the comparison of $\theta(r)$ calculated for different values of an external field with its linear initial guess in Figure 2.6 demonstrated

in section 2.2, the linear ansatz works quite well at low fields, and in the region close to the centre of a skyrmion, though at higher fields actual form of θ is clearly not linear even for a single skyrmion system.

However, it is still manageable to calculate a lot of interesting stuff as well as predict values of critical fields, β_{c_1} and β_{c_2}, just as we did.

Existence of two phase transitions, hence critical fields had been predicted even before, though, by *Bogdanov et al.* [84] *Kawaguchi et al* had also claimed calculated values for transition points, though as they had used an approximated (linear) form for skyrmion θ, hence magnetisation, their results cannot be treated as exact. We can also compare our critical fields against those experimentally observed, for example, by *Mochizuki.* [86] In our units critical fields observed in [86] are

$$\beta_{c_1}^{(experimental)} = 0.46 \tag{2.174}$$

and

$$\beta_{c_2}^{(experimental)} = 1.56, \tag{2.175}$$

that correspond exactly to the values we had obtained, whereas critical field obtained in [17] transferred in our units would be $\beta_{c_1}^{K} = 0.48$ and $\beta_{c_2}^{K} = 1.34$, which still demonstrate quite good correspondence to the experimental results (especially at low fields, which is not surprising at all, taking the linear ansanz used), though not as good as those obtained in this research.

Finally, let us compare our lattice against that obtained by *Han et al.* [43]

Han et al in their work introduced a completely new approach, however still based on *Bogdanov et al* [42] work.

They took our usual functional, (2.1), but instead of working in Cartesian coordinates as we did or parametrising magnetisation in $O(3)$ representation like *Bogdanov et al* [42] and *Kawaguchi et al*, [17] they introduced the spinor representation of

$$\vec{z} = \begin{pmatrix} z_1 \\ z_2 \end{pmatrix} = \begin{pmatrix} e^{-i\varphi}\cos\frac{\theta}{2} \\ \sin\frac{\theta}{2} \end{pmatrix} \tag{2.176}$$

that obeys $\vec{z}^{\dagger}\vec{z} = 1$ and then mapped the magnetisation via

$$\vec{M} = \vec{z}^{\dagger}\hat{\sigma}\vec{z}, \tag{2.177}$$

where $\hat{\sigma}$ is the Pauli matrix,

$$\hat{\sigma} = \sigma_x\hat{e}_x + \sigma_y\hat{e}_y + \sigma_z\hat{e}_z. \tag{2.178}$$

Ferromagnetic exchange term of the free energy functional density then becomes

$$\mathcal{F}_{ex} = \frac{1}{4}\sum_{\mu}(\partial_\mu M_\mu)\cdot(\partial_\mu M_\mu) = \sum_{\mu}(\partial_\mu\vec{z}^{\dagger})\cdot(\partial_\mu\vec{z}) - A_\mu^2 \tag{2.179}$$

with the vector potential,

$$A_\mu = -\frac{i}{2}\left[\vec{z}^\dagger \cdot (\partial_\mu \vec{z}) - (\partial_\mu \vec{z}^\dagger)\cdot \vec{z}\right], \tag{2.180}$$

that is associated with the magnetisation via

$$\frac{1}{2}\vec{M}\cdot\left(\partial_x \vec{M}\times\partial_y \vec{M}\right) = \partial_x A_y - \partial_y A_x. \tag{2.181}$$

The anisotropic term in this formulation turns into

$$\mathcal{F}_{DM} = \vec{M}\cdot\left(\nabla\times\vec{M}\right) = -2\vec{M}\cdot\vec{A} - i\vec{z}^\dagger\left(\hat{\sigma}\nabla\right)\cdot\vec{z} + i\left(\nabla\cdot\vec{z}^\dagger\right)\cdot\hat{\sigma}\vec{z}. \tag{2.182}$$

Then if we introduce

$$D_\mu = \partial_\mu - iA_\mu + i\kappa\sigma_\mu, \tag{2.183}$$

the total functional density becomes

$$\mathcal{F}\left[\vec{z}\right] = 2J\sum_\mu \left(D_\mu\vec{z}\right)^\dagger\cdot\left(D_\mu\vec{z}\right) - \vec{B}\cdot\vec{z}^\dagger\hat{\sigma}\vec{z}. \tag{2.184}$$

Saddle-point equation derived from the functional (2.184) with respect to $\vec{z}^\dagger$ is

$$2J\left(\nabla - i\vec{A} + i\kappa\hat{\sigma}\right)^2\vec{z} + 2iD\left(\vec{M}\cdot\nabla\right) + \left(\vec{B}\cdot\hat{\sigma}\right)\vec{z} = \lambda\vec{z}, \tag{2.185}$$

where λ is the Lagrange multiplier introduced in order to provide $\vec{z}^\dagger\vec{z} = 1$, just as in our case.

While turning to skyrmion lattice studies, the analogy with Abrikosov lattice was employed. With the aid of the Landau gauge,

$$\vec{A} = (0, Hx, 0), \tag{2.186}$$

magnetic length,

$$l_H = \frac{1}{\sqrt{H}}, \tag{2.187}$$

that acts as the correlation length, ξ, in Abrikosov solution, as well as the skyrmion lattice spacing through the condition of

$$l_x l_y = 2\pi l_H^2, \tag{2.188}$$

where $l_x = x_1 = a$ and $l_y = y_2 = \frac{\sqrt{3}}{2}a$ for a triangular lattice, get the Abrikosov-like solution for $\vec{z}$:

$$\vec{z}(x,y) = \sqrt{\frac{2l_x}{(1+d_0^2)l_H\sqrt{\pi}}}\sum_{j=-\infty}^{\infty} c_j e^{\frac{i2\pi jy}{l_y}}\begin{pmatrix} e^{-\frac{x_j^2}{2l_H^2}} \\ \frac{id_0\sqrt{2}x_j}{l_H}e^{-\frac{x_j^2}{2l_H^2}}\end{pmatrix}, \tag{2.189}$$

where

$$x_j = x + jl_x, \tag{2.190}$$

j is an integer, c_j is a coefficient that is 1 for even integers and i for odd integers on a triangular lattice and

$$d_0 = \frac{2\sqrt{2}\kappa l_H}{1 + 2\kappa^2 l_H^2 b + \sqrt{(1 + 2\kappa^2 l_H^2 b)^2 + 8\kappa^2 l_H^2}} \tag{2.191}$$

with

$$b = \frac{JB}{D^2} \tag{2.192}$$

and κ, J, B and D correspond to our definitions in section 2.3.1.

The lattice obtained by this method is demonstrated in Figure 2.28a.

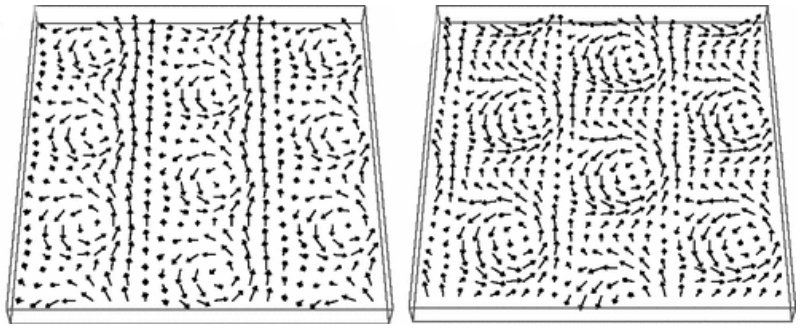

(a) Skyrmion lattice obtained with spinor decomposition (2.189).

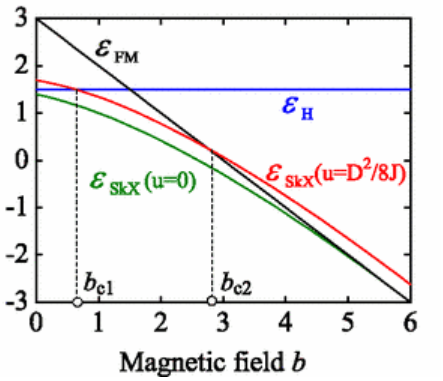

(b) Energies of different magnetic configurations against b for different values of Lagrange parameter, u.

Figure 2.28: Skyrmion lattice and energies obtained with spinor decomposition (2.189).

This method might look less intuitive than the others, though still does the job.

Notice, that *Han et al* had also predicted critical fields demonstrated in Figure 2.28b, but as they have not calculated any exact Lagrange multiplier, u, but fitted several values, their result is not to be taken as quantitatively exact and it does not pretend to be, in fact.

2.5.2 Comparison to Experimental Results

It was already mentioned above that our values of critical fields perfectly match those obtained by *Mochizuki*. [86] Let us also check how well do our other results correspond to something found experimentally.

A typical skyrmion lattice observed experimentally can be found in Figure 2.29.

By comparing results in Figure 2.29 with our lattice in Figure 2.7 conclude, that our model can be qualitatively confirmed by an experiment. In Figure 2.29 colour (brightness) indicates the direction of the magnetisation, hence spins; the black colour means that the spins are perpendicular to the plane, i.e. are pointing either upwards or downwards.

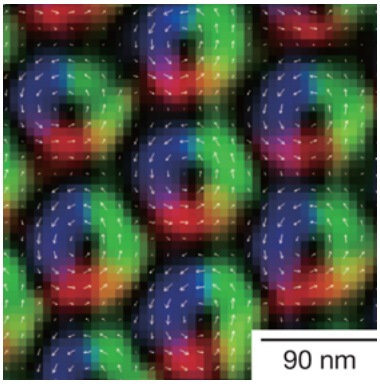

Figure 2.29: Skyrmion lattice structure observed experimentally in $Fe_{1-x}Co_xSi$ for a weak magnetic field ($50mT$). Colour scheme and arrows represent the magnetisation direction. [21]

2.6 Metastable Solutions

2.6.1 Expected Metastable Solutions

So far we have dealt with stable solutions only. However, it had been already mentioned that metastable solutions exist as well. We had even observed the evidence in Figure 2.17. Such metastable solutions are expected for a system with first order phase transitions. They are nothing more but continuations of the previous state in the region of another state just with higher energies. For example, as it can be seen from Figure 2.18, for $\beta < \beta_{c_1} = 0.46$ the system is in the helical state. But these are stable solutions. However, one can obtain metastable skyrmion solutions for $\beta < \beta_{c_1}$. Energy of these lattice solutions, obviously, is higher than the energy of helical solutions, as can be clearly seen from Figure 2.17, and the virial ratio is no longer equal to -2. An example of such a metastable solution is demonstrated in Figure 2.30a.

One can easily compare the system in Figure 2.30a with the system in Figure 2.20a to realise that they look pretty much alike. So conclude that the metastable skyrmion system in the region where a helix is a stable solution, i.e. in the helical region, is nothing more but the continuation of the skyrmion lattice solution for a lower field. This is also true for all the other metastable states of this kind and is justified by the free energy diagram in Figure 2.17. Another justification is the spacing of this metastable skyrmion state in the helical region demonstrated in Figure 2.31. We see that $a(\beta)$ is a perfect continuation of the spacing curve in the stable region. Curve in Figure 2.31 looks pretty much like that in Figure 2.27 taken from Bogdanov's work, [84] where he did not distinguish between stable and metastable states.

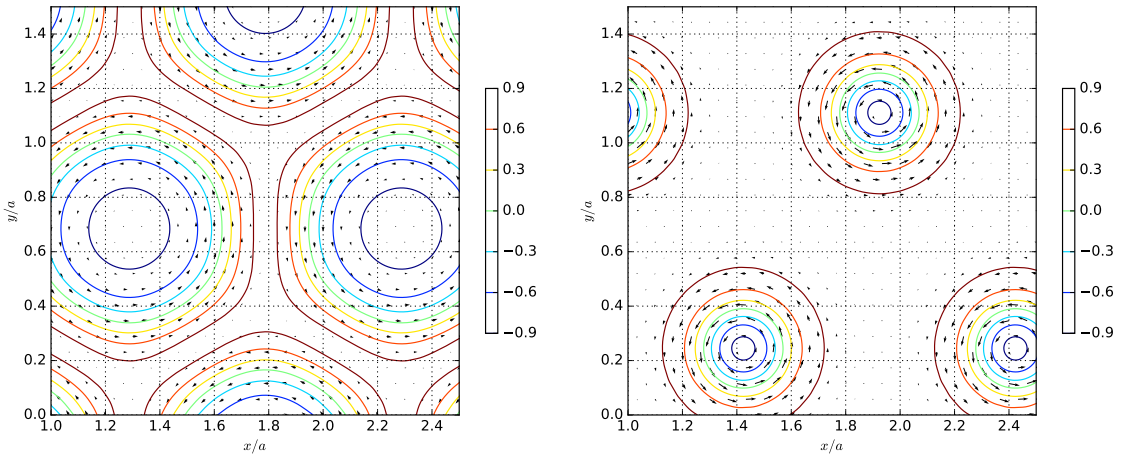

(a) Metastable lattice solution for a skyrmion system at $\beta = 0$ with $a = 4.13$.

(b) Metastable lattice solution for a skyrmion system at $\beta = 2$ with $a = 3.8$.

Figure 2.30: Metastable skyrmion lattice solutions.

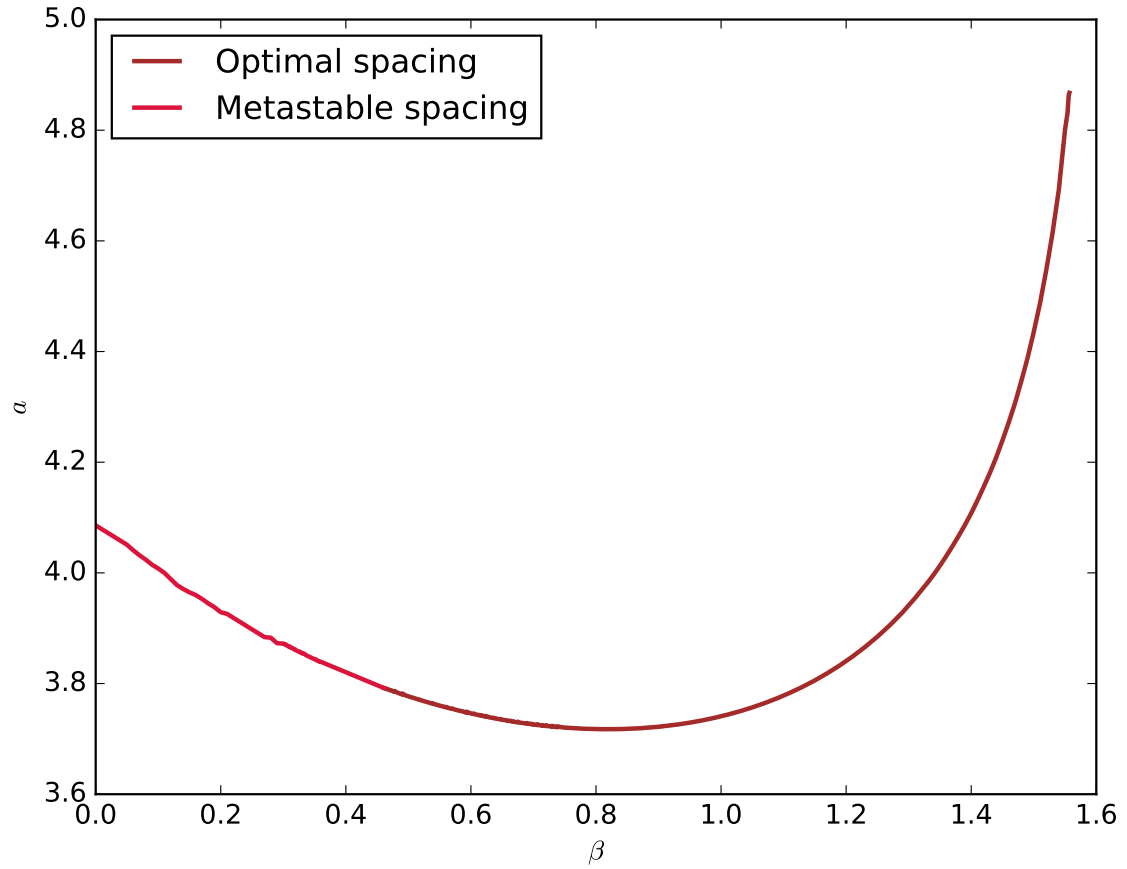

Figure 2.31: Skyrmion lattice spacing for a given β including that for a metastable region.

In fact, one can find a metastable skyrmion solution even for $\beta = 0$. Skyrmions in this case would be "fat", just like they are in proximity to the helix-skyrmion phase transition. Such a shape results from the fact that many spins tend to follow helical order, rather than the ferromagnetic one (DM-term dominates over the Zeeman term).

Eventually, one can find a metastable skyrmion system for $\beta > \beta_{c_2} = 1.56$. An example of such a lattice solution is demonstrated in Figure 2.30b. As one clearly observes from Figure 2.17, the energy of such a skyrmion system is higher than the energy of a ferromagnetic configuration, hence the solution is metastable, and from the comparison of the systems in Figure 2.30b and Figure 2.20b one concludes that they still look similar, hence the metastable skyrmion lattice in the ferromagnetic region is the continuation of the stable skyrmion lattice just with the energy that is not the lowest possible.

Numerically, we obtain these metastable solutions varying the initial guess (not to be confused with initial conditions) by using the converged result from a system with previous value of β and going in tiny steps in β. In this case we also do not seek condition (2.148) to be satisfied as it is a stable solution only that can fulfil it.

2.6.2 Unexpected Metastable Solutions

All this discussion of metastable solutions would have been useless and unnecessary (as the metastable states described in the previous section were expected and their existence was predictable), should not have we found a completely different type of skyrmion lattice that also happens to be a solution to equations (2.84) – (2.86), though the energy of the corresponding states is higher than the energy of typical stable lattice solutions and the virial relation (2.148) does not hold as well, i.e. $V \neq -2$ for these new states; though, for some of these states V is just slightly above or slightly below -2, but this is already enough to claim these states to be metastable. We call the new lattice observed to be a honeycomb lattice.

Free energy functional of these new metastable states (the golden line) along with the energies of other stable and metastable states is demonstrated in Figure 2.32. It is only slightly higher than the free energy functional of the stable configuration and while approaching β_{c_2} the difference between them becomes almost negligible.[13]

Figure 2.32 tells us that the free energy functional of honeycomb states is only slightly higher than the free energy of the states obeying triangular lattice. However, if for a stable triangular lattice we had a valid way of finding the optimal solution described in section 2.4.1 (the virial ratio), we have no such formulation for a metastable configuration (as the state cannot be optimal if it is metastable). So we need to rely on the minima of the free energy functional only. The corresponding plot of the free energy functional against the spacing for

[13]Other metastable honeycomb lattice states with higher energies have been also found, though are not demonstrated in Figure 2.32. The golden line in Figure 2.32 corresponds to the lowest values of the free energy functional calculated for honeycomb lattice states.

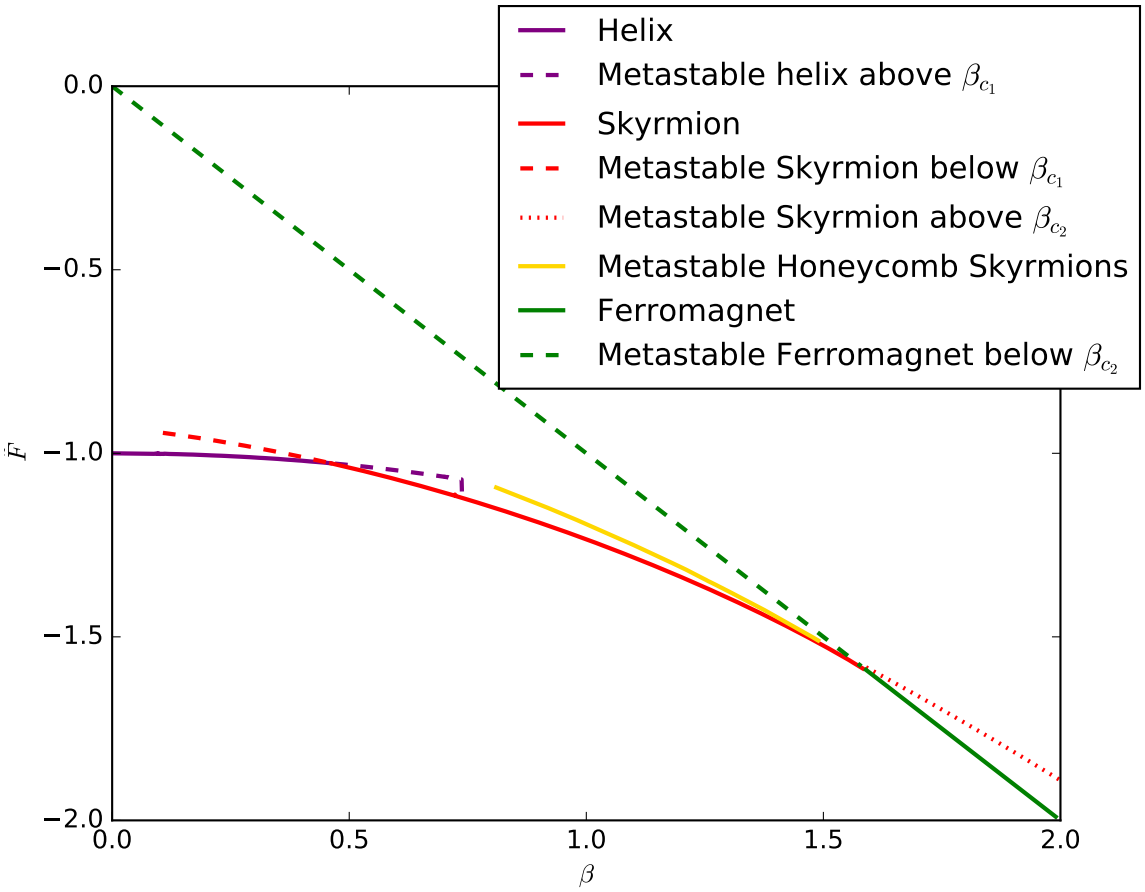

Figure 2.32: Free energy functional of a magnetic system in different regions including metastable honeycomb skyrmion lattice that is represented by a gold line. Red curve represents the optimal free energy for a skyrmion system, purple one stands for the helial system and green line is the free energy of a ferromagnetic system. Dashed lines of different colours correspond to metastable solutions of corresponding patterns.

a given β is demonstrated in Figure 2.33a.

The free energy functional is still shallow, though, as we cannot rely on the virial ratio anymore, we have to stick to the results obtained from the direct minimisation of the functional. We need to consider more points (configurations with different spacing), though, in order to obtain precise results. We also demonstrate the free energy functional against the spacing for fixed β for both triangular (optimal) and honeycomb lattices on the same plot to ensure that honeycomb solutions are actually metastable. This is demonstrated in Figure 2.33b. The value of the free energy functional that corresponds to the minima of the functional for a honeycomb configuration is higher than that for a triangular configuration. Another conclusion that can be drawn from Figure 2.33b is the fact that the optimal lattice spacing of a honeycomb lattice is a lot larger than the optimal lattice spacing of a triangular lattice.

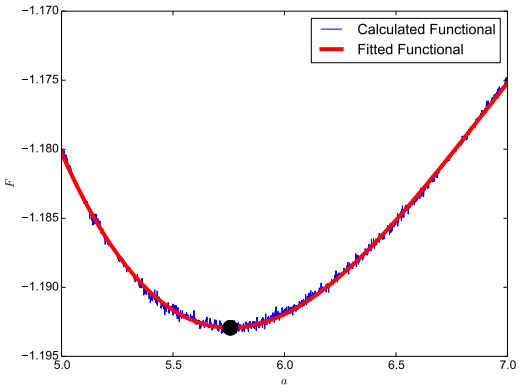

(a) Free energy functional of a honeycomb configuration against lattice spacing, a, for $\beta = 1.4$. The black dot indicates the minimal value of F.

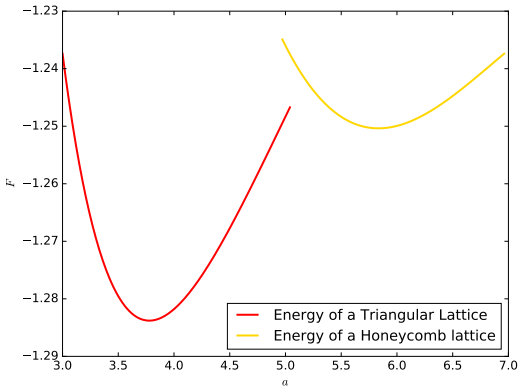

(b) Free energy functional of a honeycomb configuration along with the free energy functional of a triangular configuration against lattice spacing, a, for fixed $\beta = 1.1$.

Figure 2.33: Free energy functional of a honeycomb configuration against lattice spacing, a. In Figure 2.33b the red curve corresponds to the free energy of a triangular lattice, the golden curve corresponds to the honeycomb lattice. The minimal energy of the triangular configuration is smaller that the minimal energy of the honeycomb configuration, hence honeycomb solution is metastable. Notice that the optimal lattice spacing of a honeycomb lattice is a lot larger than the optimal spacing of a triangular lattice.

However, the fact that the free energy functional curve of the honeycomb lattice lies just above the free energy functional curve of a stable triangular lattice allows us to hope to stabilise it via some external effects and thus use it in our future research (see the following chapters). Also, especially in condensed matter physics, metastable phases sometimes can be observed and even exist in nature in some circumstances.

The magnetisation of the honeycomb lattice is demonstrated in Figure 2.34 and the spin configuration of the honeycomb lattice can be found in Figure 2.35. We notice that the skyrmions are no longer perfect circles as they used to be for the triangular lattice case. The curling pattern of M_x and M_y is preserved, though, as it depends on the Dzyaloshinksy-Moriya interaction only.

From Figure 2.34 one can yield two important conclusions:

- lattice spacing is no longer the distance between the centres of the nearest skyrmions, but the distance between the centres of honeycombs;
- a unit cell now contains exactly two skyrmions in oppose to the case of the triangular lattice where there has been exactly one skyrmion per unit cell.

One may think from the first glance, that it is impossible to obtain any but triangular lattice via the method we have used, as it was the triangular lattice we had imposed. But we

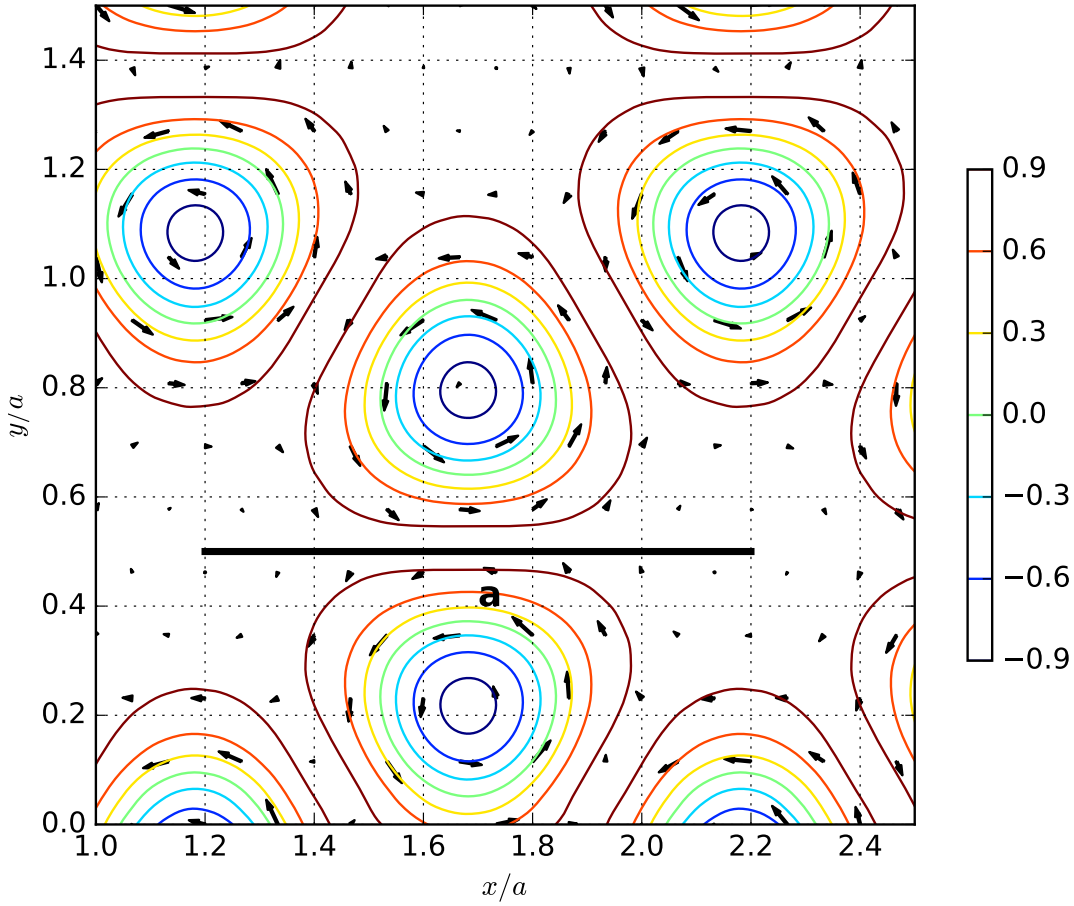

Figure 2.34: Metastable honeycomb lattice solution for a skyrmion system at $\beta = 1.2$ with $a = 4$. Lattice spacing, a, indicated in the figure is no longer the distance between the centres of the nearest skyrmions, but the distance between centres of honeycombs. Skyrmions themselves are not perfect circles as they used to be for the case of a trianguar lattice.

had actually imposed primitive cell vectors,

$$\vec{a}_1 = a\hat{e}_x \tag{2.193}$$

and

$$\vec{a}_2 = \frac{a}{2}\hat{e}_x + \frac{\sqrt{3}}{2}a\hat{e}_y, \tag{2.194}$$

that happen to coincide for both triangular and honeycomb lattices, so there is no contradiction. This can become clear if one considers a schematic representation of a honeycomb lattice given in Figure 2.36.

Comparing honeycomb lattice in Figure 2.36 with the triangular lattice in Figure 2.7 one realises that primitive lattice vectors are the same with the only difference: a honeycomb

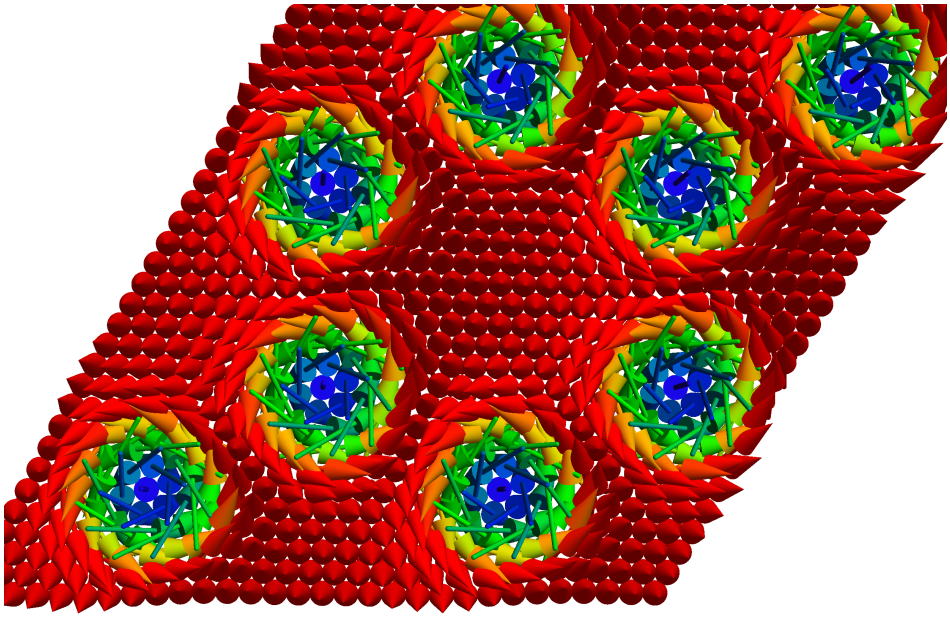

Figure 2.35: Honeycomb lattice spin configuration for a skyrmion system at $\beta = 1.$ with $a = 5.7$. Non-circular shape of skyrmions is confirmed.

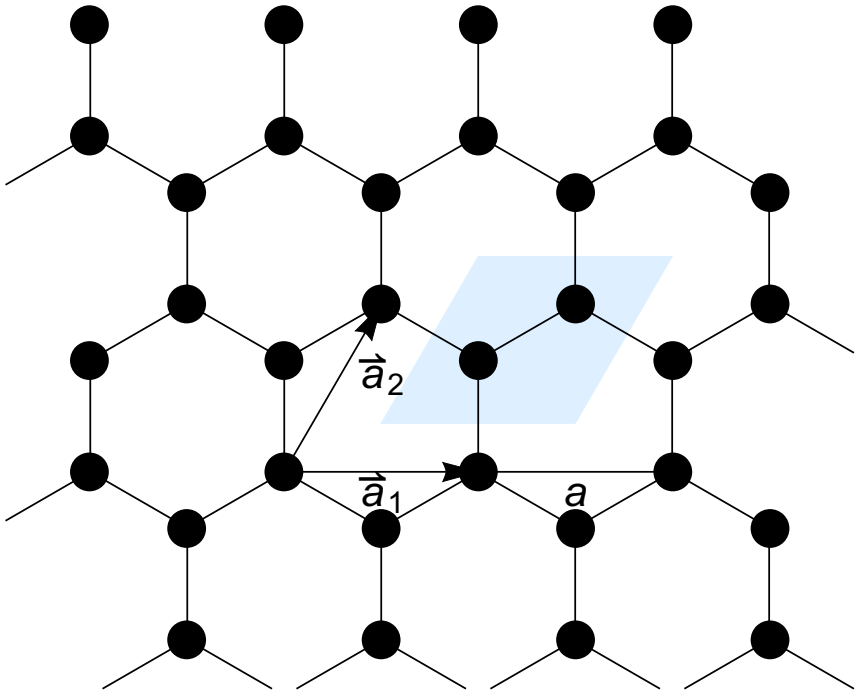

Figure 2.36: Sample honeycomb lattice with primitive lattice vetors $\vec{a}_1$ and $\vec{a}_2$ and lattice spacing a. A unit cell is depicted by a shaded parallelogram and contains exactly two vertices (skyrmions).

lattice unit cell would contain two vertices (in our case – skyrmions), while a unit cell of a triangular lattice contains only one vertex (skyrmion).

Let us compare unit cells of these two lattices directly – see Figure 2.37. Such a feature of honeycomb lattices would become extremely important in our future research, as the region between skyrmions – the region of the highest magnetisation, when all the spins are parallel to the field – is now localised by the honeycomb lattice in the periodic structure as well.

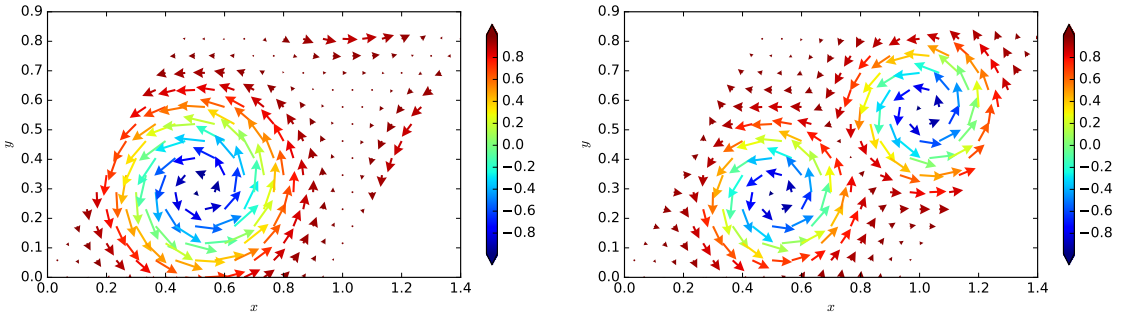

(a) A unit cell of a triangular skyrmion lattice at $\beta = 1.4$ with $a = 4$. There is exactly one skyrmion in the unit cell.

(b) A unit cell of a metastable honeycomb skyrmion lattice at $\beta = 1$ with $a = 4$. There are exactly two skyrmions in the unit cell.

Figure 2.37: Unit cells of triangular and honeycomb skyrmion lattices.

If we demonstrate the honeycomb lattice solutions in the different regions of β, just as we have done for the triangular lattice, we would realise that these are different from each other – see Figure 2.38, – though the difference is not as dramatic as it used to be for a triangular configuration. However, while moving towards β_{c_2}, the distance between skyrmions increases (the distance between skyrmions themselves, not the lattice spacing, as it not the same thing anymore, though the lattice spacing increases as well) and the ferromagnetic spin alignment becomes dominant.

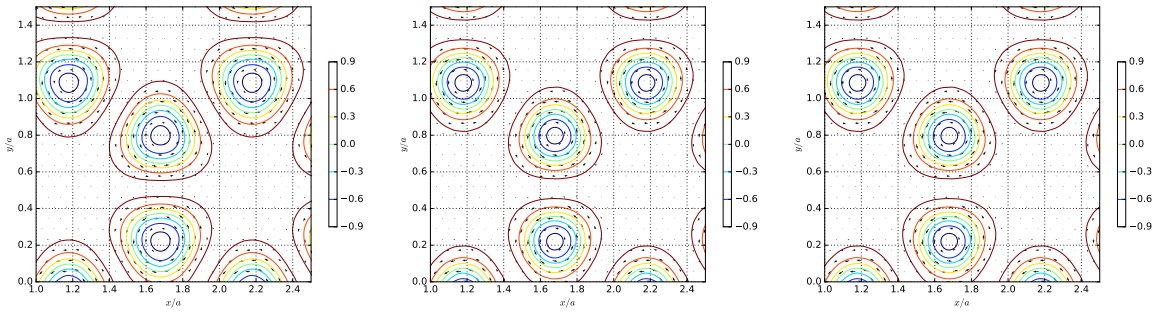

(a) Honeycomb lattice solution for a skyrmion system at $\beta = 1.$ with $a = 5.7$.

(b) Honeycomb lattice solution for a skyrmion system at $\beta = 1.25$ with $a = 6$.

(c) Honeycomb lattice solution for a skyrmion system at $\beta = 1.45$ with $a = 7.05$.

Figure 2.38: Honeycomb skyrmion lattice for different values of β.

Notice that the "optimal" lattice spacing – the one that corresponds to the minima of the free energy functional of a honeycomb lattice configuration – now is much larger than the optimal lattice spacing for a triangular system especially at larger values of an external field. We also see that by analogy with the stable case the lattice spacing is increasing with increasing β, and the radius of skyrmions is decreasing. Once again, this is related to the proximity of the ferromagnetic state and the fact that more spins would tend to align with the field.

2.6.3 Square Skyrmion Lattice

It had been predicted that skyrmions form triangular lattices in actual materials. [42] This was later confirmed by experimental evidence. [21] That is why we had imposed the triangular lattice in our calculations and defined primitive vectors in the corresponding way. So it was impossible to obtain a lattice that has different lattice vectors following the method introduced in section 2.3.2. However, one can impose a square lattice in a similar way by setting

$$\vec{R}_{vw} = (vx_s, wy_s)\,, \tag{2.195}$$

$$\vec{K}_{mn} = \frac{2\pi}{x_s y_s} \begin{pmatrix} my_s \\ nx_s \end{pmatrix}, \tag{2.196}$$

where $x_s = y_s = a$, that defines a square lattice, and v, w, m and n are dummy integers just as for the triangular or honeycomb lattice. All other assumptions we have done before (including the derivation of the virial ratio) remain unchanged as they do not depend on the lattice configuration. Skyrmion lattice obtained with such a definition of lattice vectors is demonstrated in Figure 2.39.

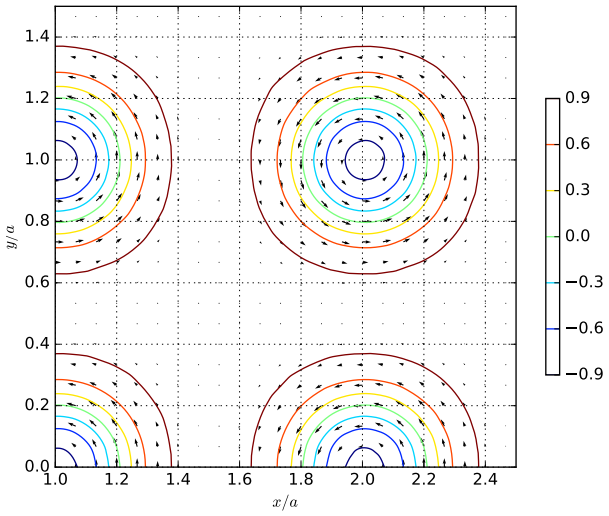

Figure 2.39: Square lattice solution for a skyrmion system at $\beta = 1.4$ with $a = 4$.

Let us now is to compare values of the free energy functional for triangular and square lattices (and honeycomb, in fact) to see which of them is actually energetically favourable. Such a comparison is demonstrated in Figure 2.40a.

We then see from Figure 2.40a that it is still a triangular lattice that is energetically more favourable than the others, though the difference in the free energy functional especially near β_{c_2} is very small – see Figure 2.40b for a better view – so one can even try to stabilise the square

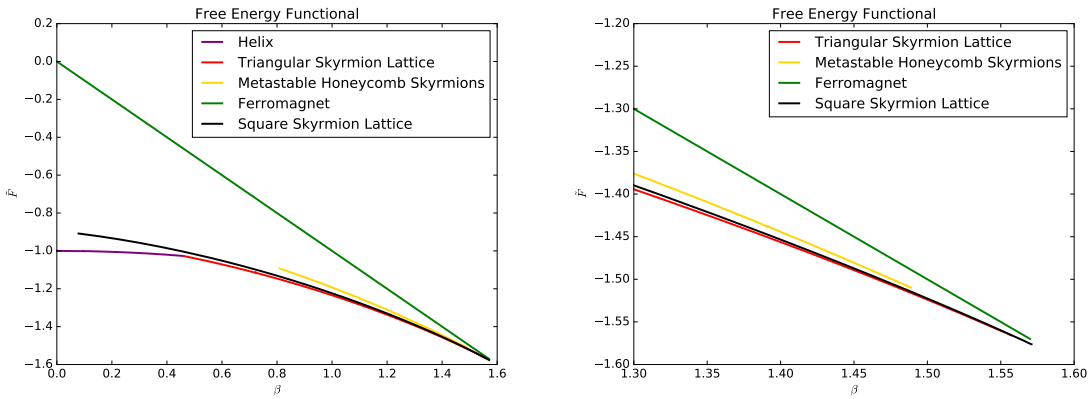

(a) Free energy functional of a magnetic system for different lattice configurations.

(b) Enlarged region near β_{c_2}.

Figure 2.40: Free energy functional of a magnetic system for different lattice configurations. Free energy functional of a triangular skyrmion lattice in represented by a Red curve, honeycomb skyrmion lattice – by a gold line, square skyrmion lattice – by a black line and a ferromagnetic configuration – by a green line.

skyrmion lattice experimentally! This is explained by the fact that it is the ferromagnetic region that is dominant near β_{c_2} for all three types of lattices (it can be seen from Figure 2.20b, Figure 2.38c and Figure 2.41b that the area between skyrmions near β_{c_2} is actually way larger than the area of skyrmions themselves), so there is in fact no much difference in the lattice configuration and then there is, again, no wonder, that at a point a pure ferromagnetic configuration dominates over all of them. One can, obviously, obtain metastable configurations of all the three types in the ferromagnetic region.

We can also see from Figure 2.41 that the difference in the configuration of our square lattice near β_{c_1} (Figure 2.41a) and β_{c_2} (Figure 2.41b) follows the same logic as that for triangular and honeycomb lattices: skyrmions are spatially large and lattice spacing is small near β_{c_1}, skyrmions are small and the lattice spacing is large near β_{c_2}. This is also confirmed by the optimal spacing plot demonstrated in Figure 2.42.

It is also notable that the numerical algorithm is way faster for the square lattice case than it is for a triangular or honeycomb lattice, so one may actually use it when investigating the region near β_{c_2} in order to save the computation time.

From all the survey done above one can conclude that skyrmion lattice becomes dilute near β_{c_2}, hence its configuration is not that crucial anymore.

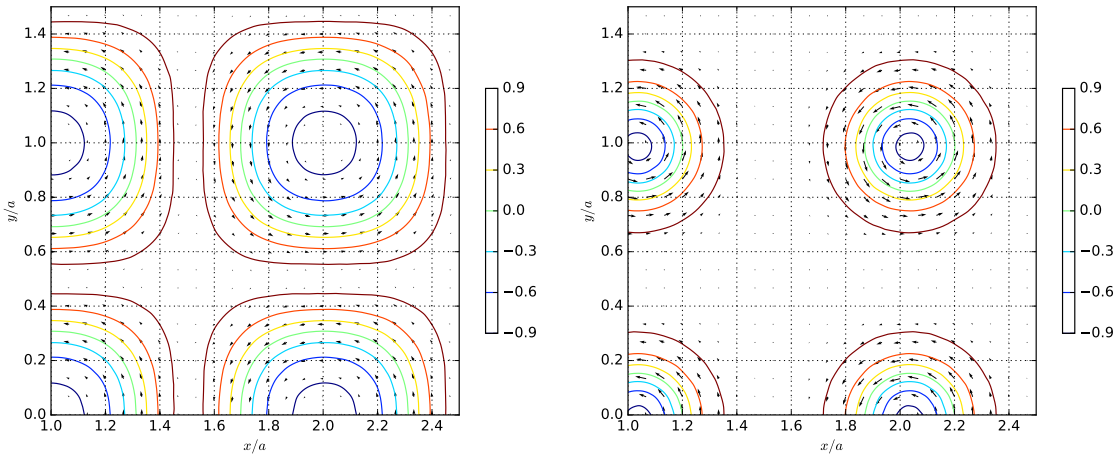

(a) Square lattice solution for a skyrmion system at $\beta = 0.461$ with $a = 3.58$.

(b) Square lattice solution for a skyrmion system at $\beta = 1.55$ with $a = 4.6$.

Figure 2.41: Square skyrmion lattice solutions for different values of β.

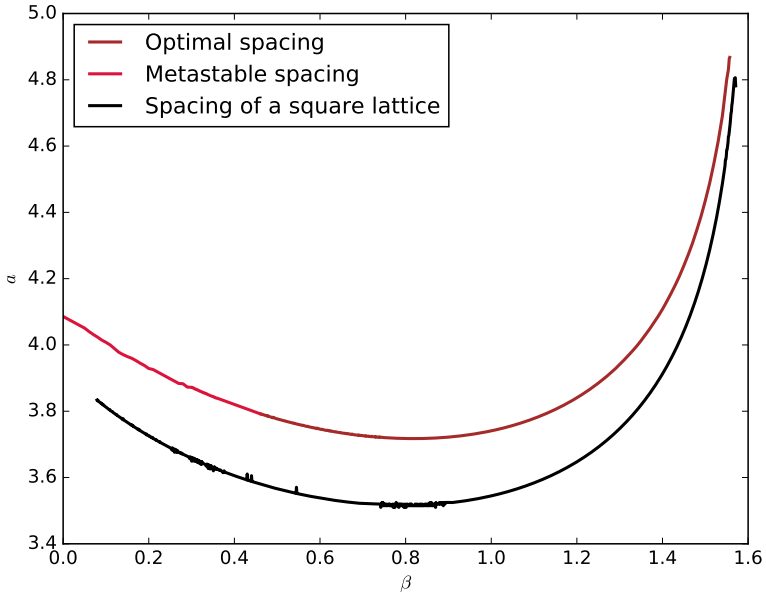

Figure 2.42: Optimal lattice spacing for triangular and square lattices compared. Brown and vinous curves represent lattice spacing for stable and metastable skyrmion lattices respectively, black curve stands for the lattice spacing of a square skyrmion lattice.

Chapter 3

Abrikosov Vortex Lattice in Type-II Superconductors

3.1 Basic Properties of Superconductors

Conductors are characterised by the presence of some particles that are free to move macroscopic distances inside an object (conductor). [87] For example, metals are good conductors because electrons are free to move between the atoms inside a metal. In metals there is also a lattice of positive ions, of course, but their movement is nothing but small oscillations about an equilibrium position, hence in general it does not contribute to the net current, or its effects are small. [87] Such a lattice generates the periodic potential. In the absence of an external electric field electrons are distributed in a free random motion interacting with the lattice as well as with each other. Once electric field is applied, electron movement becomes directed with respect to the electric force. But electrons, however, still may collide (resistivity) or pass their kinetic energy to the bulk of the metal (thermal dissipation). It is well-known that in normal metals resistance depends on temperature. A typical metal at low temperature has a T^2 behaviour leading to some finite resistivity at $T = 0$.

At low temperatures, though, some materials disobey this dependence: at a certain point their resistance suddenly drops to zero! [54] Such materials are called superconductors, as zero resistance implies infinite conductivity.

An important observation was done for mercury in 1911 by Heike Kamerlingh Onnes. [54] It was found that the resistivity does not actually decay towards zero at low temperatures continuously, but drops down to zero at some certain temperature, T_C. So the resistance in mercury (and many other materials, as it was found later) becomes zero even before $T = 0$! Such a phenomenon was called to be superconductivity. A threshold value for a current that can be carried without resistance was observed later in 1913. [88]

As it was observed, the resistivity in a perfect superconductor is zero, hence its conductivity,

σ, is infinite. Recall Ohm's law:

$$\vec{E} = \sigma \vec{J}. \tag{3.1}$$

The only possible way for Ohm's law to hold for a finite $\vec{J}$ and infinite σ is to maintain

$$\vec{E} = 0 \tag{3.2}$$

at all points inside a superconductor, so conclude that the supercurrent carries no electric field!

In 1933 Meissner and Ochsenfeld observed probably the most important feature of superconductors: they observed that a superconductor completely expels an external magnetic field, resulting in

$$\vec{B} = 0 \tag{3.3}$$

inside a superconductor. [57] Behaviour of magnetic field lines in presence of a superconductor is demonstrated in Figure 3.1.

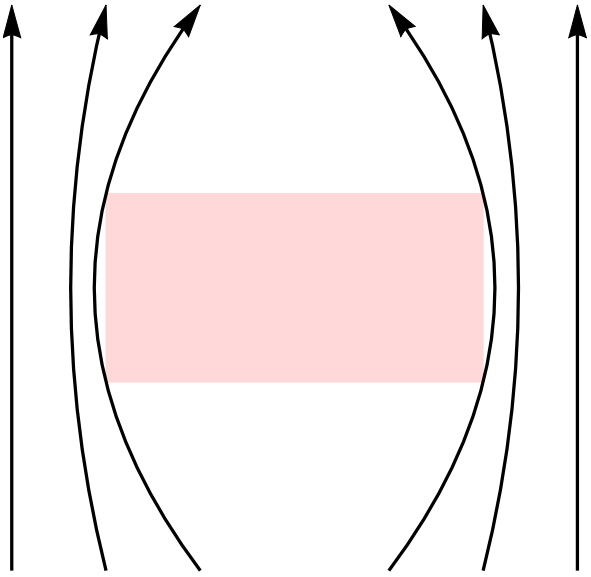

Figure 3.1: Meissner effect. Magnetic field lines are expelled by a superconductor that is held in its superconducting state, i.e. its temperature is $T < T_C$. The external field is rather small.

Notice that Meissner effect cannot be explained by the perfect conductivity of a superconductor only: $\vec{E} = 0$ implies

$$\frac{\partial \vec{B}}{\partial t} = 0, \tag{3.4}$$

as

$$\frac{\partial \vec{B}}{\partial t} = -\nabla \times \vec{E}, \tag{3.5}$$

but not $\vec{B} = 0$ on its own, so one concludes that the perfect expulsion of an external magnetic field is an essential property of a superconducting state. Nowadays a material is said to be superconducting if it demonstrates Meissner effect – this is the modern definition of a (type-I) superconductor. [9]

Nowadays, however, it is known that most materials still do not expel the external magnetic field completely: there is either an intermediate state on the boundary that allows decaying field to penetrate on some (small) depth [89] or even normal regions within a bulk superconductor – this phenomenon is related to type-II superconductors and is to be discussed later in details.

So far we have considered weak external magnetic fields only. However, large external field may destroy superconductivity as well as high temperature does. [88] Such a field is called the critical field, B_c. Microscopically, high external fields correspond to high energies that break Cooper pairs that are responsible for superconductivity and can be formed at low energies (hence low temperatures) only. Critical field is a function of temperature. [89] Empirically the dependence of the critical field on temperature was found to be

$$B_c(T) = B_c(0)\left[1 - \left(\frac{T}{T_C}\right)^2\right]. \tag{3.6}$$

An inverse conclusion is also correct: superconductivity might be destroyed by a strong current if it induces magnetic field greater than H_c that corresponds to B_c. [89]

Such a behaviour is true, however, for so-called type-I superconductors only. We will focus on type-II superconductors later.

3.2 Ginzburg-Landau Theory

3.2.1 Landau Theory of Second Order Phase Transition

It has been known since long ago that the same materials can exhibit different phases under certain conditions. Should one modify these conditions, the phase would change. Suppose a system is known to exhibit two different states at different temperatures (for example). If one of the two states is ordered and another is disordered, one can introduce an order parameter – the measure of the order in a system. [12] This order parameter would be zero in the disordered state and non-zero in the ordered state. If the temperature is involved in the phase transition, then there would always be T_c – critical temperature at which the transition occurs. In this case the state with $T > T_c$ is always disordered, whereas the state with $T < T_c$ is ordered.

One can distinguish two types of simple (isolated) phase transitions: so-called first order and second order phase transitions. [12] First order phase transition involves some latent heat, i.e. a system either adsorbs or emits some amount of energy. The most famous examples of

first order phase transitions are melting and boiling (evaporation).

Second order phase transition, in contrast to the first order one, has a major significance: the order parameter changes continuously, i.e. if the order parameter is zero in one state and non-zero in another, it has to be zero at the transition point as well.[1] This statement then leads to the conclusion that the order parameter is small in the ordered phase near the phase transition. [12] Famous examples of a second order phase transition are paramagnetic-ferromagnetic phase transition and normal-superconducting phase transition – the one we are particularly interested in. Mathematically, a point of the second order phase transition can be represented as a point characterised by some thermodynamic potential – the free energy. Moreover, at the transition point these potentials must be equal for both states. Together with an assumption of analyticity of Gibbs' free energy at the transition point, one can Taylor expand the free energy functional in terms of the order parameter, $\mathfrak{X}$: [12]

$$F_G = c_0 + c_1\mathfrak{X} + c_2\mathfrak{X}^2 + c_3\mathfrak{X}^3 + c_4\mathfrak{X}^4 + \dots. \tag{3.7}$$

However, any system tends to the minimal free energy configuration, so in equilibrium the order parameter must satisfy

$$\frac{\delta F_G}{\delta \mathfrak{X}} = 0, \tag{3.8}$$

leading to

$$c_1 + \left(2c_2 + 3c_3\mathfrak{X} + 4c_4\mathfrak{X}^2 + \dots\right)\mathfrak{X} = 0. \tag{3.9}$$

But in the normal state $\mathfrak{X} = 0$, hence the only way for the above equation to hold at any point including the transition point is to set

$$c_1 = 0. \tag{3.10}$$

Notice that one cannot stop at the odd term of the expansion, as in this case the minimal free energy would always tend to $-\infty$. The cubic term often vanishes, as otherwise the symmetry of the functional with respect to the order parameter is ruined. So need to set

$$c_3 = 0. \tag{3.11}$$

If the cubic term is present, the transition is always of the first order.

So for a general second order phase transition the free energy functional can be expanded as

$$F_G = c_0 + c_2\mathfrak{X}^2 + c_4\mathfrak{X}^4, \tag{3.12}$$

and one can truncate at order 4, so long as the corresponding coefficient is positive in order

[1] In order to avoid confusion, clarify that the symmetry of the system, hence the phase still changes spontaneously.

to make sure that the global minima exists, without any lose of physics. [11] The coefficient in from of the last term (fourth order term in our case, c_4) must be greater than zero in order to maintain $F_G \to \infty$ as $\mathfrak{X} \to \infty$. Notice also that the phase transition actually occurs when c_2 changes its sign from positive in the disordered phase to negative in the ordered one.

3.2.2 Ginzburg-Landau Functional

At low temperatures all particles tend to their ground states. For quantum systems this state can be described by a macroscopic wave function that is the same for all the particles sharing the state. This macroscopic wave function would act as an order parameter for a normal-superconducting phase transition, as it is zero in the normal state and non-zero in the superconducting state.[2] [90]

For a normal-superconducting phase transition define the order parameter to be [90]

$$\mathfrak{X} = \psi = |\psi| e^{i\theta}, \tag{3.13}$$

where θ is the phase of the macroscopic wave function, leading to

$$\mathfrak{X}^2 = |\psi|^2, \tag{3.14}$$

$$\mathfrak{X}^4 = |\psi|^4, \tag{3.15}$$

with $|\psi|^2 = \psi\psi^*$, as usual for complex quantities.

Notice that as $\psi = \psi(\vec{r})$, it might be convenient sometimes to work with the free energy functional density, $\mathcal{F}$, instead of the functional itself. So the free energy functional density of a free superconductor is

$$\mathcal{F} = \alpha|\psi|^2 + \frac{\beta}{2}|\psi|^2 + \frac{\hbar^2}{2m}|\nabla\psi|^2, \tag{3.16}$$

where α and β are phenomenological Ginzburg-Landau constants and we add the kinetic term to the phase transition term. So the free energy functional per unit area is then

$$F = \int \mathcal{F}\frac{d^2r}{A}, \tag{3.17}$$

for a system that does not exhibit any z-dependence, i.e. for a system with $\vec{r} = (x, y)$.[3]

[2] It is macroscopic wave function that is zero in normal state. Some ground state wave function still exists.

[3] This is not a general requirement, though. Derivations of Ginzburg-Landau equations that we are about to demonstrate would be valid for any arbitrary $\vec{r}$. We assume $\vec{r} = (x, y)$ in order to be consistent with the Abrikosov solution that is to follow.

In the presence of a magnetic field, Ginzburg-Landau functional density is modified to [90]

$$\mathcal{F} = \alpha|\psi|^2 + \frac{\beta}{2}|\psi|^2 + \frac{\left|\left(-i\hbar\nabla - q\vec{A}\right)\psi\right|^2}{2m} + \frac{|\vec{B}|^2}{2\mu_0}, \tag{3.18}$$

where the last term corresponds to the energy of the magnetic field and $\vec{B} = \nabla \times \vec{A}$ with $\vec{A}$ being the vector potential.[4]

N.B.: for a superconductor m and q are effective mass and charge respectively, i.e. $m = 2m_e$ and $q = 2e$, where m_e is the mass of an electron and e is the electron charge.

3.2.3 Ginzburg-Landau Equations

Let us now recall that a system would always tend to the configuration of the minimal free energy, hence minimise the functional (3.18) with respect to ψ[5] and $\vec{A}$.

The variation of the functional with respect to ψ^* in absence of an external field (i.e. in the simplest case of $\vec{A} = 0$) gives us

$$-\frac{\hbar^2}{2m}\nabla^2\psi + \alpha\psi + \beta\psi|\psi|^2 = 0. \tag{3.20}$$

Equation (3.20) can be solved analytically. Consider a 1D case with the interface between normal and superconducting states situated at $x = 0$. The wave function for such a system is found to be[6]

$$\psi(x) = \sqrt{\frac{|\alpha|}{\beta}}\,\tanh\frac{x}{\sqrt{2}\,\xi}, \tag{3.21}$$

where ξ is the coherence length defined as

$$\xi^2 = \frac{\hbar^2}{2m|\alpha|}, \tag{3.22}$$

and this solution is demonstrated in Figure 3.2.

[4] In general, however, Ginzburg-Landau functional density is written as

$$\mathcal{F}_s = \mathcal{F}_n + \alpha|\psi|^2 + \frac{\beta}{2}|\psi|^2 + \frac{\left|\left(-i\hbar\nabla - q\vec{A}\right)\psi\right|^2}{2m} + \frac{\left(\vec{B} - \mu_0\vec{H}\right)^2}{2\mu_0}, \tag{3.19}$$

where $\mathcal{F}_s$ is the energy density of a superconducting state, $\mathcal{F}_n$ is the energy density of a normal state and $\vec{H}$ stands for the magnetic field intensity that is the same as for an external field, hence constant for a uniform field. We have defined $\mathcal{F} = \mathcal{F}_s - \mathcal{F}_n$ for convenience. We also omit the constant term that corresponds to an external field, as we are going to find Euler-Lagrange equations for this functional (that would become the famous Ginzburg-Landau equations), hence the constant terms would drop out.

[5] ψ^* in fact.

[6] See Appendix B.5 for the full derivations and solution.

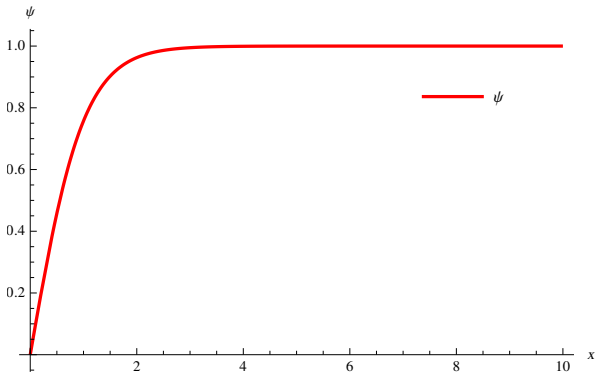

Figure 3.2: Order parameter of a 1D free superconductor for $T < T_C$. Suppose that the interface with the normal state is located at $x = 0$.

In presence of some non-zero magnetic field equation (3.20) modifies to

$$\frac{\delta \mathcal{F}}{\delta \psi^*} = \frac{\left(-i\hbar\nabla - q\vec{A}\right)^2}{2m}\psi + \alpha\psi + \beta|\psi|^2\psi = 0. \tag{3.23}$$

Now let us vary the functional (3.18) with respect to $\vec{A}$. The outcome is the second Ginzburg-Landau equation:[7]

$$\frac{i\hbar q}{2m}\left(\psi^*\nabla\psi - \psi\nabla\psi^*\right) + \frac{q^2}{m}|\psi|^2\vec{A} = \vec{J}_s. \tag{3.24}$$

3.2.4 Flux quantisation

Let us work with the second Ginzburg-Landau equation a bit. Define the macroscopic wave function through the density, ν:

$$|\psi|^2 = \psi\psi^* = \nu, \tag{3.25}$$

then

$$\psi = \sqrt{\nu}\, e^{i\theta}, \tag{3.26}$$

and

$$\psi^* = \sqrt{\nu}\, e^{-i\theta}, \tag{3.27}$$

where $\theta = \theta(\vec{r})$, hence

$$\psi^*\nabla\psi - \psi\nabla\psi^* = i\nu\nabla\theta + i\nu\nabla\theta = 2i\nu\nabla\theta. \tag{3.28}$$

[7] Once again, consult with Appendix B.5 for the detailed derivation.

Substitute this result in (3.24) to get:

$$-\frac{q\hbar}{m}\nu\nabla\theta + \frac{q^2}{m}\nu\vec{A} = \vec{J}_s. \tag{3.29}$$

Now take the integral of both sides around a closed contour:

$$\oint \left[\frac{q^2}{m}\nu\vec{A} - \frac{q\hbar}{m}\nu\nabla\theta\right]\vec{dl} = \oint \vec{J}_s \cdot \vec{dl} \tag{3.30}$$

and notice that q, m, ν and $\hbar$ are constants and the integral of the current along the closed loop is zero:

$$\oint \vec{J}_s \cdot \vec{dl} = 0.^8 \tag{3.31}$$

From Stokes' theorem it follows that

$$\oint \vec{A} \cdot \vec{dl} = \int \left(\nabla \times \vec{A}\right) \cdot \vec{dS} = \int \vec{B} \cdot \vec{dS} = \Phi \tag{3.32}$$

– magnetic flux.

Integral of the gradient part then follows from the gradient theorem (fundamental theorem of calculus for line integrals):

$$\oint \nabla\theta \cdot \vec{dl} = \lim_{\vec{r}_1 \to \vec{r}_2} \{\theta(\vec{r}_2) - \theta(\vec{r}_1)\} = 2\pi n, \tag{3.33}$$

as we integrate along a closed path and the shape of the path does not matter; n is an integer. Thus finally get an expression for the magnetic flux[9]

$$\Phi = 2\pi n\frac{\hbar}{q} = n\frac{h}{q} = n\Phi_0, \tag{3.34}$$

where Φ_0 is known as the flux quanta. This is an important result to remember for the future.

3.2.5 Ginzburg-Landau Parameters

Ginzburg-Landau theory introduces two important lengths scales. We have already met one of them in section 3.2.3: it was ξ, coherence length, that works as an indicator of a typical length scale of the variation of the order parameter within a superconductor. Coherence length is defined as

$$\xi = \frac{\hbar}{\sqrt{2m|\alpha|}}. \tag{3.35}$$

[8] In general this might not be true. In this case we would label the integral to be the vortex strength and speak about the fluxoid quantisation. [89]

[9] Or fluxoid if $\oint \vec{J}_s \cdot \vec{dl} \neq 0$.

Similar scale – the one that allows the variation – exists for the magnetic field as well. This is the penetration depth mentioned in section 3.1. It can be derived from the simplified second Ginzburg-Landau equation to be

$$\lambda_{GL} = \sqrt{\frac{m\beta}{q^2|\alpha|\mu_0}}. \tag{3.36}$$

Both ξ and λ_{GL} have dimensions of length. The are demonstrated schematically in Figure 3.3 for a typical type-I superconductor.

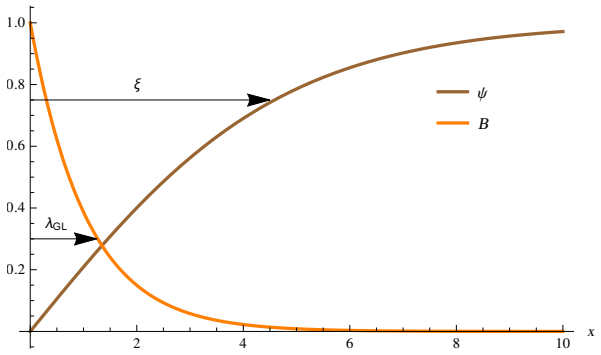

Figure 3.3: The spatial distribution of the order parameter and the magnetic field at the boundary between a superconducting and a normal state. Coherence length, ξ, and penetration depth, λ_{GL}, are indicated in the superconducting state. Notice that for a type-I superconductor $\xi > \lambda_{GL}$.

Another important quantity is the ratio of λ_{GL} and ξ – Ginzburg-Landau parameter, κ_{GL}:

$$\kappa_{GL} = \frac{\lambda_{GL}}{\xi} = \sqrt{\frac{2m^2\beta}{\hbar^2 q^2 \mu_0}}. \tag{3.37}$$

κ_{GL} would become extremely important soon enough.

3.2.6 Dimensionless Form of Ginzburg-Landau Equations

We would apply numerical analysis to superconducting vortices as well as we did for skyrmions, hence let us now introduce some dimensionless quantities in order to make our Ginzburg-Landau functional and equations dimensionless. We would widely use ξ, λ_{GL} and κ_{GL} defined in the previous section.

It is usual for a superconducting system to scale the coordinates with λ_{GL}, that is a measure of length itself. We would start off with the dimensional coordinates scaled with λ_{GL}

and hence scale all other dimensional quantities. By defining the dimensionless coordinate,

$$\vec{\mathsf{X}} = \frac{\vec{r}}{\lambda_{GL}} = \vec{r}\sqrt{\frac{q^2|\alpha|\mu_0}{m\beta}}, \tag{3.38}$$

obtain

$$\left(-\frac{i}{\kappa_{GL}}\nabla - \vec{A}\right)^2 \psi + \psi + |\psi|^2\psi = 0, \tag{3.39}$$

$$\vec{i} = -\frac{i}{2\kappa_{GL}}\left(\psi^*\nabla\psi - \psi\nabla\psi^*\right) - |\psi|^2\vec{A}, \tag{3.40}$$

where ψ, $\vec{A}$ and $\vec{i}$ are now all dimensionless and the only material-specific parameter involved is the dimensionless κ_{GL} – the Ginzburg-Landau parameter.

3.3 Type-II Superconductors

The main feature learnt about superconductors was their ability to completely expel magnetic field. This, however, appeared not to be the general truth. Some superconductors demonstrate an ability to be penetrated by a magnetic field, though still remain superconducting. Such materials are called to be type-II superconductors. [90]

It was Lev Shubnikov who discovered type-II superconductors experimentally and it was Alexei Abrikosov who first described them theoretically. [63] Before Abrikosov Ginzburg-Landau theory was applied to superconductors with

$$\kappa_{GL} < \frac{1}{\sqrt{2}} \tag{3.41}$$

only. Abrikosov, however, showed that all materials with Ginzburg-Landau parameter

$$\kappa_{GL} > \frac{1}{\sqrt{2}} \tag{3.42}$$

are in fact type-II superconductors and developed an extension of Ginzburg-Landau theory that holds for these values of κ_{GL}.

So one can say that Meissner-Normal phase transition in type-II superconductors is not instant – there is a region – Abrikosov phase (sometimes referred to as the *vortex phase* or *Shubnikov phase*) – in between. This statement also yields existence of two critical fields: the lower critical field, B_{c_1}, corresponding to Meissner-Abrikosov phase transition and the upper critical field, B_{c_2}, corresponding to Abrikosov-normal phase transition. Clearly, both B_{c_1} and B_{c_2} depend on temperature, and there are no phase transitions beyond T_c. [91] The phase diagram for a type-II superconductor is demonstrated in Figure 3.4.

Though type-II superconductors allow magnetic field to penetrate, their existence does not

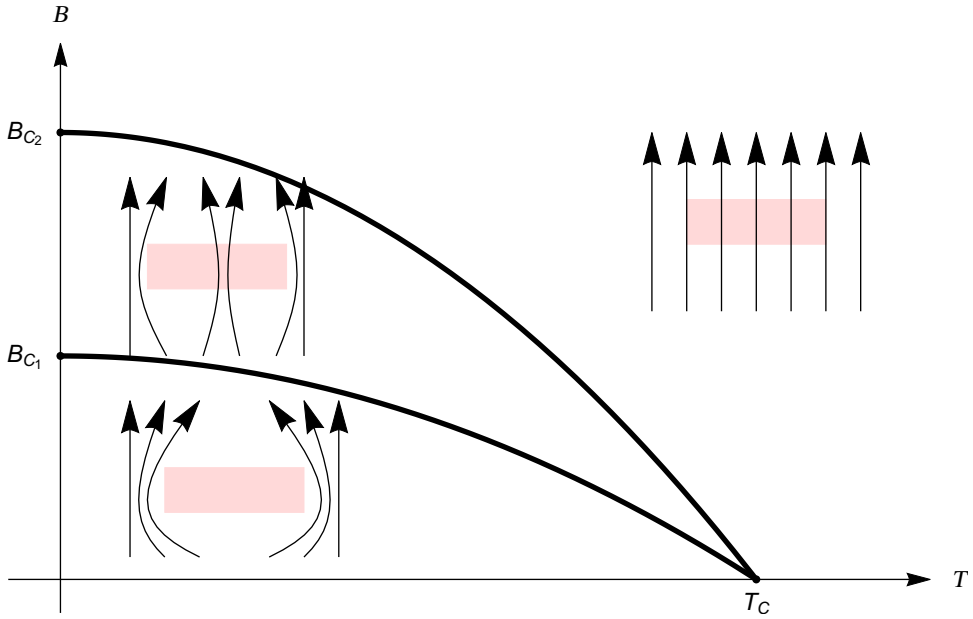

Figure 3.4: Phase diagram for a type-II superconductor demonstrating the dependence of critical fields on temperature. This diagram also shows the behaviour of magnetic field lines with respect to the material in different phases. In the Meissner phase (below B_{c_1}) field lines are completely expelled by a superconductor; in the Abrikosov phase (between B_{c_1} and B_{c_2}) field lines penetrate the superconductor, in certain places only, though; in the normal phase field lines penetrate the sample everywhere as it is no longer superconducting.

violate the general theory of superconductivity. Following this argument, Abrikosov proposed existence of some small non-superconducting domains inside a superconductor. [63] So the flux is carried through these domains, being expelled by a superconducting part. Keeping in mind that the sample tends to split onto normal and superconducting domains in the best possible (energetically most optimal) way, it was later established that such regions typically have cylindrical-like shape, projected to circles – vortices – in 2D, that form a triangular lattice – such a configuration corresponds to the minima of the free energy as in the case of a triangular lattice the distance between vortices is the largest possible, as the triangular lattice is in general the best-packed one in 2D. [65] It was then determined that every single vortex carries exactly one flux quanta. [63] It is known that the flux is quantised, as we derived it in section 3.2.4,

$$\Phi = n\Phi_0. \tag{3.43}$$

For a vortex we take $n = 1$, as any other configuration would lead to agglutinate vortices near the upper critical field; such a conclusion arises from the fact that we would need to minimise the free energy, and this would anyway lead to the narrowest possible vortex, i.e. $n = 1$; in addition to that, it is easier to form a little vortex rather than the large one, so small fields near the lower critical field would correspond to $n = 1$ vortices only. [92]

It is then trivial that inside a normal region the order parameter, ψ, is zero, as we are still within the limits of the Landau theory of phase transitions. However, the order parameter does not jump down to zero on the N-S boundary, though varies continuously over the vortex. We can define a so-called vortex core of radius $\sim \xi$ – the radius of change of the order parameter from zero to its finite superconducting value. Rate of change of B is a lot larger, however, of order λ_{GL}. [91]

Notice that in contrast to type-I superconductors in type-II superconductors λ_{GL} is typically larger than ξ. This is demonstrated in Figure 3.5.

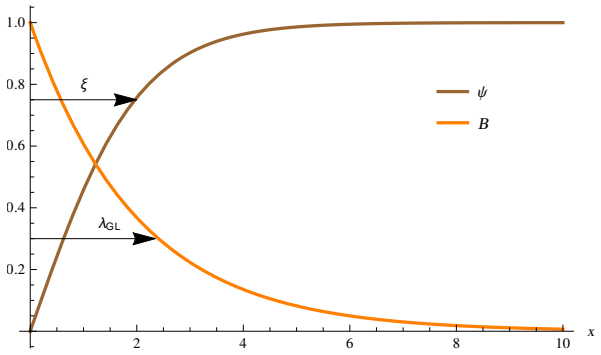

Figure 3.5: The spatial distribution of the order parameter and the magnetic field for a type-II superconductor. Coherence length, ξ, and penetration depth, λ_{GL}, are indicated in the superconducting state. λ_{GL} is greater than ξ.

3.4 Abrikosov Solution

We had already mentioned that it was Alexei Abrikosov who first described type-II superconductors theoretically. In this section we would demonstrate Abrikosov's solution of the first Ginzburg-Landau equation that made him a Noble prize winner.

Let us recall Ginzburg-Landau functional density for a superconductor in the magnetic field that is

$$\mathcal{F} = \alpha|\psi|^2 + \frac{\beta}{2}|\psi|^4 + \frac{\left|\left(-i\hbar\nabla - q\vec{A}\right)\psi\right|^2}{2m} + \frac{|\vec{B}|^2}{2\mu_0}. \tag{3.44}$$

The first Ginzburg-Landau equation in presence of an external magnetic field is then

$$\frac{\left(-i\hbar\nabla - q\vec{A}\right)^2}{2m}\psi + \alpha\psi + \beta|\psi|^2\psi = 0, \tag{3.45}$$

which can be modified to [90]

$$-\frac{\hbar^2}{2m}\left(\nabla+\frac{iq}{\hbar}\vec{A}\right)^2\psi(\vec{r})+\left(\alpha+\beta|\psi|^2\right)\psi(\vec{r})=0. \tag{3.46}$$

Now assume

$$\vec{B}=(0,0,B)\,, \tag{3.47}$$

with $B=const$, and consider the corresponding Landau gauge:

$$\vec{A}=(0,xB,0)\,, \tag{3.48}$$

then the kinetic term gets expanded as

$$\left(\nabla+\frac{iq}{\hbar}\vec{A}\right)^2=\nabla^2+\frac{2iq}{\hbar}xB\frac{\partial}{\partial y}-\frac{q^2}{\hbar^2}x^2B^2. \tag{3.49}$$

Dropping off the cubic term, [63] the first Ginzburg-Landau equation becomes:

$$-\frac{\hbar^2}{2m}\left(\nabla^2+\frac{2iq}{\hbar}xB\frac{\partial}{\partial y}-\frac{q^2}{\hbar^2}x^2B^2\right)\psi+\alpha\psi=0. \tag{3.50}$$

As we work in the superconducting region, we are not interested in the trivial solution of $\psi=0$. This also yields the fact that α is negative, hence $\alpha=-|\alpha|$, as it is conventional for a superconducting state.

Introduce the cyclotron frequency:

$$\omega=\frac{qB}{m}, \tag{3.51}$$

for convenience, so the first Ginzburg-Landau equation transforms to

$$\left(-\frac{\hbar^2}{2m}\nabla^2-i\hbar\omega x\frac{\partial}{\partial y}+\frac{m\omega^2}{2}x^2\right)\psi=|\alpha|\psi. \tag{3.52}$$

Notice that in this chapter we consider a 2D system, not a 3D that is just invariant in z-direction, and $\vec{A}=\vec{A}(x)$ only. So one can introduce[10]

$$\psi(\vec{r})=e^{ik_y y}f(x), \tag{3.53}$$

[10]We notice the mathematical similarity with the Schrödinger equation for a simple harmonic oscillator. Modify the equation for this correspondence to become obvious. This is a standard technique when dealing with some quantum systems, for example, Landau levels (see Appendix B.6).

then the gradient term is expanded as

$$\nabla^2\psi(\vec{r}) = -k_y^2\psi(\vec{r}) + \frac{d^2f}{dx^2}e^{ik_y y}, \tag{3.54}$$

and the derivative in y-direction is nothing more but

$$\frac{\partial}{\partial y}\psi(\vec{r}) = ik_y\psi(\vec{r}), \tag{3.55}$$

which leads to

$$\frac{\hbar^2k_y^2}{2m}f(x) - \frac{\hbar^2}{2m}\frac{d^2f}{dx^2} + \hbar\omega x k_y f(x) + \frac{m\omega^2}{2}x^2 f(x) = |\alpha|f(x), \tag{3.56}$$

as we had cancelled $e^{i(k_y y + k_z z)}$ term out.

Rearrange:

$$-\frac{\hbar^2}{2m}\frac{d^2f}{dx^2} + \left(\hbar\omega x k_y + \frac{m\omega^2}{2}x^2\right)f(x) = \left(|\alpha| - \frac{\hbar^2k_y^2}{2m}\right)f(x). \tag{3.57}$$

Define

$$x_0 = -\frac{\hbar k_y}{m\omega}, \tag{3.58}$$

then

$$\hbar\omega x k_y + \frac{m\omega^2}{2}x^2 = \frac{m\omega^2}{2}(x - x_0)^2 - \frac{m\omega^2}{2}x_0^2, \tag{3.59}$$

so the equation (3.52) becomes

$$-\frac{\hbar^2}{2m}\frac{d^2f}{dx^2} + \left(\frac{m\omega^2}{2}(x - x_0)^2 - \frac{m\omega^2}{2}x_0^2\right)f(x) = \left(|\alpha| - \frac{\hbar^2k_y^2}{2m}\right)f(x). \tag{3.60}$$

Notice that

$$\frac{m\omega^2}{2}x_0^2 = \frac{\hbar^2k_y^2}{2m}, \tag{3.61}$$

hence can drastically simplify equation (3.52) to

$$-\frac{\hbar^2}{2m}\frac{d^2f}{dx^2} + \frac{m\omega^2}{2}(x - x_0)^2 f(x) = |\alpha|f(x), \tag{3.62}$$

which looks extremely similar[11] to the Schrödinger equation for a shifted simple harmonic oscillator. Then one can use this analogy in order to obtain a solution of

$$\left(n + \frac{1}{2}\right)\hbar\omega = |\alpha|, \tag{3.63}$$

[11] In terms of its mathematical form, not physical meaning.

for "energies" and

$$f(x) = \frac{1}{\sqrt{2^n n!}} \left(\frac{m\omega}{\pi\hbar}\right)^2 e^{-\frac{m\omega(x-x_0)^2}{2\hbar}} \mathtt{H}_n(\sqrt{\frac{m\omega}{\hbar}}\, x), \tag{3.64}$$

for wave functions, where $\mathtt{H}_n$ are Hermite polynomials (see Appendix A.3).

For the ground state one has $n = 0$, $k_z = 0$, so

$$\mathtt{H}_0 = 1, \tag{3.65}$$

$$f(x) = Ce^{-\frac{m\omega(x-x_0)^2}{2\hbar}} = Ce^{-\frac{2m|\alpha|(x-x_0)^2}{\hbar}} = Ce^{-\frac{(x-x_0)^2}{\xi^2}}, \tag{3.66}$$

where

$$C = \left(\frac{m\omega}{\pi\hbar}\right)^2 \tag{3.67}$$

and

$$\xi = \sqrt{\frac{\hbar}{2m|\alpha|}} \tag{3.68}$$

is the Ginzburg-Landau coherence length.

Hence the full solution is written as

$$\psi(\vec{r}) = Ce^{ik_y y} e^{-\frac{(x-x_0)^2}{\xi^2}}, \tag{3.69}$$

as $\vec{r} = (x, y, 0)$, yet there is no z-dependence.

But this is not the end of the story. Now employ the periodic lattice conditions:

$$k_x = \frac{2\pi}{L_x} l, \tag{3.70}$$

$$k_y = \frac{2\pi}{L_y} j, \tag{3.71}$$

where l and j are integers and L_x and L_y are periods in x and y directions respectively.

An important property of an Abrikosov vortex is the fact that it carries exactly one flux quanta. Recall:

$$\Phi_0 = \int \vec{B} \cdot d\vec{S}, \tag{3.72}$$

but $\vec{B} = (0, 0, B)$ and $B = const$, hence we are left with

$$\int dS = \frac{\Phi_0}{B}. \tag{3.73}$$

For a triangular lattice one knows that

$$\int dS = S = L_x L_y, \tag{3.74}$$

hence

$$L_x L_y = \frac{\Phi_0}{B}. \tag{3.75}$$

As x_0 was expressed as

$$x_0 = -\frac{\hbar k_y}{m\omega}, \tag{3.76}$$

can now re-express it as

$$x_0 = -\frac{\Phi_0}{BL_y} j. \tag{3.77}$$

The full solution is then

$$\psi(x,y) = \sum_j C_j e^{\frac{2\pi i j y}{L_y}} e^{-\frac{(x-jL_x)^2}{\xi^2}}, \tag{3.78}$$

and this is the famous Abrikosov solution for a type-II superconductor. [63]

3.5 Brandt-Fourier Ansatz

3.5.1 Alternative Form of the Ginzburg-Landau Functional

Let us now return to the Ginzburg-Landau functional density:

$$\mathcal{F} = \alpha|\psi|^2 + \frac{\beta}{2}|\psi|^4 + \frac{\left|\left(-i\hbar\nabla - q\vec{A}\right)\psi\right|^2}{2m} + \frac{|\vec{B}|^2}{2\mu_0}. \tag{3.79}$$

Following the approach introduced in section 3.2.6, it can be converted to the dimensionless form:

$$\mathcal{F} = \frac{|\alpha|^2}{\beta}\left[-|\psi|^2 + \frac{1}{2}|\psi|^4 + \left|\left(-\frac{i}{\kappa_{GL}}\nabla - \vec{A}\right)\psi\right|^2 + |\vec{B}|^2\right] \tag{3.80}$$

for a superconducting state, hence the minus sign in front of $|\psi|^2$.

We have already considered the variation of the functional (3.80) with respect to ψ^* and $\vec{A}$ in order to obtain Ginzburg-Landau equations that describe a superconductor, however, there exists another approach, which is more convenient for numerical methods that are to be applied. [93] Let us write

$$\psi = \mathsf{f} e^{i\theta} = \sqrt{f}\, e^{i\theta}, \tag{3.81}$$

where

$$f = |\psi|^2. \tag{3.82}$$

Also introduce the superfluid velocity or supervelocity,

$$\vec{Q} = \vec{A} - \frac{1}{\kappa_{GL}}\nabla\theta \tag{3.83}$$

and recall $\vec{B} = \nabla \times \vec{A}$.

Then one can expand the kinetic term as

$$\left(-\frac{i}{\kappa_{GL}}\nabla - \vec{A}\right)\psi = \frac{\nabla \mathsf{f}}{i\kappa_{GL}}e^{i\theta} + \frac{\mathsf{f}}{\kappa_{GL}}e^{i\theta}\nabla\theta - \vec{Q}\mathsf{f}e^{i\theta} - \frac{\mathsf{f}}{\kappa_{GL}}e^{i\theta}\nabla\theta = \left(\frac{\nabla \mathsf{f}}{i\kappa_{GL}} - \vec{Q}\mathsf{f}\right)e^{i\theta}. \quad (3.84)$$

Noting that

$$f = |\mathsf{f}|^2, \quad (3.85)$$

then gradient of f^2 can be expanded as

$$\nabla \mathsf{f}^2 = 2\mathsf{f}\nabla \mathsf{f} \quad (3.86)$$

in order to express $\nabla \mathsf{f}$, and thus

$$(\nabla \mathsf{f})^2 = \left(\frac{\nabla \mathsf{f}^2}{2\mathsf{f}}\right) = \frac{\left(\nabla \mathsf{f}^2\right)^2}{4\mathsf{f}^2} = \frac{(\nabla f)^2}{4f}, \quad (3.87)$$

as $|\mathsf{f}|^2 = f$, and therefore obtain

$$\left|\left(-\frac{i}{\kappa_{GL}}\nabla - \vec{A}\right)\psi\right|^2 = \frac{(\nabla \mathsf{f})^2}{\kappa_{GL}^2} + \left(\vec{Q}\mathsf{f}\right)^2 = \frac{(\nabla f)^2}{4\kappa_{GL} f} + f\left|\vec{Q}\right|^2, \quad (3.88)$$

which then leads to the formulation of the functional in terms of f and $\vec{Q}$:

$$\mathcal{F} = \frac{\alpha^2}{\beta}\left[-f + \frac{f^2}{2} + \frac{(\nabla f)^2}{4\kappa_{GL}^2 f} + f\left|\vec{Q}\right|^2 + |\nabla \times \vec{Q}|^2\right], \quad (3.89)$$

where we have made use of

$$\nabla \times \vec{Q} = \nabla \times \vec{A} = \vec{B}. \quad (3.90)$$

N.B.: Here $f = f(x, y)$, $\vec{Q} = \vec{Q}(x, y)$, $\theta = \theta(x, y)$, as $\psi = \psi(x, y)$, $\vec{A} = \vec{A}(x, y)$ and $\vec{B} = \vec{B}(x, y)$. Also notice that $\vec{Q}$ follows the same gauge as $\vec{A}$.

3.5.2 Alternative Derivation of Ginzburg-Landau Equations

Let us now construct Euler-Lagrange equations for the functional (3.89) by variating it with respect to f and $\vec{Q}$, keeping in mind that both f and $\vec{Q}$ are functions of Cartesian x and y.

For f (first Gizburg-Landau equation):

$$\frac{\partial \mathcal{F}}{\partial f} - \nabla \frac{\partial \mathcal{F}}{\partial(\nabla f)} = 0. \quad (3.91)$$

Do it step by step. Start with

$$\frac{\partial \mathcal{F}}{\partial f} = -1 + f + |\vec{Q}|^2 - \frac{(\nabla f)^2}{4\kappa_{GL}^2 f^2}, \tag{3.92}$$

and

$$\nabla \frac{\partial \mathcal{F}}{\partial (\nabla f)} = \frac{f\nabla^2 f - (\nabla f)^2}{4\kappa_{GL}^2 f^2}, \tag{3.93}$$

so the full Euler-Lagrange equation now reads:

$$-1 + f + |\vec{Q}|^2 - \frac{(\nabla f)^2}{4\kappa_{GL}^2 f^2} = \frac{f\nabla^2 f - (\nabla f)^2}{2\kappa_{GL}^2 f^2} \tag{3.94}$$

that can be transformed to

$$-\nabla^2 f = 2\kappa_{GL}^2 \left[f - f^2 - f|\vec{Q}|^2 - g \right], \tag{3.95}$$

where

$$g = \frac{(\nabla f)^2}{4\kappa_{GL}^2 f}. \tag{3.96}$$

Equation (3.95) is just the first Ginzburg-Landau equation in the so-called Brandt form. However, it was demonstrated [71] that the numerical solution converges faster if one isolates $(-\nabla^2 + const)f(x, y)$ term on the LHS, so equation (3.95) then becomes

$$\left(-\nabla^2 + 2\kappa_{GL}^2\right) f = 2\kappa_{GL}^2 \left[2f - f^2 - f|\vec{Q}|^2 - g \right], \tag{3.97}$$

as we have added a $2\kappa_{GL}^2 f$ term to both sides.

Let us now derive an alternative formulation for the second Ginzburg-Landau equation. We start from the same functional (3.89) and vary it with respect to $\vec{Q}$. Such a variation leads to the following equation:

$$f\vec{Q} + \nabla \times \vec{Q} = 0. \tag{3.98}$$

Notice that from the gauge choice

$$\nabla \cdot \vec{Q} = 0, \tag{3.99}$$

hence equation (3.98) can be transformed to

$$f\vec{Q} - \nabla^2 \vec{Q} = 0, \tag{3.100}$$

and this is the Brandt's form of the second Ginzburg-Landau equation.

Again, we seek for some numerical acceleration, so let us now introduce

$$\vec{Q}_b = \vec{Q} - \vec{Q}_A, \tag{3.101}$$

where $\vec{Q}_A$ is the supervelocity of the Abrikosov solution,

$$\vec{Q}_A = \frac{\nabla f_A \times \hat{e}_z}{2\kappa_{GL} f_A}, \tag{3.102}$$

with f_A being the Abrikosov solution at B_{c_2} (can be calculated analytically). $\vec{Q}_A$ satisfies

$$\nabla \times \vec{Q}_A = \left[\bar{B} - \Phi_0 \sum_{\vec{R}} \left(\vec{r} - \vec{R} \right) \right] \hat{e}_z, \tag{3.103}$$

where $\vec{R}$ are positions of vortices (see later),

$$\bar{B} = \langle B(x,y) \rangle = \frac{\Phi_0}{S}, \tag{3.104}$$

is the spatially averaged over a unit cell[12] magnetic field; S is the area of the unit cell and Φ_0 is the flux quanta.

Also,

$$\nabla \times \vec{Q}_b = \left(B - \bar{B} \right) \hat{e}_z. \tag{3.107}$$

With $\vec{Q}_b$ introduced, equation (3.100) becomes

$$-\nabla^2 \vec{Q}_b - \nabla^2 \vec{Q}_A = -f\vec{Q}_b - f\vec{Q}_A, \tag{3.108}$$

but following the definition of $\vec{Q}_A$, equation (3.102), and condition (3.103) notice that

$$\nabla^2 \vec{Q}_A = 0, \tag{3.109}$$

hence we are left with

$$-\nabla^2 \vec{Q}_b = -f\vec{Q}_b - f\vec{Q}_A. \tag{3.110}$$

[12]By spatial averaging over a uinit cell we mean

$$\langle F(\vec{r}) \rangle = \frac{1}{L^n} \int F(\vec{r}) d^n r \tag{3.105}$$

for a continuous system and

$$\langle F(\vec{r}) \rangle = \frac{1}{N^n} \sum_k F_k \tag{3.106}$$

for a discrete one. Here n is the dimensionality and N is the number of points along one of the axes. For all the systems studied in this Theses $n = 2$.

Just as before, isolate $(-\nabla^2 + const)f(x,y)$ term on the LHS:

$$\left(-\nabla^2 + \bar{f}\right)\vec{Q}_b = -f\vec{Q}_A - \left(f - \bar{f}\right)\vec{Q}_b, \tag{3.111}$$

where

$$\bar{f} = \langle f \rangle . \tag{3.112}$$

So to conclude, two Ginzburg-Landau equations in Brandt form are:

$$\left(-\nabla^2 + 2\kappa_{GL}^2\right) f = 2\kappa_{GL}^2 \left[2f - f^2 - f|\vec{Q}|^2 - g\right] \tag{3.113}$$

and

$$\left(-\nabla^2 + \bar{f}\right)\vec{Q}_b = -f\vec{Q}_A - \left(f - \bar{f}\right)\vec{Q}_b. \tag{3.114}$$

3.5.3 Fourier Series Ansatz

3.5.3.1 The Lattice

One of the main Abrikosov's assumptions was the periodicity of the vortex lattice. [92] Suppose one has a lattice with constant a, then vortex positions can be set as

$$\vec{R}_{vw} = \begin{pmatrix} vx_1 + wx_2 \\ wy_2 \end{pmatrix}, \tag{3.115}$$

where $x_1 = a$, $x_2 = \frac{x_1}{2}$, $y_2 = x_1\frac{\sqrt{3}}{2}$ for a triangular lattice ($x_1 = L_x$, $y_2 = L_y$ to be consistent with Abrikosov's definitions introduced before) and v and w are integers. [93]

Reciprocal lattice vectors then are

$$\vec{k}_{mn} = \frac{2\pi}{S}\begin{pmatrix} my_2 \\ nx_1 + mx_2 \end{pmatrix}, \tag{3.116}$$

where

$$S = x_1 y_2 = \frac{\Phi_0}{\bar{B}} \tag{3.117}$$

and m and n are integers. [94]

One shall also notice that the position vector in the real space, $\vec{r}$, is continuous,

$$\vec{r} = (x, y), \tag{3.118}$$

but the reciprocal lattice vector, $\vec{k}$, is discrete:

$$\vec{k} = \left\{\vec{k}_{mn}\right\}. \tag{3.119}$$

We have used the same formalism for our skyrmion lattice studies in chapter 2.

3.5.3.2 Fourier Coefficients

The main achievement of *Brandt* [71] was to introduce the Fourier series ansatz for f, $B = B_z$ and $\vec{Q}$:

$$f(\vec{r}) = \sum_{\vec{k}} a_{\vec{k}} \left(1 - \cos\left(\vec{k}\cdot\vec{r}\right)\right), \tag{3.120}$$

$$B(\vec{r}) = \bar{B} + \sum_{\vec{k}} b_{\vec{k}} \cos\left(\vec{k}\cdot\vec{r}\right), \tag{3.121}$$

$$\vec{Q}(\vec{r}) = \vec{Q}_A(\vec{r}) + \sum_{\vec{k}} b_{\vec{k}} \frac{\hat{e}_z \times \vec{k}}{k^2} \sin\left(\vec{k}\cdot\vec{r}\right), \tag{3.122}$$

where $\vec{r} = (x, y)$, the sums go over $k_{mn} \neq 0$ to avoid ill-defined terms in equation (3.122) ($k_{mn} = 0$ terms are handled separately, as one can see from equations (3.120) – (3.122)), $\vec{k}$ is defined in (3.116) and $\vec{B}$ is assumed to be $\vec{B} = (0, 0, B)$.

Let us now focus on the Fourier series for f. According to equation (3.120),

$$\nabla f = \sum_{\vec{k}} \vec{k} a_{\vec{k}} \sin\left(\vec{k}\cdot\vec{r}\right), \tag{3.123}$$

$$\nabla^2 f = \sum_{\vec{k}} k^2 a_{\vec{k}} \cos\left(\vec{k}\cdot\vec{r}\right). \tag{3.124}$$

RHS of the equation (3.97) then becomes:

$$-\sum_{\vec{k}} a_{\vec{k}} k^2 \cos\left(\vec{k}\cdot\vec{r}\right) + 2\kappa_{GL}^2 \sum_{\vec{k}} a_{\vec{k}} - 2\kappa_{GL}^2 \sum_{\vec{k}} a_{\vec{k}} \cos\left(\vec{k}\cdot\vec{r}\right) = \tag{3.125}$$

$$= -\sum_{\vec{k}} a_{\vec{k}} \left(k^2 + 2\kappa_{GL}^2\right) \cos\left(\vec{k}\cdot\vec{r}\right) + 2\kappa_{GL}^2 \sum_{\vec{k}} a_{\vec{k}} \tag{3.126}$$

$$= -\sum_{\vec{k}} a_{\vec{k}} \left(k^2 + 2\kappa_{GL}^2\right) \cos\left(\vec{k}\cdot\vec{r}\right) + 2\kappa_{GL}^2 \bar{f}, \tag{3.127}$$

according to *Brandt.* [93]

The full equation (3.97) now reads:

$$-\sum_{\vec{k}} a_{\vec{k}} \left(k^2 + 2\kappa_{GL}^2\right) \cos\left(\vec{k}\cdot\vec{r}\right) + 2\kappa_{GL}^2 \bar{f} = 2\kappa_{GL}^2 \left(2f - f^2 - f|\vec{Q}|^2 - g\right). \tag{3.128}$$

Multiply both sides by $\cos\left(\vec{k}'\cdot\vec{r}\right)$, integrate (spatially average) with respect to x and y:

$$\begin{aligned} - & \sum_{\vec{k}} a_{\vec{k}}\left(k^2+2\kappa_{GL}^2\right)\int\cos\left(\vec{k}\cdot\vec{r}\right)\cos\left(\vec{k}'\cdot\vec{r}\right)\frac{dxdy}{A}+2\kappa_{GL}^2\bar{f}\int\cos\left(\vec{k}'\cdot\vec{r}\right)\frac{dxdy}{A} \\ = & \int 2\kappa_{GL}^2\left(2f-f^2-f|\vec{Q}|^2-g\right)\cos\left(\vec{k}'\cdot\vec{r}\right)\frac{dxdy}{A}. \end{aligned} \tag{3.129}$$

Apply cosine orthogonality relation,

$$\int\cos\left(\vec{k}\cdot\vec{r}\right)\cos\left(\vec{k}'\cdot\vec{r}\right)\frac{dxdy}{A}=\frac{\delta_{\vec{k},\vec{k}'}}{2}, \tag{3.130}$$

notice that

$$\int\cos\left(\vec{k}'\cdot\vec{r}\right)\frac{dxdy}{A}=0, \tag{3.131}$$

re-label $\vec{k}'\to\vec{k}$ and define

$$\int\left(2f-f^2-f|\vec{Q}|^2-g\right)\cos\left(\vec{k}'\cdot\vec{r}\right)\frac{dxdy}{A}=\left\langle\left(2f-f^2-f|\vec{Q}|^2-g\right)\cos\left(\vec{k}\cdot\vec{r}\right)\right\rangle \tag{3.132}$$

to get

$$a_{\vec{k}}=4\kappa_{GL}^2\frac{\left\langle\left(2f-f^2-f|\vec{Q}|^2-g\right)\cos\left(\vec{k}\cdot\vec{r}\right)\right\rangle}{k^2+2\kappa_{GL}^2}. \tag{3.133}$$

In order to improve the performance, one can also add an auxiliary equation that follows from the minimisation of the functional (3.89) with respect to the amplitude of f, i.e. $\frac{\delta\mathcal{F}}{\delta\bar{f}}=0$: [93]

$$a_{\vec{k}}=a_{\vec{k}}\frac{\left\langle f-f|\vec{Q}|^2-g\right\rangle}{\langle f^2\rangle}, \tag{3.134}$$

though this step is not necessary.

Following the same logic, one can obtain an expression for $b_{\vec{k}}$ from the second Ginzburg-Landau equation in Brandt's form. Curl equation (3.111):

$$\nabla\times\left[\left(-\nabla^2+\bar{f}\right)\vec{Q}_b\right]=-\nabla\times\left(f\vec{Q}_A\right)-\nabla\times\left[\left(f-\bar{f}\right)\vec{Q}_b\right]. \tag{3.135}$$

Deal with the LHS first. As

$$\nabla\times\vec{Q}_b=\vec{B}-\bar{B}\hat{e}_z, \tag{3.136}$$

and $\bar{f}$ is a constant, we get

$$\nabla\times\left[\left(-\nabla^2+\bar{f}\right)\vec{Q}_b\right]=\left(-\nabla^2+\bar{f}\right)B\hat{e}_z-\bar{f}\bar{B}\hat{e}_z. \tag{3.137}$$

For the RHS it gets a bit trickier:

$$-\nabla\times\left(f\vec{Q}_A\right) - \nabla\times\left[\left(f-\bar{f}\right)\vec{Q}_b\right] = \tag{3.138}$$

$$= -f\nabla\times\vec{Q}_A - \nabla f\times\vec{Q}_A - (f-\bar{f})\nabla\times\vec{Q}_b - \nabla f\times\vec{Q}_b \tag{3.139}$$

$$= -f\nabla\times\vec{Q}_A - \nabla f\times\left(\vec{Q}_A+\vec{Q}_b\right) - (f-\bar{f})\nabla\times\vec{Q}_b. \tag{3.140}$$

Notice that as

$$\vec{Q}_A+\vec{Q}_b=\vec{Q}, \tag{3.141}$$

$$\nabla\times\vec{Q}_b=\vec{B}-\bar{B}\hat{e}_z, \tag{3.142}$$

hence the equation transforms to

$$-\nabla\times\left(f\vec{Q}_A\right)-\nabla\times\left[\left(f-\bar{f}\right)\vec{Q}_b\right]=-\nabla f\times\vec{Q}-\left(f-\bar{f}\right)\left(B-\bar{B}\right)\hat{e}_z. \tag{3.143}$$

Call

$$\vec{p}=\nabla f\times\vec{Q}, \tag{3.144}$$

then

$$\vec{p}\cdot\hat{e}_z=\frac{\partial f}{\partial x}Q_y-\frac{\partial f}{\partial y}Q_x=p, \tag{3.145}$$

hence equation (3.111) finally transforms to

$$\left(-\nabla^2+\bar{f}\right)B=-\left[(f-\bar{f})B-f\bar{B}+p\right]. \tag{3.146}$$

Now let us apply the Fourier expansion of B, (3.121), to get

$$\bar{f}\bar{B}+\sum_{\vec{k}}\left(k^2+\bar{f}\right)b_{\vec{k}}\cos\left(\vec{k}\cdot\vec{r}\right)=-\left[(f-\bar{f})B-f\bar{B}+p\right]. \tag{3.147}$$

Just as before, multiply both sides of (3.147) by $\cos\left(\vec{k}'\cdot\vec{r}\right)$, integrate (spatially average) and apply cosine orthogonality relation to get

$$b_{\vec{k}}=-2\frac{\left\langle\left[(f-\bar{f})B-f\bar{B}+p\right]\cos\left(\vec{k}\cdot\vec{r}\right)\right\rangle}{k^2+\bar{f}}, \tag{3.148}$$

as

$$\int\cos\left(\vec{k}'\cdot\vec{r}\right)\frac{dxdy}{A}=0. \tag{3.149}$$

The best initial guess to use in numerical simulations that are applied to solve the equations obtained is the one that would give a triangular lattice itself. Corresponding Fourier coefficients

then are [93]

$$a_{\vec{k}} = -(-1)^{m+mn+n} e^{-\frac{k_{mn}^2 S}{8\pi}}, \tag{3.150}$$

$$b_{\vec{k}} = 0, \tag{3.151}$$

f_A, required for the formulation of $\vec{Q}_A$, is found from combining series (3.120) and the coefficients have the form stated above:

$$f_A = -\sum_{mn} (-1)^{m+mn+n} e^{-\frac{k_{mn}^2 S}{8\pi}} \left(1 - \cos\left(\vec{k}_{mn} \cdot \vec{r}\right)\right). \tag{3.152}$$

It then leads to the normalisation of $\langle f_A(x,y)\rangle = 1$.

3.5.3.3 Vortex Lattice

We have noticed already that the only material parameter introduced in the model is the Ginzburg-Landau parameter, κ_{GL}. Obviously, different values of an external field can be applied. However, the lattice constant, a, depends on the average field, B, via

$$\Phi_0 = \int B dx dy. \tag{3.153}$$

In our dimensionless units $\Phi_0 = \frac{2\pi}{\kappa_{GL}}$, $B_{c_2} = \kappa_{GL}$, so the area of the unit cell governed by the field B is

$$S = \frac{2\pi}{\kappa_{GL} B}. \tag{3.154}$$

On the other hand,

$$S = x_1 y_2 = a^2 \frac{\sqrt{3}}{2} \tag{3.155}$$

for a triangular lattice, hence one obtains a relation between the average field and the lattice spacing:

$$B = \frac{4\pi}{a^2 \kappa_{GL} \sqrt{3}}, \tag{3.156}$$

or just $B \propto a^{-2}$ if we do not want to bother with the configuration of the lattice.

In our calculations we shall use either external field or lattice spacing as a control parameter, as we want to deal with stable configurations only. It is more convenient to use the spacing and then calculate the external field that corresponds to this spacing if need be.

An example of a vortex lattice calculated by the approach introduced before is demonstrated in Figure 3.6. We demonstrate f (Figure 3.6a) and B (Figure 3.6b) calculated.

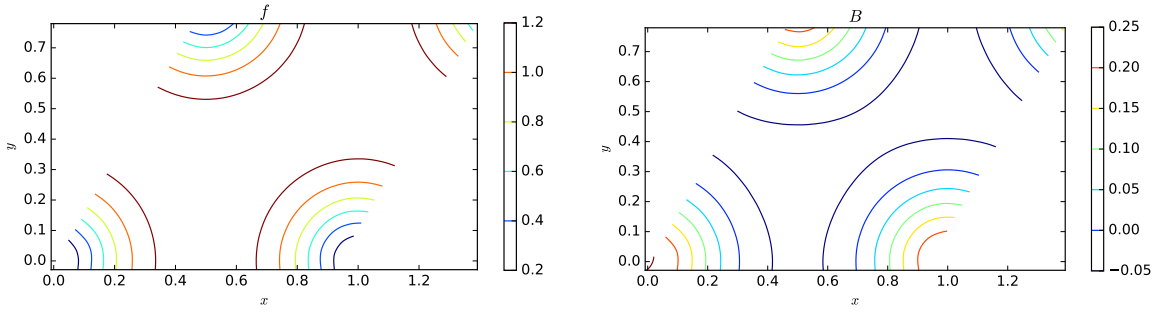

(a) f calculated for $\kappa = 1.43$ and $a = 4$.

(b) B calculated for $\kappa = 1.43$ and $a = 4$.

Figure 3.6: Order parameter and magnetic field on the unit cell of an Abrikosov lattice for $\kappa = 1.43$ and $a = 4$. Coordinates x and y are scaled by a: $x \equiv \frac{x}{a}$ and $y \equiv \frac{y}{a}$. Order parameter is zero in the vortex core and non-zero in the bulk, whereas the field is non-zero in the vortex core and decays in the bulk, as expected.

Chapter 4

Magnetic Skyrmions in Proximity to Superconducting Vortex Lattice

4.1 Introduction and Motivation

In chapter 2 we have discussed skyrmion lattices. We have noticed their similarities to Abrikosov vortex lattices, described in section 3.4, and applied Fourier approach similar to that of Brandt's for superconductors (see section 3.5 to recall the approach). As both skyrmion and Abrikosov vortex lattices are triangular and both allow magnetic field to penetrate, quite an obvious idea rises then: to combine two systems and study the obtained one, i.e. consider a system that consists of a bilayer of a material that exhibits a skyrmion lattice and a type-II superconductor that has a vortex lattice. A good example to consider might be a bilayer of $Fe_{1-x}Co_xSi$ as a material with skyrmion lattice and Nb as a superconducting one, as their critical temperatures and fields should allow skyrmion lattice and Abrikosov lattice to exist simultaneously. For instance, $Fe_{1-x}Co_xSi$ exhibits skyrmion phase when an applied field, B_a, lies in a region of $40mT < B_a < 80mT$; [43] niobium demonstrates superconducting vortex lattice when an applied field is $40mT < B_a < 280mT$. [95]

An example of the visualisation of the combined system we are about to study can be found in Figure 4.1a, if we take a skyrmion material that exhibits a triangular lattice, or in Figure 4.1b, if we take a skyrmion material that exhibits a honeycomb lattice. Regions of the maximal fields must coincide for both Abrikosov vortex lattice and skyrmion lattice. In the vortex lattice the field is maximal in the vortex core and then decays to zero in the bulk of a superconductor; on the skyrmion lattice the field is maximal in those regions far from skyrmions themselves, i.e. where all the spins align along the field. So we would position vortices above those 'ferromagnetic' regions and use such a system as an initial configuration for our calculations.

Notice that the position of the vortex lattice in Figure 4.1a is not unique: there are two

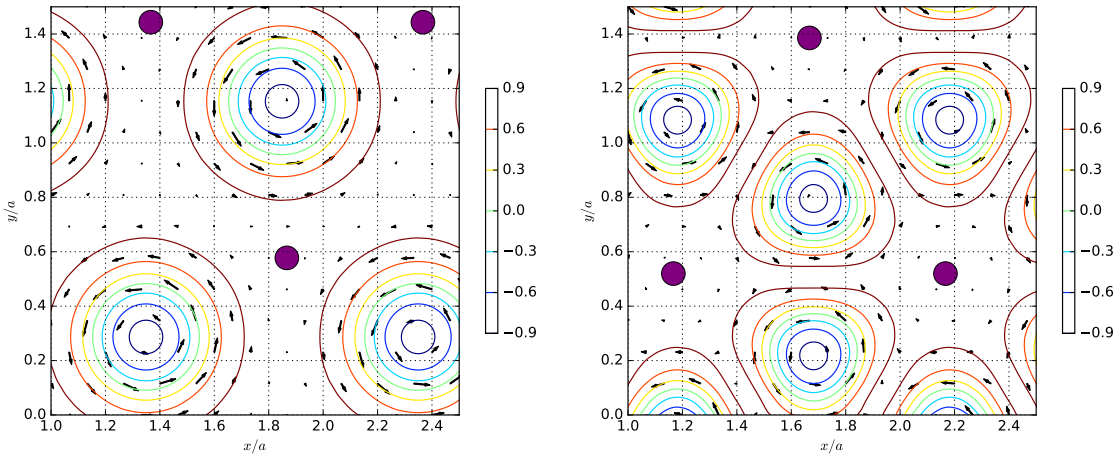

(a) Schematic representation of a triangular skyrmion lattice interacting with Abrikosov vortices.

(b) Schematic representation of a honeycomb skyrmion lattice interacting with Abrikosov vortices.

Figure 4.1: Schematic representation of combined systems to be studied. Vortices are located in the regions of the highest field and are denoted by purple dots.

possibilities to combine triangular skyrmion lattice with the triangular vortex lattice, however the position of the vortex lattice in Figure 4.1b is unique: a vortex always happens to be surrounded by skyrmions should they form a honeycomb lattice.

Attempts to study a similar system are known, however. For example, *Hals et al* [96] considered a skyrmion-vortex pair in a hybrid system of coupled ferromagnetic and superconducting layers like it is demonstrated in Figure 4.2. They have considered effects of a single skyrmion on a single vortex, though, whereas we are going to consider how does one lattice affect another.

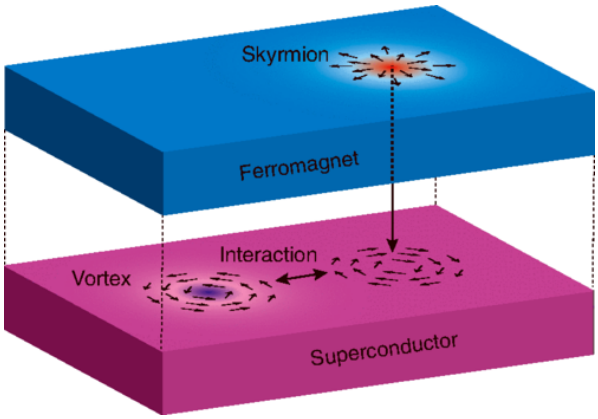

Figure 4.2: Schematic representation of a skyrmion-vortex pair. [96]

In previous chapters we considered the behaviour of the order parameter and magnetic

field of a type-II superconductor in an external field and the behaviour of the magnetisation of a magnetic (skyrmion) material in an external field with this field varying. In fact, skyrmion lattice cannot even exist in the absence of an external field, as it is a type of magnetic ordering resulting as a reaction to the field. Abrikosov vortices would not exist either. We have observed skyrmion lattices and Abrikosov vortex lattices in the regions between critical fields. However, the external field was held to be uniform for both cases. Now that we combine two systems, external field would no longer stay uniform for any of them: the total field that would cause (or not cause – depending on its value) ordering in a magnetic material would be an external field modified by a superconductor, while the field acting on a superconductor would be a combination of an external field and the magnetisation field due to the skyrmion lattice. Proper interface conditions have to be derived as well.

In this chapter we would introduce a mathematical representation of the bilayer of a skyrmion lattice and a type-II superconductor with some separation between them (that can be zero in the simplest case); the total free energy functional of such a system consists of the combination of a free energy functional for a magnetic system and Ginzburg-Landau functional for a superconductor. As we are going to see later, there is only one coupling term in the combined functional, so it would make sense to derive Ginzburg-Landau equations for the superconducting system and Euler-Lagrange equations for the magnetic system and solve them separately in order to save the computation time. Thus we would demonstrate how does a type-II superconductor affect the skyrmion lattice and how does the skyrmion lattice affect Abrikosov vortex lattice in a superconductor.

4.2 Extending Brandt's Approach

We have described Brandt's approach to Abrikosov vortex lattice in details in section 3.5. Let us just quote some important results here. First Ginzburg-Landau equation in Brandt's form is written as

$$\left(-\nabla^2 + 2\kappa_{GL}^2\right) f = 2\kappa_{GL}^2 \left[2f - f^2 - f\left|\vec{Q}\right|^2 - g\right], \tag{4.1}$$

and second Ginzburg-Landau equation in Brandt's form[1] is

$$\left(-\nabla^2 + \bar{f}\right)\vec{Q}_b = -f\vec{Q}_A - \left(f - \bar{f}\right)\vec{Q}_b, \tag{4.2}$$

for $\vec{Q}_b$, that can be transformed into an equation for B:

$$\left(-\nabla^2 + \bar{f}\right) B = -\left[\left(f - \bar{f}\right) B - f\bar{B} + p\right], \tag{4.3}$$

[1]Call them to be Ginzburg-Landau-Brandt equations from here on.

where B is defined from

$$\vec{B} = (0, 0, B)\,, \tag{4.4}$$

f, $\vec{Q}$, $\vec{Q}_A$, $\vec{Q}_b$, $\bar{f}$ and g are defined in section 3.5.1,

$$p = \vec{p} \cdot \hat{z} = \frac{\partial f}{\partial x} Q_y - \frac{\partial f}{\partial y} Q_x, \tag{4.5}$$

and κ_{GL} is the Ginzburg-Landau parameter (not to be confused with κ we have used in our dimensionless formulation of the free energy functional for a skyrmion system).

Expanding f and $\vec{Q}$ in Fourier form,

$$f(\vec{r}) = \sum_{\vec{k}} a_{\vec{k}} \left(1 - \cos\left(\vec{k} \cdot \vec{r}\right)\right), \tag{4.6}$$

$$B(\vec{r}) = \bar{B} + \sum_{\vec{k}} b_{\vec{k}} \cos\left(\vec{k} \cdot \vec{r}\right), \tag{4.7}$$

$$\vec{Q}(\vec{r}) = \vec{Q}_A(\vec{r}) + \sum_{\vec{k}} b_{\vec{k}} \frac{\hat{e}_z \times \vec{k}}{k^2} \sin\left(\vec{k} \cdot \vec{r}\right), \tag{4.8}$$

where $\vec{B} - \bar{B}\hat{e}_z = \nabla \times \vec{Q}_b$, substituting these expressions into LHS of Ginzburg-Landau-Brandt equations, multiplying these equations by $\frac{1}{A}\cos\left(\vec{k}' \cdot \vec{r}\right)$ and spatial averaging, get formulations for Fourier coefficients, $a_{\vec{k}}$, $b_{\vec{k}}$,

$$a_{\vec{k}} = 4\kappa_{GL}^2 \frac{\left\langle \left(2f - f^2 - f|\vec{Q}|^2 - g\right) \cos\left(\vec{k} \cdot \vec{r}\right) \right\rangle}{k^2 + 2\kappa_{GL}^2}, \tag{4.9}$$

$$b_{\vec{k}} = -2 \frac{\left\langle \left[(f - \bar{f})B - f\bar{B} + p\right] \cos\left(\vec{k} \cdot \vec{r}\right) \right\rangle}{k^2 + \bar{f}}. \tag{4.10}$$

However, these formulations are based on the assumption of $\vec{B} = (0, 0, B)$ with $B = const$ and the corresponding Landau gauge for $\vec{A}$, hence $\vec{Q}$. But once we combine the Abrikosov lattice with the skyrmion lattice, $\vec{B}$ would not remain necessarily directed solely along z-axis, as the total field, $\vec{B}$, would be the combination of an external field (still constant and aligned with z-axis) and the magnetisation of the skyrmion system (three active components, all spatially-dependent). Hence we need to derive Ginzburg-Landau-Brandt equations that would be valid for any shape of $\vec{B}$ and $\vec{Q}$. Also, we have used exponential form of Fourier expansion for the magnetisation components in our skyrmion lattice survey, so we would like

to convert Brandt's formulation to the exponential form for consistency. Write

$$f = \sum_{\vec{k}} a_{\vec{k}} \left(1 - e^{-i\vec{k}\vec{r}}\right), \tag{4.11}$$

hence the expression for $a_{\vec{k}}$ gets modified to

$$a_{\vec{k}} = 4\kappa_{GL}^2 \frac{\left\langle \left(2f - f^2 - f|\vec{Q}|^2 - g\right) e^{i\vec{k}\vec{r}} \right\rangle}{k^2 + 2\kappa_{GL}^2}, \tag{4.12}$$

and everything else regarding first Ginzburg-Landau-Brandt equation remains unchanged. Dealing with the second equation, however, becomes more tricky. As

$$\vec{B} = (B_x, B_y, B_z) \tag{4.13}$$

now, need to write

$$\vec{B} = \bar{\vec{B}} + \sum \vec{b}_{\vec{k}} e^{-i\vec{k}\vec{r}}, \tag{4.14}$$

or in component form:

$$B_\mu = \bar{B}_\mu + \sum = b_{\mu_{\vec{k}}} e^{-i\vec{k}\vec{r}}, \tag{4.15}$$

where $\mu = x, y, z$.

Condition (4.13) automatically means that instead of having one equation (4.3), we would have three equations for three components of $\vec{B}$:

$$\left(-\nabla^2 + \bar{f}\right) B_x = -\left[\left(f - \bar{f}\right) B_x - f\bar{B}_x + p_x\right], \tag{4.16}$$

$$\left(-\nabla^2 + \bar{f}\right) B_y = -\left[\left(f - \bar{f}\right) B_y - f\bar{B}_y + p_y\right], \tag{4.17}$$

$$\left(-\nabla^2 + \bar{f}\right) B_z = -\left[\left(f - \bar{f}\right) B_z - f\bar{B}_z + p_z\right], \tag{4.18}$$

where

$$p_x = \frac{\partial f}{\partial y} Q_z, \tag{4.19}$$

$$p_y = -\frac{\partial f}{\partial x} Q_z, \tag{4.20}$$

$$p_z = \frac{\partial f}{\partial x} Q_y - \frac{\partial f}{\partial y} Q_x, \tag{4.21}$$

hence

$$b_{x_{\vec{k}}} = -2 \frac{\left\langle \left[(f - \bar{f})B_x - f\bar{B}_x + p_x\right] e^{i\vec{k}\vec{r}} \right\rangle}{k^2 + \bar{f}}, \tag{4.22}$$

$$b_{y_{\vec{k}}} = -2\frac{\left\langle \left[(f-\bar{f})B_y - f\bar{B}_y + p_y\right] e^{i\vec{k}\vec{r}} \right\rangle}{k^2+\bar{f}}, \tag{4.23}$$

$$b_{z_{\vec{k}}} = -2\frac{\left\langle \left[(f-\bar{f})B_z - f\bar{B}_z + p_z\right] e^{i\vec{k}\vec{r}} \right\rangle}{k^2+\bar{f}}, \tag{4.24}$$

by analogy to the formulation of $b_{\vec{k}}$. Fourier formulation of $\vec{Q}$ is, however, less trivial.

Let us first convert Fourier formulation of $\vec{Q}$, (4.8), to the exponential form:

$$\vec{Q} = \vec{Q}_A + i\sum_{\vec{k}} \frac{\vec{b}_{\vec{k}} \times \vec{k}}{k^2} e^{-i\vec{k}\vec{r}}, \tag{4.25}$$

and if $\vec{B} = (0,0,B)$, then $\vec{b}_{\vec{k}} = \left(0,0,b_{\vec{k}}\right)$, hence one can write

$$\vec{Q} = \vec{Q}_A + i\sum_{\vec{k}} b_{\vec{k}} \frac{\hat{e}_z \times \vec{k}}{k^2} e^{-i\vec{k}\vec{r}}. \tag{4.26}$$

Now check that the curl of $\vec{Q}$ defined in (4.26) actually gives us $\vec{B}$:

$$\hat{e}_z \times \vec{k} = (-k_y, k_x) = \vec{k}_\perp, \tag{4.27}$$

$$\nabla \times \vec{Q} = \bar{B} + \sum_{\vec{k}} b_{\vec{k}} \frac{\vec{k} \times \vec{k}_\perp}{k^2} e^{-i\vec{k}\vec{r}}. \tag{4.28}$$

Calculate the cross product:

$$\vec{k} \times \vec{k}_\perp = \begin{vmatrix} \hat{e}_x & \hat{e}_y & \hat{e}_z \\ k_x & k_y & 0 \\ -k_y & k_x & 0 \end{vmatrix} = \left(0,0,k_x^2+k_y^2\right) = k^2\hat{e}_z, \tag{4.29}$$

then

$$\nabla \times \vec{Q} = \bar{B} + \sum_{\vec{k}} b_{\vec{k}} \hat{e}_z e^{-i\vec{k}\vec{r}} = \vec{B}, \tag{4.30}$$

as it was defined in (4.14) just for $\vec{B} = (0,0,B)$.

Let us then extend the Fourier formulation of $\vec{Q}$, (4.25), for $\vec{B} = (B_x, B_y, B_z)$:

$$\vec{Q} = \vec{Q}_A + i\sum_{\vec{k}} \frac{\vec{b}_{\vec{k}} \times \vec{k}}{k^2} e^{-i\vec{k}\vec{r}}, \tag{4.31}$$

where

$$\vec{b}_{\vec{k}} = \left(b_{x_{\vec{k}}}, b_{y_{\vec{k}}}, b_{z_{\vec{k}}}\right) \tag{4.32}$$

and

$$\vec{Q}_A = \left(Q_{A_x}, Q_{A_y}, 0\right), \tag{4.33}$$

as this form is still consistent with its definition, (3.83).

The cross product inside (4.25) can be expanded as

$$\vec{b}_{\vec{k}} \times \vec{k} = \left(-k_y b_{z_{\vec{k}}}\ ,\ k_x b_{z_{\vec{k}}}\ ,\ k_y b_{x_{\vec{k}}} - k_x b_{y_{\vec{k}}}\right), \tag{4.34}$$

thus curl of $\vec{Q}$ is

$$\nabla \times \vec{Q} = \sum_{\vec{k}} \frac{1}{k^2}\left(b_{x_{\vec{k}}} k_y^2 - b_{y_{\vec{k}}} k_x k_y\ ,\ -b_{x_{\vec{k}}} k_x k_y + b_{y_{\vec{k}}} k_x^2\ ,\ k^2 b_{z_{\vec{k}}}\right) e^{-i\vec{k}\vec{r}} = \sum_{\vec{k}} \vec{T}_{b_{\vec{k}}} e^{-i\vec{k}\vec{r}}. \tag{4.35}$$

The result may look incorrect from the first glance as it does not seem to correspond to the definition of B_x and B_y from (4.15), though, if we simplify it a bit, the situation may become different. Write

$$\vec{T}^T_{b_{\vec{k}}} = \frac{1}{k^2}\begin{pmatrix} b_{x_{\vec{k}}} k_y^2 - b_{y_{\vec{k}}} k_x k_y \\ -b_{x_{\vec{k}}} k_x k_y + b_{y_{\vec{k}}} k_x^2 \\ k^2 b_{z_{\vec{k}}} \end{pmatrix} \tag{4.36}$$

for convenience. Then complete the k^2 in two components of $\vec{T}^T_{b_{\vec{k}}}$ by adding corresponding terms to them:

$$\begin{aligned} \vec{T}^T_{b_{\vec{k}}} &= \frac{1}{k^2}\begin{pmatrix} b_{x_{\vec{k}}} k_x^2 - b_{x_{\vec{k}}} k_x^2 + b_{x_{\vec{k}}} k_y^2 - b_{y_{\vec{k}}} k_x k_y \\ -b_{x_{\vec{k}}} k_x k_y + b_{y_{\vec{k}}} k_x^2 + b_{y_{\vec{k}}} k_y^2 - b_{y_{\vec{k}}} k_y^2 \\ k^2 b_{z_{\vec{k}}} \end{pmatrix} \\ &= \begin{pmatrix} b_{x_{\vec{k}}} \\ b_{y_{\vec{k}}} \\ b_{z_{\vec{k}}} \end{pmatrix} - \frac{1}{k^2}\begin{pmatrix} k_x\left(b_{x_{\vec{k}}} k_x + b_{y_{\vec{k}}} k_y\right) \\ k_y\left(b_{x_{\vec{k}}} k_y + b_{y_{\vec{k}}} k_y\right) \\ 0 \end{pmatrix} \\ &= \begin{pmatrix} b_{x_{\vec{k}}} \\ b_{y_{\vec{k}}} \\ b_{z_{\vec{k}}} \end{pmatrix} - \frac{1}{k^2}\begin{pmatrix} k_x\left(\vec{b}_{\vec{k}} \cdot \vec{k}\right) \\ k_y\left(\vec{b}_{\vec{k}} \cdot \vec{k}\right) \\ 0 \end{pmatrix}, \end{aligned} \tag{4.37}$$

as $\vec{k} = (k_x, k_y, 0)$ if one wants to express it in 3D.

On the other hand, one can define $\vec{b}_{\vec{k}}$ as

$$\vec{b}_{\vec{k}} = b_{x_{\vec{k}}}\hat{e}_x + b_{y_{\vec{k}}}\hat{e}_y + b_{z_{\vec{k}}}\hat{e}_z = b_{\perp\vec{k}}\hat{e}_\perp + b_{z_{\vec{k}}}\hat{e}_z \tag{4.38}$$

with

$$b_{\perp\vec{k}}\hat{e}_\perp = b_{x_{\vec{k}}}\hat{e}_x + b_{y_{\vec{k}}}\hat{e}_y \tag{4.39}$$

and $\hat{e}_\perp$ is defined in Figure 4.3.

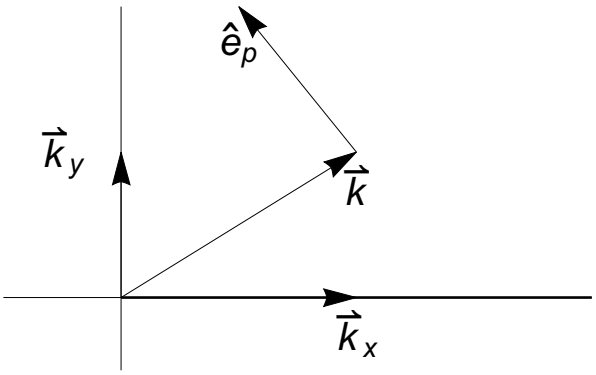

Figure 4.3: Definition of $\hat{e}_\perp$ vector – $\hat{e}_p$ in the figure – as a vector that is perpendicular to $\vec{k}$.

From Figure 4.3 it is then clear that

$$\hat{e}_\perp \cdot \vec{k} = 0, \tag{4.40}$$

but if $\hat{e}_\perp \cdot \vec{k} = 0$, then $\vec{b}_{\perp_{\vec{k}}} \cdot \vec{k} = 0$ and therefore

$$\vec{b}_{\vec{k}} \cdot \vec{k} = 0, \tag{4.41}$$

as there is no z-dependence in $\vec{k}$, so conclude that

$$b_{x_{\vec{k}}} k_x + b_{y_{\vec{k}}} k_y = \vec{b}_{\vec{k}} \cdot \vec{k} = 0, \tag{4.42}$$

hence

$$\vec{T}^T_{b_{\vec{k}}} = \begin{pmatrix} b_{x_{\vec{k}}} \\ b_{y_{\vec{k}}} \\ b_{z_{\vec{k}}} \end{pmatrix} \tag{4.43}$$

and

$$\nabla \times \vec{Q} = \sum_{\vec{k}} \left(b_{x_{\vec{k}}}, b_{y_{\vec{k}}}, b_{z_{\vec{k}}} \right) e^{-i\vec{k}\vec{r}} = (B_x, B_y, B_z)\,, \tag{4.44}$$

which allows us to conclude that the generalisation (4.25) was correct.

To summarise: in the exponential form we write

$$f = \sum_{\vec{k}} a_{\vec{k}} \left(1 - e^{-i\vec{k}\vec{r}} \right), \tag{4.45}$$

$$\vec{B} = \vec{\bar{B}} + \sum \vec{b}_{\vec{k}} e^{-i\vec{k}\vec{r}} \tag{4.46}$$

and

$$\vec{Q} = \vec{Q}_A + i \sum_{\vec{k}} \frac{\vec{b}_{\vec{k}} \times \vec{k}}{k^2} e^{-i\vec{k}\vec{r}}. \tag{4.47}$$

Notice that if an external field is aligned along z-direction only, as it was assumed in section 3.5.1, B_x and B_y would still remain zeros, hence one can use this formulation as the general one for all the cases. The calculations are a bit slower than those using the original Brandt's approach, though the difference in speed is negligible on modern machines.

4.3 Coupling Skyrmion Lattice with a Superconductor

4.3.1 The Total Functional

All this study is about finding optimal solutions for thermodynamical systems in the first place, minimising the free energy functional, in other words. As we have a system of a magnetic material and a superconductor combined, we need to write a free energy functional for this system. Such a free energy functional would be a combination of free energy functionals for those systems when they are not interacting with each other. However, some modifications have to be made to both functionals in order to combine them correctly and take the actual interactions into account.

Recall Ginzburg-Landau functional as it was stated in section 3.2.2:

$$F_{SC} = \int \left\{ -|\alpha| |\psi|^2 + \frac{\beta}{2} |\psi|^4 + \frac{1}{2m} \left| \left(-i\hbar\nabla - q\vec{A} \right) \psi \right|^2 + \frac{\left|\vec{B}\right|^2}{2\mu_0} \right\} \frac{dxdy}{A}. \tag{4.48}$$

This functional is not dimensionless itself, and we cannot use the dimensionless formulation introduced in section 3.2.6 as the coordinate scaling would be different in our new problem (related to skyrmion coordinate scaling, in fact, as we want to combine functionals, hence combine integrals, hence make sure we integrate with respect to the same variable(-s)), so should develop a new one.

So let us derive this new dimensionless formulation. Write

$$\psi = \psi_0 \tilde{\psi} \tag{4.49}$$

with

$$\psi_0^2 = \frac{|\alpha|}{\beta}. \tag{4.50}$$

Ginzburg-Landau coherence length and the penetration depth are defined as usually,

$$\xi = \frac{\hbar}{\sqrt{2m|\alpha|}} \tag{4.51}$$

and

$$\lambda_{GL} = \sqrt{\frac{m\beta}{q^2|\alpha|\mu_0}} \tag{4.52}$$

respectively. These are unchanged with respect to those defined in section 3.2.5.

The functional then becomes

$$F_{SC} = \int \left\{ -\frac{|\alpha|^2}{\beta}\left|\tilde{\psi}\right|^2 + \frac{1}{2}\frac{|\alpha|^2}{\beta}\left|\tilde{\psi}\right|^4 + \frac{1}{2m|\alpha|}\frac{|\alpha|^2}{\beta}\left|\left(-i\hbar\nabla - q\vec{A}\right)\tilde{\psi}\right|^2 + \frac{\left|\vec{B}\right|^2}{2\mu_0} \right\} \frac{dxdy}{A}, \tag{4.53}$$

that can be simplified to

$$F_{SC} = \frac{|\alpha|^2}{\beta}\int \left\{ -\left|\tilde{\psi}\right|^2 + \frac{1}{2}\left|\tilde{\psi}\right|^4 + \frac{1}{2m|\alpha|}\left|\left(-i\hbar\nabla - q\vec{A}\right)\tilde{\psi}\right|^2 + \frac{\beta}{|\alpha|^2}\frac{\left|\vec{B}\right|^2}{2\mu_0} \right\} \frac{dxdy}{A}. \tag{4.54}$$

Define

$$B_c = \sqrt{\frac{\mu_0|\alpha|^2}{\beta}}, \tag{4.55}$$

in order to write

$$\left|\vec{B}\right|^2 = B_c^2\left|\vec{b}\right|^2, \tag{4.56}$$

also rearrange

$$\frac{1}{2m|\alpha|}\left|\left(-i\hbar\nabla - q\vec{A}\right)\tilde{\psi}\right|^2 = \frac{\hbar^2}{2m|\alpha|}\left|\left(-i\nabla - \frac{q}{\hbar}\vec{A}\right)\tilde{\psi}\right|^2 = \xi^2\left|\left(-i\nabla - \frac{q}{\hbar}\vec{A}\right)\tilde{\psi}\right|^2. \tag{4.57}$$

Notice that

$$\xi\frac{q}{\hbar} = \frac{q}{\sqrt{2m|\alpha|}} = \frac{1}{\sqrt{2}\lambda_{GL}B_c}, \tag{4.58}$$

then define

$$\vec{a} = \frac{q}{\hbar}\xi\vec{A} = \frac{\vec{A}}{\sqrt{2}\lambda_{GL}B_c}. \tag{4.59}$$

Also notice that

$$\nabla\times\vec{a} = \frac{1}{\sqrt{2}\lambda_{GL}B_c}\nabla\times\vec{A} = \frac{1}{\sqrt{2}\lambda_{GL}B_c}\vec{B} = \frac{1}{\lambda_{GL}}\vec{b}, \tag{4.60}$$

or just

$$\vec{b} = \lambda_{GL}\nabla\times\vec{a}, \tag{4.61}$$

that would be useful in the future.

So finally the functional turns into

$$F_{SC} = H_c^2 \int \left\{ -\left|\tilde{\psi}\right|^2 + \frac{1}{2}\left|\tilde{\psi}\right|^4 + \left|\left(-i\xi\nabla - \vec{a}\right)\tilde{\psi}\right|^2 + \left|\vec{b}\right|^2 \right\} \frac{dxdy}{A}, \tag{4.62}$$

where

$$H_c^2 = \frac{B_c^2}{\mu_0^2}. \tag{4.63}$$

Coordinates, though, are still dimensionful. As it was mentioned before, we cannot use the scaling introduced in section 3.2.6, as that one was related to λ_{GL}. We want our coordinates to be the same as in the free energy functional for a magnetic material,

$$F_{SkX} = 2J\kappa^2 \int \left\{ \frac{1}{4}\left(\partial_\mu \vec{M}\right)\cdot\left(\partial_\mu \vec{M}\right) + \vec{M}\cdot\left(\nabla\times\vec{M}\right) - \vec{\beta}\cdot\vec{M} + \lambda\left(|\vec{M}|^2 - 1\right)\right\} \frac{dxdy}{A}, \tag{4.64}$$

and the coordinates are dimensionless for this functional. So define

$$\vec{r}_\kappa = \kappa\vec{r}, \tag{4.65}$$

where κ is defined in section 2.3.1 and has dimensions of $\vec{r}^{-1}$, hence

$$\tilde{\nabla} = \frac{1}{\kappa}\nabla \tag{4.66}$$

and

$$\tilde{A} = \kappa^2 A, \tag{4.67}$$

with $\vec{r}_\kappa$ being dimensionless. One can also introduce

$$\tilde{\lambda} = \kappa\lambda_{GL}, \tag{4.68}$$

$$\tilde{\xi} = \kappa\xi, \tag{4.69}$$

then the Ginzburg-Landau functional would turn into

$$F_{SC} = H_c^2 \int \left\{ -\left|\tilde{\psi}\right|^2 + \frac{1}{2}\left|\tilde{\psi}\right|^4 + \left|\left(-i\tilde{\xi}\tilde{\nabla} - \vec{a}\right)\tilde{\psi}\right|^2 + \left|\vec{b}\right|^2 \right\} \frac{d\tilde{x}d\tilde{y}}{\tilde{A}}. \tag{4.70}$$

We also want functionals (4.64) and (4.70) to be consistent with each other, hence define

$$\tilde{H}_c = \frac{H_c}{\sqrt{2J\kappa^2}} \tag{4.71}$$

to get

$$H_c^2 = 2J\kappa^2\tilde{H}_c^2, \tag{4.72}$$

and yet the Ginzburg-Landau functional finally becomes

$$F_{SC} = 2J\kappa^2 \tilde{H}_c^2 \int \left\{ -\left|\tilde{\psi}\right|^2 + \frac{1}{2}\left|\tilde{\psi}\right|^4 + \left|\left(-i\tilde{\xi}\tilde{\nabla} - \vec{a}\right)\tilde{\psi}\right|^2 + \left|\vec{b}\right|^2 \right\} \frac{d\tilde{x}d\tilde{y}}{\tilde{A}}. \tag{4.73}$$

One may notice, though, that the magnetic field in (4.73) is represented by $\vec{b}$, whereas in (4.64) it is represented by $\vec{\beta}$ that is also scaled with κ (κ^2, in fact).

Let us recall its definition from section 2.3.1 and relate it to $\vec{b}$:

$$\vec{\beta}_\kappa = \frac{\vec{B}_Z}{2J\kappa^2} = \frac{\mu_s}{2J\kappa^2}\vec{B} = \frac{\mu_s\sqrt{2}B_c}{2J\kappa^2}\vec{b}, \tag{4.74}$$

where $\vec{B}_Z$ is the Zeeman field and

$$\mu_s = g\mu_B \tag{4.75}$$

– the magnetic moment of the spins in the skyrmion material.

Define

$$\tilde{\mu}_s = \frac{\mu_s}{2J\kappa^2\mu_0}, \tag{4.76}$$

then

$$\vec{\beta}_\kappa = \sqrt{2}\,\tilde{\mu}_s\tilde{H}_c\vec{b}, \tag{4.77}$$

or

$$\vec{b} = \frac{1}{\sqrt{2}\,\tilde{\mu}_s\tilde{H}_c}\vec{\beta}_\kappa, \tag{4.78}$$

and then we re-label back $\vec{\beta}_\kappa \to \vec{\beta}$. This is the way $\vec{b}$ and $\vec{\beta}$ are related. We would juggle between them for computational convenience, though keeping in mind that it is actually the same mathematical quantity with different constant prefactor.

In contrast with systems considered in previous chapters, we are not working in quasi 2D system anymore. Moreover, the system is not uniform in z-direction, as it is composite of two different media: skyrmion and superconducting materials with possible gap between them. Hence stray field and interface effects have to be taken into account.

Let us derive the interface conditions first. Recall from the general electrodynamics, that on the interface between two media we get

$$B_{\perp_1} = B_{\perp_2} \tag{4.79}$$

and

$$H_{\parallel_1} = H_{\parallel_2}, \tag{4.80}$$

i.e. the component of $\vec{B}$ that is perpendicular to the interface (B_z in our case) is continuous, and so is the component of $\vec{H}$ that is parallel to the interface.

Ginzburg-Landau functional, (4.73), describes a superconductor in an external field that is uniform. Even in this case, though, the full free energy functional is written as

$$F_{SC} = 2J\kappa^2 \tilde{H}_c^2 \int \left\{ -\left|\tilde{\psi}\right|^2 + \frac{1}{2}\left|\tilde{\psi}\right|^4 + \left|\left(-i\tilde{\xi}\tilde{\nabla} - \vec{a}\right)\tilde{\psi}\right|^2 + \left(\vec{b} - \vec{h}\right)^2 \right\} \frac{d\tilde{x}d\tilde{y}}{\tilde{A}}, \tag{4.81}$$

but h-part is often omitted, as for the uniform external field

$$\vec{h} = (0, 0, h_0) \tag{4.82}$$

and $h_0 = const$, hence it does not affect Ginzburg-Landau equations derived from (4.81). It was already discussed in section 3.2.2.

However, the presence of a skyrmion lattice in proximity to a superconductor means that the field external to a superconductor is no longer uniform, hence the functional in (4.73) needs to be modified as in (4.81), just with

$$\vec{h} = h_0\hat{e}_z + \tilde{\mu}_s M_z \hat{e}_z + \vec{h}_d, \tag{4.83}$$

where $\vec{h}_d = \left(h_{d_x}, h_{d_y}, 0\right)$ is the demagnetisation (stray) field of a magnetic material expressed in our usual dimensionless units, obeying

$$\nabla \times \vec{h}_d = 0, \tag{4.84}$$

M_z is z-component of the magnetisation of the skyrmion lattice, $\vec{M}$, that is normalised by $\left|\vec{M}\right|^2 = 1$, $\tilde{\mu}_s$ is the magnetic moment of spins in the skyrmion material and h_0 is the uniform external field, related to the initial $\vec{\beta}$ applied to a magnetic material in our skyrmion lattice study (we used it as a control parameter). Call it to be $\vec{\beta}_0$ now,

$$\vec{\beta}_0 = (0, 0, \beta_0)\,, \tag{4.85}$$

$\beta_0 = const$. One shall also keep in mind that the magnetisation, $\vec{M}$, in equation (4.83) arises due to the skyrmion lattice, hence has nothing to do with the usual expansion of the magnetic induction, $\vec{B} = \mu_0\left(\vec{H} + \vec{M}_{SC}\right)$, as this is related to a superconductor only, and it is $\vec{H}$ ($\vec{h}$ in the dimensionless formulation) itself that is modified by skyrmions. The final outfit of $\vec{h}$ is now

$$\vec{h} = h_0\hat{e}_z + \tilde{\mu}_s M_z \hat{e}_z + h_{d_x}\hat{e}_x + h_{d_y}\hat{e}_y, \tag{4.86}$$

For notational convenience relabel:

$$\tilde{\psi} \to \psi, \tag{4.87}$$

$$\tilde{\nabla} \to \nabla, \tag{4.88}$$

$$\tilde{A} \to A, \tag{4.89}$$

$$\tilde{\xi} \to \xi, \tag{4.90}$$

$$\vec{a} \to \vec{A}, \tag{4.91}$$

$$\vec{b} \to \vec{B}, \tag{4.92}$$

$$\vec{h} \to \vec{H}, \tag{4.93}$$

$$\vec{h}_d \to \vec{H}_d, \tag{4.94}$$

$$\vec{h}_0 \to \vec{H}_0, \tag{4.95}$$

$$\tilde{H}_c \to H_c, \tag{4.96}$$

$$\tilde{\mu}_s \to \mu_s, \tag{4.97}$$

etc. Keep $\tilde{\lambda}$, though, in order to avoid confusion with the Lagrange multiplier.

Ginzburg-Landau functional for a superconductor in proximity to a skyrmion lattice is then written as

$$\begin{aligned} F_{SC} &= 2J\kappa^2 H_c^2 \int \left\{ -|\psi|^2 + \frac{1}{2}|\psi|^4 + \left|\left(-i\xi\nabla - \vec{A}\right)\psi\right|^2 + \left|\vec{B}\right|^2 \right. \\ &- 2\vec{B}\cdot\left(H_0\hat{e}_z + \mu_s M_z \hat{e}_z + H_{d_x}\hat{e}_x + H_{d_y}\hat{e}_y\right) \\ &+ \left.\left(H_0\hat{e}_z + \mu_s M_z \hat{e}_z + H_{d_x}\hat{e}_x + H_{d_y}\hat{e}_y\right)^2 \right\} \frac{dxdy}{A}, \\ &= 2J\kappa^2 H_c^2 \int \left\{ -|\psi|^2 + \frac{1}{2}|\psi|^4 + \left|\left(-i\xi\nabla - \vec{A}\right)\psi\right|^2 + \left|\vec{B}\right|^2 \right. \\ &- 2\vec{B}\cdot\left(H_0\hat{e}_z + \mu_s M_z \hat{e}_z + H_{d_x}\hat{e}_x + H_{d_y}\hat{e}_y\right) \\ &+ \left. H_0^2 + H_{d_x}^2 + H_{d_y}^2 + 2\mu_s H_0 M_z + \mu_s^2 M_z^2 \right\} \frac{dxdy}{A}, \end{aligned} \tag{4.98}$$

or just

$$F_{SC} = 2J\kappa^2 H_c^2 \tilde{F}_{SC}. \tag{4.99}$$

Finally, let us combine the Ginzburg-Landau functional, (4.98), with the free energy functional of a magnetic material, (4.64):

$$F = 2J\kappa^2 \left(H_c^2 \tilde{F}_{SC} + \tilde{F}_{SkX}\right) = 2J\kappa^2 H_c^2 \left(\tilde{F}_{SC} + \gamma \tilde{F}_{SkX}\right), \tag{4.100}$$

where we have defined

$$\gamma = \frac{1}{H_c^2}, \tag{4.101}$$

and

$$\tilde{F}_{SkX} = \int \left\{ \frac{1}{4} \left(\partial_\mu \vec{M} \right) \cdot \left(\partial_\mu \vec{M} \right) + \vec{M} \cdot \left(\nabla \times \vec{M} \right) - \vec{\beta} \cdot \vec{M} + \lambda \left(\left| \vec{M} \right|^2 - 1 \right) \right\} \frac{dxdy}{A} \quad (4.102)$$

is the dimensionless free energy functional for a magnetic material.

The total, combined functional, then reads as

$$\begin{aligned} F &= 2J\kappa^2 H_c^2 \left(\tilde{F}_{SC} + \gamma \tilde{F}_{SkX} \right) \quad (4.103) \\ &= 2J\kappa^2 H_c^2 \int \left\{ - |\psi|^2 + \frac{1}{2} |\psi|^4 + \left| \left(-i\xi\nabla - \vec{A} \right) \psi \right|^2 + \left| \vec{B} \right|^2 \right. \\ &- 2\vec{B} \cdot \left(H_0 \hat{e}_z + \mu_s M_z \hat{e}_z + H_{d_x} \hat{e}_x + H_{d_y} \hat{e}_y \right) \\ &+ H_0^2 + H_{d_x}^2 + H_{d_y}^2 + 2\mu_s H_0 M_z + \mu_s^2 M_z^2 \\ &+ \left. \gamma \left[\frac{1}{4} \left(\partial_\mu \vec{M} \right) \cdot \left(\partial_\mu \vec{M} \right) + \vec{M} \cdot \left(\nabla \times \vec{M} \right) - \vec{\beta} \cdot \vec{M} + \lambda \left(\left| \vec{M} \right|^2 - 1 \right) \right] \right\} \frac{dxdy}{A}, \end{aligned}$$

and now γ and μ_s are our new control parameters that represent the contribution of the skyrmion part to the total energy and the magnitude of the magnetic moment of spins in the magnetic (helical, skyrmion or ferromagnetic) system respectively.

In the real world $\mu_s \sim \mu_B$ and $\gamma \sim \frac{1}{H_c^2}$. For example, for MnSi $\mu_s = 0.4\mu_B$; for Nb $H_c \sim 200mT$ and depends on temperature.

4.3.2 Modified Equations

We have mentioned in the section 4.1, that as there is a skyrmion lattice in proximity to a superconductor, the total external field would not necessarily stay uniform. However, this is also true for the skyrmion lattice itself: the external field, β, can be modified by a superconductor. It is no longer constant, hence has to be Fourier expanded in the same way as the components of $\vec{M}$ are:

$$\vec{\beta} = \vec{\beta}(x, y) = \sum_{\vec{k}} \vec{\beta}_{\vec{k}} e^{-i\vec{k}\vec{r}}, \quad (4.104)$$

hence Euler-Lagrange equations derived from the free energy functional for a magnetic material would be modified to

$$\left(\partial_x^2 + \partial_y^2 \right) M_x - 4\partial_y M_z - 4\lambda M_x = -2\beta_x, \quad (4.105)$$

$$\left(\partial_x^2 + \partial_y^2 \right) M_y + 4\partial_x M_z - 4\lambda M_y = -2\beta_y, \quad (4.106)$$

$$\left(\partial_x^2 + \partial_y^2 \right) M_z - 4 \left(\partial_x M_y - \partial_y M_x \right) - 4\lambda M_z = -2\beta_z. \quad (4.107)$$

and thus in Fourier form they become:

$$\sum_{\vec{k}'}\left[\left\{-k'^2X_{\vec{k}'}+4ik'_yZ_{\vec{k}'}\right\}\delta_{\vec{k}\vec{k}'}-4X_{\vec{k}'}\lambda_{\vec{k}-\vec{k}'}\right]=-2\sum_{\vec{k}'}\beta_{x_{\vec{k}'}}\delta_{\vec{k}\vec{k}'}, \tag{4.108}$$

$$\sum_{\vec{k}'}\left[\left\{-k'^2Y_{\vec{k}'}-4ik'_xZ_{\vec{k}'}\right\}\delta_{\vec{k}\vec{k}'}-4Y_{\vec{k}'}\lambda_{\vec{k}-\vec{k}'}\right]=-2\sum_{\vec{k}'}\beta_{y_{\vec{k}'}}\delta_{\vec{k}\vec{k}'}, \tag{4.109}$$

$$\sum_{\vec{k}'}\left[\left\{-k'^2Z_{\vec{k}'}+4i\left(k'_xY_{\vec{k}'}-k'_yX_{\vec{k}'}\right)\right\}\delta_{\vec{k}\vec{k}'}-4Z_{\vec{k}'}\lambda_{\vec{k}-\vec{k}'}\right]=-2\sum_{\vec{k}'}\beta_{z_{\vec{k}'}}\delta_{\vec{k}\vec{k}'}, \tag{4.110}$$

i.e. $\vec{\beta}$ is no longer constant and we need to take into account Fourier coefficients of $\vec{\beta}$ – $\vec{\beta}_{\vec{k}}=\left(\beta_{x_{\vec{k}}},\beta_{y_{\vec{k}}},\beta_{z_{\vec{k}}}\right)$, but this is the only change that one has to make to the skyrmion part of our survey. Superconducting part, however, gets a bit more tricky.

In order to take into account effects of a skyrmion lattice on a superconductor introduced via relation (4.86) in the most efficient way, let us introduce a vector that combines them:

$$\vec{P}=\begin{pmatrix}H_{d_x}\\H_{d_y}\\\mu_sM_z\end{pmatrix}. \tag{4.111}$$

Notice that vector $\vec{P}$ on its own has no physical meaning.

The effective Ginzburg-Landau functional in Brandt's form derived from (4.98) is

$$\tilde{F}_{eff}=\int\left\{-f+\frac{f^2}{2}+\frac{\xi^2\left(\nabla f\right)^2}{4f}+f\left|\vec{Q}\right|^2+\tilde{\lambda}^2\left|\nabla\times\vec{Q}\right|^2-2\tilde{\lambda}\left(\nabla\times\vec{Q}\right)\cdot\vec{P}\right\}\frac{dxdy}{A}, \tag{4.112}$$

where we have omitted H_0 term, as we are interested in Euler-Lagrange equations derived from this functional only at the moment.

Minimisation of the functional (4.112) with respect to f, however, is not different from the minimisation of Ginzburg-Landau-Brandt functional from section 3.5.2, as there is no interaction between f and $\vec{M}$ or $\vec{H}_d$, so the first Ginzburg-Landau-Brandt equation remains unchanged, though shall be now formulated via ξ, not via κ_{GL}, in order to satisfy our new dimensionless formulation. Hence the formulation for $a_{\vec{k}}$, that is a Fourier coefficient for f, is

$$a_{\vec{k}}=\frac{4}{\xi^2}\frac{\left\langle\left(2f-f^2-f|\vec{Q}|^2-g\right)e^{i\vec{k}\vec{r}}\right\rangle}{k^2+2\xi^{-2}}, \tag{4.113}$$

where g is now

$$g=\frac{\xi^2(\nabla f)^2}{4f}. \tag{4.114}$$

The second Ginzburg-Landau-Brandt equation does change, however. It is derived to be

$$2f\vec{Q} + 2\tilde{\lambda}^2\left(\nabla \times \nabla \times \vec{Q}\right) - 2\tilde{\lambda}\nabla \times \vec{P} = 0, \tag{4.115}$$

but as the triple cross product can be simplified to

$$\nabla \times \nabla \times \vec{Q} = -\nabla^2\vec{Q} + \nabla\left(\nabla \cdot \vec{Q}\right) \tag{4.116}$$

and

$$\nabla \cdot \vec{Q} = 0 \tag{4.117}$$

because of the gauge choice, equation (4.115) becomes:

$$f\vec{Q} - \tilde{\lambda}^2\nabla^2\vec{Q} - \tilde{\lambda}\nabla \times \vec{P} = 0, \tag{4.118}$$

that can be transformed to

$$-\tilde{\lambda}^2\nabla^2\vec{Q} = -f\vec{Q} + \tilde{\lambda}\nabla \times \vec{P}, \tag{4.119}$$

and this is the second Ginzburg-Landau-Brandt equation for a system of a superconductor and a magnetic material combined.

Let us now apply Brandt's trick described in section 3.5.2, i.e. write $\vec{Q} = \vec{Q}_A + \vec{Q}_b$, curl both sides of equation (4.119), add $\bar{f}\vec{B}$ to them (to stay consistent with Brandt's approach) and divide the whole equation by $\tilde{\lambda}$. Thus obtain

$$\left(-\nabla^2 + \bar{f}\right)\vec{B} = -\frac{1}{\tilde{\lambda}^2}\left(f - \tilde{\lambda}^2\bar{f}\right)\vec{B} + \frac{1}{\tilde{\lambda}^2}f\vec{\bar{B}} - \frac{1}{\tilde{\lambda}}\vec{p} + \nabla \times \nabla \times \vec{P}, \tag{4.120}$$

and f, $\bar{f}$ and $\vec{p}$ are defined in section 4.2.

Expand the coupling term:

$$\nabla \times \nabla \times \vec{P} = \nabla\left(\nabla \cdot \vec{P}\right) - \nabla^2\vec{P} = \begin{pmatrix} -\partial_y^2 H_{d_x} + \partial_x\partial_y H_{d_y} \\ \partial_x\partial_y H_{d_x} - \partial_x^2 H_{d_y} \\ -\mu_s\partial_x^2 M_z - \mu_s\partial_y^2 M_z \end{pmatrix}, \tag{4.121}$$

and notice that the first two components of this vector correspond to $\nabla \times \vec{H}_d$, but

$$\nabla \times \vec{H}_d = 0, \tag{4.122}$$

hence the equations for three components of $\vec{B}$ become:

$$\left(-\nabla^2 + \bar{f}\right)B_x = -\frac{1}{\tilde{\lambda}^2}\left[\tilde{\lambda}\left(f - \tilde{\lambda}^2\bar{f}\right)B_x - f\bar{B}_x + \tilde{\lambda}p_x\right], \tag{4.123}$$

$$\left(-\nabla^2+\bar{f}\right)B_y=-\frac{1}{\tilde{\lambda}^2}\left[\tilde{\lambda}\left(f-\tilde{\lambda}^2\bar{f}\right)B_y-f\bar{B}_y+\tilde{\lambda}p_y\right], \tag{4.124}$$

$$\left(-\nabla^2+\bar{f}\right)B_z=-\frac{1}{\tilde{\lambda}^2}\left[\tilde{\lambda}\left(f-\tilde{\lambda}^2\bar{f}\right)B_z-f\bar{B}_z+\tilde{\lambda}p_z-\mu_s\tilde{\lambda}^2\left(-\partial_x^2M_z-\partial_y^2M_z\right)\right]. \tag{4.125}$$

Now expand B_x, B_y and B_z on the LHS via Fourier transform, then multiply all the equations by $\frac{1}{A}e^{i\vec{k}'\vec{r}}$ and integrate with respect to x and y (just as we did in section 4.2) to get expressions for Fourier coefficients for $\vec{B}$:

$$b_{x_{\vec{k}}}=-2\frac{\left\langle\left[\tilde{\lambda}\left(f-\tilde{\lambda}^2\bar{f}\right)B_x-f\bar{B}_x+\tilde{\lambda}p_x\right]e^{i\vec{k}\vec{r}}\right\rangle}{\tilde{\lambda}^2\left(k^2+\bar{f}\right)}, \tag{4.126}$$

$$b_{y_{\vec{k}}}=-2\frac{\left\langle\left[\tilde{\lambda}\left(f-\tilde{\lambda}^2\bar{f}\right)B_y-f\bar{B}_y+\tilde{\lambda}p_y\right]e^{i\vec{k}\vec{r}}\right\rangle}{\tilde{\lambda}^2\left(k^2+\bar{f}\right)}, \tag{4.127}$$

$$b_{z_{\vec{k}}}=-2\frac{\left\langle\left[\tilde{\lambda}\left(f-\tilde{\lambda}^2\bar{f}\right)B_z-f\bar{B}_z+\tilde{\lambda}p_z-\mu_s\tilde{\lambda}^2\left(-\partial_x^2M_z-\partial_y^2M_z\right)\right]e^{i\vec{k}\vec{r}}\right\rangle}{\tilde{\lambda}^2\left(k^2+\bar{f}\right)}, \tag{4.128}$$

and these are to be used in our future calculations.

It follows, though, from expressions (4.126) and (4.127) that B_x and B_y are not different from the case of no skyrmion lattice present, hence $B_x=B_y=0$, but we would still keep them in the model should we want to extend it in the future.

4.3.3 Modified Ginzburg-Landau-Brandt Functional in Fourier Form

In the previous section we had mentioned the free energy functional calculations (not to be confused with the minimisation). We have already derived the form of the free energy functional for a magnetic material that is the most convenient for calculations if $\vec{M}$ is Fourier transformed in section 2.4.5. Let us now derive such an expression for the Ginzburg-Landau-Brandt functional. Recall the Ginzburg-Landau functional:

$$\begin{aligned}\tilde{F}_{SC} &= \int\Big\{-|\psi|^2+\frac{1}{2}|\psi|^4+\left|\left(-i\xi\nabla-\vec{A}\right)\psi\right|^2+\left|\vec{B}\right|^2 \\ &- 2\vec{B}\cdot\left(H_0\hat{e}_z+\mu_sM_z\hat{e}_z+H_{d_x}\hat{e}_x+H_{d_y}\hat{e}_y\right) \\ &+ H_0^2+H_{d_x}^2+H_{d_y}^2+2\mu_sH_0M_z+\mu_s^2M_z^2\Big\}\frac{dxdy}{A}.\end{aligned} \tag{4.129}$$

This can be converted into Brandt's form, i.e. to

$$\begin{aligned}\tilde{F}_B &= \int \Big\{ -f + \frac{f^2}{2} + \frac{\xi^2 (\nabla f)^2}{4f} + f \left|\vec{Q}\right|^2 + \left|\vec{B}\right|^2 \\ &- 2\vec{B} \cdot \left(H_0 \hat{e}_z + \mu_s M_z \hat{e}_z + H_{d_x} \hat{e}_x + H_{d_y} \hat{e}_y \right) \\ &+ H_0^2 + H_{d_x}^2 + H_{d_y}^2 + 2\mu_s H_0 M_z + \mu_s^2 M_z^2 \Big\} \frac{dxdy}{A},\end{aligned} \tag{4.130}$$

where M_z is Fourier expanded as in section 2.3.2,

$$M_z = \sum_{\vec{k}} Z_{\vec{k}} e^{-i\vec{k}\vec{r}}, \tag{4.131}$$

but Fourier expansion of other quantities is different from that introduced in section 4.2:

$$f = \sum_{\vec{k}} a'_{\vec{k}} e^{-i\vec{k}\vec{r}}, \tag{4.132}$$

hence its derivative is

$$\nabla f = -i \sum_{\vec{k}} a'_{\vec{k}} \vec{k} e^{-i\vec{k}\vec{r}}, \tag{4.133}$$

also define Fourier expansion of the inverse f separately:

$$\frac{1}{f} = \omega = \sum_{\vec{k}} \omega_{\vec{k}} e^{-i\vec{k}\vec{r}}, \tag{4.134}$$

field components are also redefined as

$$B_x = \sum_{\vec{k}} b'_{x_{\vec{k}}} e^{-i\vec{k}\vec{r}}, \tag{4.135}$$

$$B_y = \sum_{\vec{k}} b'_{y_{\vec{k}}} e^{-i\vec{k}\vec{r}}, \tag{4.136}$$

$$B_z = \sum_{\vec{k}} b'_{z_{\vec{k}}} e^{-i\vec{k}\vec{r}}, \tag{4.137}$$

and $\vec{Q}$ components as well:

$$Q_x = \sum_{\vec{k}} q_{x_{\vec{k}}} e^{-i\vec{k}\vec{r}}, \tag{4.138}$$

$$Q_y = \sum_{\vec{k}} q_{y_{\vec{k}}} e^{-i\vec{k}\vec{r}}, \tag{4.139}$$

$$Q_z = \sum_{\vec{k}} q_{z_{\vec{k}}} e^{-i\vec{k}\vec{r}}. \tag{4.140}$$

Fourier formulations were changed against those used in section 4.2 in order to simplify the calculations of the functional, as there is no need to calculate Fourier coefficients via any external algorithm: they can be found directly from the converged quantities. For example, for converged $f = f(x, y)$ that can be expanded as

$$f = \sum_{\vec{k}} a'_{\vec{k}} e^{-i\vec{k}\vec{r}}, \tag{4.141}$$

Fourier coefficient, $a'_{\vec{k}}$, is found via

$$a'_{\vec{k}} = \left\langle f(x, y) e^{i\vec{k}\vec{r}} \right\rangle \tag{4.142}$$

for a given $\vec{k}$.

Now let us calculate all the separate terms of the functional step by step. In order to calculate of them we would need integrals of δ-function that can be found in Appendix A.2.2 along with derivations. Write

$$\tilde{F}_B = F_1 + F_2 + F_3 + F_4 + F_5 + F_6, \tag{4.143}$$

then F_1 is found to be

$$F_1 = \int (-f) \frac{dxdy}{A} = -\int \sum_{\vec{k}} a'_{\vec{k}} e^{-i\vec{k}\vec{r}} \frac{dxdy}{A} = -a'_{\vec{k}} \delta_{\vec{k},0} = -a'_0. \tag{4.144}$$

Similarly, F_2 is

$$F_2 = \frac{1}{2} \int f^2 \frac{dxdy}{A} = \frac{1}{2} \int \sum_{\vec{k}\vec{k}'} a'_{\vec{k}} a'_{\vec{k}'} e^{-i(\vec{k}+\vec{k}')\vec{r}} = \frac{1}{2} \sum_{\vec{k}\vec{k}'} a'_{\vec{k}} a'_{\vec{k}'} \delta_{\vec{k},-\vec{k}'} = \frac{1}{2} \sum_{\vec{k}\vec{k}'} a'_{\vec{k}} a'^{*}_{\vec{k}'} = \frac{1}{2} \sum_{\vec{k}} \left| a'_{\vec{k}} \right|^2. \tag{4.145}$$

And hence all the other terms. F_3:

$$\begin{aligned} F_3 &= \frac{\xi^2}{4} \int \nabla f \nabla f \omega \frac{dxdy}{A} = -\frac{\xi^2}{4} \int \sum_{\vec{k}\vec{k}'\vec{k}''} a'_{\vec{k}} a'_{\vec{k}'} \omega_{\vec{k}''} \vec{k} \cdot \vec{k}' e^{-i(\vec{k}+\vec{k}'+\vec{k}'')\vec{r}} \frac{dxdy}{A} \\ &= -\frac{\xi^2}{4} \sum_{\vec{k}\vec{k}'\vec{k}''} a'_{\vec{k}} a'_{\vec{k}'} \omega_{\vec{k}''} \vec{k} \cdot \vec{k}' \delta_{\vec{k}+\vec{k}',-\vec{k}''} = -\frac{\xi^2}{4} \sum_{\vec{k}\vec{k}'} a'_{\vec{k}} a'_{\vec{k}'} \omega^*_{\vec{k}+\vec{k}'} \vec{k} \cdot \vec{k}'. \end{aligned} \tag{4.146}$$

F_4:

$$F_4 = \int f \left| \vec{Q} \right|^2 \frac{dxdy}{A}. \tag{4.147}$$

In order to simplify our life, expand $\left|\vec{Q}\right|^2$ first:

$$\left|\vec{Q}\right|^2 = Q_x^2 + Q_y^2 + Q_z^2, \tag{4.148}$$

where

$$Q_\mu^2 = \sum_{\vec{k}\vec{k}'} q_{\mu_{\vec{k}}} q_{\mu_{\vec{k}'}} e^{-i(\vec{k}+\vec{k}')\vec{r}}, \tag{4.149}$$

hence

$$\left|\vec{Q}\right|^2 = \sum_{\vec{k}\vec{k}'} \left(q_{x_{\vec{k}}} q_{x_{\vec{k}'}} + q_{y_{\vec{k}}} q_{y_{\vec{k}'}} + q_{z_{\vec{k}}} q_{z_{\vec{k}'}} \right) e^{-i(\vec{k}+\vec{k}')\vec{r}}. \tag{4.150}$$

Define

$$\vec{q}_{\vec{k}\vec{k}'}{}^2 = q_{x_{\vec{k}}} q_{x_{\vec{k}'}} + q_{y_{\vec{k}}} q_{y_{\vec{k}'}} + q_{z_{\vec{k}}} q_{z_{\vec{k}'}} \tag{4.151}$$

to simplify:

$$\left|\vec{Q}\right|^2 = \sum_{\vec{k}\vec{k}'} \vec{q}_{\vec{k}\vec{k}'}{}^2 e^{-i(\vec{k}+\vec{k}')\vec{r}}, \tag{4.152}$$

hence F_4 is

$$F_4 = \int \sum_{\vec{k}\vec{k}'\vec{k}''} \vec{q}_{\vec{k}\vec{k}'}{}^2 a'_{\vec{k}''} e^{-i(\vec{k}+\vec{k}'+\vec{k}'')\vec{r}} \frac{dxdy}{A} = \sum_{\vec{k}\vec{k}'} \vec{q}_{\vec{k}\vec{k}'}{}^2 a'^*_{\vec{k}+\vec{k}'}. \tag{4.153}$$

F_5:

$$F_5 = \int \left|\vec{B}\right| \frac{dxdy}{A} = \int \sum_{\vec{k}\vec{k}'} \vec{b}'_{\vec{k}\vec{k}'}{}^2 e^{-i(\vec{k}+\vec{k}')\vec{r}} = \sum_{\vec{k}\vec{k}'} \vec{b}'_{\vec{k}\vec{k}'}{}^2 \delta_{\vec{k},-\vec{k}'} = \sum_{\vec{k}} \left|\vec{b}'_{\vec{k}}\right|^2, \tag{4.154}$$

where

$$\vec{b}'^2_{\vec{k}} = b'_{x_{\vec{k}}} b'_{x_{\vec{k}}} + b'_{y_{\vec{k}}} b'_{y_{\vec{k}}} + b'_{z_{\vec{k}}} b'_{z_{\vec{k}}}. \tag{4.155}$$

and

$$\left|\vec{b}'_{\vec{k}}\right|^2 = b'_{x_{\vec{k}}} b'^*_{x_{\vec{k}}} + b'_{y_{\vec{k}}} b'^*_{y_{\vec{k}}} + b'_{z_{\vec{k}}} b'^*_{z_{\vec{k}}}. \tag{4.156}$$

F_6:

$$\begin{aligned} F_6 &= \int \Big\{ -2\vec{B} \cdot \left(H_0 \hat{e}_z + \mu_s M_z \hat{e}_z + H_{d_x} \hat{e}_x + H_{d_y} \hat{e}_y \right) \\ &+ H_0^2 + H_{d_x}^2 + H_{d_y}^2 + 2\mu_s H_0 M_z + \mu_s^2 M_z^2 \Big\} \frac{dxdy}{A}, \end{aligned} \tag{4.157}$$

now deal with H_{d_x} and H_{d_y}. As $\nabla \times \vec{H}_d = 0$, one can define a potential, U_d, such that

$$\nabla U_d = \vec{H}_d. \tag{4.158}$$

The magnetic induction, $\vec{B}$, in a magnetic material can be also written in terms of $\vec{H}_d$ and

$\vec{M}$:

$$\vec{B} = \mu_0 \left(\vec{H} + \mu_s \vec{M} \right), \tag{4.159}$$

and as

$$\nabla \cdot \vec{B} = 0, \tag{4.160}$$

obtain the relation of

$$\nabla \cdot \vec{H}_d = -\mu_s \nabla \cdot \vec{M}. \tag{4.161}$$

Now let us Fourier expand U_d just as we expanded M_μ:

$$U_d = \sum_{\vec{k}} u_{\vec{k}} e^{-i\vec{k}\vec{r}}. \tag{4.162}$$

The expression (4.161) then leads to the following relation for U_d:

$$\nabla^2 U_d = -\mu_s \nabla \cdot \vec{M}. \tag{4.163}$$

In Fourier form this then leads to the formulation of Fourier coefficients of U_d:

$$u_{\vec{k}} = -i\mu_s \frac{k_x X_k + k_y Y_k}{k^2} \tag{4.164}$$

for $k \neq 0$; for the case of $k = 0$, $u_{\vec{k}} = u_0 = 0$.

Let us now Fourier expand $\vec{H}_d$ itself,

$$\vec{H}_d = \sum_{\vec{k}} \vec{h}_{\vec{k}} e^{-i\vec{k}\vec{r}}, \tag{4.165}$$

where

$$\vec{h}_{\vec{k}} = \left(h_{x_{\vec{k}}}, h_{y_{\vec{k}}}, 0 \right) \tag{4.166}$$

with

$$h_{x_{\vec{k}}} = -\mu_s \frac{k_x^2 X_k + k_x k_y Y_k}{k^2}, \tag{4.167}$$

$$h_{y_{\vec{k}}} = -\mu_s \frac{k_x k_y X_k + k_y^2 Y_k}{k^2}, \tag{4.168}$$

following from (4.163) and (4.164).

With the aid of (4.167) and (4.168), required for the Fourier formulations of H_{d_x} and H_{d_y},

one obtains the following expression for F_6:

$$\begin{aligned}
F_6 &= \int \Big\{ -2\vec{B}\cdot\left(H_0\hat{e}_z + \mu_s M_z \hat{e}_z + H_{d_x}\hat{e}_x + H_{d_y}\hat{e}_y\right) \\
&+ H_0^2 + H_{d_x}^2 + H_{d_y}^2 + 2\mu_s H_0 M_z + \mu_s^2 M_z^2 \Big\} \frac{dxdy}{A} \\
&= \int \Bigg\{ H_0^2 + \sum_{\vec{k}\vec{k}'} \Big[-2b'_{z_{\vec{k}}} H_0 + 2\mu_s H_0 Z_{\vec{k}} \\
&+ \left(h_{x_{\vec{k}}} h_{xk'} + h_{y_{\vec{k}}} h_{yk'} + \mu_s^2 Z_{\vec{k}} Z_{\vec{k}'} - 2b'_{x_{\vec{k}}} h_{xk'} - 2b'_{y_{\vec{k}}} h_{yk'} - 2\mu_s b'_{z_{\vec{k}}} Z_{\vec{k}'} \right) e^{-i\vec{k}'\vec{r}} \Big] e^{-i\vec{k}\vec{r}} \Bigg\} \frac{dxdy}{A} \\
&= H_0^2 - 2H_0 b'_{z_0} + 2\mu_s H_0 Z_0 \\
&+ \sum_{\vec{k}} \left(h_{x_{\vec{k}}} h^*_{x_{\vec{k}}} + h_{y_{\vec{k}}} h^*_{y_{\vec{k}}} + \mu_s^2 Z_{\vec{k}} Z^*_{\vec{k}} - 2b'_{x_{\vec{k}}} h^*_{x_{\vec{k}}} - 2b'_{y_{\vec{k}}} h^*_{y_{\vec{k}}} - 2\mu_s b'_{z_{\vec{k}}} Z^*_{\vec{k}} \right).
\end{aligned} \tag{4.169}$$

The total Ginzburg-Landau-Brandt functional in terms of Fourier coefficients is then written as

$$\begin{aligned}
\tilde{F}_B &= -a'_0 + \sum_{\vec{k}} \left[\frac{1}{2} \left| a'_{\vec{k}} \right|^2 + \left| \vec{b}'_{\vec{k}} \right|^2 \right] + \sum_{\vec{k}\vec{k}'} \left[-\frac{\xi^2}{4} a'_{\vec{k}} a'_{\vec{k}'} \omega^*_{\vec{k}+\vec{k}'} \vec{k}\cdot\vec{k}' + \vec{q}_{\vec{k}\vec{k}'}{}^2 a'^*_{\vec{k}+\vec{k}'} \right] \\
&+ H_0^2 - 2H_0 b'_{z_0} + 2\mu_s H_0 Z_0 \\
&+ \sum_{\vec{k}} \left(h_{x_{\vec{k}}} h^*_{x_{\vec{k}}} + h_{y_{\vec{k}}} h^*_{y_{\vec{k}}} + \mu_s^2 Z_{\vec{k}} Z^*_{\vec{k}} - 2b'_{x_{\vec{k}}} h^*_{x_{\vec{k}}} - 2b'_{y_{\vec{k}}} h^*_{y_{\vec{k}}} - 2\mu_s b'_{z_{\vec{k}}} Z^*_{\vec{k}} \right).
\end{aligned} \tag{4.170}$$

4.3.4 Summary of the Full Algorithm

Now that we have derived all the modified equations for both magnetic material and superconductor, it is time to summarise the approach. Our new calculation would be based on the following algorithm:

1. calculate the solution for the magnetic system as if there is no superconductor in proximity to it (i.e. with $\vec{\beta} = \vec{\beta_0} = const$);
2. use β_0 to obtain H_0;
3. using modified expressions for Fourier coefficients for f and $\vec{B}$,

$$a_{\vec{k}} = \frac{4}{\xi^2} \frac{\left\langle \left(2f - f^2 - f|\vec{Q}|^2 - g \right) e^{i\vec{k}\vec{r}} \right\rangle}{k^2 + 2\xi^{-2}}, \tag{4.171}$$

$$b_{x_{\vec{k}}} = -2 \frac{\left\langle \left[\tilde{\lambda} \left(f - \tilde{\lambda}^2 \bar{f} \right) B_x - f\bar{B}_x + \tilde{\lambda} p_x \right] e^{i\vec{k}\vec{r}} \right\rangle}{\tilde{\lambda}^2 \left(k^2 + \bar{f} \right)}, \tag{4.172}$$

$$b_{y_{\vec{k}}} = -2\frac{\left\langle \left[\tilde{\lambda}\left(f - \tilde{\lambda}^2\bar{f}\right)B_y - f\bar{B}_y + \tilde{\lambda}p_y\right]e^{i\vec{k}\vec{r}}\right\rangle}{\tilde{\lambda}^2\left(k^2 + \bar{f}\right)}, \tag{4.173}$$

$$b_{z_{\vec{k}}} = -2\frac{\left\langle \left[\tilde{\lambda}\left(f - \tilde{\lambda}^2\bar{f}\right)B_z - f\bar{B}_z + \tilde{\lambda}p_z - \mu_s\tilde{\lambda}^2\left(-\partial_x^2 M_z - \partial_y^2 M_z\right)\right]e^{i\vec{k}\vec{r}}\right\rangle}{\tilde{\lambda}^2\left(k^2 + \bar{f}\right)}, \tag{4.174}$$

calculate f and $\vec{B}$;

4. use $\vec{B}$ to obtain new $\vec{\beta}$ via

$$\vec{\beta} = \sqrt{\frac{2}{\gamma}}\,\mu_s\vec{B}, \tag{4.175}$$

5. calculate new solution for the magnetic system with new $\vec{\beta}$:

$$\left(\partial_x^2 + \partial_y^2\right)M_x - 4\partial_y M_z - 4\lambda M_x = -2\beta_x, \tag{4.176}$$

$$\left(\partial_x^2 + \partial_y^2\right)M_y + 4\partial_x M_z - 4\lambda M_y = -2\beta_y, \tag{4.177}$$

$$\left(\partial_x^2 + \partial_y^2\right)M_z - 4\left(\partial_x M_y - \partial_y M_x\right) - 4\lambda M_z = -2\beta_z; \tag{4.178}$$

6. repeat steps 3-5 until the solution converges (use a and $\vec{M}$ from the previous step);[2]

7. calculate the free energy functional:

$$\begin{aligned}
\tilde{F} &= -a'_0 + H_0^2 + 2H_0\left[\mu_s Z_0 - b'_{z_0}\right] + \sum_{\vec{k}}\left[\frac{1}{2}\left|a'_{\vec{k}}\right|^2 + \left|\vec{b}'_{\vec{k}}\right|^2\right] \\
&+ \sum_{\vec{k}}\left(h_{x_{\vec{k}}}h^*_{x_{\vec{k}}} + h_{y_{\vec{k}}}h^*_{y_{\vec{k}}} + \mu_s^2 Z_{\vec{k}}Z^*_{\vec{k}} - 2b'_{x_{\vec{k}}}h^*_{x_{\vec{k}}} - 2b'_{y_{\vec{k}}}h^*_{y_{\vec{k}}} - 2\mu_s b'_{z_{\vec{k}}}Z^*_{\vec{k}}\right) \\
&+ \sum_{\vec{k}\vec{k}'}\left[-\frac{\xi^2}{4}a'_{\vec{k}}a'_{\vec{k}'}\omega^*_{\vec{k}+\vec{k}'}\vec{k}\cdot\vec{k}' + \vec{q}_{\vec{k}\vec{k}'}{}^2 a'^*_{\vec{k}+\vec{k}'}\right] \\
&+ \gamma\left[\sum_{\vec{k}}\left\{\frac{1}{4}k^2\left(\left|X_{\vec{k}}\right|^2 + \left|Y_{\vec{k}}\right|^2 + \left|Z_{\vec{k}}\right|^2\right)\right.\right. \\
&+ k_y X_{\vec{k}}Z^*_{\vec{k}} - k_x Y_{\vec{k}}Z^*_{\vec{k}} + k_x Y^*_{\vec{k}}Z_{\vec{k}} - k_y X^*_{\vec{k}}Z_{\vec{k}} \\
&- \left.\left.\left(\beta^*_{x_{\vec{k}}}X_{\vec{k}} + \beta^*_{y_{\vec{k}}}Y_{\vec{k}} + \beta^*_{z_{\vec{k}}}Z_{\vec{k}}\right)\right\}\right];
\end{aligned} \tag{4.179}$$

8. find the optimal spacing for a given β_0.

All the procedure can be repeated for different values of μ_s and γ.

[2]This usually takes several iterations for small μ_s if the initial guess is good enough.

4.4 Superconducting Vortex Lattice

4.4.1 Vortex Lattice with no Skyrmions in Proximity to it

Despite the fact that it is the skyrmion lattice of our main concern, let us briefly consider a pure superconducting vortex lattice in order to remind ourselves important relations and dependences that would make our life easier in the future. We would also be able to use the results from this section for comparison purposes just as we would use the results for skyrmion lattices obtained in chapter 2.

We have mentioned in section 4.3.2 that our Ginzburg-Landau-Brandt equations are now formulated with the aid of dimensionless coherence length, ξ, and dimensionless penetration depth, $\tilde{\lambda}$, hence varying them would naturally correspond to considering different superconducting materials. In this section we would like to revisit the optimal spacing of a vortex lattice for given ξ, $\tilde{\lambda}$ and an external filed H_0. This is important, as while considering a combined system of a superconductor and a magnet we assume the lattice spacing to be the same for both materials,[3] hence we would rather adjust ξ and $\tilde{\lambda}$ for the optimal lattice spacing at a given field, H_0, to correspond to that of a skyrmion lattice, than consider a random material, as the shape of the final solution in this case might become unpredictable and numerical procedures would require additional time.

One shall remember, though, that the optimal lattice spacing is bound by an average field, $B_0 = \langle B \rangle = \bar{B}$, that corresponds to some external field H_0, via the following expression:

$$a = \sqrt{\frac{4\pi}{\tilde{\lambda}\xi B_0 \sqrt{3}}}\,. \tag{4.180}$$

However, we would find the optimal spacing numerically in order to be consistent with our approach to skyrmion systems, as when the skyrmion system is attached, the relation between a and $\bar{B}$ becomes non-trivial.

Let us first stick to the external filed of $H_0 = 1.1$ that corresponds to $\beta_0 = 1.1$ for coupling of $\gamma = 2\mu_s^2$. Notice, that while γ is fixed to $2\mu_s^2$, the actual value of μ_s would not affect the relation between H_0 and β_0.

The closer the lattice spacings of disjoint systems are to each other, the easier it would be to couple them. But the lattice spacing is not the only thing of our concern here: another one is the total field of a superconductor, as this is the field acting on a skyrmion system and we would like to make sure it fits into skyrmion region on the filed scale demonstrated in Figure 2.18. Examples of the field distribution on the vortex lattice can be found in Figure 4.4.

[3] Although, This is not a necessary requirement, it makes our calculations a lot easier as there is no need to find the general lattice which would have a huge unit cell comparing to that we have for a system with coinciding lattice spacings of a vortex lattice and a skyrmion lattice. A more general case can be studied in the future.

The dependence of the average total field on the lattice spacing is presented in Figure 4.5.

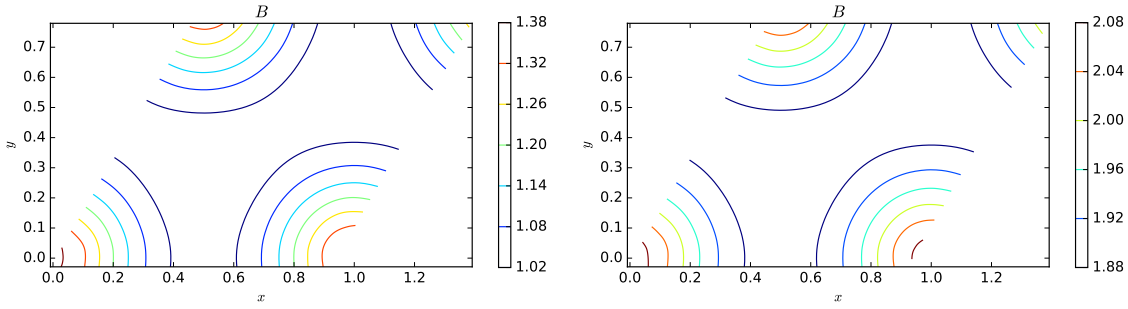

(a) Magnetic field of the vortex lattice for $\xi = 0.5$, $\tilde{\lambda} = 4.5$.

(b) Magnetic field of the vortex lattice $\xi = 0.5$, $\tilde{\lambda} = 8$.

Figure 4.4: Magnetic field of the superconducting vortex lattice for different parameters. In this model $\vec{B} = (0, 0, B_z)$ and B_z is represented by coloured contours. The field presented in this figure is the total field; in order to obtain the pure field that penetrates the superconductor, the external field has to be subtracted.

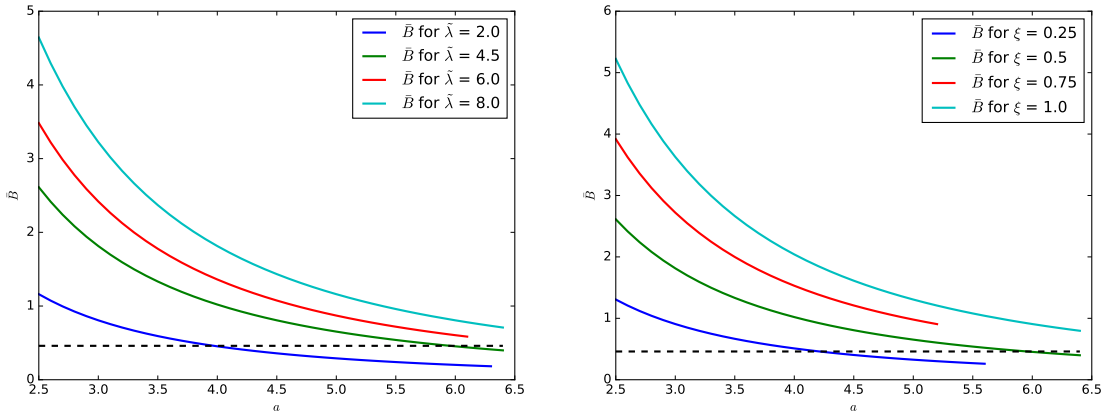

(a) Average magnetic field of the vortex lattice for various values of $\tilde{\lambda}$ with ξ fixed to $\xi = 0.5$.

(b) Average magnetic field of the vortex lattice for various values of ξ with $\tilde{\lambda}$ fixed to $\tilde{\lambda} = 4.5$.

Figure 4.5: Average magnetic field of the superconducting vortex lattice for different parameters. Colour lines indicate the filed for corresponding parameters. A dashed line corresponds to the critical field β_{c_1} (expressed in the same units as B) that stands for the transition from a helical to skyrmionic state.

We can also fix ξ and $\tilde{\lambda}$ and consider the behaviour of the Ginzburg-Landau Functional for different values of an external field, H_0. Such a dependence is demonstrated in Figure 4.6 for several values of H_0 with fixed $\xi = 0.5$ and $\tilde{\lambda} = 4.5$.[4]

[4]We fix these particular values of ξ and $\tilde{\lambda}$ for this demonstration as they are to play extremely important role in the nearest future; the motivation of their choice is just about to follow.

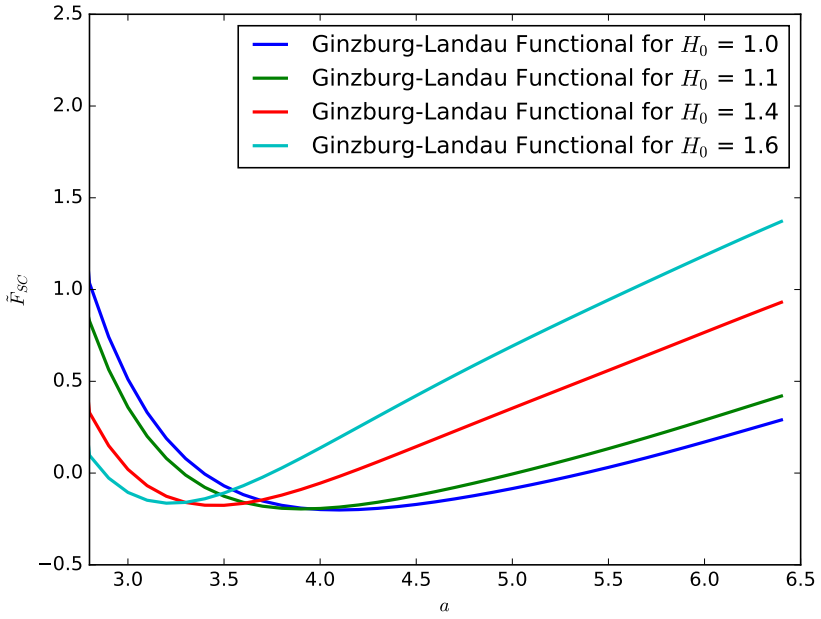

Figure 4.6: Ginzburg-Landau functional for various values of H_0 with fixed $\xi = 0.5$ and $\tilde{\lambda} = 4.5$. Colour lines indicate the Ginzburg-Landau functional calculated for corresponding parameters.

Following the information obtained from Figure 4.5 and Figure 4.6, we conclude that if we would like to couple a skyrmion lattice at an external field of $\beta_0 = 1.1$ that has an optimal spacing of $a = 3.9$, we shall choose ξ and $\tilde{\lambda}$ to be $\xi = 0.5$ and $\tilde{\lambda} = 4.5$ in order to provide the best convergence of the total solution. It is also handy to keep in mind the proper dependence of the optimal spacing on ξ and $\tilde{\lambda}$ when other parameters are fixed. These are demonstrated in Figure 4.7. Such a knowledge would help us to tune ξ and $\tilde{\lambda}$ that would provide the best optimal spacing, hence convergence, while coupled with a stable or metastable skyrmion system of a given spacing.

4.4.2 Vortex Lattice with no Feedback on Skyrmions

Before making use of the method introduced in section 4.3.4 and study an actual bilayer of a skyrmion material and a superconductor, let us consider how does a skyrmion lattice act on a superconductor experiencing no feedback from it. This will be our last test before we proceed to a proper combined system. As we are going to introduce a skyrmion lattice to the superconductor, the coupling, μ_s, becomes important. The higher μ_s is, the higher the effects of skyrmions on a superconductor would be. Let us first of all demonstrate the distribution of the magnetic field on a vortex lattice once the skyrmion lattice is introduced to it for different couplings. The patterns can be observed in Figure 4.8. Notice that we are connecting a

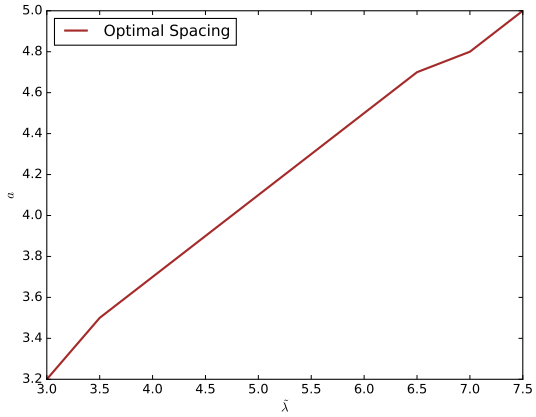

(a) Optimal spacing of the vortex lattice against $\tilde{\lambda}$ with ξ fixed to $\xi = 0.2$.

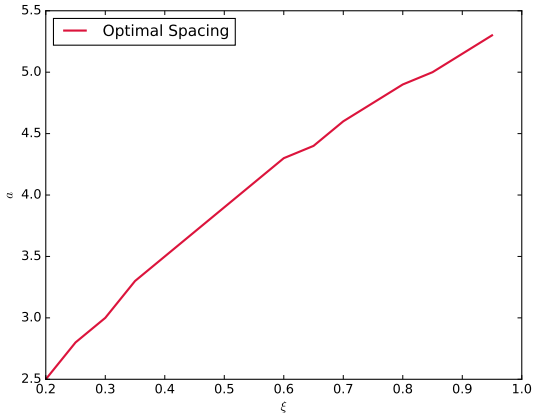

(b) Optimal spacing of the vortex lattice against ξ with $\tilde{\lambda}$ fixed to $\tilde{\lambda} = 4.5$.

Figure 4.7: Optimal spacing of the vortex lattice against $\tilde{\lambda}$ and ξ. For the fixed ξ the optimal spacing increases with $\tilde{\lambda}$ almost linearly; for fixed $\tilde{\lambda}$ the optimal spacing increases with ξ as well.

triangular skyrmion lattice so far. Lattices were obtained for the same values of an external field.

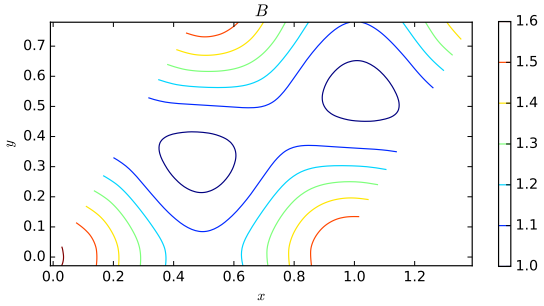

(a) Magnetic field of the vortex lattice coupled with skyrmions. Coupling strength is $\mu_s = 0.1$.

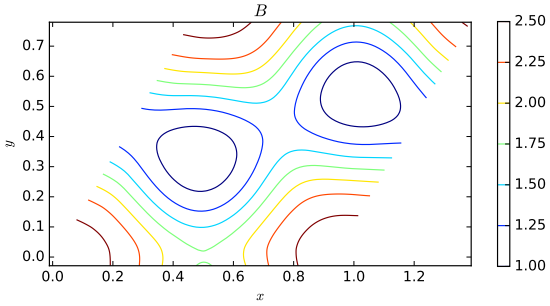

(b) Magnetic field of the vortex lattice coupled with skyrmions. Coupling strength is $\mu_s = 1$.

Figure 4.8: Magnetic field of the vortex lattice for $\xi = 0.5$, $\tilde{\lambda} = 4.5$ coupled with a skyrmion lattice with differnet values of coupling, μ_s. The field presented in this figure is the total field.

As one can see from Figure 4.8, the higher the coupling is, the stronger effects of a skyrmion lattice on the vortex lattice would be. The effects of the skyrmion lattice are seen even better if one compares field profiles from Figure 4.8 with superconducting vortices in absence of any skyrmions around as demonstrated in Figure 3.6. Very large coupling could even destroy the vortex lattice completely. Another important conclusion one can yield is the change of the optimal lattice spacing of a superconducting vortex lattice. For the same external field, ξ and

$\tilde{\lambda}$ as before, the optimal spacing would become smaller. This was actually expected as well, as the total average field increases with coupling increasing, and the optimal lattice spacing of the vortex lattice is related to the total average field. So if we would like to calibrate ξ and $\tilde{\lambda}$ for better convergence of the solution for a proper combined system, it is better to calibrate them on a system with skyrmions already attached, though not experiencing any feedback from the superconductor, as the lattice spacing may differ drastically especially for large values of coupling, μ_s.

4.5 Skyrmion-Superconductor Bilayer

We are just about to study actual systems of combined skyrmion and Abrikosov vortex lattices. There is a huge variety of lattices we can consider, though we would not study all of them, as this seems to be physically impossible timewise. Many of them are also similar to each other, so there is no sense to study two systems that are almost identical. A reasonable approach goes as follows:

- choose a skyrmion lattice to combine with a superconductor, determine the corresponding optimal spacing;
- choose superconducting parameters, ξ and $\tilde{\lambda}$ such that the optimal spacing of a superconductor would coincide with that of the skyrmion lattice or at list lie close to it (this step is not necessary, though will significantly help to obtain stable solutions in oppose to those metastable or not stable at all and speed up the numerical algorithm);
- start with small values of μ_s, as numerical procedures are faster in this case and some physical effects found can still be clarified, do single calculations for fixed β_0 and a;
- bound $\gamma = 2\mu_s^2$ as this maintains the simplest possible relation between superconducting $\vec{B}$ and skyrmion $\vec{\beta}$, hence is the easiest case to control;
- choose other values of γ;
- increase μ_s;
- perform calculations for various values of β_0 and determine the optimal spacing for each value of β_0 for a chosen combination of μ_s and γ.

From our formulation described in section 4.3 we know that changing μ_s affects the vortex part of the system (μ_s is the measure of how much does the skyrmion lattice affects the vortex one) and the relation between $\vec{B}$ and $\vec{\beta}$. On the other hand, γ determines how much the skyrmion free energy contributes to the total free energy and affects the relation between $\vec{B}$ and $\vec{\beta}$. Expected effects of changing μ_s and γ are summarised in Table 4.1.

	small μ_s	large μ_s
small γ	skyrmions do not affect vortex lattice a lot $F_{SC} \gg F_{SkX}$ $\vec{B} \sim \vec{\beta}$, hence the system is easy to control	skyrmions affect vortex lattice a lot $F_{SC} \gg F_{SkX}$ $\vec{\beta}$ is large skyrmions would tend to tear apart
large γ	$F_{SC} \sim F_{SkX}$ skyrmions do not affect vortex lattice a lot $\vec{\beta}$ is small skyrmion lattice would tend to helices	$F_{SC} \sim F_{SkX}$ skyrmions affect vortex lattice a lot $\vec{\beta}$ depends on $\frac{\mu_s}{\sqrt{\gamma}}$ a lot the lattice is unpredictable

Table 4.1: Expected effects of variating coupling parameters μ_s and γ.

Let us quote our first ever results for a combined system here. As it was proposed above, we start with a small coupling, $\mu_s = 0.001$. According to Table 4.1, we do not expect dramatic changes in both systems with respect to their isolated behaviour, but there are some qualitative differences we would like to point out. Let us first of all compare the skyrmion lattice obtained in this combined case against the lattice that is free from a superconductor for the same values of β (β_0 in case of the combined system) and a. This comparison is demonstrated in Figure 4.9. Solution demonstrated in Figure 4.9b was obtained for superconducting $\xi = 0.5$ and $\tilde{\lambda} = 4.5$ in our dimensionless units. The choice of ξ and $\tilde{\lambda}$ was motivated by the fact that the pure superconducting system has its minimal free energy for $\beta_0 = 1.1$ at $a = 3.92$, which is close to the optimal spacing at $\beta = 1.1$ of the free skyrmion system ($a = 3.9$).

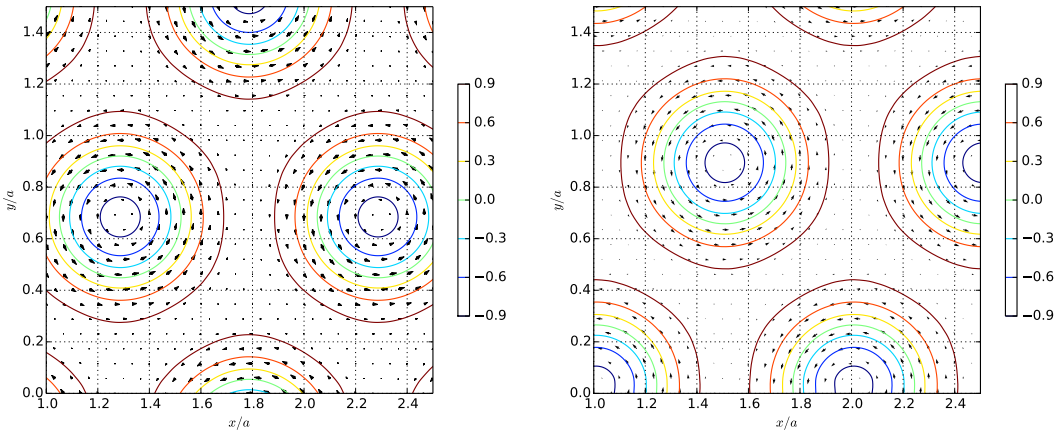

(a) Free skyrmion lattice solution for $\beta = 1.1$ with $a = 3.92$.

(b) Skyrmion lattice combined with a superconductor for $\beta_0 = 1.1$ with $a = 3.92$.

Figure 4.9: Stable solutions for a free skyrmion lattice and a skyrmion lattice that is coupled with a superconductor for the same values of β (β_0) and a. Coupling factors are $\mu_s = 0.001$ and $\gamma = 2\mu_s^2$. Notice that the free solution is not stable (though is quite close to the stable one), whereas the combined one is.

One may conclude straight away from Figure 4.9 that the skyrmion lattice does not change

much if the interaction with a superconductor is weak.

Let us now see how does the skyrmion lattice affect the superconductor. Compare the superconducting field, $\vec{B}$. The comparison is demonstrated in Figure 4.10.

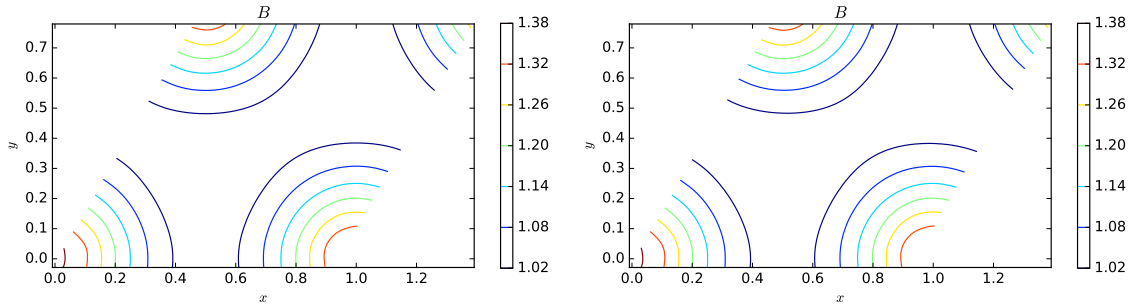

(a) Magnetic field of the vortex lattice.

(b) Magnetic field of the vortex lattice coupled with skyrmions. Coupling strength is $\mu_s = 0.001$.

Figure 4.10: Comparison of the magnetic field of the free vortex lattice for $\xi = 0.5$, $\tilde{\lambda} = 4.5$ with the one coupled with a skyrmion lattice with small coupling, $\mu_s = 0.001$. The field presented in this figure is the total field.

Figure 4.10 tells us that the field pattern on a superconducting vortex lattice is almost not affected by a skyrmion lattice if the coupling is small, and this was predicted and expected.

Finally, let us demonstrate the free energy functional of this combined system. First of all, let us study the dependence of the free energy on the spacing, a. Consult Figure 4.11 for the plot.

For the system of a free skyrmion lattice we have employed the virial theorem in order to determine the optimal spacing for a given β, hence the dependence $\tilde{F}(a)$ was not important itself (though, it was demonstrated in Figure 2.12a with optimal spacing indicated). The shape of skyrmions did not vary much even for completely different spacings (i.e. the shape of a skyrmion remained almost the same for $a = 3$ and for $a = 4$ for a given β). As the virial ratio derived in section 2.4.1 is not valid anymore, $\tilde{F}(a)$ becomes more important – we would use it directly in order to calculate the optimal spacing for a given external field, β_0.

We see from Figure 4.11 that the shape of skyrmions is now quite different for different values of the spacing. As we have mentioned before, for a system of magnetic skyrmions that is not affected by a superconductor there is no much difference in shape of skyrmions despite the different spacing. For a superconductor, though, the relation between the external field and the lattice spacing is well-known. So while changing the spacing, the average field (that later acts on a skyrmion lattice) changes automatically. And the field obviously has a huge impact on the skyrmion structure. If we recall the relation between the field and the spacing

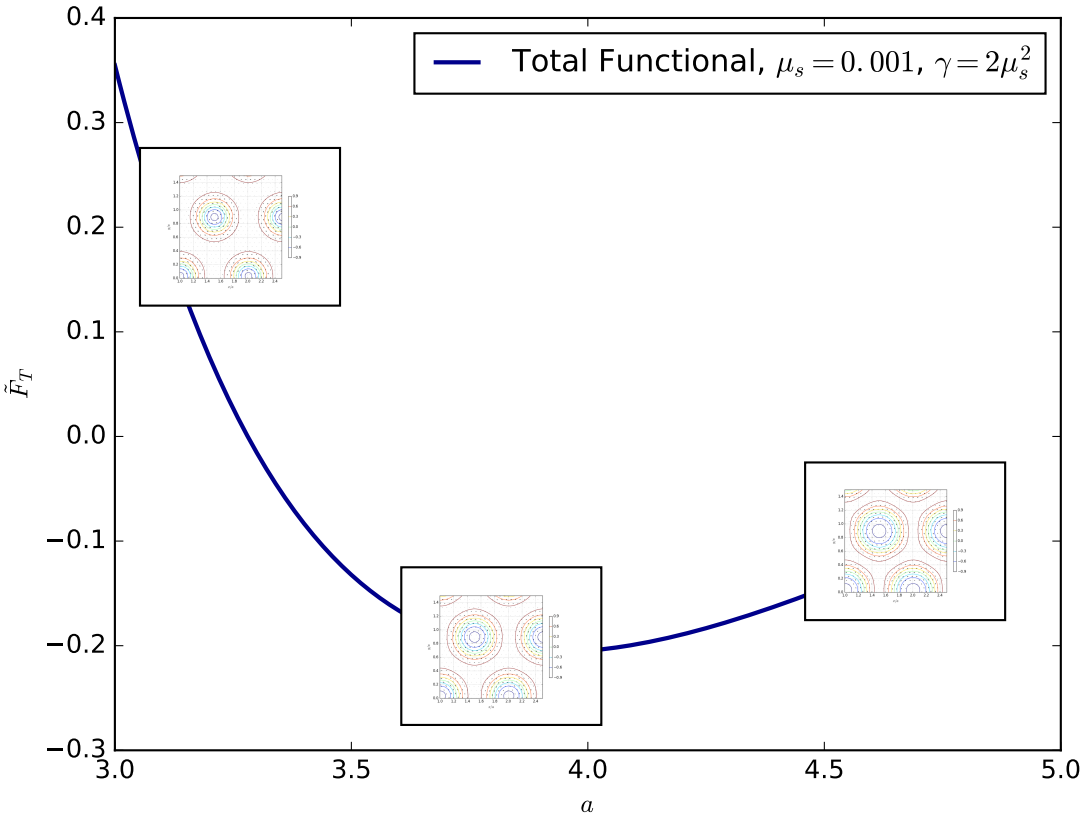

Figure 4.11: Free energy of the combined system of a superconductor and a skyrmion material. Skyrmion lattice is demonstrated in different regions of the functional. The structure of the skyrmions is different with spacing changing, which was not the case for a free skyrmion system.

in superconductors,

$$a = \sqrt{\frac{4\pi}{\tilde{\lambda}\xi B_0 \sqrt{3}}}\,, \tag{4.181}$$

for a triangular lattice in units introduced in section 4.3.4 with B_0 being the average field,[5]

$$B_0 = \langle B \rangle\,, \tag{4.182}$$

we conclude, that large spacings require small fields and vice versa. Large fields, however, as we remember, destroy the skyrmion lattice, and turn the sample into a ferromagnetic state, while small fields would make the lattice tend to the helical state. Hence we conclude that varying the lattice spacing one may obtain a solution of a completely different pattern than

[5]Notice that it is not related to β_0 via relation (4.78).

that expected for a given β_0. For example, a large spacing corresponds to a small field, hence the corresponding skyrmion lattice shall be similar to that near the helix-skyrmion phase transition. From Figure 4.11 we see that our expectations are completely fulfilled.

Remember, so far we are working with weak coupling of $\mu_s = 0.001$. Our γ so far was bound to μ_s in order to simplify the relation between $\vec{\beta}$ and $\vec{B}$. Let us now consider the case when $\gamma > \gamma_0 = 2\mu_s^2$.

Skyrmion lattice as well as the total field of a superconductor does not change drastically while considering $\gamma > \gamma_0$, though still small, so they are not worth to be demonstrated here. Let us, however, study the total free energy functional and its dependence on the spacing (hence determine the optimal one) and applied field, β_0. Corresponding plots can be found in Figure 4.12a and Figure 4.12b respectively.

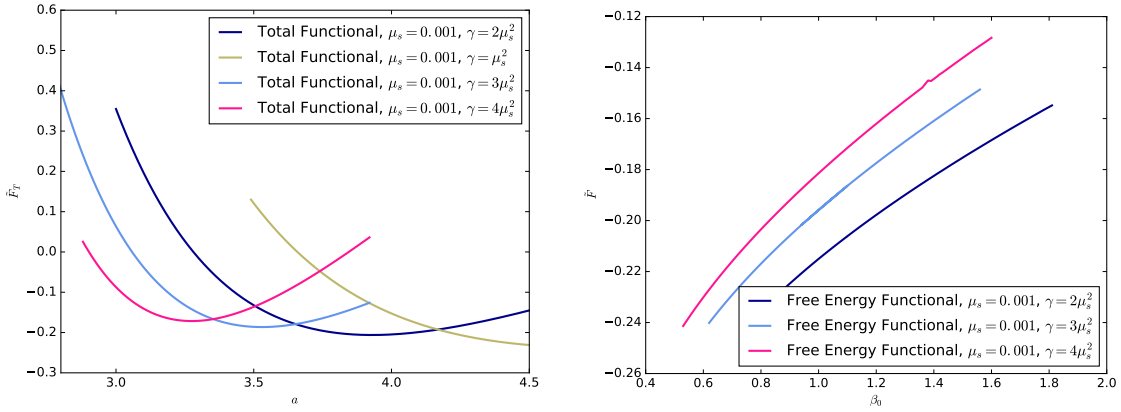

(a) Free energy functional of the combined system against lattice spacing.

(b) Free energy functional of the combined system against the external field.

Figure 4.12: Free energy functional of the combined system against spacing and the external field for different values of γ, though for the same small value of $\mu_s = 0.001$. The optimal spacing becomes quite different with γ changing.

One shall remember, that γ is still rather small, so the main contributor to the total free energy functional is the superconductor. In Figure 4.13 one can find the Ginzburg-Landau functional plotted against the spacing for a fixed value of an external field as well as against the applied field itself.

Comparing graphs in Figure 4.12a and Figure 4.13a, we realise that they are almost identical as well as graphs in Figure 4.12b and Figure 4.13b are. It then confirms the fact that the energy of a superconductor still remains the main contributor to the total energy while slightly increasing γ, though keeping it of the same order. Changing γ drastically would seriously affect $\vec{B} \to \vec{\beta}$ transformation, making the field that is external to a skyrmion lattice either extremely large (which would lead to a ferromagnetic configuration), or extremely small, hence leading to a helical solution for a magnet. Despite being physically correct, helical and ferromagnetic

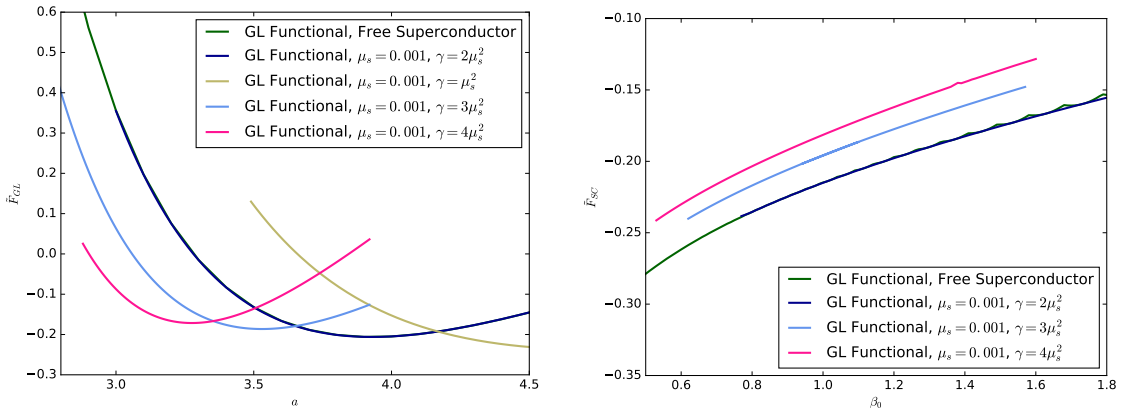

(a) Ginzburg-Landau part of the total free energy functional of the combined system against lattice spacing.

(b) Ginzburg-Landau part of the total free energy functional of the combined system against the external field.

Figure 4.13: Ginzburg-Landau part of the total free energy functional of the combined system of a superconducotr and a skyrmion lattice against spacing and the external field for different values of γ, though for the same small value of $\mu_s = 0.001$.

solutions are not of our primary concern in this research, hence we should avoid considering values of γ that are extreme with respect to $\gamma_0 = 2\mu_s^2$.

From Figure 4.12a one can conclude that the optimal spacing of a combined system differs rather drastically with γ: the higher γ is, the lower the optimal spacing gets. Let us now consider the optimal lattice spacing against the applied field, β_0 and demonstrate this dependence for different values of γ explicitly in Figure 4.14.

From Figure 4.14 we confirm that the optimal lattice spacing that correspond to the same value of an external field, β_0, becomes smaller with γ increasing. In Figure 4.14 we also compare the lattice spacing against the combined system against the lattice spacing of the disjoint systems. We then conclude that it follows the behaviour of a lattice spacing of a superconducting vortex lattice, though the actual value of the optimal spacing is smaller, and the larger γ is, the smaller the optimal spacing gets. Such a behaviour can be related to the fact that decreasing γ implies the increase in the field that acts on a skyrmion lattice (recall equation (4.77) for the effects of γ on $\vec{B}$, keeping in mind the relation between γ and H_c: $\gamma = \frac{1}{H_c^2}$), pushing it towards the ferromagnetic region, hence increasing the total field of a skyrmion lattice acting back on the superconductor and larger applied field implements smaller optimal spacing in the vortex lattice case.

So far we have dealt with a small coupling only. We did not expect any dramatic effects, though we wanted to observe some qualitative dependences that would become more important should we increase the coupling strength, μ_s. Let us now consider $\mu_s = 0.1$. The comparison of a free skyrmion lattice with the lattice coupled with a superconductor with coupling of

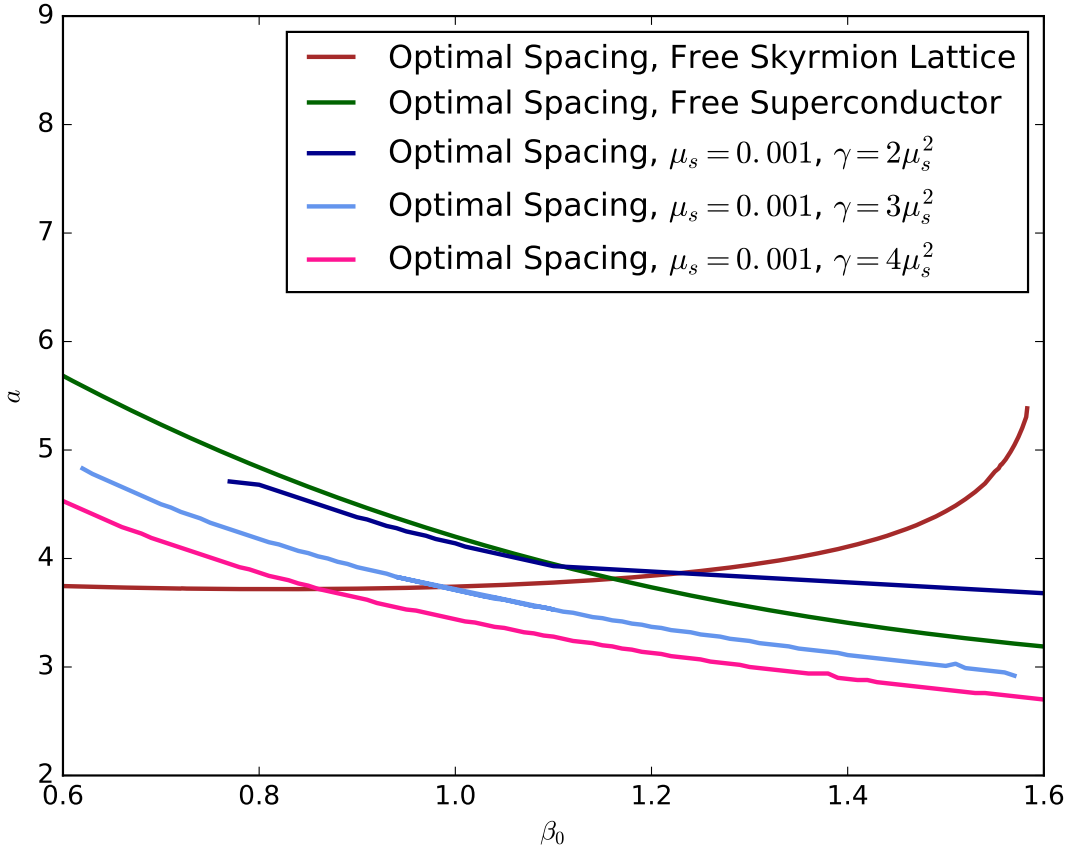

Figure 4.14: Lattice spacing for differnet values of γ. As μ_s is small, the lattice spacing follows the behaviour of that for a pure superconductor, though gets smaller with γ increasing.

$\mu_s = 0.1$, holding $\gamma = 2\mu_s^2$ is demonstrated in Figure 4.15.[6]

Figure 4.15 tells us that skyrmions themselves (shape-wise) are modified by a superconductor. They elongate like they are slowly turning into helices, and the direction of this change of the shape is governed by the position of vortices with respect to skyrmions. Also, the optimal lattice spacing is smaller than that of a free skyrmion system, just as we have seen it for smaller couplings. In order to explain such a behaviour, let us compare the total field of our combined system with the pure field of a vortex lattice. The comparison is demonstrated in Figure 4.16.

From Figure 4.16 we see that the skyrmion lattice affects the field of a superconducting vortex lattice quite drastically, hence the total field becomes larger. For a coupling of $\mu_s = 0.1$, $\gamma = 2\mu_s^2$ the dominant term of the functional is still the superconducting one, so the optimal spacing shall still follow the law for a superconductor, though the effects of a skyrmion lattice

[6]We had to consider slightly higher external field than we usually did in order to be sure that the solution of the combined system would fit into the skyrmion region.

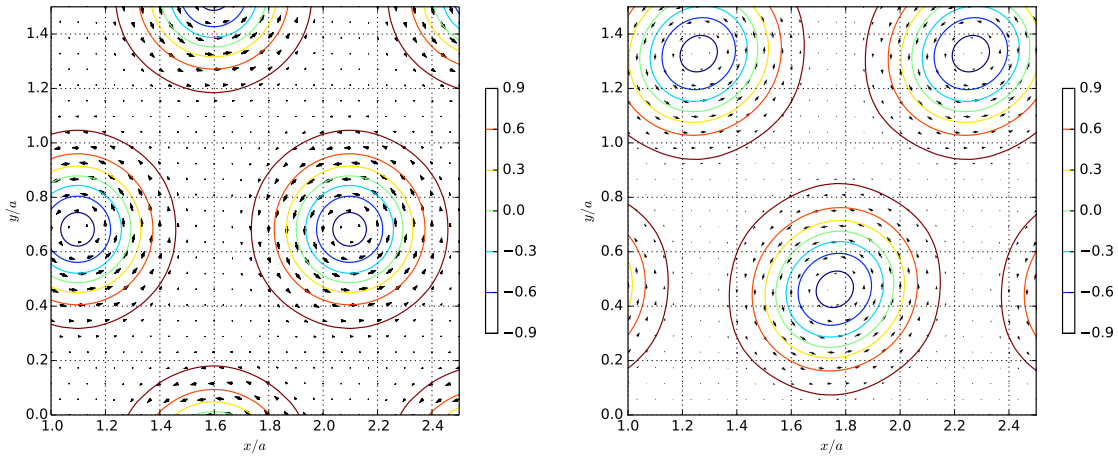

(a) Free skyrmion lattice solution for $\beta = 1.4$ with $a = 4.1$.

(b) Skyrmion lattice combined with a superconductor for $\beta_0 = 1.4$ with $a = 3.37$.

Figure 4.15: Stable solutions for a free skyrmion lattice and a skyrmion lattice that is coupled with a superconductor for the same value of β (β_0). Coupling factors are $\mu_s = 0.1$ and $\gamma = 2\mu_s^2$. Notice how the shape of skyrmions is different now: skyrmions that are coupled with a superconductor do not look like perfect circles anymore.

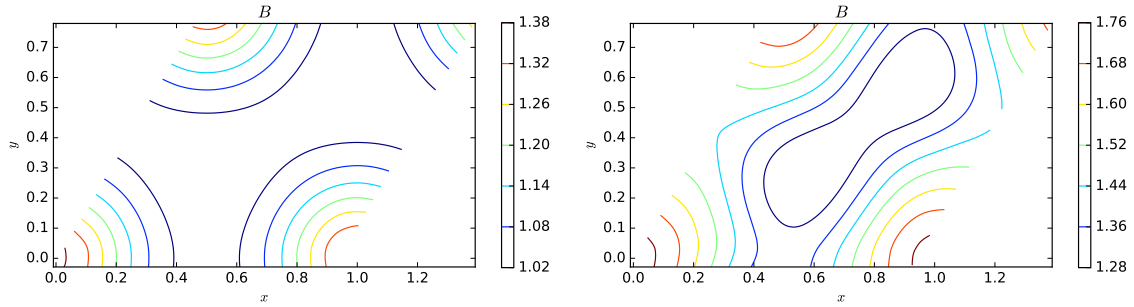

(a) Magnetic field of the vortex lattice.

(b) Magnetic field of the vortex lattice coupled with skyrmions. Coupling strength is $\mu_s = 0.1$.

Figure 4.16: Comparison of the magnetic field of a free vortex lattice for $\xi = 0.5$, $\tilde{\lambda} = 4.5$ with the one coupled with a skyrmion lattice with small coupling, $\mu_s = 0.1$. The field presented in this figure is the total field.

cannot be neglected anymore. That is why the total spacing is still smaller, than it used to be for a free skyrmion lattice for the same external field applied, and smaller than that for a vortex lattice with no skyrmions in proximity to it. The total free energy functional is plotted together with the Ginzburg-Landau part of this functional in Figure 4.17 in order to demonstrate that they follow the same pattern, though not coinciding like they used to for smaller values of coupling μ_s. The positions of their minimas almost coincide.

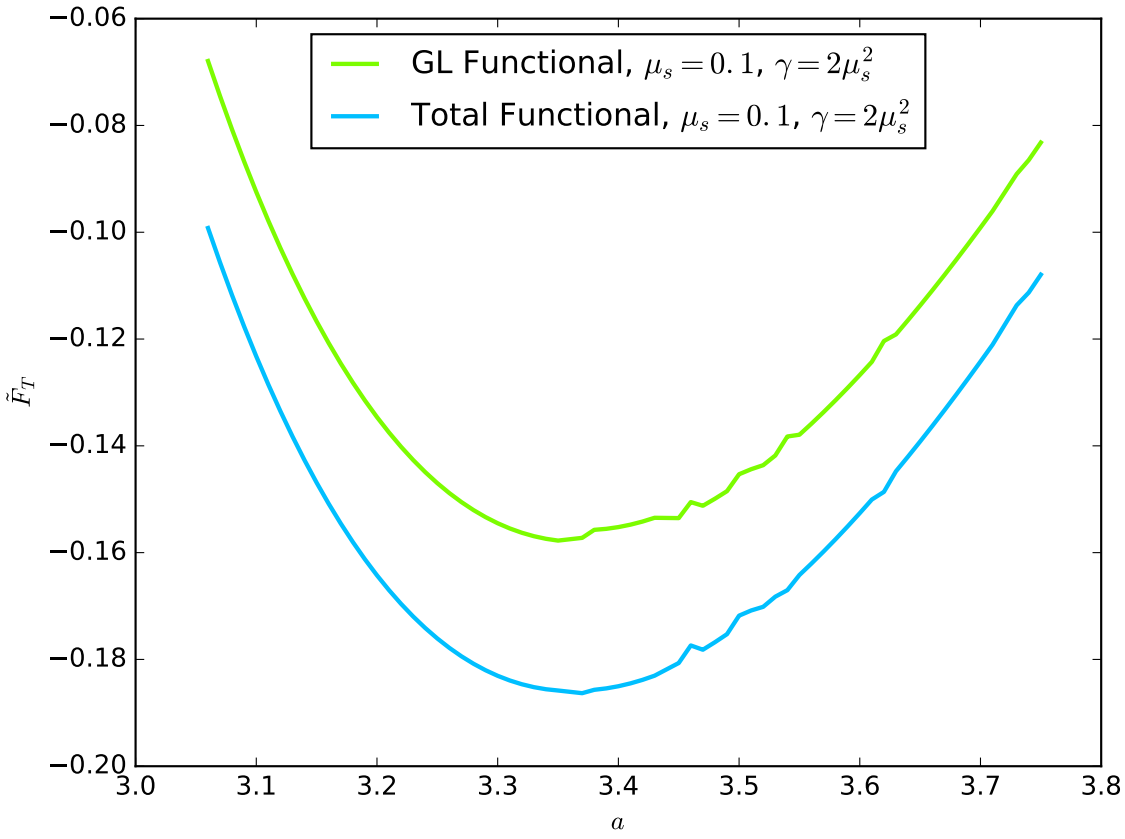

Figure 4.17: Total free energy functional of the combined system with coupling $\mu_s = 0.1$ and $\gamma = 2\mu_s^2$ and the Ginzburg-Landau part of this functional. Both follow the same pattern, though they do not coincide, though their minimas almost do.

Chapter 5

Conclusions and Future Directions

Here comes our time to leave the wonderful world of micromagnetism. But before we go, let us summarise everything we have discussed.

In this work we have introduced a new method of dealing with micromagnetic systems that was mainly applied to magnetic skyrmion systems. The method consists of Fourier decomposition of the magnetisation components and thus converting Euler-Lagrange equations,

$$\left(\partial_x^2 + \partial_y^2\right) M_x - 4\partial_y M_z - 4\lambda M_x = 0, \tag{5.1}$$

$$\left(\partial_x^2 + \partial_y^2\right) M_y + 4\partial_x M_z - 4\lambda M_y = 0, \tag{5.2}$$

$$\left(\partial_x^2 + \partial_y^2\right) M_z - 4\left(\partial_x M_y - \partial_y M_x\right) - 4\lambda M_z = -2\beta. \tag{5.3}$$

derived from the free energy functional,

$$F = 2J \int \left\{ \frac{1}{4} \sum_{\mu} \left(\partial_\mu \vec{M}\right) \cdot \left(\partial_\mu \vec{M}\right) + \vec{M} \cdot \left(\nabla \times \vec{M}\right) - \vec{\beta} \cdot \vec{M} + \lambda \left(\left|\vec{M}\right|^2 - 1 \right) \right\} \frac{dxdy}{A}, \tag{5.4}$$

into Fourier form. We claim our method to be more efficient and universal than any of those existed before. It is particularly well-designed for studying periodic structures, such as skyrmion lattices, where the Fourier approach does an amazing job in simplifying the problem. Fixing the constraint on the magnetisation of $\left|\vec{M}\right|^2 = 1$ via Lagrange multiplier technique (λ in functional (5.4)) provides more accurate results than other methods.[1] We have also employed the virial theorem in order to fix the optimal spacing that corresponds to a certain value of an applied field precisely via ratio

$$\frac{\tilde{F}_{DM}}{\tilde{F}_{ex}} = -2, \tag{5.5}$$

[1] And it was actually λ that required numerical approach, as the components of the magnetisation were reconstructed from the corresponding Fourier coefficients calculated analytically for a given λ.

where $\tilde{F}_{ex}$ is the ferromagnetic exchange part of the free energy functional and $\tilde{F}_{DM}$ is the anisotropic exchange part of the functional. A typical skyrmion lattice found via the method described above is demonstrated in Figure 5.1.

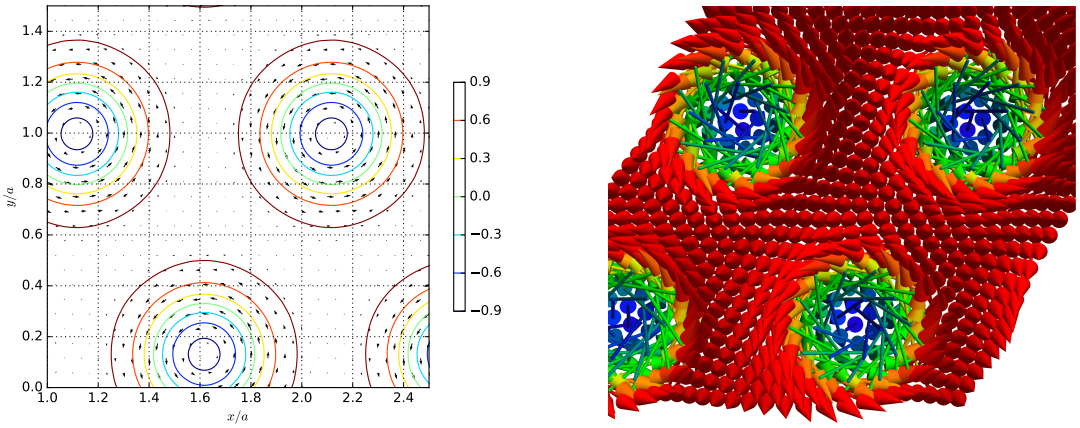

(a) A typical skyrmion lattice. Magnetisation.

(b) Spin distribution on the skyrmion lattice.

Figure 5.1: Skyrmion lattice obtained by Fourier expansion method.

The new method also allows us to follow the real-space configuration of the system (magnetisation or spin), not just the energy scale.

In this Thesis we have mainly focused on Bloch skyrmions. Our method, however, is universal enough to deal with Néel skyrmions as well. The free energy functional, hence the numerical approach has to be modified, though. The only mathematical difference between free energy functionals of Bloch and Néel skyrmion systems is the formulation of the anisotropic exchange term. In continuum approximation it was derived for Bloch skyrmions to be

$$\mathcal{F}_{DM} = \vec{M} \cdot \left(\nabla \times \vec{M} \right). \tag{5.6}$$

In Néel case anisotropic exchange term is written as

$$\mathcal{F}_{DM} = \left(\hat{e}_z \cdot \vec{M} \right) \left(\nabla \cdot \vec{M} \right) - \left(\vec{M} \cdot \nabla \right) \left(\hat{e}_z \cdot \vec{M} \right). \tag{5.7}$$

Spin distribution on a unit cell of a Néel skyrmion lattice obtained by the method introduced in this Thesis is demonstrated in Figure 5.2 in order to prove the method's universality.

We have studied the magnetic system under the effects of an external magnetic field and thus obtained a bestiary of skyrmion lattices and other solutions as well as the phase diagram for a magnetic system demonstrated in Figure 5.3.

As we can see from Figure 5.3, exact critical fields were found. For the helical-skyrmion

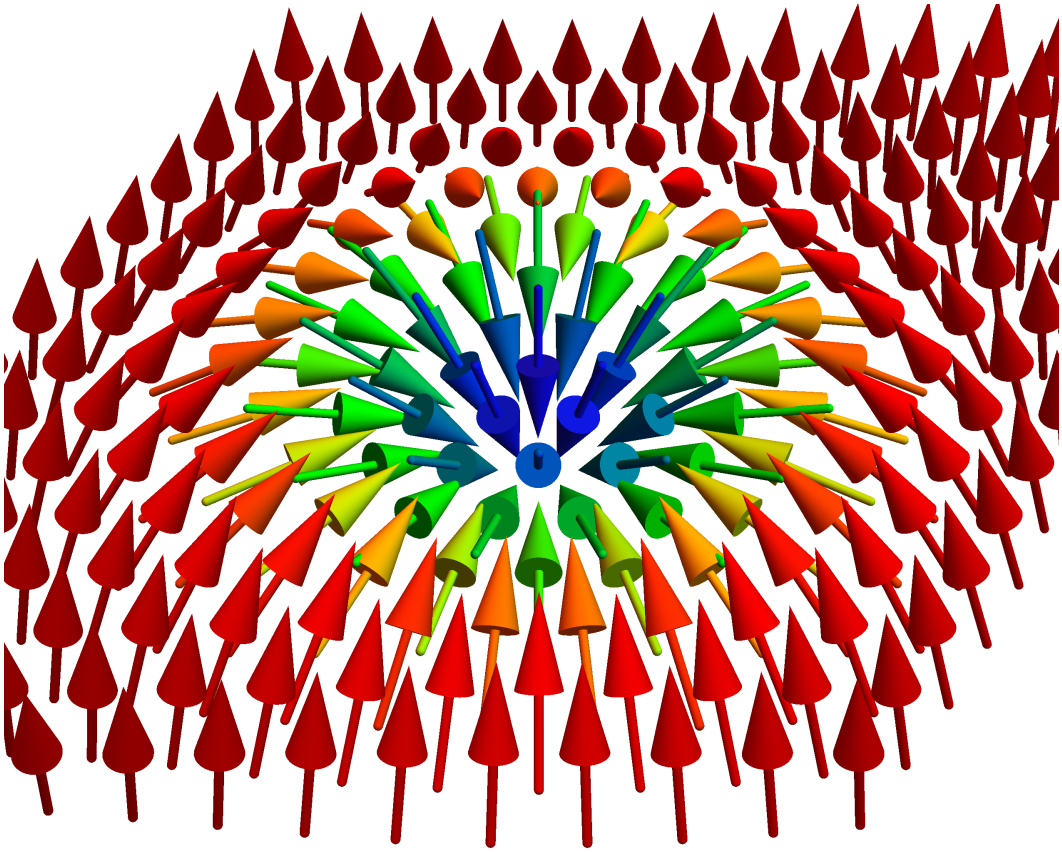

Figure 5.2: Spin distribution on a unit cell of a Néel skyrmion lattice obtained by the method introduced in this Thesis.

state phase transition the value of the critical field is claimed to be

$$\beta_{c_1} = 0.46, \tag{5.8}$$

for the skyrmion-ferromagnet phase transition:

$$\beta_{c_2} = 1.56. \tag{5.9}$$

Both β_{c_1} and β_{c_2} are expressed in dimensionless units introduced in section 2.3.1. Both β_{c_1} and β_{c_2} correspond to critical field values found experimentally, for example by *Mochizuki*, [86] exactly.

Notice that Figure 5.3 contains the free energy of metastable states along with that of stable states. We have studied metastable skyrmion states that can be obtained in ferromagnetic and helical regions and found them to be rather similar to the stable states near the transition. Notable metastable skyrmion states that exhibit honeycomb lattice in oppose to triangular one have been found. These are demonstrated in Figure 5.4 and the proof of their metastability

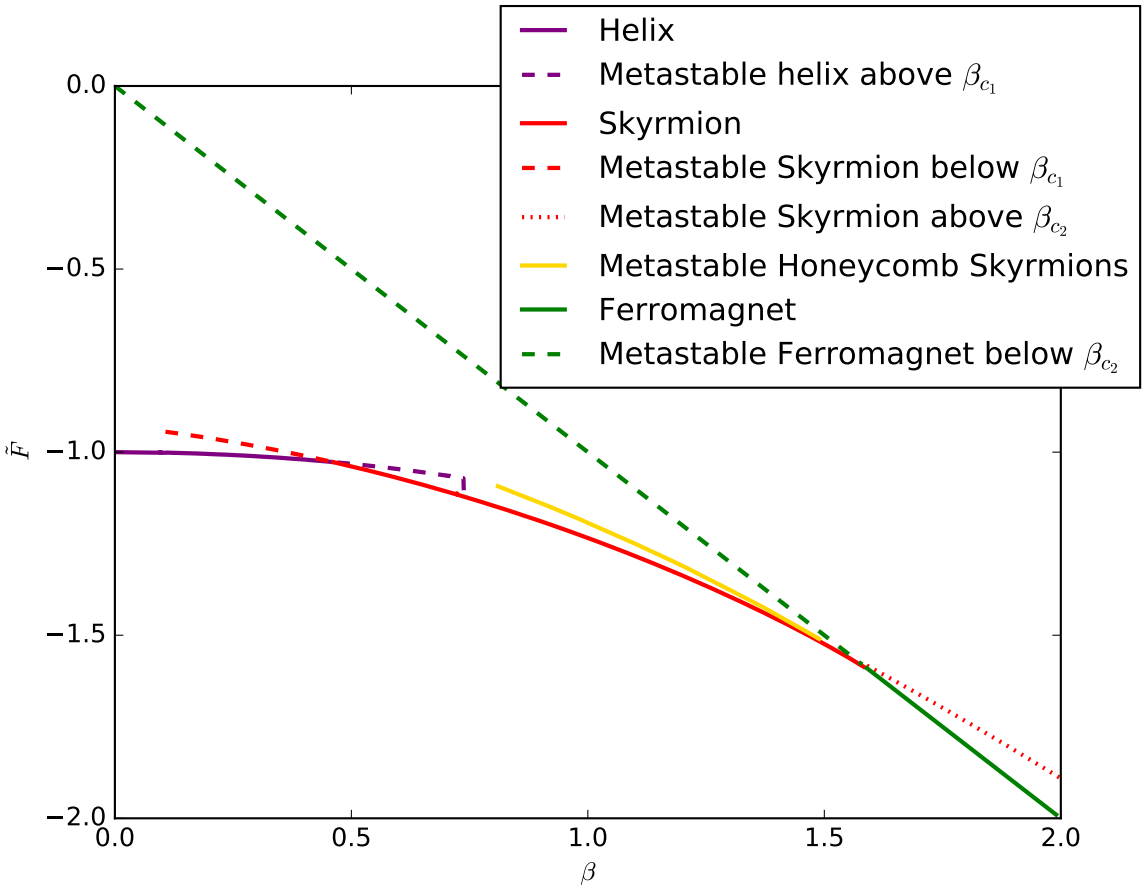

Figure 5.3: Free energy functional of a magnetic system in different regions including metastable honeycomb skyrmion lattice that is represented by a gold line. Red curve represents the optimal free energy for a skyrmion system, purple one stands for the helial system and green line is the free energy of a ferromagnetic system. Dashed lines of different colours correspond to metastable solutions of corresponding patterns.

can be found in Figure 5.5. Such a pattern had never been observed for skyrmions before.

These honeycomb configurations were found to be metastable only. However, their energy is only slightly higher than the energy of stable triangular lattices especially in proximity to β_{c_2}, so it might be even possible to observe them experimentally.

Another important conclusion that can be drawn from our calculations is the behaviour of the optimal lattice spacing for a given field. This is demonstrated in Figure 5.6.

We have observed that the lattice spacing is increasing drastically with increasing field – this happens because the area of the ferromagnetic region (the number of spins that align along the field) is increasing; on the other hand, with decreasing field at some point the spacing starts increasing again. This is explained by the fact that the radius of skyrmions is increasing with decreasing field, so at a point the distance between skyrmions has to become larger so

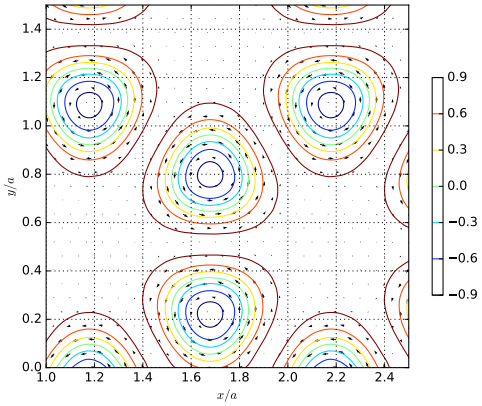

(a) Honeycomb Skyrmion lattice. Magnetisation.

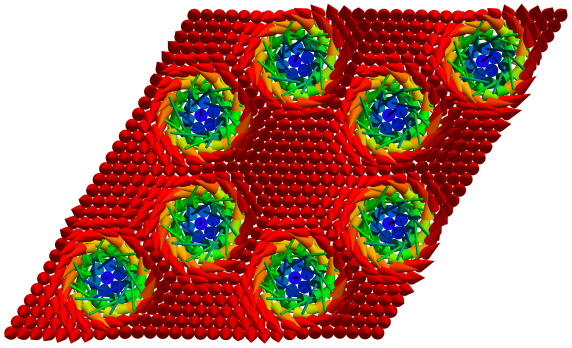

(b) Spin distribution on the honeycomb skyrmion lattice.

Figure 5.4: Metastable honeycomb skyrmion lattice.

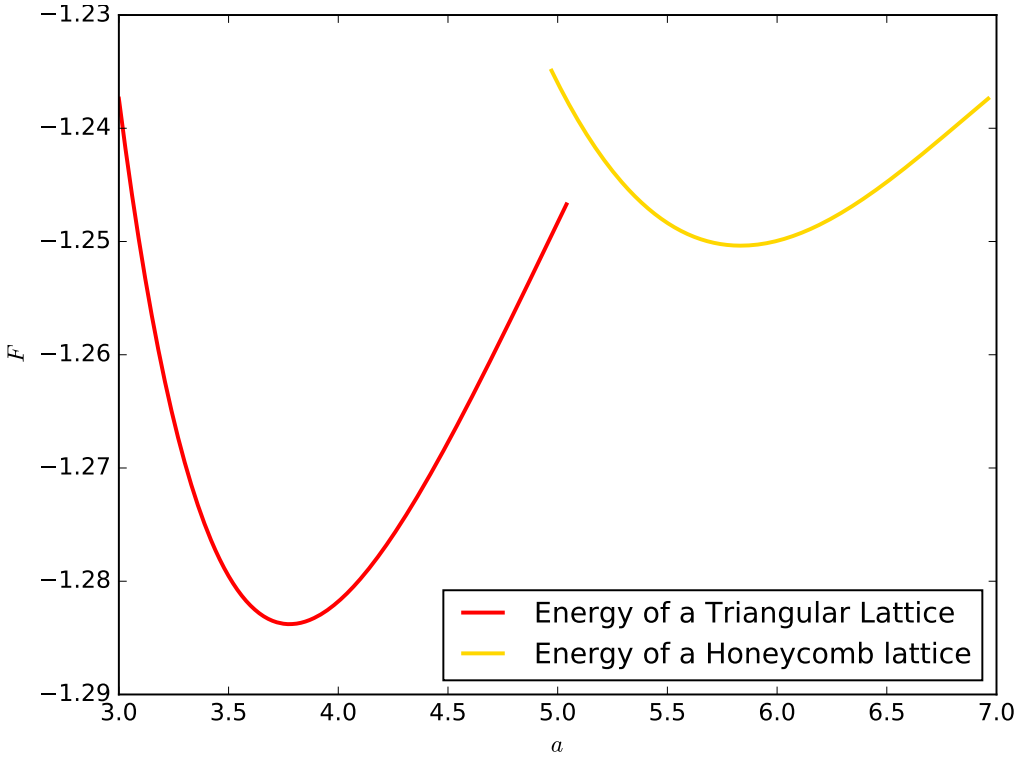

Figure 5.5: Free energy functional of a honeycomb configuration along with the free energy functional of a triangular configuration against lattice spacing, a, for fixed $\beta = 1.1$. The red curve corresponds to the free energy of a triangular lattice, the golden curve corresponds to the honeycomb lattice. The minimal energy of the triangular configuration is smaller that the minimal energy of the honeycomb configuration, hence honeycomb solution is metastable. Notice that the optimal lattice spacing of a honeycomb lattice is a lot larger than the optimal spacing of a triangular lattice.

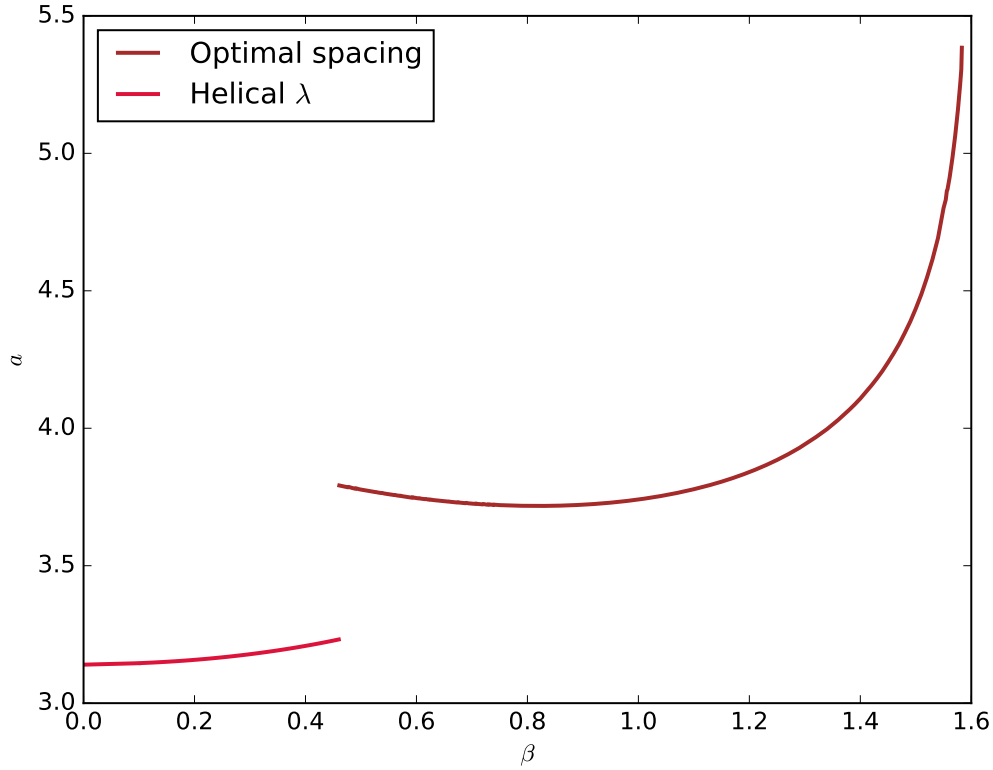

Figure 5.6: Optimal skyrmion lattice spacing vs β. Brown curve stands for the optimal lattice spacing, vinous curve – for λ_H. The spacing is increasing drastically when the field is approaching β_{c_2}, when the field is near β_{c_1}, the spacing is slightly increasing as well.

that skyrmions would not overlap.

Another way to demonstrate the universality of the method developed is to consider a more complicated system, for example, by coupling a skyrmion lattice with a superconductor. Therefore we considered a bilayer of a 2D magnetic material and a type-II superconductor. Lattices were adjusted in such a way that the regions of the largest field coincided. The actual coupling was performed via magnetic field and the total free energy functional of the whole combined system was derived to be

$$\begin{aligned} F &= 2J\kappa^2 H_c^2 \left(\tilde{F}_{SC} + \gamma \tilde{F}_{SkX}\right) \\ &= 2J\kappa^2 H_c^2 \int \left\{ -|\psi|^2 + \frac{1}{2}|\psi|^4 + \left|\left(-i\xi\nabla - \vec{A}\right)\psi\right|^2 + \left|\vec{B}\right|^2 \right. \\ &- 2\vec{B}\cdot\left(H_0\hat{e}_z + \mu_s M_z \hat{e}_z + H_{d_x}\hat{e}_x + H_{d_y}\hat{e}_y\right) \\ &+ H_0^2 + H_{d_x}^2 + H_{d_y}^2 + 2\mu_s H_0 M_z + \mu_s^2 M_z^2 \\ &+ \left. \gamma\left[\frac{1}{4}\left(\partial_\mu \vec{M}\right)\cdot\left(\partial_\mu \vec{M}\right) + \vec{M}\cdot\left(\nabla\times\vec{M}\right) - \vec{\beta}\cdot\vec{M} + \lambda\left(\left|\vec{M}\right|^2 - 1\right)\right]\right\}\frac{dxdy}{A}, \end{aligned} \tag{5.10}$$

where ψ is the order parameter of the superconductor, $\vec{B}$ is the magnetic field of the superconductor, H_0 is the external field in $\hat{e}_z$-direction, $\vec{H}_d$ is the stray field due to the skyrmion lattice, μ_s is the magnetic moment of spins in a skyrmion material and γ is the measure of the contribution of the skyrmion part to the total energy. $\vec{B}$ and $\vec{\beta}$ are related via

$$\vec{B} = \sqrt{\frac{\gamma}{2}} \frac{1}{\mu_s} \vec{\beta}. \tag{5.11}$$

We also had to modify Brandt's approach to the superconductor to match with our new functional. Corresponding Ginzburg-Landau equations in Brandt's form then are:

$$\left(-\nabla^2 + \frac{2}{\xi^2}\right) f = \frac{2}{\xi^2} \left[2f - f^2 - f\left|\vec{Q}\right|^2 - g\right], \tag{5.12}$$

and

$$\left(-\nabla^2 + \bar{f}\right) \vec{B} = -\frac{1}{\tilde{\lambda}^2} \left(f - \tilde{\lambda}^2 \bar{f}\right) \vec{B} + \frac{1}{\tilde{\lambda}^2} f \vec{B} - \frac{1}{\tilde{\lambda}} \vec{p} + \nabla \times \nabla \times \vec{P}, \tag{5.13}$$

where

$$\vec{P} = \begin{pmatrix} H_{d_x} \\ H_{d_y} \\ \mu_s M_z \end{pmatrix} \tag{5.14}$$

and f, $\bar{f}$, g, and $\vec{p}$ are defined in section 4.2. New Euler-Lagrange equations for a skyrmion part of the system were derived from the functional (5.10) to be

$$\left(\partial_x^2 + \partial_y^2\right) M_x - 4\partial_y M_z - 4\lambda M_x = -2\beta_x, \tag{5.15}$$

$$\left(\partial_x^2 + \partial_y^2\right) M_y + 4\partial_x M_z - 4\lambda M_y = -2\beta_y, \tag{5.16}$$

$$\left(\partial_x^2 + \partial_y^2\right) M_z - 4\left(\partial_x M_y - \partial_y M_x\right) - 4\lambda M_z = -2\beta_z, \tag{5.17}$$

keeping in mind that components of $\vec{\beta}$ are to be Fourier-expanded in the same manner as the components of the magnetisation, $\vec{M}$, had been.

We have observed that the presence of a skyrmion lattice next to a superconductor makes the total lattice spacing smaller, than it used to be for the same set of parameters for a disjoint system. The comparisonal demonstration of free energy functional against the spacing for different values of coupling, μ_s is demonstrated in Figure 5.7. On the other hand, one can use a superconductor in order to stabilise a magnetic system that used to be metastable without it. This can be performed via careful choice of ξ and $\tilde{\lambda}$, i.e. of a superconductor itself.

There is always space for development, no matter what you do. In the case of our combined system one should take into account the stray field of a superconductor as well as the stray field of a magnet. Stabilising the honeycomb lattices found for a free system to be unstable is also a good point for future studies. Also, one can perform studies of the larger region of β_0

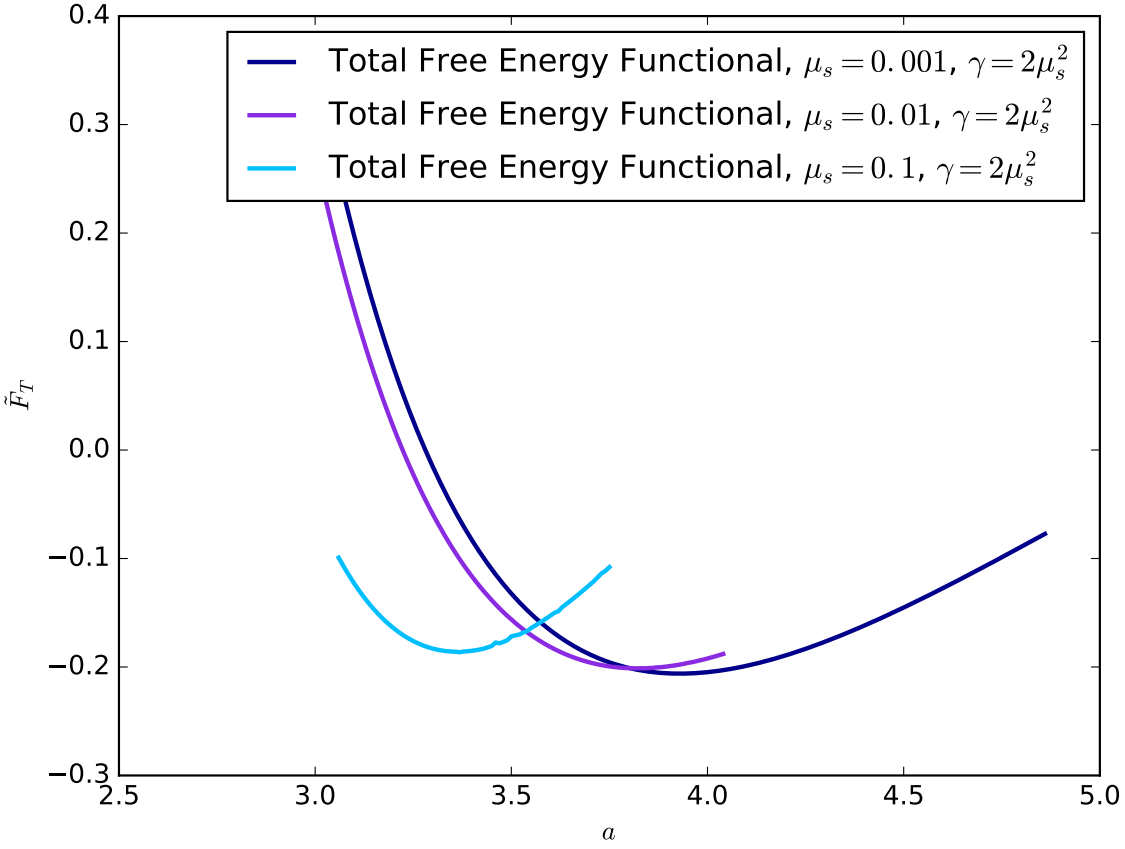

Figure 5.7: Free energy functional against the spacing for different values of μ_s. The optimal spacing is decreasing with μ_s increasing.

and determine how a superconductor affects helix-skyrmion and skyrmion-ferromagnet phase transitions.

Another possible future direction is to study different systems, a magnetic superconductor, for example, a superconductor with magnetic skyrmions in it. On the other hand, if one does not want to leave the bilayer case so quickly, one can try to locate skyrmions exactly on top of the vortices and study a system of this kind (in this case the z-component of the magnetisation of skyrmions, M_z, changes its sign, i.e. the spins shall align along the field in the centre and opposite to it on the edge).

There are many more possible systems to study as the method was proved to be universal and so long as the system can exist in nature (and sometimes even if it cannot) with a bit of thought one shall be able to adjust the method for it.

Appendices

Appendix A

General Mathematics

A.1 ∇ in Polar Parametrisation

The usual conversion from Cartesian to polar coordinates is performed via [97]

$$x = r \sin\varphi \cos\vartheta, \tag{A.1}$$

$$y = r \sin\varphi \sin\vartheta, \tag{A.2}$$

$$z = r \cos\varphi, \tag{A.3}$$

or, in vector form:

$$\begin{pmatrix} x \\ y \\ z \end{pmatrix} = \begin{pmatrix} r \sin\varphi \cos\vartheta \\ r \sin\varphi \sin\vartheta \\ r \cos\varphi \end{pmatrix}. \tag{A.4}$$

The corresponding transformation matrix is [97]

$$\hat{J} = \begin{pmatrix} \frac{\partial x}{\partial r} & \frac{\partial x}{\partial \vartheta} & \frac{\partial x}{\partial \varphi} \\ \frac{\partial y}{\partial r} & \frac{\partial y}{\partial \vartheta} & \frac{\partial y}{\partial \varphi} \\ \frac{\partial z}{\partial r} & \frac{\partial z}{\partial \vartheta} & \frac{\partial z}{\partial \varphi} \end{pmatrix} = \begin{pmatrix} \sin\varphi \cos\vartheta & -r \sin\varphi \sin\vartheta & r \cos\varphi \cos\vartheta \\ \sin\varphi \sin\vartheta & r \sin\varphi \cos\vartheta & r \cos\varphi \sin\vartheta \\ \cos\varphi & 0 & -r \sin\varphi \end{pmatrix}, \tag{A.5}$$

so one can write the general transformation relation for a Cartesian vector, $\vec{v}_C$, and a polar vector, $\vec{v}_p$, as

$$\vec{v}_C = \hat{J}\vec{v}_p, \tag{A.6}$$

or, upon inversion,

$$\vec{v}_p = \hat{J}^{-1}\vec{v}_C, \tag{A.7}$$

where $\hat{J}^{-1}$ is the inverse of $\hat{J}$, given by

$$\hat{J}^{-1} = \begin{pmatrix} \sin\varphi\cos\vartheta & \sin\varphi\sin\vartheta & \cos\varphi \\ -\frac{\sin\vartheta}{r\sin\varphi} & \frac{\cos\vartheta}{r\sin\varphi} & 0 \\ \frac{\cos\varphi\cos\vartheta}{r} & \frac{\cos\varphi\sin\vartheta}{r} & -\frac{\sin\varphi}{r} \end{pmatrix}. \tag{A.8}$$

The vector we would like to transform is

$$\nabla = \begin{pmatrix} \frac{\partial}{\partial x} \\ \frac{\partial}{\partial y} \\ \frac{\partial}{\partial z} \end{pmatrix}. \tag{A.9}$$

Notice, that the result we will obtain would not be equivalent to the polar formulation of ∇, as we are not going to transform the unit vectors, $\hat{e}_x$, $\hat{e}_y$ and $\hat{e}_z$.

The transformed vector of partial derivatives then becomes:

$$\begin{pmatrix} \frac{\partial}{\partial x} \\ \frac{\partial}{\partial y} \\ \frac{\partial}{\partial z} \end{pmatrix} = \hat{J} \begin{pmatrix} \frac{\partial}{\partial r} \\ \frac{\partial}{\partial \vartheta} \\ \frac{\partial}{\partial \varphi} \end{pmatrix} = \begin{pmatrix} \cos\vartheta\sin\varphi\frac{\partial}{\partial r} - \frac{\sin\vartheta}{r\sin\varphi}\frac{\partial}{\partial\vartheta} + \frac{\cos\vartheta\cos\varphi}{r}\frac{\partial}{\partial\varphi} \\ \sin\vartheta\sin\varphi\frac{\partial}{\partial r} + \frac{\cos\vartheta}{r\sin\varphi}\frac{\partial}{\partial\vartheta} + \frac{\sin\vartheta\cos\varphi}{r}\frac{\partial}{\partial\varphi} \\ \cos\varphi\frac{\partial}{\partial r} - \frac{\sin\varphi}{r}\frac{\partial}{\partial\varphi} \end{pmatrix}. \tag{A.10}$$

A.2 δ-function

A.2.1 Dirac δ-function and Fourier Transform

In general Dirac δ-function can be expressed as a Fourier transform: [97]

$$\delta(x) = \frac{1}{2\pi}\int_{-\infty}^{\infty} e^{ikx}dk, \tag{A.11}$$

or

$$\delta(k) = \int_{-\infty}^{\infty} e^{-2\pi ikx}dx. \tag{A.12}$$

The most important properties of a δ-function to remember are [97]

$$\int_{-\infty}^{\infty} f(x)\delta(x - x_0) = f(x_0) \tag{A.13}$$

and

$$\delta(-x) = \delta(x). \tag{A.14}$$

A.2.2 Kronecker δ and Discrete Fourier Transform

For discrete quantities Kronecker δ is the analogue of a continuous Dirac δ-function. [97] We are mainly interested in the integrals of discrete sums involving exponentials (discrete Fourier

transforms), namely:

$$\int \sum_{\vec{k}} a_{\vec{k}} \frac{dxdy}{A} = \sum_{\vec{k}} a_{\vec{k}} \int \frac{dxdy}{A} = \sum_{\vec{k}} a_{\vec{k}}, \tag{A.15}$$

$$\int \sum_{\vec{k}} a_{\vec{k}} e^{-i\vec{k}\vec{r}} \frac{dxdy}{A} = \sum_{\vec{k}} a_{\vec{k}} \delta_{\vec{k},0} = a_0, \tag{A.16}$$

$$\int \sum_{\vec{k}\vec{k}'} a_{\vec{k}} b_{\vec{k}'} e^{-i(\vec{k}-\vec{k}')\vec{r}} \frac{dxdy}{A} = \sum_{\vec{k}\vec{k}'} a_{\vec{k}} b_{\vec{k}'} \delta_{\vec{k}\vec{k}'} = \sum_{\vec{k}'} a_{\vec{k}'} b_{\vec{k}'} = \sum_{\vec{k}} a_{\vec{k}} b_{\vec{k}}, \tag{A.17}$$

$$\int \sum_{\vec{k}\vec{k}'} a_{\vec{k}} b_{\vec{k}'} e^{-i(\vec{k}+\vec{k}')\vec{r}} \frac{dxdy}{A} = \sum_{\vec{k}\vec{k}'} a_{\vec{k}} b_{\vec{k}'} \delta_{\vec{k},-\vec{k}'} = \sum_{\vec{k}'} a_{-\vec{k}'} b_{\vec{k}'} = \sum_{\vec{k}'} a^*_{\vec{k}'} b_{\vec{k}'} = \sum_{\vec{k}} a^*_{\vec{k}} b_{\vec{k}}, \tag{A.18}$$

provided the symmetry of $a_{-\vec{k}} = a^*_{\vec{k}}$,

$$\begin{aligned} \int \sum_{\vec{k}\vec{k}'\vec{k}''} a_{\vec{k}} b_{\vec{k}'} c_{\vec{k}''} e^{-i(\vec{k}+\vec{k}'-\vec{k}'')\vec{r}} \frac{dxdy}{A} &= \sum_{\vec{k}\vec{k}'\vec{k}''} a_{\vec{k}} b_{\vec{k}'} c_{\vec{k}''} \delta_{\vec{k}+\vec{k}',\vec{k}''} \\ &= \sum_{\vec{k}\vec{k}''} a_{\vec{k}} b_{\vec{k}''-\vec{k}} c_{\vec{k}''} = \sum_{\vec{k}\vec{k}'} a_{\vec{k}'} b_{\vec{k}'-\vec{k}} c_{\vec{k}}, \end{aligned} \tag{A.19}$$

$$\begin{aligned} \int \sum_{\vec{k}\vec{k}'\vec{k}''} a_{\vec{k}} b_{\vec{k}'} c_{\vec{k}''} e^{-i(\vec{k}+\vec{k}'+\vec{k}'')\vec{r}} \frac{dxdy}{A} &= \sum_{\vec{k}\vec{k}'\vec{k}''} a_{\vec{k}} b_{\vec{k}'} c_{\vec{k}''} \delta_{\vec{k}+\vec{k}',-\vec{k}''} \\ &= \sum_{\vec{k}\vec{k}''} a_{\vec{k}} b_{-(\vec{k}''+\vec{k})} c_{\vec{k}''} = \sum_{\vec{k}\vec{k}'} a_{\vec{k}'} b^*_{\vec{k}'+\vec{k}} c_{\vec{k}}. \end{aligned} \tag{A.20}$$

A.3 Hermite Polynomials

Hermite polynomials [98] form an orthogonal series that is a solution to the Hermite differential equation,

$$y'' - 2xy' = -2\mu y. \tag{A.21}$$

Hermite polynomials are given by

$$\mathtt{H}_n(x) = (-1)^n e^{x^2} \frac{d^n}{dx^n} e^{-x^2}. \tag{A.22}$$

Several first Hermite polynomials are:

$$\mathtt{H}_0(x) = 1, \tag{A.23}$$

$$\mathtt{H}_1(x) = 2x, \tag{A.24}$$

$$\mathtt{H}_2(x) = 4x^2 - 2, \tag{A.25}$$

$$\mathtt{H}_3(x) = 8x^3 - 12x. \tag{A.26}$$

Important properties of Hermite polynomials:

- orthogonality:
$$\int_{-\infty}^{\infty} \mathtt{H}_m(x)\mathtt{H}_n(x)e^{-x^2}dx = 2^n\sqrt{\pi}\,n!\delta_{nm}; \tag{A.27}$$
- recursion relation:
$$\mathtt{H}_{n+1}(x) = 2x\mathtt{H}_n(x) - \mathtt{H}_n'(x), \tag{A.28}$$
$$\mathtt{H}_{n+1}(x) = 2x\mathtt{H}_n(x) - 2n\mathtt{H}_{n-1}(x). \tag{A.29}$$

The main application of Hermite polynomials a physicist may face is the solution of a Schrödinger equation for a simple harmonic oscillator:

$$\psi(x) = \sum_n C_n \frac{1}{\sqrt{2^n n!}} \left(\frac{m\omega}{\pi\hbar}\right)^{\frac{1}{4}} e^{-\frac{m\omega x^2}{2\hbar}} \mathtt{H}_n\left(\sqrt{\frac{m\omega}{\hbar}}\,x\right). \tag{A.30}$$

Appendix B

General Physics

B.1 Basic Electromagnetism

B.1.1 Maxwell's Equations

The heart of electromagnetism theory, Maxwell's equations are: [99]

$$\nabla \cdot \vec{E} = \frac{\rho}{\varepsilon_0}, \tag{B.1}$$

$$\nabla \cdot \vec{B} = 0, \tag{B.2}$$

$$\nabla \times \vec{E} = -\frac{\partial \vec{B}}{\partial t}, \tag{B.3}$$

$$\nabla \times \vec{B} = \mu_0 \vec{J} + \mu_0 \varepsilon_0 \frac{\partial \vec{E}}{\partial t}, \tag{B.4}$$

where $\vec{E}$ is the electric field, $\vec{B}$ is the magnetic field, $\vec{J}$ is the total current density, ρ is the total charge density, μ_0 is the permeability of the free space, ε_0 is the permittivity of the free space.

B.1.2 Supplementary Equations of Electromagnetism

B.1.2.1 Magnetisation

Define

$$\vec{B} = \mu_0 \left(\vec{H} + \vec{M} \right), \tag{B.5}$$

where $\vec{H}$ is the magnetic field intensity and $\vec{M}$ is the magnetisation. [99] Magnetisation is defined as the average magnetic moment over the volume:

$$\vec{M} = \varrho \vec{\mu}, \tag{B.6}$$

where ϱ is the material density:

$$\varrho = \frac{m}{V}. \tag{B.7}$$

B.1.2.2 Stray Field

The stray field (sometimes also referred to as a demagnetisation field) is the magnetic intensity, $\vec{H}_d$, generated by the magnetisation of a material. [99] It often acts on the magnetisation and reduces the total magnetic moment, hence the total free energy of a sample, giving rise to shape anisotropy and other effects.

Demagnetisation field, $\vec{H}_d$, obeys [99]

$$\nabla \times \vec{H}_d = 0, \tag{B.8}$$

which in combination with the second Maxwell's equation, (B.2), provides

$$\vec{H}_d = -\vec{M}. \tag{B.9}$$

B.1.2.3 Electromagnetic Potentials

Define scalar and vector potentials such that

$$\vec{E} = -\nabla\varphi - \frac{\partial \vec{A}}{\partial t} \tag{B.10}$$

and

$$\vec{B} = \nabla \times \vec{A}. \tag{B.11}$$

B.1.2.4 Flux Equations

Electric flux:

$$\Phi_E = \int \vec{E} \cdot d\vec{S}. \tag{B.12}$$

Magnetic flux:

$$\Phi_B = \int \vec{B} \cdot d\vec{S} = \oint \vec{A} \cdot \vec{dl}. \tag{B.13}$$

B.1.2.5 Ohm's law

Ohm's law:

$$\vec{J} = \sigma\vec{E}, \tag{B.14}$$

where σ is the conductivity.

B.2 Free Energy

In general, the free energy is defined as an amount of work a system can perform. [100] The free energy, F is the difference between the internal energy, U, and the energy that cannot be used to perform work. Typically we work with Helmholtz free energy that is defined as

$$F_H = U - TS, \tag{B.15}$$

where T is the absolute temperature and S is the entropy. The change of the Helmholtz free energy is equal to the amount of reversible work performed on a system. Natural variables of the Helmholtz free energy are T and V, i.e. $F_H = F_H(T, V)$. [100]

One can also define Gibbs free energy by

$$F_G = F_H + pV, \tag{B.16}$$

and natural variables for Gibbs free energy are T and p, hence $F_G = F_G(T, p)$. [100] In presence of a magnetic field Gibbs free energy writes as

$$F_G = F_H - \vec{H} \cdot \vec{M}. \tag{B.17}$$

B.3 Electron in an External Magnetic Field

Being a charged particle, electron obviously experiences effects of an external magnetic field. In this chapter we are mainly interested in the energy contribution of these effects.

General Hamiltonian of a particle in an external field can be written as [101]

$$\hat{H} = \frac{\hat{p}^2}{2m} + V(r) = \hat{H}_0. \tag{B.18}$$

However, if the particle is charged and an external magnetic field is turned on, the momenta gets modified $\hat{p} \to \vec{p} - q\vec{A}$, where q is the charge of the particle and $\vec{A}$ is the vector potential of the magnetic field. [101] The Hamiltonian (B.18) has to be changed accordingly to

$$\hat{H} = \frac{1}{2m}\left(\vec{p} - q\vec{A}\right)^2 + V(r), \tag{B.19}$$

that can be expanded to

$$\hat{H} = \frac{\hat{p}^2}{2m} - \frac{q}{2m}\left(\vec{p}\cdot\vec{A} + \vec{A}\cdot\vec{p}\right) + \frac{q^2}{2m} + V(r) = \hat{H}_0 + \frac{q^2}{2m} - \frac{q}{2m}\left(\vec{p}\cdot\vec{A} + \vec{A}\cdot\vec{p}\right). \tag{B.20}$$

Let us consider how does $\vec{p}\cdot\vec{A}$ part of a general Hamiltonian operator act on an arbitrary

quantum mechanical state vector, recalling $\hat{p} = -i\hbar\nabla$:

$$\vec{p}\cdot\vec{A}\,|\psi\rangle = -i\hbar\left(\nabla\cdot\vec{A}\right)|\psi\rangle - i\hbar\vec{A}\nabla\,|\psi\rangle = \vec{A}\cdot\vec{p}|\psi\rangle\,, \tag{B.21}$$

as

$$\nabla\cdot\vec{A} = 0 \tag{B.22}$$

according to Coulomb gauge. So conclude that

$$\vec{p}\cdot\vec{A} = \vec{A}\cdot\vec{p}, \tag{B.23}$$

hence the Hamiltonian becomes

$$\hat{H} = \hat{H}_0 - \frac{q}{m}\vec{A}\cdot\vec{p} + \frac{q^2}{2m}. \tag{B.24}$$

Here and later on we are interested in the interaction part of the Hamiltonian only: [101]

$$\hat{H}_{int} = -\frac{q}{m}\vec{A}\cdot\vec{p}. \tag{B.25}$$

Now let us expand the vector potential of the magnetic field via[1]

$$\vec{A} = \frac{1}{2}\vec{B}\times\vec{r}, \tag{B.26}$$

then

$$\vec{A}\cdot\vec{p} = \frac{1}{2}\left(\vec{B}\times\vec{r}\right)\cdot\vec{p} = \frac{1}{2}\vec{B}\cdot(\vec{r}\times\vec{p}) = \frac{1}{2}\vec{B}\cdot\vec{L}, \tag{B.27}$$

where $\vec{L}$ is the angular momentum, that can be either orbital or spin angular momentum or combination of both.

One can also define magnetic moment of an electron,

$$\vec{\mu} = \frac{q}{2m}\vec{L} = \frac{\mu_B}{\hbar}\vec{L}, \tag{B.28}$$

where μ_B is Bohr's magneton and spin magnetic moment is thus

$$\vec{\mu}_s = g\mu_B\vec{S}, \tag{B.29}$$

where g is Langé factor.

Finally, the Hamiltonian becomes

$$\hat{H}_{int} = -\vec{\mu}\cdot\vec{B}, \tag{B.30}$$

[1]Such an expansion provides both $\vec{B} = \nabla\times\vec{A}$ and $\nabla\cdot\vec{A} = 0$.

where $\vec{\mu}$ is either $\vec{\mu}_L$ (magnetic moment due to the orbital angular momentum) or $\vec{\mu}_s$ (magnetic moment due to spin) or the combination of both.

B.4 Spin-orbit Interaction

Another important quantum phenomenon one should refer to while dealing with magnetism is the spin-orbit interaction. In this section we would briefly discuss it and its effects in solids.

The spin-orbit interaction is one of the few complicated and non-trivial relativistic phenomena that can be actually to a some extend explained in simple words: an electron being a charged particle is orbiting, hence moving, hence induces some magnetic field; it's spin then interacts with the field induced by electrons' own movements and one should remember that electromagnetism is relativistic itself. [101]

As we know from Maxwell's equations, moving charges induce the magnetic field, so in the reference frame that moves with velocity $\vec{v}$ relative to an electric field $\vec{E}$ one finds

$$\vec{B} = \frac{\vec{E} \times \vec{v}}{c^2}, \tag{B.31}$$

where

$$\vec{E} = -\nabla V(\vec{r}) = -\frac{\vec{r}}{r}\frac{dV}{dr} \tag{B.32}$$

is $V(\vec{r})$ is the electric potential corresponding to the field $\vec{E}$. If the field has the Coulomb origin, then

$$\frac{1}{r}\frac{dV}{dr} = \frac{Nq}{4\pi\varepsilon_0 r^3}, \tag{B.33}$$

where N is the number of electrons on the outer shell.

The field induced by moving electrons, $\vec{B}$, then becomes:

$$\vec{B} = -\frac{Nq}{4\pi\varepsilon_0 c^2 r^3}(\vec{r} \times \vec{v}) = -\frac{Nq}{4\pi m\varepsilon_0 c^2 r^3}(\vec{r} \times \vec{p}) = -\frac{Nq}{4\pi m\varepsilon_0 c^2 r^3}\vec{L}, \tag{B.34}$$

and this field interacts with the magnetic moment of an electron via[2]

$$\hat{H}_{SO} = -\frac{1}{2}\vec{\mu} \cdot \vec{B} = \frac{q\hbar^2}{2m}\frac{Nq}{4\pi m\varepsilon_0 c^2 r^3}\vec{S} \cdot \vec{L} = \frac{\mu_0 N q^2 \hbar^2}{8\pi m^2 r^3}\vec{S} \cdot \vec{L} = \alpha_{SO}\vec{S} \cdot \vec{L}, \tag{B.35}$$

where α_{SO} is the spin-orbit coupling constant.

Spin-orbit coupling is a relativistic effect itself and was first derived by comparing Dirac and Schrödinger equations. [102] It is Dirac equation then that explains the spin-orbit interaction from the first principles but we would not discuss it here.

[2]The factor of $\frac{1}{2}$ – Thomas factor – rises from the change in the precession frequency of the electron spin due to the change of reference frame. [9]

In solid state physics spin-orbit interaction has its great importance while studying crystals that lack inversion symmetry, as it does not affect the total energy in other cases with some minor exceptions.

B.5 Ginzburg-Landau Equations

B.5.1 First Ginzburg-Landau Equation

Let us derive first Ginzburg-Landau equation by the direct variation of the Ginzburg-Landau functional,

$$F_{SC} = \int \left\{ \alpha|\psi|^2 + \frac{\beta}{2}|\psi|^4 + \frac{\hbar^2}{2m}|\nabla\psi|^2 \right\} \frac{d^3r}{L^3}, \tag{B.36}$$

with respect to ψ and ψ^*. Start with ψ-minimisation. Define the variation in ψ and ψ^* as

$$\psi'(\vec{r}) \to \psi(\vec{r}) + \delta\psi(\vec{r}), \tag{B.37}$$

$$\psi'^*(\vec{r}) \to \psi^*(\vec{r}) + \delta\psi^*(\vec{r}), \tag{B.38}$$

hence the quantities we are interested in (those appearing in the functional) become:

$$|\psi'|^2 = (\psi + \delta\psi)(\psi^* + \delta\psi^*) = \psi\psi^* + \psi\delta\psi^* + \psi^*\delta\psi + \mathcal{O}(\delta\psi^2), \tag{B.39}$$

$$\begin{aligned} |\psi'|^4 &= (\psi\psi^* + \psi\delta\psi^* + \psi^*\delta\psi)(\psi\psi^* + \psi\delta\psi^* + \psi^*\delta\psi) \\ &= |\psi|^4 + 2|\psi|^2\psi\delta\psi^* + 2|\psi|^2\psi^*\delta\psi + \mathcal{O}(\delta\psi^2), \end{aligned} \tag{B.40}$$

$$\left|\nabla\psi'\right| = \left|\nabla\psi + \nabla\delta\psi\right|, \tag{B.41}$$

$$\left|\nabla\psi'\right|^2 = \nabla\psi'\nabla\psi'^* = |\nabla\psi|^2 + \nabla\psi\nabla\delta\psi^* + \nabla\psi^*\nabla\delta\psi + \mathcal{O}(\delta\psi^2). \tag{B.42}$$

Variation of the functional then can be written as

$$\begin{aligned} \mathcal{F} + \delta\mathcal{F} &= \int \left[\frac{\hbar^2}{2m} \left(|\nabla\psi|^2 + \nabla\psi\nabla\delta\psi^* + \nabla\psi^*\nabla\delta\psi \right) + \alpha \left(|\psi|^2 + \psi\delta\psi^* + \psi^*\delta\psi \right) \right. \\ &+ \left. \frac{\beta}{2} \left(|\psi|^4 + 2|\psi|^2\psi\delta\psi^* + 2|\psi|^2\psi^*\delta\psi \right) \right] \frac{d^3r}{L^3}, \end{aligned} \tag{B.43}$$

and then the variation term can be deduced to be

$$\delta\mathcal{F} = \int \left[-\frac{\hbar^2}{2m}\nabla^2\psi + \alpha\psi + \beta\psi|\psi|^2 \right] \delta\psi^* d^3r + \int \left[-\frac{\hbar^2}{2m}\nabla^2\psi^* + \alpha\psi^* + \beta\psi^*|\psi|^2 \right] \delta\psi \frac{d^3r}{L^3}, \tag{B.44}$$

where we have used the consequence of the product rule for $\nabla(\nabla\psi\delta\psi)$,

$$\nabla\psi\nabla\delta\psi^* = \nabla(\nabla\psi\delta\psi^*) - \nabla^2\psi\delta\psi^*, \tag{B.45}$$

$$\nabla\psi^*\nabla\delta\psi = \nabla(\nabla\psi^*\delta\psi) - \nabla^2\psi^*\delta\psi, \tag{B.46}$$

and

$$\int \nabla(\nabla\psi\delta\psi^* + \nabla\psi^*\delta\psi)\frac{d^3r}{L^3} = 0, \tag{B.47}$$

so the variation of the functional with respect to ψ^* gives us

$$-\frac{\hbar^2}{2m}\nabla^2\psi + \alpha\psi + \beta\psi|\psi|^2 = 0 \tag{B.48}$$

– the first Ginzburg-Landau Equation for a free superconductor.

B.5.2 First Ginzburg-Landau Equation via Euler-Lagrange Method

Let us apply an alternative approach: derive first Ginzburg-Landau equation by writing Euler-Lagrange equation for the Ginzburg-Landau functional density:

$$\mathcal{F} = \alpha|\psi|^2 + \frac{\beta}{2}|\psi|^4 + \frac{\hbar^2}{2m}|\nabla\psi|^2, \tag{B.49}$$

hence Euler-Lagrange equation is:

$$\frac{\partial\mathcal{F}}{\partial\psi^*} - \nabla\frac{\partial\mathcal{F}}{\partial(\nabla\psi^*)} = 0, \tag{B.50}$$

which directly leads to

$$\alpha\psi + \beta\psi|\psi|^2 - \frac{\hbar^2}{2m}\nabla^2\psi = 0 \tag{B.51}$$

– the first Ginzburg-Landau equation for a free superconductor.

B.5.3 Analytical Solution of First Ginzburg-Landau Equation

Consider the simplest possible case:

$$\psi = \psi(x), \tag{B.52}$$

first Ginzburg-Landau then writes as

$$-\frac{\hbar^2}{2m}\frac{d\psi^2}{dx^2} + \alpha\psi + \beta\psi|\psi|^2 = 0. \tag{B.53}$$

With the aid of the coherence length,

$$\xi^2 = \frac{\hbar^2}{2m|\alpha|}, \tag{B.54}$$

convert the first Ginzburg-Landau equation into a dimensionless form:

$$-\xi^2\psi'' - \psi - \psi^3 = 0, \tag{B.55}$$

where ψ'' is the second derivative with respect to x.

Multiply both sides of (B.55) by ψ' and notice that

$$\frac{d}{dx}\left[\psi^4\right] = \psi^3\psi' + \psi\frac{d}{dx}\left[\psi^3\right] = \psi^3\psi' + 3\psi^3\psi' = 4\psi^3\psi', \tag{B.56}$$

$$\frac{d}{dx}\left[\psi^2\right] = 2\psi\psi', \tag{B.57}$$

$$\frac{d}{dx}\left[\psi'^2\right] = 2\psi'\psi'', \tag{B.58}$$

hence (B.55) can be modified to

$$\frac{d}{dx}\left[\frac{\xi^2}{2}\psi'^2 - \frac{1}{2}\psi^2 + \frac{1}{4}\psi^4\right] = 0, \tag{B.59}$$

or just

$$\frac{\xi^2}{2}\psi'^2 - \frac{1}{2}\psi^2 + \frac{1}{4}\psi^4 = const. \tag{B.60}$$

Apply boundary conditions of

$$\psi'(\infty) = 0 \tag{B.61}$$

and

$$\psi^2(\infty) = 1, \tag{B.62}$$

obtain

$$const = -\frac{1}{4}, \tag{B.63}$$

hence (B.60) transforms to

$$\xi^2\psi'^2 = \frac{1}{2}\left(1 - \psi^2\right)^2, \tag{B.64}$$

that can be square-rooted to

$$\xi\psi' = \frac{1}{\sqrt{2}}\left(1 - \psi^2\right), \tag{B.65}$$

which is solved to

$$\psi = \tanh\frac{x}{\xi\sqrt{2}}, \tag{B.66}$$

that is the simplest possible solution of the first Ginzburg-Landau equation.

B.5.4 Second Ginzburg-Landau Equation

Now let us vary the functional (B.36) with respect to $\vec{A}$. Do this with the aid of Euler-Lagrange technique:

$$\frac{\partial \mathcal{F}}{\partial \vec{A}} - \nabla \frac{\partial \mathcal{F}}{\partial \nabla \cdot \vec{A}} + \nabla \times \frac{\partial \mathcal{F}}{\partial \nabla \times \vec{A}} = 0. \tag{B.67}$$

Notice that there is no $\nabla \cdot \vec{A}$ term present in the functional, hence

$$\nabla \frac{\partial \mathcal{F}}{\partial \nabla \cdot \vec{A}} = 0. \tag{B.68}$$

Also,

$$\nabla \times \frac{\partial \mathcal{F}}{\partial \nabla \times \vec{A}} = \nabla \times \frac{2\nabla \times \vec{A}}{2\mu_0} = \frac{\nabla \times \vec{B}}{\mu_0} = \vec{J}_s, \tag{B.69}$$

where we define a supercurrent as

$$\vec{J}_s = \frac{1}{\mu_0} \nabla \times \vec{B}. \tag{B.70}$$

Focus on the first term now:

$$\begin{aligned} \frac{\partial \mathcal{F}}{\partial \vec{A}} &= \frac{\partial}{\partial \vec{A}} \left[\frac{\left| \left(-i\hbar\nabla - q\vec{A} \right) \psi \right|^2}{2m} \right] \\ &= \frac{1}{2m} \frac{\partial}{\partial \vec{A}} \left[\left(i\hbar\nabla\psi^* - q\vec{A}\psi^* \right) \left(-i\hbar\nabla\psi - q\vec{A}\psi \right) \right] \\ &= \frac{1}{2m} \left[-q\psi^* \left(-i\hbar\nabla\psi - q\vec{A}\psi \right) - q\psi \left(i\hbar\nabla\psi^* - q\vec{A}\psi^* \right) \right] \\ &= \frac{i\hbar q}{2m} \left(\psi^* \nabla\psi - \psi \nabla\psi^* \right) + \frac{q^2}{m} |\psi|^2 \vec{A}, \end{aligned} \tag{B.71}$$

so finally get

$$\frac{i\hbar q}{2m} \left(\psi^* \nabla\psi - \psi \nabla\psi^* \right) + \frac{q^2}{m} |\psi|^2 \vec{A} = \vec{J}_s \tag{B.72}$$

– the second Ginzburg-Landau equation.

B.5.5 Ginzburg-Landau Equations in Dimensionless Form

B.5.5.1 Dimensionless Quantities

Dimensionless quantities we are interested in are:

- the dimensionless coordinates:

$$\vec{\mathsf{X}} = \frac{\vec{r}}{\lambda_{GL}} = \vec{r}\sqrt{\frac{q^2|\alpha|\mu_0}{m\beta}}, \tag{B.73}$$

hence

$$\frac{\partial}{\partial\vec{\mathsf{X}}} = \lambda_{GL}\nabla; \tag{B.74}$$

- the dimensionless order parameter:

$$\mathcal{X} = \frac{\psi}{\psi_0} = \psi\sqrt{\frac{\beta}{|\alpha|}}; \tag{B.75}$$

- the dimensionless magnetic field:

$$\vec{b} = \frac{\vec{B}}{\sqrt{2}B_c} = \frac{\vec{B}}{|\alpha|}\sqrt{\frac{\beta}{2\mu_0}}, \tag{B.76}$$

where B_c corresponds to H_c – the thermodynamic critical field;

- the dimensionless vector potential:

$$\vec{a} = \frac{\vec{A}}{\sqrt{2}\lambda_{GL}B_c} = \frac{q\vec{A}}{\sqrt{2}}\sqrt{\frac{1}{m|\alpha|}}, \tag{B.77}$$

hence

$$\vec{b} = \frac{\partial}{\partial\vec{\mathsf{X}}} \times \vec{a}; \tag{B.78}$$

- the dimensionless current:

$$\vec{i} = \frac{\lambda_{GL}\mu_0\vec{J}_s}{\sqrt{2}B_c}, \tag{B.79}$$

hence

$$\vec{i} = \frac{\partial}{\partial\vec{\mathsf{X}}} \times \vec{b}. \tag{B.80}$$

B.5.5.2 First Ginzburg-Landau Equation in the Dimensionless Form

Let us now convert the first Ginzburg-Landau Equation, (3.23), in the dimensionless form. Making use of the definitions of $\vec{\mathsf{X}}$, $\vec{a}$ and $\mathcal{X}$ from the previous paragraph, we get

$$\left(-\frac{i}{\hbar}\frac{\partial}{\partial\vec{\mathsf{X}}} - \sqrt{2m|\alpha|}\vec{a}\right)^2 \mathcal{X} + 2m\alpha\mathcal{X} + 2m\beta\psi_0^2|\mathcal{X}|^2\mathcal{X} = 0, \tag{B.81}$$

which then transforms to

$$\left(-\frac{i}{\kappa_{GL}}\sqrt{2m|\alpha|}\frac{\partial}{\partial\vec{\mathsf{X}}}-\sqrt{2m|\alpha|}\vec{a}\right)^2\mathcal{X}+2m\alpha\mathcal{X}+2m\beta\psi_0^2|\mathcal{X}|^2\mathcal{X}=0, \tag{B.82}$$

then use the definition of ψ_0^2,

$$\psi_0^2=\frac{\alpha}{\beta}, \tag{B.83}$$

and thus cancel out $2m\alpha$ term to get

$$\left(-\frac{i}{\kappa_{GL}}\frac{\partial}{\partial\vec{\mathsf{X}}}-\vec{a}\right)^2\mathcal{X}+\mathcal{X}+|\mathcal{X}|^2\mathcal{X}=0 \tag{B.84}$$

– the first Ginzburg-Landau equation in the dimensionless form.

B.5.5.3 Second Ginzburg-Landau Equation in the Dimensionless Form

Now it is time to convert the second Ginzburg-Landau Equation in the dimensionless form. It seems to be slightly more complicated than the procedure we have just followed, so let us do it step by step. In the second Ginzburg-Landau Equation one has three terms. Call them to be J-term,

$$T_J=\vec{J}_s=\frac{\sqrt{2}B_c}{\lambda_{GL}\mu_0}\vec{i}, \tag{B.85}$$

∇-term,

$$T_\nabla=(\psi^*\nabla\psi-\psi\nabla\psi^*) \tag{B.86}$$

and A-term,

$$T_A=-\frac{q^2}{m}\psi_0^2|\mathcal{X}|^2\vec{A}\sqrt{2}B_c\lambda_{GL} \tag{B.87}$$

Start with the J-term:

$$T_J=\vec{J}_s=\frac{\sqrt{2}B_c}{\lambda_{GL}\mu_0}\vec{i}=q\psi_0\sqrt{\frac{2|\alpha|}{m}}\vec{i}, \tag{B.88}$$

continue with ∇-term:

$$T_\nabla=(\psi^*\nabla\psi-\psi\nabla\psi^*)=\frac{\psi_0^2}{\lambda_{GL}}\left(\mathcal{X}^*\frac{\partial}{\partial\vec{\mathsf{X}}}\mathcal{X}-\mathcal{X}\frac{\partial}{\partial\vec{\mathsf{X}}}\mathcal{X}^*\right), \tag{B.89}$$

and finish with the A-term:

$$T_A=-\frac{q^2}{m}\psi_0^2|\mathcal{X}|^2\vec{A}\sqrt{2}B_c\lambda_{GL}=-q\psi_0^2\sqrt{\frac{2|\alpha|}{m}}|\mathcal{X}|^2\vec{a}. \tag{B.90}$$

Combine all the terms together:

$$\sqrt{\frac{2|\alpha|}{m}}\vec{i} = -\frac{i\hbar}{2m\lambda_{GL}}\left(\mathcal{X}^*\frac{\partial}{\partial\vec{\mathsf{X}}}\mathcal{X} - \mathcal{X}\frac{\partial}{\partial\vec{\mathsf{X}}}\mathcal{X}^*\right) - \sqrt{\frac{2|\alpha|}{m}}|\mathcal{X}|^2\vec{a}, \tag{B.91}$$

divide both sides by $\sqrt{\frac{2|\alpha|}{m}}$ and make use of definitions of ξ and κ_{GL} to obtain

$$\vec{i} = -\frac{i}{2\kappa_{GL}}\left(\mathcal{X}^*\frac{\partial}{\partial\vec{\mathsf{X}}}\mathcal{X} - \mathcal{X}\frac{\partial}{\partial\vec{\mathsf{X}}}\mathcal{X}^*\right) - |\mathcal{X}|^2\vec{a}, \tag{B.92}$$

and this is the second Ginzburg-Landau equation in the dimensionless form.

B.5.5.4 Summary

In order to work with more convenient notation in the future re-label back:

$$\mathcal{X} \to \psi, \tag{B.93}$$

$$\vec{b} \to \vec{B}, \tag{B.94}$$

$$\vec{a} \to \vec{A}, \tag{B.95}$$

$$\frac{\partial}{\partial\vec{\mathsf{X}}} \to \nabla, \tag{B.96}$$

so Ginzburg-Landau equations in the dimensionless form read as

$$\left(-\frac{i}{\kappa_{GL}}\nabla - \vec{A}\right)^2\psi + \psi + |\psi|^2\psi = 0, \tag{B.97}$$

$$\vec{i} = -\frac{i}{2\kappa_{GL}}\left(\psi^*\nabla\psi - \psi\nabla\psi^*\right) - |\psi|^2\vec{A}, \tag{B.98}$$

and the only material-specific parameter involved is the dimensionless κ_{GL} – the Ginzburg-Landau parameter.

B.6 Landau Levels

Let us consider a particle in a magnetic field $\vec{B} = (0, 0, B)$. A possible form of a vector potential is $\vec{A} = (0, xB, 0)$ – the Landau gauge.

The Hamiltonian in the coordinate representation then is

$$\hat{H} = \frac{1}{2m}\left(\frac{\hbar}{i}\nabla - q\vec{A}\right)^2 = -\frac{\hbar^2}{2m}\left(\nabla + \frac{iq}{\hbar}\vec{A}\right)^2 = -\frac{\hbar^2}{2m}\nabla^2 + \frac{q^2B^2}{2m} - \frac{qB}{m}x\hat{p}_y. \tag{B.99}$$

Schroedinger equation for such a particle reads as

$$\hat{H}\psi(x,y,z) = E\psi(x,y,z). \tag{B.100}$$

Studying the form of the Hamiltonian (B.99), try a separable solution of the form [103]

$$\psi(x,y,z) = \psi_x(x)\psi_y(y)\psi_z(z). \tag{B.101}$$

So get three equations to solve. Start with those simple ones:

$$-\frac{\hbar^2}{2m}\frac{d^2\psi_y}{d^2y} = E_y\psi_y(y), \tag{B.102}$$

which can be converted to

$$\frac{d^2\psi_y}{d^2y} = -k_y^2\psi_y(y), \tag{B.103}$$

if we define

$$k_y^2 = \frac{2mE_y}{\hbar^2}, \tag{B.104}$$

that is solved to

$$\psi_y(y) = e^{ik_y y}. \tag{B.105}$$

Similarly get

$$\psi_z(z) = e^{ik_z z}. \tag{B.106}$$

So we are left with an equation for ψ_x only, that now turns into

$$\left(-\frac{\hbar^2}{2m}\frac{d^2}{dx^2} + \frac{q^2B^2}{2m}x^2 + \frac{q\hbar k_y}{2m}x\right)\psi_x(x) = E_x\psi_x(x). \tag{B.107}$$

Introduce:

$$\omega = \frac{qB}{m}, \tag{B.108}$$

$$x_0 = \frac{\hbar k_y}{m\omega} \tag{B.109}$$

to get

$$\left(-\frac{\hbar^2}{2m}\frac{d^2}{dx^2} + \frac{m\omega^2}{2}(x-x_0)^2 - \frac{\hbar^2k_y^2}{2m}\right)\psi_x(x) = E_x\psi_x(x) \tag{B.110}$$

And this can be transformed to

$$\left(-\frac{\hbar^2}{2m}\frac{d^2}{dx^2} + \frac{m\omega^2}{2}(x-x_0)^2\right)\psi_x(x) = \tilde{E}\psi_x(x), \tag{B.111}$$

which is an equation for a shifted simple harmonic oscillator with

$$\tilde{E} = E_x + \frac{\hbar^2 k_y^2}{2m}, \tag{B.112}$$

and it can be solved to [103]

$$\tilde{E} = \hbar\omega\left(n + \frac{1}{2}\right), \tag{B.113}$$

or just

$$E_x = \hbar\omega\left(n + \frac{1}{2}\right) - \frac{\hbar^2 k_y^2}{2m}. \tag{B.114}$$

So the total solution for energy is

$$E = \hbar\omega\left(n + \frac{1}{2}\right) + \frac{\hbar^2 k_z^2}{2m}, \tag{B.115}$$

and corresponding eigenstates are

$$\psi_{x_n}(x) = \frac{1}{\sqrt{2^n n!}}\left(\frac{m\omega}{\pi\hbar}\right)^{\frac{1}{4}} e^{-\frac{m\omega(x-x_0)^2}{2\hbar}} \mathtt{H}_n\left(\sqrt{\frac{m\omega}{\hbar}}(x - x_0)\right), \tag{B.116}$$

where $\mathtt{H}_n$ are Hermite polynomials (see Appendix A.3), and the total wave function in then

$$\psi(x, y, z) = \sum_n C_n \frac{1}{\sqrt{2^n n!}}\left(\frac{m\omega}{\pi\hbar}\right)^{\frac{1}{4}} e^{-\frac{m\omega(x-x_0)^2}{2\hbar}} \mathtt{H}_n\left(\sqrt{\frac{m\omega}{\hbar}}(x - x_0)\right) e^{ik_y y} e^{ik_z z}. \tag{B.117}$$

Appendix C

Technical Details

C.1 Convergence Algorithm

C.1.1 General Formulation

We believe that it is important to give a reader an opportunity to reproduce the results obtained in this Thesis. In order to make it possible, we present our full convergence algorithm starting with the general formulation here.

Any convergence problem can written as a stationary point problem, i.e. for an n-dimensional vector,

$$\vec{x} = \vec{G}(\vec{x}) \tag{C.1}$$

one can define

$$\vec{f} = \vec{G}(\vec{x}) - \vec{x} \tag{C.2}$$

along with the map

$$\vec{x} \to \vec{f}. \tag{C.3}$$

A fixed-point problem is solved if

$$\left|\vec{f}(\vec{x})\right| = 0 \tag{C.4}$$

$\forall \vec{x}$.

In general, $\left|\vec{f}(\vec{x})\right| \geq 0 \quad \forall \vec{x}$, hence $\left|\vec{f}(\vec{x})\right| = 0$ is the minimal-most possible configuration.

Assume we have a pair of $\left(\vec{x}_m, \vec{f}_m\right)$, where

$$\vec{f}_m = \vec{f}_m(\vec{x}). \tag{C.5}$$

For m iterations one can define a linear interpolation of

$$\vec{f}\,[g_l] = \vec{f}_m + \sum_{l=1}^{m-1} g_l \left(\vec{f}_l - \vec{f}_m\right). \tag{C.6}$$

Note that the coefficient g_l is to be determined.

The absolute value of any quantity can be written as

$$\left|\vec{f}(\vec{x})\right| = \sqrt{\vec{f}\cdot\vec{f}^*}, \tag{C.7}$$

hence for the minimal configuration one can write:

$$\vec{f}\,[g_l]\cdot\vec{f}^*\,[g_l] \to \min, \tag{C.8}$$

that is

$$\vec{f}\,[g_l]\cdot\vec{f}^*\,[g_l] \to 0 \tag{C.9}$$

for a fixed-value problem. Therefore

$$\vec{f}\,[g_l]\cdot\vec{f}^*\,[g_l] = \vec{f}_m\cdot\left(\vec{f}_k^* - \vec{f}_m^*\right) + \sum_{l=1}^{m-1} g_l\left(\vec{f}_l - \vec{f}_m\right)\cdot\left(\vec{f}_k^* - \vec{f}_m^*\right) = 0, \tag{C.10}$$

hence g_l can be calculated for a given l from 1 to $m-1$. Define

$$S_{kl}^{(i)} = \left(\vec{f}_l - \vec{f}_i\right)\cdot\left(\vec{f}_k^* - \vec{f}_i^*\right), \tag{C.11}$$

$$T_k^{(i)} = -\vec{f}_i\cdot\left(\vec{f}_k^* - \vec{f}_i^*\right), \tag{C.12}$$

hence

$$g_l^{(i)} = \left(S^{-1}T\right)_l. \tag{C.13}$$

By analogy to (C.6) expand $\vec{x}$:

$$\vec{x}^{\min} = \vec{x}_m + \sum_{l=1}^{m-1} g_l\left(\vec{x}_l - \vec{x}_m\right), \tag{C.14}$$

as $\vec{x}^{\min}$ maps to the neighbourhood of $\vec{f}^{\min}$.

Finally introduce the coupling, the measure of change in $\vec{x}$, p_m:

$$\vec{x}_{m+1} = \vec{x}^{\min} + p_m\vec{f}^{\min}, \tag{C.15}$$

where

$$\vec{f}^{\min} = \vec{f}(\vec{x}^{\min}), \tag{C.16}$$

$$p_m = \frac{\left|\vec{x}_{m-1} - \vec{x}^{\min}\right|}{\vec{f}^{\min}}, \tag{C.17}$$

hence

$$\vec{f}_{m+1} = \vec{f}(\vec{x}_{m+1}). \tag{C.18}$$

C.1.2 Calculations of the Lagrange Multiplier

Let us now apply the formalism developed in the previous section to the problem solved in this Thesis. It would not only accelerate the convergence of numerical solutions, but also help us find the Lagrange multiplier itself. Recall the functional we are to minimise:

$$F = \int \left\{ \frac{J}{2} \sum_{\mu} \left(\partial_\mu \vec{M}\right) \cdot \left(\partial_\mu \vec{M}\right) + D\vec{M} \cdot \left(\nabla \times \vec{M}\right) - \vec{B} \cdot \vec{M} + \lambda \left(\left|\vec{M}\right|^2 - 1 \right) \right\} \frac{dxdy}{A}, \tag{C.19}$$

where $\vec{M} = \vec{M}(x, y)$ and $\lambda = \lambda(x, y)$ is the Lagrange multiplier. In chapter 2 we have discussed this functional and its minimisation in details. Particularly, we have concluded that if we Fourier expand both $\vec{M}$ and λ, then Fourier coefficients for the components of $\vec{M}$ can be found analytically for a given λ. So one can write $M_\mu = M_\mu(\lambda)$ for a component of the magnetisation.

In order to be consistent with the algorithm described in the previous section, state

$$\vec{x} \to \vec{\lambda}. \tag{C.20}$$

Vector sign here means that $\vec{\lambda}$ is a multidimensional function, i.e. $\vec{\lambda} = \vec{\lambda}(x, y)$. Also define

$$\underline{\lambda} = \left\{ \vec{\lambda}_1(x, y), \vec{\lambda}_2(x, y), \ldots, \vec{\lambda}_m(x, y) \right\}, \tag{C.21}$$

a vector of m vectors $\vec{\lambda}$. The vector of functions of $\vec{x}$, $\vec{f}$, is then defined as

$$\vec{f}_j = \vec{f}_j(\vec{\lambda}_j) \tag{C.22}$$

and for a given j f_j is written as

$$f_j = M_x^2 + M_y^2 + M_z^2 - 1, \tag{C.23}$$

and this is the actual constraint we want to implement.

It was found that it is enough to consider $m = 5$ iterations. So the full algorithm for finding λ writes:

- for iteration $i < 3$[1]:

  1 load initial guess for λ_i;

  2 calculate M_x, M_y, M_z;

  3 report the average $\vec{M}$;

  4 calculate $f_i \to \vec{f_i}$, then write $\vec{f_i}$ to $\vec{f}$ and $\vec{\lambda}_i$ to $\vec{\lambda}$;

- for iteration $3 \leq i < m$:

  1 calculate g_l coefficients:

$$g_l = \left(S^{-1}T\right)_l \tag{C.24}$$

  with

$$S_{kl}^{(i)} = \left(\vec{f}_k - \vec{f}_{i-1}\right)\left(\vec{f}_l - \vec{f}_{i-1}\right) \tag{C.25}$$

  and

$$T_k^{(i)} = -\vec{f}_{i-1}\left(\vec{f}_k - \vec{f}_{i-1}\right), \tag{C.26}$$

  where l, k go from 1 to $i-2$;

  2 find $\vec{\lambda}^{min}$:

$$\vec{\lambda}^{min} = \vec{\lambda}_{i-1} + \sum_{l=1}^{i-2} g_l \left(\vec{\lambda}_l - \vec{\lambda}_{i-1}\right), \tag{C.27}$$

  3 find $\vec{f}^{min}$:

$$\vec{f}^{min} = \vec{f}_{i-1} + \sum_{l=1}^{i-2} g_l \left(\vec{f}_l - \vec{f}_{i-1}\right); \tag{C.28}$$

  4 update the mixing parameter, p_i;

  5 find mixed $\vec{\lambda}_i$:

$$\vec{\lambda}_i = \vec{\lambda}^{min} + p_i \vec{f}^{min}; \tag{C.29}$$

  6 calculate M_x, M_y, M_z;

  7 calculate $f_i \to \vec{f_i}$, then write $\vec{f_i}$ to $\vec{f}$ and $\vec{\lambda}_i$ to $\vec{\lambda}$;

  8 test the convergence, if

$$|\vec{f_i}| < 10^{-15}, \tag{C.30}$$

$$|\lambda_i - \lambda_{i-1}| < 10^{-15}, \tag{C.31}$$

$$|M_{x_i} - M_{x_{i-1}}| < 10^{-15}, \tag{C.32}$$

$$|M_{y_i} - M_{y_{i-1}}| < 10^{-15}, \tag{C.33}$$

[1] To avoid confusion, here all the counting starts at 1, though the vast majority of programming languages start their conuting at 0.

$$|M_{z_i} - M_{z_{i-1}}| < 10^{-15} \tag{C.34}$$

are all true;

- for $i \geq m$:

  1 calculate g_l coefficients:

  $$g_l = \left(S^{-1}T\right)_l \tag{C.35}$$

  with

  $$S_{kl}^{(m)} = \left(\vec{f}_k - \vec{f}_{m-1}\right)\left(\vec{f}_l - \vec{f}_{m-1}\right) \tag{C.36}$$

  and

  $$T_k^{(m)} = -\vec{f}_{m-1}\left(\vec{f}_k - \vec{f}_{m-1}\right), \tag{C.37}$$

  where l, k go from 1 to $m-2$;

  2 find $\vec{\lambda}^{min}$:

  $$\vec{\lambda}^{min} = \vec{\lambda}_{m-1} + \sum_{l=1}^{m-2} g_l \left(\vec{\lambda}_l - \vec{\lambda}_{m-1}\right), \tag{C.38}$$

  3 find $\vec{f}^{min}$:

  $$\vec{f}^{min} = \vec{f}_{m-1} + \sum_{l=1}^{m-2} g_l \left(\vec{f}_l - \vec{f}_{m-1}\right); \tag{C.39}$$

  4 update the mixing parameter, p_m;

  5 find mixed $\vec{\lambda}_m$:

  $$\vec{\lambda}_m = \vec{\lambda}^{min} + p_m \vec{f}^{min}; \tag{C.40}$$

  6 calculate M_x, M_y, M_z;

  7 calculate $f_m \to \vec{f}_m$, then write $\vec{f}_m$ to $\vec{f}$ and $\vec{\lambda}_m$ to $\vec{\lambda}$;

  8 test the convergence, if

  $$|\vec{f}_m| < 10^{-15}, \tag{C.41}$$

  $$|\lambda_m - \lambda_{m-1}| < 10^{-15}, \tag{C.42}$$

  $$|M_{x_m} - M_{x_{m-1}}| < 10^{-15}, \tag{C.43}$$

  $$|M_{y_m} - M_{y_{m-1}}| < 10^{-15}, \tag{C.44}$$

  $$|M_{z_m} - M_{z_{m-1}}| < 10^{-15} \tag{C.45}$$

  are all true;

  9 step back in $\vec{f}$ and $\vec{\lambda}$:

  $$\vec{f}_k = \vec{f}_{k+1}, \tag{C.46}$$

etc, starting with

$$\vec{f}_1 = \vec{f}_2, \tag{C.47}$$

up to

$$\vec{f}_{m-1} = \vec{f}_m, \tag{C.48}$$

etc. Notice that in the end one has $\vec{f}_{m-1} = \vec{f}_m$, so two last elements of $\vec{f}$ vector are the same, but it is ok, as $\vec{f}_m$ is overwritten in the next iteration.

C.1.3 Initial Guess for λ

In the previous section we have discussed how to obtain the Lagrange multiplier, λ, from its previous iterations, however, one shall always begin with something. Initial guess for λ is important, as the better it is, the faster the solution would converge. We need at least two linearly independent initial guesses for λ in order to implement the algorithm described in the previous section.

The condition we would like to implement with the aid of the Lagrange multiplier, λ, is the condition on the magnetisation, hence one may suggest that λ shall repeat the shape of components of $\vec{M}$ somehow. If we Fourier transform both λ and $\vec{M}$, then an initial guess that seems good for λ can be written as

$$\lambda_1(x, y) = \sum_{\vec{k}} \left(X_{\vec{k}}^2 + Y_{\vec{k}}^2 + Z_{\vec{k}}^2 \right) \tag{C.49}$$

and

$$\lambda_2(x, y) = \sum_{\vec{k}} Z_{\vec{k}} Z_{\vec{k}}^*, \tag{C.50}$$

where $X_{\vec{k}}$, $Y_{\vec{k}}$ and $Z_{\vec{k}}$ are Fourier coefficients for M_x, M_y and M_z respectively.

C.1.4 Full Algorithm

The full algorithm of a run for a single value of an external field, β, for a system of skyrmions only is then as follows:

1. define the lattice for a given lattice spacing a;
2. calculate the k-matrix, $\hat{K}_{\vec{k}\vec{k}'}$;
3. if there is no better choice, implement the initial guess for the Lagrange multiplier from section C.1.3;
4. find Fourier coefficients for λ from the numerical algorithm introduced in this chapter;

5. find Fourier coefficients for the magnetisation components analytically for λ found just before;

6. implement the virial theorem in order to find the optimal spacing for a given external field, β.

C.2 Software Used

The main code created in order to implement the numerical algorithms required to solve the model presented in this Thesis was written mainly on Python [104] with come inserts of C^{++} [105] for bits that required heavy computations. Python was also used for all the supplementary calculations, analysis and representation that followed the main calculations. We have used standard python libraries (methods) only: numpy, [106] scipy [107] and matplotlib, [108] no external packages were required. Wolfram Mathematica [109] was also used in order to present some high quality plots.

Bibliography

[1] E. M. Purcell. Electricity and Magnetism, Vol. II: v. 2 (Berkeley Physics Course) *McGraw-Hill Higher Education*, Oct 1984.

[2] `https://en.wikipedia.org/wiki/Curie_temperature`

[3] `https://en.wikipedia.org/wiki/Magnetic_domain`

[4] T. Koyama, D. Chiba, K. Ueda, K. Kondou, H. Tanigawa, S. Fukami, T. Suzuki, N. Ohshima, N. Ishiwata, Y. Nakatani, K. Kobayashi, T. Ono. Observation of the intrinsic pinning of a magnetic domain wall in a ferromagnetic nanowire. *Nature Materials*, 10, 194–197, Jan 2011.

[5] V. L. Sivuhin. General course of physics. Vol. III. Electricity. *FIZMATLIT*, Edition 3, 2006.

[6] D. Wagner, D. Ter Haar. Introduction to the Theory of Magnetism: International Series of Monographs in Natural Philosophy. *Pergamon*, Oct 2013

[7] S. Blundell. Magnetism in Condensed Matter. *Oxford University Press*, Nov 2000.

[8] R. Shankar. Principles of Quantum Mechanics. Second Edition. *Springer*, 1994.

[9] C. Kittel. Introduction to Solid State Physics, 5th ed., *Wiley*, 1976.

[10] N. W. Ashcroft, D. N. Mermin. Solid State Physics. *Thomson Press (India) Ltd*, Dec 2003.

[11] L. Landau. Theory of phase transformations. I. *Zh. Eksp. Teor. Fiz.*, 7 19, 1937.

[12] L. D. Landau, E. M. Lifshitz. Course of Theoretical Physics. Volume V. Statistical Physics. Part 1. 3rd Edition. *Butterworth-Heinemann, Oxford*. 1980.

[13] R. J. Baxter. Exactly solved models in statistical mechanics. *Academic Press, London*, 1982.

[14] A. Fert, V. Cros, J. Sampaio. Skyrmions on the track. *Nature Nanotechnology*, 8, 152-156, Mar 2013.

[15] I. Dzyaloshinsky. A thermodynamic theory of "weak" ferromagnetism of antiferromagnetics. *Journal of Physics and Chemistry of Solids*, 4:241–255, 1957.

[16] T. Moriya. Anisotropic superexchange interaction and weak ferromagnetism. *Physical Review*, 120(1):91–99, 1960.

[17] Y. Kawaguchi, Y. Tanaka, N. Nagaosa. Skyrmionic magnetization configurations at chiral magnet/ferromagnet heterostructures. *Phys. Rev. B*, 93, 064416, Feb 2016.

[18] `http://www.staff.uni-mainz.de/kaeversc/research-talks-and-posters.html`

[19] J. Iwasaki, M. Mochizuki, N. Nagaosa. Universal current-velocity relation of skyrmion motion in chiral magnets. *Nature Communications*, 4, 1463, Jan 2013.

[20] S. Mühlbauer, B. Binz, F. Jonietz, C. Pfleiderer, A. Rosch, A. Neubauer, R. Georgii, P. Böni. Skyrmion Lattice in a Chiral Magnet. *Science*, Vol. 323, Issue 5916, pp. 915-919, Feb 2009.

[21] X. Z. Yu, Y. Onose, N. Kanazawa, J. H. Park, J. H. Han, Y. Matsui, N. Nagaosa, Y. Tokura. Real-space observation of a two-dimensional skyrmion crystal. *Nature*, 465, 901–904, Jun 2010.

[22] T. H. R. Skyrme. A Non-Linear Field Theory. *Proc. R. Soc. A*, 260, 127, 1961.

[23] R. H. Hobart. On the Instability of a Class of Unitary Field Models. *Proc. Phys. Soc. Lond.*, 82, 201, 1963.

[24] G. H. Derrick. Comments on Nonlinear Wave Equations as Models for Elementary Particles. *J. Math. Phys.*, 5, 1252, 1964.

[25] U. A. Khawaja, H. Stoof. Skyrmions in a ferromagnetic Bose-Einstein condensate. *Nature*, 411, 918-920, Jun 2001

[26] T. L. Ho. Spinor Bose condensates in optical traps. *Phys. Rev. Lett.*, 81, 742–745, 1998.

[27] S. L. Sondhi, A. Karlhede, S. A. Kivelson, E. H. Rezayi. Skyrmions and the crossover from the integer to fractional quantum Hall effect at small Zeeman energies. *Phys. Rev. B*, 47, 16419–16426, 1993.

[28] P. M. Walmsley, A. I. Golov. Chirality of Superfluid $^3He - A$. *Phys. Rev. Lett.*, 109, 215301, Nov 2012.

[29] D. C. Wright, N. D. Mermin. Crystalline liquids: the blue phases. *Rev. Mod. Phys.*, 61, 385, 1989.

[30] J. P. Sethna. Frustration, curvature, and defect lines in metallic glasses and the cholesteric blue phase. *Phys. Rev. B*, 31, 6278, 1985.

[31] P. Jaikumar, M. Bagchi, R. Ouyed. High-Density Skyrmion Matter and Neutron Stars. *The Astrophysical Journal*, Volume 678, Number 1, May 2008.

[32] C. Adam, C. Naya, J. Sanchez-Guillen, R. Vazquez, A. Wereszczynski. BPS Skyrmions as neutron stars. *Physics Letters B*, Volume 742, Pages 136-142, Mar 2015.

[33] X. Z. Yu, N. Kanazawa, Y. Onose, K. Kimoto, W. Z. Zhang, S. Ishiwata, Y. Matsui, Y. Tokura. Near room-temperature formation of a skyrmion crystal in thin-films of the helimagnet FeGe. *Nature Mater.*, 10, 106, Dec 2011.

[34] T. Sato, T. Ando, T. Oku, M. Furusaka. Helical-spin-glass reentrant transition in itinerant electron type magnet $Cr_{1-x}Mn_xGe$. *J. Magn. Magn. Matt.*, 140, 1785, 1995.

[35] R. Bügel, A. Faißt, H. V. Löhneysen, J. Wosnitza, U. Schotte. Magnetic phase diagram of $CsCuCl_3$ for in-plane magnetic fields up to $14T$. *Phys. Rev. B*, 65, 052402, Dec 2002.

[36] S. Maruyama, H. Tanaka, Y. Narumi, K. Kindo, H. Nojiri, M. Motokawa, K. Nagata. Susceptibility, Magnetization Process and ESR Studies on the Helical Spin System $RbCuCl_3$. *J. Phys. Soc. Jpn.*, 70, 859, 2001.

[37] S. Seki, X. Z. Yu, S. Ishiwata, Y. Tokura. Observation of Skyrmions in a Multiferroic Material, *Science*, 336, 198, Apr 2012.

[38] A. Zheludev, S. Maslov, G. Shirane, Y. Sasago, N. Koide, K. Uchinokura. Field-Induced Commensurate-Incommensurate Phase Transition in a Dzyaloshinsky-Moriya Spiral Antiferromagnet. *Phys. Rev. Lett.*, 78, 4857, Jun 1997.

[39] I. Kézsmárki, S. Bordács, P. Milde, E. Neuber, L. M. Eng, J. S. White, H. M. Rønnow, C. D. Dewhurst, M. Mochizuki, K. Yanai, H. Nakamura, D. Ehlers, V. Tsurkan, A. Loidl. Néel-type skyrmion lattice with confined orientation in the polar magnetic semiconductor GaV_4S_8. *Nature Materials*, 14, 1116–1122, Jul 2015.

[40] A. N. Bogdanov, D. A. Yablonskii. Thermodynamically stable "vortices" in magnetically ordered crystals. The mixed state of magnets. *JETP*, Vol. 68, No. 1, p. 101, Jan 1989.

[41] A. N. Bogdanov, A. Hubert. The Properties of Isolated Magnetic Vortices. *phys. stat. sol. (b)*, 186, 1521-3951, Dec 1994.

[42] A. N. Bogdanov, A. Hubert. Thermodynamically stable magnetic vortex states in magnetic crystals. *J. Magn. Magn. Mater.*, Volume 138, Issue 3, Pages 255-269, Dec 1994.

[43] J. H. Han, J. Zang, Z. Yang, J. Park, N. Nagaosa. Skyrmion lattice in a two-dimensional chiral magnet. *Phys. Rev. B*, 82, 094429, Sep 2010.

[44] M. Garst. Topological skyrmion dynamics in chiral magnets. Chapter in "Topological structures in ferroic materials", ed. J. Seidel, *Springer International Publishing*, 2016.

[45] A. O. Leonov, I. E. Dragunov, U. K. Rößler, A. N. Bogdanov. Theory of skyrmion states in liquid crystals. *Phys. Rev. E*, 90, 042502, Oct 2014.

[46] T. Yokoyama, J. Linder. Josephson effect through magnetic skyrmions. *Phys. Rev. B*, 92, 060503(R), Aug 2015.

[47] S. Heinze, K. V. Bergmann, M. Menzel, J. Brede, A. Kubetzka, R. Wiesendanger, G. Bihlmayer, S. Blügel. Spontaneous atomic-scale magnetic skyrmion lattice in two dimensions. *Nature Phys.*, 7, 713–718, Jul 2011.

[48] N. Romming, A. Kubetzka, C. Hanneken, K. V. Bergmann, R. Wiesendanger. Field-Dependent Size and Shape of Single Magnetic Skyrmions. *Phys. Rev. Lett.*, 114, 177203, May 2015.

[49] S. Woo, K. Litzius, B. Krüger, M. Im, L. Caretta, K. Richter, M. Mann, A. Krone, R. M. Reeve, M. Weigand, P. Agrawal, I. Lemesh, M. Mawass, P. Fischer, M. Kläui, G. S. D. Beach. Observation of room-temperature magnetic skyrmions and their current-driven dynamics in ultrathin metallic ferromagnets. *Nature Materials*, 15, 501–506, Jan 2016.

[50] H. Du, R. Che, L. Kong, X. Zhao, C. Jin, C. Wang, J. Yang, W. Ning, R. Li, C. Jin, X. Chen, J. Zang, Y. Zhang, M. Tian. Edge-mediated skyrmion chain and its collective dynamics in a confined geometry. *Nature Communications*, 6, 8504. Oct 2015.

[51] N. Romming, C. Hanneken, M. Menzel, J. E. Bickel, B. Wolter, K. V. Bergmann, A. Kubetzka, R. Wiesendanger. Writing and Deleting Single Magnetic Skyrmions. *Science*, Vol. 341, Issue 6146, pp. 636-639, Aug 2013.

[52] X. Zhang, M. Ezawa, Y. Zhou. Magnetic skyrmion logic gates: conversion, duplication and merging of skyrmions. *Scientific Reports*, 5, Article number: 9400 , Mar 2015.

[53] X. Zhang, M. Ezawa, Y. Zhou. Magnetic skyrmion transistor: skyrmion motion in a voltage-gated nanotrack. *Scientific Reports*, 5, Article number: 11369, May 2015.

[54] H. Kamerlingh Onnes. *Commun. Phys. Lab. Univ. Leiden*, 12, 120, 1911.

[55] A. Schilling, M. Cantoni, J. D. Guo, H. R. Ott. Superconductivity in the Hg-Ba-Ca-Cu-O system. *Nature*, 363 (6424): 56-58, 1993.

[56] A. P. Drozdov, M. I. Eremets, I. A. Troyan, V. Ksenofontov, S. I. Shylin. Conventional superconductivity at 203 kelvin at high pressures in the sulfur hydride system. *Nature*, 525, 73–76, 03 SEP 2015.

[57] W. Meissner, R. Ochsenfeld. *Die Naturwissenschaften*, 44.787, 1933.

[58] E. H. Brandt. The flux-line lattice in superconductors. *Reports on Progress in Physics*, Volume 58, Number 11, Jun 1995.

[59] V. L. Ginzburg, L. D. Landau, On the theory of superconductivity. *Zh. Eksp. Teor. Fiz.*, 20, 1064, 1950.

[60] R. Peierls, *Proc. Roy. Soc.*, A155, 613, 1936.

[61] F. London, *Physica* 3, 450, 1936.

[62] W. J. de Haas, J. M. Casimir-Jonker. Penetration of a Magnetic Field into Supra-Conductive Alloys. *Nature*, 135, 30-31, Jan 1935.

[63] A. A. Abrikosov. On the magnetic properties of superconductors of the second group. *Sov. Phys. JETP* 5, 1174, 1957.

[64] L. V. Shubnikov, V. I. Khotkevich, Y. D. Shepelev, Y. N. Riabinin. Magnetic properties of superconducting metals and alloys. *Zh. Exper. Teor. Fiz. (USSR)*, V.7, No 2, p.221-237, 1937.

[65] W. H. Kleiner, L. M. Roth, S. H. Autler. Bulk Solution of Ginzburg-Landau Equations for Type II Superconductors: Upper Critical Field Region. *Phys. Rev.*, 133, A1226, Mar 1964,

[66] D. Cribier, B. Jacrot, L. Madhav Rao, B. Farnoux. Mise en evidence par diffraction de neutrons d'une structure periodique du champ magnetique dans le niobium supraconducteur. *Phys. Lett.* 9, 106, Apr 1964.

[67] U. Essmann, H. Trauble. The direct observation of individual flux lines in type-II superconductors. *Phys. Lett.* 24A, 526, May 1967.

[68] H. F. Hess, R. B. Robinson, R. C. Dynes, J. M. Valles Jr., J. V. Waszczak. Scanning-Tunneling-Microscope Observation of the Abrikosov Flux Lattice and the Density of States near and inside a Fluxoid. *Phys. Rev. Lett.*, 62, 214, Jan 1989.

[69] L. Y. Vinnikov, J. Karpinski, S. M. Kazakov, J. Jun, J. Anderegg, S. L. Budko, P. C. Canfield. Vortex structure in MgB_2 single crystals observed by the Bitter decoration technique. *Phys. Rev. B*, 67, 092512, Mar 2013.

[70] D. F. Agterberg. Square vortex lattices for two-component superconducting order parameters. *Phys. Rev. B*, 58, 14484, Dec 1998.

[71] E. H. Brandt, *Phys. Status Solidi*, 36, 381, 393, 1969.

[72] D. F. Agterberg, E. Babaev, J. Garaud. Microscopic prediction of skyrmion lattice state in clean interface superconductors. *Phys. Rev. B*, 90, 064509, Aug 2014.

[73] A. Knigavko, B. Rosenstein, Y. F. Chen. Magnetic skyrmions and their lattices in triplet superconductors. *Phys. Rev. B*, 60, 550, Jul 1999.

[74] T. Okubo, S. Chung, H. Kawamura. Multiple-q States and the Skyrmion Lattice of the Triangular-Lattice Heisenberg Antiferromagnet under Magnetic Fields. *Phys. Rev. Lett.*, 108, 017206, Jan 2012.

[75] N. Nagaosa, Y. Tokura. Topological properties and dynamics of magnetic skyrmions. *Nature Nanotechnology*, 8, 899–911, Dec 2013.

[76] Y. S. Lin, P. J. Grundy, E. A. Giess. *Appl. Phys. Lett.*, 23, 485, 1973.

[77] S. Takao. A study of magnetization distribution of submicron bubbles in sputtered Ho-Co thin films. *Journal of Magnetism and Magnetic Materials.*, Volumes 31–34, Part 2, Feb 1983.

[78] M. N. Wilson, A. B. Butenko, A. N. Bogdanov, T. L. Monchesky. Chiral skyrmions in cubic helimagnet films: The role of uniaxial anisotropy. *Phys. Rev. B*, 89, 094411, Mar 2014.

[79] I. Klebanov. Nuclear matter in the Skyrme model. *Nuclear Physics B*, Volume 262, Issue 1, Pages 133-143, Dec 1985.

[80] A. Bogdanov, A. Hubert. Stability of vortex-like structures in uniaxial ferromagnets. *J. Magn. Magn. Mater.*, 195, 182, 1999.

[81] A. Bogdanov. New localized solutions of the nonlinear field equations. *Pis'ma Zh. Eksp. Teor. Fiz.*, 62, No 3, 231-235, Aug 1995.

[82] K. Everschor, M. Garst, B. Binz, F. Jonietz, S. Mühlbauer, C. Pfleiderer, A. Rosch. Rotating skyrmion lattices by spin torques and field or temperature gradients. *Phys. Rev. B*, 86, 054432, Aug 2012.

[83] P. M. Chaikin, T. C. Lubensky. Principles of Condensed Matter Physics. *Cambridge University Press*, Sep. 2000.

[84] A. N. Bogdanov, U.K. Rößler, C. Pfleiderer. Modulated and localized structures in cubic helimagnets. *Physica B Condensed Matter.* 359-361:1162-1164, Dec 2004.

[85] M. M. Doria, J. E. Gubernatis, D. Rainer. Virial theorem for Ginzburg-Landau theories with potential applications to numerical studies of type-II superconductors. *Phys. Rev. B*, 39, 9573, May 1989.

[86] M. Mochizuki. Spin-Wave Modes and Their Intense Excitation Effects in Skyrmion Crystals. *Phys. Rev. Lett.*, 108, 017601, Jan 2012.

[87] G. L. Pollack, D. R. Stump. Electromagnetism. *Addison-Wesley*, 2012.

[88] H. Kamerlingh Onnes. *Commun. Phys. Lab. Univ. Leiden*, Suppl, 34b, 1913.

[89] M. Tinkham. Introduction to Superconductivity: v. 1. *McGraw-Hill, New York*, Jun 2004.

[90] J. F. Annett. Superconductivity, superfluids and condensates. Oxford master series in physics. *Oxford Univ. Press, Oxford*, 2004.

[91] L. D. Landau, E. M. Lifshitz. Course of Theoretical Physics. Volume IX. Statistical Physics. Part 2. 3rd Edition. *Butterworth-Heinemann, Oxford*, 1980.

[92] A. A. Abrikosov. Fundamentals of the Theory of Metals. *Elsevier Science Ltd*, 1988.

[93] E. H. Brandt. Precision Ginzburg-Landau Solution of Ideal Vortex Lattices for Any Induction and Symmetry. *Phys. Rev. Lett.*, 78, 2208, Mar 1997.

[94] E. H. Brandt. Properties of the ideal Ginzburg-Landau vortex lattice. *Phys. Rev. B*, 68, 054506, Aug 2003.

[95] V. Dikovsky, V. Sokolovsky, B. Zhang, C. Henkel, R. Folman. Superconducting atom chips: advantages and challenges. *The European Physical Journal D*, 51, Issue 2, pp 247-259, Feb 2009.

[96] K. M. D. Hals, M. Schecter, M. S. Rudner. Composite Topological Excitations in Ferromagnet-Superconductor Heterostructures. *Phys. Rev. Lett. 117, 017001*, Jul 2016.

[97] G. B. Arfken, H. J. Weber, F. E. Harris. Mathematical Methods for Physicists: A Comprehensive Guide. *Academic Press*, 7 edition, Feb. 2012.

[98] W. E. Boyce, R. C. DiPrima. Elementary Differential Equations. *John Wiley and Sons*, 9th Edition edition, Nov 2008.

[99] J. D. Jackson. Classical Electrodynamics. *John Wiley and Sons*, 3rd Revised edition edition, Dec 1998

[100] V. L. Sivuhin. General course of physics. Vol. II. Thermodynamics. *FIZMATLIT*, Edition 3, 2006.

[101] N. Zettili. Quantum Mechanics: Concepts and Applications. *Wiley*, 2nd Edition edition, Feb 2009.

[102] J. Kessler. Polarized Electrons. *Springer*, Berlin, Heidelberg, 1985.

[103] Lectures delivered in academic year 2010-2011 by prof Niels Walet in the University of Manchester.

[104] `https://www.python.org`

[105] `https://isocpp.org/`

[106] `http://www.numpy.org/`

[107] `http://www.scipy.org/`

[108] `http://matplotlib.org/`

[109] `https://www.wolfram.com/mathematica/`

Acknowledgments

Since I was old enough to think about my future, I wanted to be a scientist. Three or four years prior to my graduation from the high school I already knew that I would go to a university, it would be a university in the UK and the degree would be related to physics in one or another way. I have to thank my physics teacher, Roza Isaakovna, for that. She taught me tonnes of physics, maths that was beyond the curriculum, trained for National Olympiads, but what was far more important, with her I learned that if you want to achieve something, you should bloody work on it; stop complaining and blaming someone else in your failures. Simple truth, one may say. Well, I was lucky to learn it while being young enough. There was also an institution that influenced me a lot: a pre-university school for (especially) gifted youngsters "Fizikos Olimpas" – "The Olympus of Physics" to be translated – that selected the best pupils from the National Olympiad in Physics and trained them for the international one and introduced them (us!) to the university life. These are also my parents to thank after all, for having let me leave for another, foreign and unknown country, probably feeling even back then that I would not come back.

The route to the position I am in now was quite straightforward: I was accepted at the University of Manchester, where I spent four great years learning fascinating stuff and exploring a culture that was new to me. I would like to thank my lecturers for the guidance they have provided, especially my maths and quantum mechanics lecturers. Also, I would like to thank Andre Geim for not having accepted me on the summer placement in 2010 – I might have ended up as an experimentalist if he had – and Henggui Zhang for accepting me the year after. Towards the end of my Masters degree, I was applying for several PhD positions and, eventually, chose the supervisor I liked the most – professor Matthias Eschrig from Royal Holloway University of London. That is how my PhD adventure began.

I have met amazing people during these four years here in Egham, at Royal Holloway. Thank you guys, thank you for being there! Thank you, Matthias and Anna, Andrew and Giovanni, Aldo, Niclas and Paco, Gabriele and Lorenzo, Eugene and Tom, Franco, David, Teresa, Luke, Seb, Jorge and all the others! I would also like to thank my friend Daniel (Danila for those who know him for as long as I do) for introducing me to Amazon AWS systems – this turned out to be bloody handy especially in the last few months, Vitaly for keeping telling

me that I should “release it if I truly love”, Valduk and his precious wife Angela (I delivered my first ever public talk just the day after a sleepless night of their wedding) for being “tough as the place they’ve been born in” and maintaining my belief in this very world, Peter for some discussions on spin ordering in magnets, Taya, Maria and other people of London for reminding me that there is occasionally life outside Physics Department, Gabriele for helping me overcome the syntax of Wolfram’s Mathematica and produce some of the wonderful pictures presented in this Thesis. Also, I would like to thank Tim and Glen for letting me try myself in teaching here in Royal Holloway. This has been an amazing experience! I enjoyed working with them, as well as with Andrew, Nikolas, Anna and the others. I would also like to thank my students for always keeping me “in shape”. But most of all I would like to thank my sister Nika, who has recently started her career as an English language teacher, for proofreading this Thesis – should one find any grammar mistakes now, they are as much hers as they are mine, – my closest collaborator Aldo for long and intensive discussions, all the advice he had provided, and my supervisor Matthias who has been a great supervisor, sometimes answering my questions before I managed to ask. Thank you all guys, these four years have been bloody awesome and I am ready for new challenges and adventures!